Università degli Studi di Torino

**Scuola di Dottorato**

---

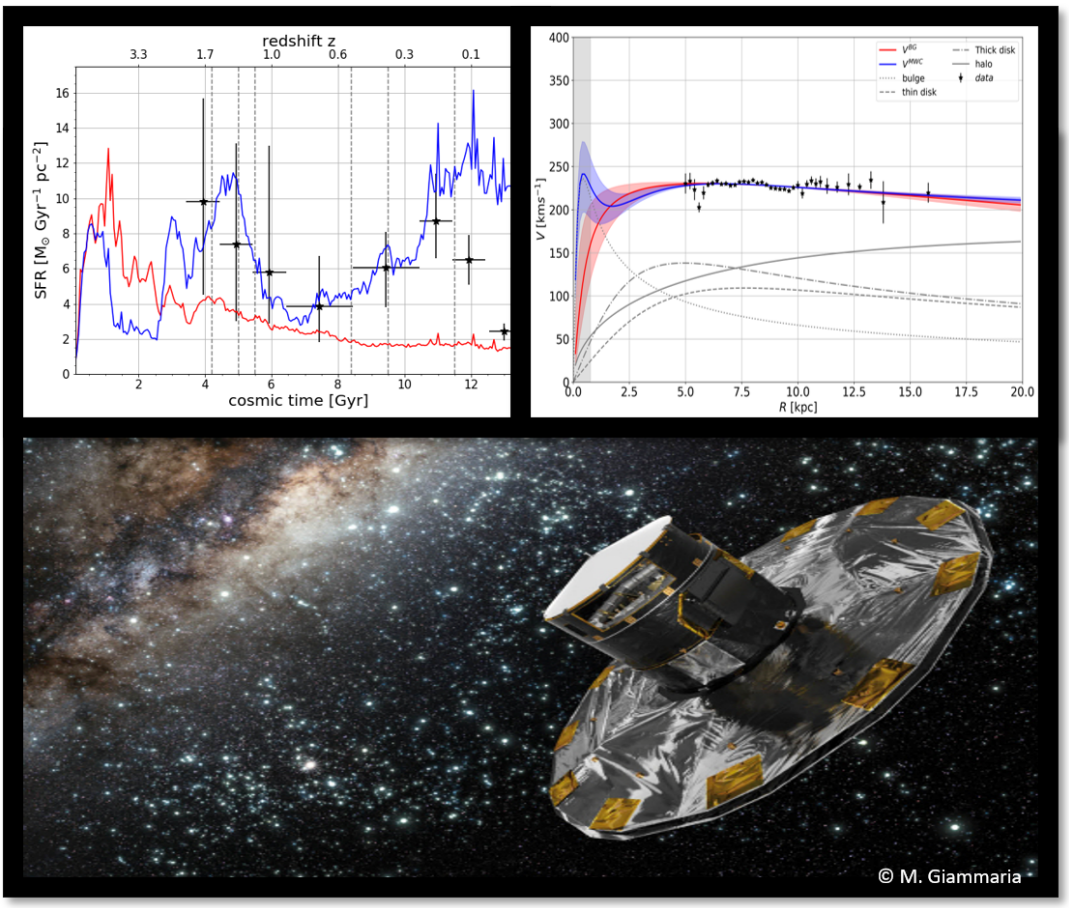


# Milky Way simulations and tests with Gaia-DR2 in the context of Local Cosmology and Relativistic Astrometry

**Marco Giammaria**

Università degli Studi di Torino
**Scuola di Dottorato**

---

**Dottorato in Fisica ed Astrofisica**

# Milky Way simulations and tests with Gaia-DR2 in the context of Local Cosmology and Relativistic Astrometry

**Marco Giammaria**

**Tutor: Dr. Mariateresa Crosta**
**Co-Tutor: Dr. Mario G. Lattanzi**

# *Abstract*

Local Cosmology aims to provide a link between the local scenario at redshift $z = 0$ and the distant Universe. In this context, we may certainly assert that the evolution of the Milky Way, and its constituents, is the product of the action of gravity according to General Relativity. In the era of Gaia, the weak-gravity regime is playing a pivotal role in Galactic observation surveys, together with the implementation of high-resolution cosmological simulations. Therefore, the quests nowadays and the motivation of this Thesis are to put several observational constraints on the structure and origin of the Galaxy as a "standard candle" for disc-like galaxies and to push on the use of General Relativity to ensure a robust Local Cosmology Laboratory against which any model at first for the Galaxy can be tested. In this work, the high-resolution simulation AqC4 was investigated to disentangle the complex overlapping of stellar generations that rises from the top-down and inside-out formation of the galactic disc. Several cosmological signatures, stemming from past and recent dynamical perturbations, confirm that the Galactic thick disc was produced by a satellite with a stellar mass ratio $\Delta \sim 5.5$ % accreted at $z \sim 1.6$ which resembles the major merger Gaia-Sausage-Enceladus ($\Delta \sim 6$ %), while at $z \sim 0.5 - 0.4$ two merging satellites with a stellar mass of $\sim 10^8$ $M_\odot$ each are associated to a strong starburst in the Star Formation History which appears fairly similar to that recently found in the Solar Neighbourhood. On the other hand, from the Gaia DR2 catalogue was extracted one of the most suitable angular-momentum supported stellar sample that better traces the Milky Way observed rotation curve. To explain its flatness, two models were fitted to such data: a classical velocity profile including a dark matter halo, and a general relativistic one derived from a stationary axisymmetric Galactic-scale metric. The latter provides a statistically indistinguishable result from its state-of-the-art dark matter analogue. These findings suggest no need for extra matter to account for the Galactic disc kinematics and a baryonic-only Milky Way. The results of this Thesis confirm that detailed studies of stellar kinematics based on current and future Gaia data releases and in synergy with simulations are fundamental to unravel the formation and evolution of the Milky Way in the context of Local Cosmology.

## List of publications:

- Mariateresa Crosta et al. (June 2020). "On testing CDM and geometry-driven Milky Way rotation curve models with Gaia DR2". In: *Monthly Notices of the Royal Astronomical Society* 496.2, pp. 2107–2122. DOI: 10.1093/mnras/staa1511. arXiv: 1810.04445 [astro-ph.GA]

- Marco Giammaria et al. (Apr. 2021). "The formation history of the Milky Way disc with high-resolution cosmological simulations". In: *Monthly Notices of the Royal Astronomical Society* 502.2, pp. 2251–2265. DOI: 10.1093/mnras/stab136. arXiv: 2102.02652 [astro-ph.GA]

### In proceedings:

- Mariateresa Crosta et al. (Apr. 2019). "Shedding light on the Milky Way rotation curve with Gaia DR2". In: *The Gaia Universe*, p. 63. DOI: 10.5281/zenodo.3237518

- Alessandro Spagna et al. (Apr. 2019). "The thick disk rotation-metallicity correlation, comparison with Galactic cosmological simulations". In: *The Gaia Universe*, p. 38. DOI: 10.5281/zenodo.3059063

# *Acknowledgements*

I would like to start thanking the people who most helped me throughout my PhD in my daily routine and non-Academic life. My girlfriend, my parents and my sister were and are my first supporters and only (Space-)Time will tell how much important they are for me. Most of what I am and the goals I reach I owe to them. Thanks.

This PhD project has made use of data from the European Space Agency (ESA) mission *Gaia* (*ESA Web Portal*) and processed by the *Gaia* Data Processing and Analysis Consortium (DPAC, *Gaia DPAC*). Funding for the DPAC has been provided by national institutions, in particular the institutions participating in the *Gaia* Multilateral Agreement. Also data from the Two Micron All Sky Survey (2MASS; Skrutskie et al., 2006, www.ipac.caltech.edu/2mass) has been used.

The cosmological simulation considered for the project was carried out using ULISSE at SISSA and Marconi at CINECA, Italy (*CINECA Web Portal*, project IsB16DSKAGN, PI: G. Murante). The post-processing has been performed using the PICO HPC cluster at CINECA. The GADGET3 code was made available by Volker Springel.

I am indebted to the Italian Space Agency (ASI) for their continuing support through contract 2014-025-R.1.2015 and 2018-24-HH.0 to the National Institute for Astrophysics (INAF).

This research made use of python libraries scipy (Virtanen et al., 2020), corner (Foreman-Mackey, 2016), PyMC3 (Salvatier, Wiecki, and Fonnesbeck, 2016), and galpy (Bovy, 2015). I am are grateful to and acknowledge the work of anonymous referee and Assistant Editor whose valuable comments and suggestions improved the publications correlated to this work.

I acknowledge Marco Bruni, Ronald Drimmel, Eloisa Poggio for fruitful discussions on computational schemes and selection of stellar samples. Many thanks to Giuseppe Murante and Milena Valentini for making available to my research project the AqC4 simulation and their immense knowledge on numerical issues and cosmological framework. I would also greatly thank Paola Re Fiorentin, and Alessandro Spagna for their support during my PhD and for their fundamental help to learn how a good research should be compiled and published. Finally, I must thank my advisor, Mariateresa Crosta, and co-advisor, Mario G. Lattanzi, for their guide throughout this incredible, three-years long adventure. They let me and help me to understand what does Scientific Research mean and how much hard work hides behind

any publication, report or presentation. Together we faced many sceptical opinions but, in the end, the content of this thesis reveals that perseverance, coherence, hard work and genuine scientific interest can make the difference to obtain results and reach any goal.

In Science we trust!

# Contents

# List of Figures

# List of Tables

# List of Abbreviations

| | |
|---|---|
| **AqC4** | **Aq**uila-**C**-**4** (simulation) |
| **BG** | **B**alasin **G**rumiller (model or metric) |
| **CI** | **C**redible **I**nterval (for bayesian statistics) |
| **DM** | **D**ark **M**atter |
| **FRLW** | **F**riedmann-**L**emaître-**R**obertson-**W**alker metric |
| **Gaia DRx** | **Gaia D**ata **R**elease number **x** (x = 1,2,3 . . . ) |
| **GR** | **G**eneral **R**elativity |
| **GSE** | **G**aia-**S**ausage-**E**nceladus |
| **ΛCDM** | Λ (i.e. cosmological constant) **C**old **D**ark **M**atter |
| **MW** | **M**ilky **W**ay |
| **MWC** | **M**ilky **W**ay **C**lassic (model) |
| **NG** | **N**ewtonian **G**ravity |
| **RC** | **R**otation **C**urve |
| **SFH** | **S**tar **F**ormation **H**istory |
| **SFR** | **S**tar **F**ormation **R**ate |
| **SPH** | **S**moothed **P**article **H**ydrodynamic |
| **SSR** | **S**imulated **S**olar **R**ing |

# Physical Constants

| | | |
|---|---|---|
| Gravitational constant | G | $4.30091 \cdot 10^{-6}$ kpc $M_\odot$ km$^2$ s$^{-2}$ |
| Speed of Light | c | $2.99792458 \cdot 10^{8}$ m s$^{-1}$ (exact) |
| Solar Mass | $M_\odot$ | $2.99 \cdot 10^{30}$ kg |
| Milli-arcsecond | 1 mas | $10^{-3}$ arcsecond |
| Micro-arcsecond | 1 $\mu$as | $10^{-6}$ arcsecond |
| Parsec | 1 pc | $3.08568 \cdot 10^{16}$ m |

# Notations and units

| | | |
|---|---|---|
| $(X, Y, Z)$ | cartesian coordinates | kpc |
| $(V_X, V_Y, V_Z)$ | cartesian velocities | $\mathrm{km\,s^{-1}}$ |
| $r$ | spherical radius | kpc |
| $(R, Z)$ | cylindrical coordinates | kpc |
| $\phi$ | azimuthal angle in Galactocentric coordinates frame | rad |
| $(V_R, V_\phi, V_Z)$ | cylindrical velocities | $\mathrm{km\,s^{-1}}$ |
| $M$ | mass | $\mathrm{M_\odot}$ |
| $\mu$ | proper motion | $\mathrm{mas\ yr^{-1}}$ |
| $\sigma_V$ | velocity dispersion | $\mathrm{km\,s^{-1}}$ |

# Part I

# Introduction

# Chapter 1

# The context of Local Cosmology

What does it mean Local Cosmology? From the Greek *kósmos* (i.e. "world") and *-logia* (in the figurative sense, "study of"), the term cosmology refers to the studies of the origin and evolution of the Universe, from the beginning of spacetime with the Big Bang to today and on into the future. It concerns the scientific study of the largest-scale structures, as well as the laws that govern their formation and dynamics.

Since immemorial time, indeed, our ancestors have been observing the night sky and trying to make sense of the world around them in some "theoretical framework", but it is from the 20$^{th}$ century that cosmology raises as a modern science. In 1915, Albert Einstein published his theory of General Relativity and advanced that the Universe should be evolving; then in 1929, Edwin Hubble claimed that it was not only changing in time but actually expanding. In the same period, Harlow Shapley and Heber Curtis proposed two different models on the structure of our galaxy, the Milky Way, and their discussion led to the famous Great Debate in 1920. Again, in 1929, observations of the Andromeda "nebula" using the period-luminosity relation for Cepheids stars, now called the Leavitt Law (Leavitt and Pickering, 1912), confirmed unambiguously that our Milky Way is one among a large variety of galaxies in the observable universe with similar evolution process, as well as peculiar properties. The discovery in 1965 of the Cosmic Microwave Background, or CMB, showed that the Universe was hotter and denser in the past (Penzias and Wilson, 1965; Wright et al., 1992; Planck Collaboration et al., 2016).

By the 1970s, the Holy Grail of cosmology soon emerged: starting from a theory of gravity, defining a standard cosmological model to describe the origin of galaxies became one of the major research goals of astrophysicists. In this respect, the history of modern cosmology highlights a dichotomy, a contrast between the *whole* Universe and our relatively small *Local* corner, our Galaxy. On one hand, is our observable Universe all there is, homogeneous

and isotropic as implied by the Cosmological Principle? How the large scale structures could have been formed from the primordial density fluctuations in the Cosmic Microwave Background? On the other hand, is our Galaxy just a Local, atypical "bubble" which just happens to have the properties we can observe today or is it a typical cosmological product with which we can test and study cosmological models?

Indeed, the cosmological consequences of the evolution of the Universe "could manifest themselves as characteristic signatures in the main constituents of the Milky Way (i.e. halo, disc) or as small perturbations in the gravity in action within our Solar System" (Lattanzi, 2012). Then, many of the chemo-kinematic properties of the Milky Way and nearby galaxies relate to events that occurred a long time ago.

Therefore, the terminology *Local* associated with *Cosmology* gains its full meaning and importance in the wider and more global interest of modern astrophysics: the aim is to provide a link between the local scenario at redshift $z = 0$ and the distant Universe.

This new perspective highlights that the domain of *far-field*, concerning cosmic structures, CMB, galaxy clusters etc., and *near-field* cosmology, focused on the local Group, Galactic Archaeology, stellar and gas astrophysics, are no more separate research fields. From now on, the whole and the local studies of the Universe, the high-redshift and the low-redshift observations have converged in the Milky Way thanks to the tremendous improvements of astrometry given by space mission as Gaia (Gaia Collaboration et al., 2016) and of ground-based spectro-photometric surveys (e.g. Majewski et al., 2017; De Silva et al., 2015).

In particular, it is the few-micro-arcsecond ($\mu$as) accuracy achievable with Gaia measurements that allows astronomers to reach the kilo-parsec (kpc) scale and acquire detailed phase space coordinates for about one billion stars, within a sphere of 20 kpc of diameters (the "Gaia sphere"). This impressive result requires "a fully general-relativistic analysis of the inverse ray-tracing problem, from the observational data (e.g. stellar images on a digital detector) back to the positions of light-emitting stars" (Crosta et al., 2017). In this respect, cosmology becomes "local" not only because we are observing and studying a small portion of the Universe, but also from a relativistic point of view: due to the ever present and ever changing overlapping weak local gravitational field of the Solar System, the *local* Gaia-observer must be properly defined, and in this framework of modern Relativistic Astrometry, the

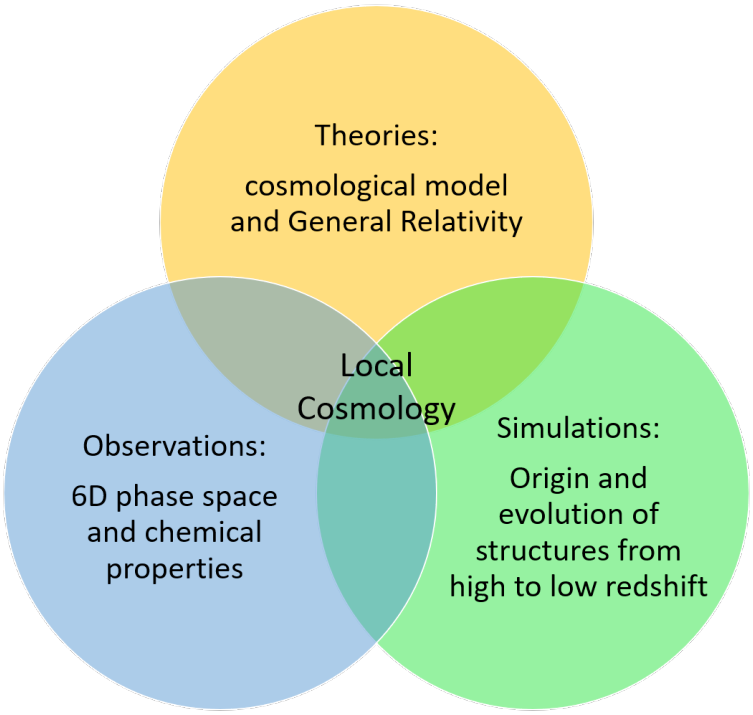


**Figure 1.1:** The fields of interest of Local Cosmology.

weak gravitational regime is playing a pivotal role for understanding gravity (Crosta, 2019, and references therein). Moreover, "once a relativistic model for the data reduction is in place, any subsequent scientific exploitation and investigation should be consistent with those prescriptions and, consequentially, fully compliant with the precepts of the standard theory of gravity adopted, i.e. the General Relativity" (Crosta et al. 2017; Crosta, Giammaria, Lattanzi, and Poggio 2020).

A last but not less important field of interest for Local Cosmology is the comparison between observations and high-resolution cosmological simulations that recently have produced quantitative predictions on the present-day structure of our Galaxy.

This is mandatory in order to create a coherent laboratory for Local Cosmology studies to perform extensive experimental tests on the Standard Cosmological Model, also called *Concordance model*: the ΛCDM.

## 1.1 The Concordance model

The Concordance model, as introduced before, is the state-of-the-art of modern cosmology, the culmination of almost all the investigations made in the last century on the physics of the Universe and structures

formation. This paradigm is based upon the Cosmological Principle within the framework of General Relativity (Bland-Hawthorn, Freeman, and Matteucci, 2014; Read, 2014; Bullock and Boylan-Kolchin, 2017). The former is the hypothesis that the Universe is spatially homogeneous and isotropic at least at large scales, and it is mathematically expressed with the Friedmann-Lemaître-Robertson-Walker (FLRW) metric, i.e.

$$ds^2 = c^2dt - a(t)^2\left[\frac{dr^2}{1-Kr^2} + r^2(d\theta^2 + sin^2\theta d\phi^2)\right] \tag{1.1}$$

that takes into account the expansion of the Universe. Here, spherical polar coordinates are used: $r$, $\theta$ and $\phi$ are the comoving coordinates[1] ($r$ is by convention dimensionless); $t$ is the proper time; $a(t)$ is a function to be determined which has the dimensions of a length and is called the cosmic scale factor or the expansion parameter; the curvature parameter $K$ is a constant which can be scaled in such a way that it takes only the values +1, 0 or -1. The framework is the standard theory of gravity, expressed by the famous Einstein's field equation

$$G_{\mu\nu} = R_{\mu\nu} - \frac{1}{2}g_{\mu\nu}R\left(+\Lambda g_{\mu\nu}\right) = \frac{8\pi G}{c^4}T_{\mu\nu} \tag{1.2}$$

where $R_{\mu\nu}$ is the Ricci curvature tensor, $R$ is the scalar curvature, $g_{\mu\nu}$ is the metric tensor, $\Lambda$ is the cosmological constant[2], $G$ is Newton's gravitational constant, $c$ is the speed of light in vacuum, and $T_{\mu\nu}$ is the stress-energy tensor. According to this equation, gravity is the manifestation of the geometry of spacetime encapsulated in the metric tensor $g_{\mu\nu}$, and determined by the energy-mass distribution, i.e. the physical sources of the gravitational field $T_{\mu\nu}$.

In this respect, the Concordance model, or ΛCDM (expression that will be divulged just a little later) describes the expanding Universe that obeys to Cosmological Principle, and, within the framework of General Relativity, explains how primordial fluctuations grew in time to become the seeds of all structure formation (Liddle and Lyth, 2000). A graphical representation of this process is shown in Fig. 1.2.

[1] Comoving coordinates assign constant spatial coordinate values to observers who perceive the Universe as isotropic. Such observers are called "comoving" observers because they move along with the Hubble flow.

[2] To be precise, Einstein included a cosmological constant in 1917 (Einstein, 1917) to counterbalance the effects of gravity and achieve a static universe. If moved onto the right-hand side of the equation, the $\Lambda = 8\pi(G/c^2)\rho_{vac}$ becomes proportional to the intrinsic energy density of space, or vacuum energy, $\rho_{vac}$.

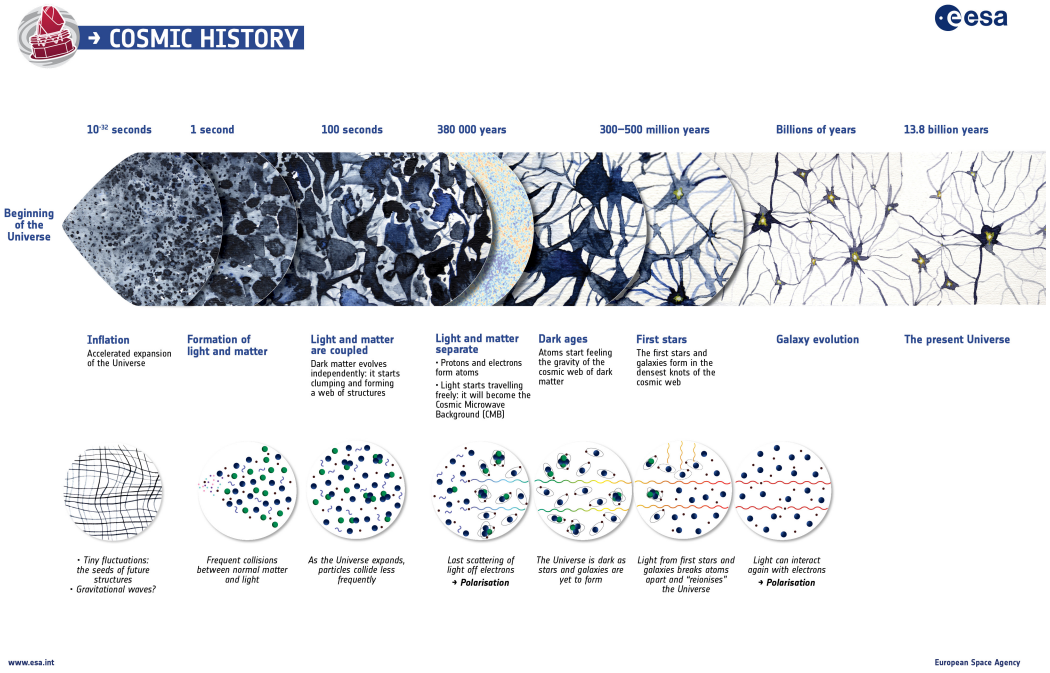


**Figure 1.2:** Graphic picture of the history of the Universe according to the Standard Model of Cosmology ΛCDM. Copyright: ESA

According to this model, the Universe should be dominated today by Dark Energy ($\Lambda$, $\sim$ 70 % of the total budget, Planck Collaboration et al., 2016), that produce an apparent accelerated expansion (Riess et al., 1998), and by Cold dark matter (CDM, $\sim$ 25 %), a collisionless, non-relativistic and non-baryonic fluid that is gravitationally dominant and determines the structures formation. Baryons contributes only for a $\sim$ 5 % to the energy density (Planck Collaboration et al., 2016; Guo et al., 2016).

### 1.1.1 Galactic formation scenario

In this context, the Concordance model predicts that structures in the Universe form hierarchically, driven by the gravitational forces of the large-scale distribution of Cold dark matter (see Fig. 1.2).

Starting from sub-galactic scales, via mergers, larger and large systems such as our Galaxy growth. Fig. 1.3 provides a good exemplification of this process. At early times mergers were more frequent because of the higher density of the Universe, and depending on the accretion history and the mass ratio between the main galaxy and the accreted satellite, such events could lead to the formation of all the great variety of galactic morphologies, as well as the internal substructures of these galaxies.

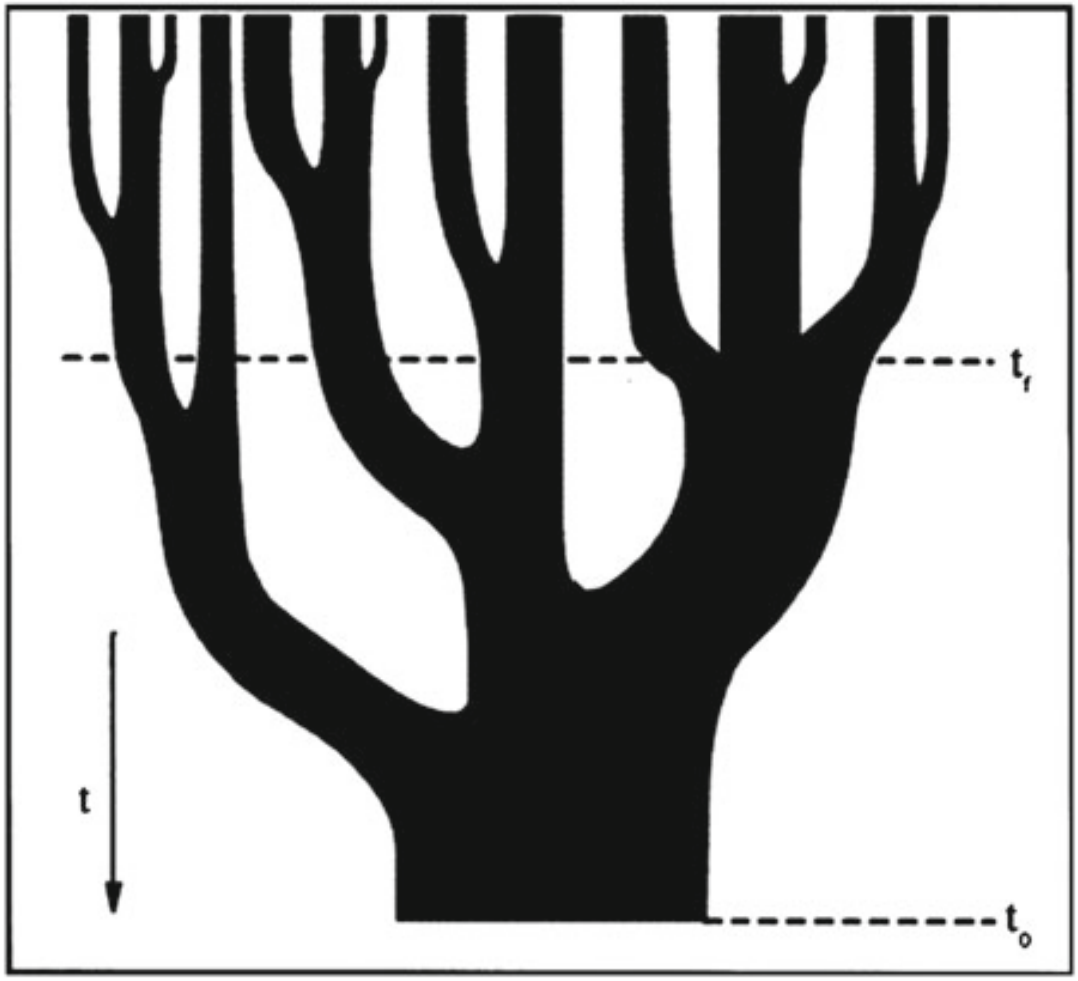


**Figure 1.3:** Schematic representation of a merger tree showing the growth of dark matter halos in time. Time increases from top to bottom, and the widths of branches are proportional to the masses of the progenitor halo. Credits: Lacey and Cole (1993).

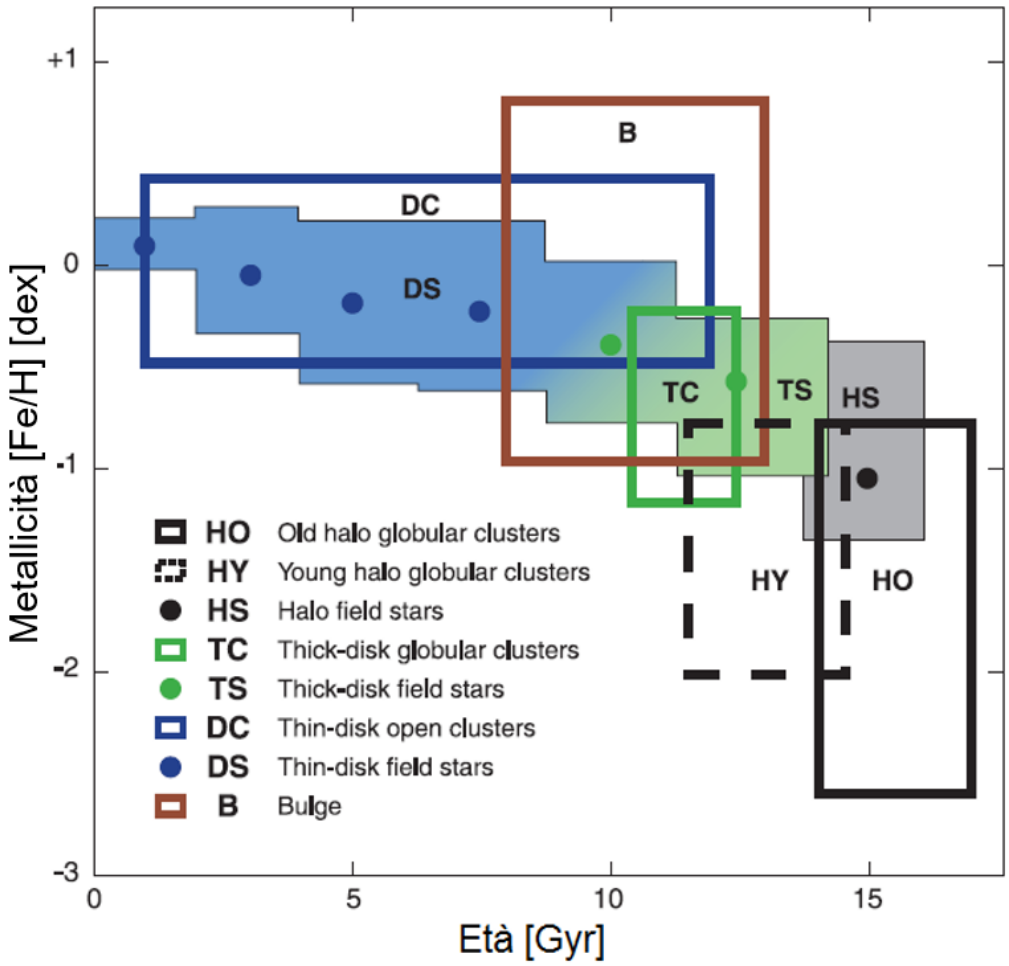


**Figure 1.4:** The age-metallicity relation of the Galaxy for the different components. Credits: Buser (2000).

This is also the case of our Galaxy: the mergers that the Milky Way experienced should have left "fossil" (i.e. long-lived) signatures that can be inferred from the observation today of the stellar populations in the Galactic bulge, disc, and halo and their peculiar chemo-kinematic properties as shown in Fig. 1.4 with the age-metallicity relation. Another case study is, for example, the investigation of co-moving groups of stars: these stars, stripped by the Milky Way from a merging satellite, continue to follow similar trajectories as their progenitor system and should define streams that crisscross the whole Galaxy and let us reconstruct the accretion history of the Galactic halo (Helmi et al., 2018; Re Fiorentin et al., 2015, and references therein). Another particularly useful way to track Galactic history is through precise measurements of stellar ages in order to date the sequence of events that led to the formation of the different components. However obtaining precise ages for very old stars is very difficult.

On the other hand, "with the advent of cosmological hydrodynamical zoom-in simulations of Milky Way-like galaxies, we are able to analyse in details the complex interplay of physical processes (e.g. dynamics of collisionless systems, gas flows, radiative cooling and heating, star formation, stellar nucleosynthesis, . . . ) that generated our Galaxy, which represents the Rosetta stone of galaxy evolution" (Giammaria et al., 2021). To the interested reader, the review by Helmi (2020) describes extensivelly the early accretion history of the Milky Way, while Buck et al. (2019) and Grand et al. (2020) discuss in details on the chemical and dynamical properties of the Galaxy, respectively.

Today, thanks to all of these parallel and complementary studies the definition "Galactic archaeology", namely the branch of Galactic studies that investigate the formation and history of the Milky Way and its stellar populations, has been adopted widely by the community, and it begins to appear more frequently both in talks as in the literature (see for example the very influential reviews Freeman and Bland-Hawthorn, 2002; Bland-Hawthorn, Freeman, and Matteucci, 2014, who introduced the term "near-field cosmology"). The idea behind is to use the properties of long-lived stars to reconstruct the history much in the same way archaeologists use artifacts or "rubble", to learn about the past.

This is again the context of Local Cosmology that, guided by theory and observation, could test the main aspects of the cosmological models directly from the perspective of the Milky Way.

## 1.2 Solutions and open questions

There are several observations that supports the ΛCDM model at different scales that range from the cosmic horizon ($\sim$ 15 000 Mpc Planck Collaboration et al., 2016; Slosar et al., 2013; Riess et al., 1998; Riess et al., 2016) to the typical distance that separate galaxies ($\sim$ 1 Mpc Zwicky, 1933; Croft et al., 2002; Markevitch et al., 2004; Clowe et al., 2006) to Galactic scale (order of $\sim$ 100 kpc and lower Rubin, Ford, and Thonnard, 1980; Eilers et al., 2019; Crosta et al., 2020).

Nevertheless, despite many attempts to explain their physical nature, at least 95% of the fundamental ingredients that compose the Universe, i.e. the dark matter and the Dark Energy, are still unknown. Therefore, the validity of the Concordance model is still a matter of debate among the cosmology and astrophysics community. In the following, the discussion will be mainly

focused on the first one of this two undisclosed elements because, within the context of the Concordance model and Local Cosmology, dark matter plays a key role in the cosmic structures formation and galaxies evolution, included the Milky Way.

### 1.2.1 In the dark mirror

Historically, the dark matter paradigm was for a long time termed the "missing matter" problem. This is because the astrophysicists are not completely sure where to find the solution: is it a new kind of fundamental particle beyond the Standard Model of nuclear physics? Or the standard theory of gravity, General Relativity, is wrong and need to be modified (e.g. MOdified Newtonian Dynamics, $f(R)$ gravity and scalar-tensor theories, etc.)? Or the approximations such as low speed and weak-field limits we are considering are no more valid for the accuracy of new data?

Almost all information on celestial bodies and the Universe comes to us via photons, and the majority of objects are observed because they emit light. Despite the great efforts made in identifying dark matter, we have only indirect observations that may suggest the presence of an "invisible" component which manifests itself only by gravitational interaction.

The strength of the dark matter hypothesis as a solution to the dynamics and evolution of the Universe lies in the fact that solve a lot of problems in a very large range of scales, from galactic dynamics to cosmic scale structures, in a simple way with a few *ad hoc* considerations on the possible nature of its constituent particles (e.g. non-relativistic, weakly interactive). Currently, no other scenario seems to have the same robustness describing coherently the Universe, however there are several problems within this context that in some cases appear to be totally inconsistent and unsolvable. Some of these issues are reported in the following.

### 1.2.2 $\Lambda$CDM at cosmological scales

The most important observation that supports the Concordance model and suggests the presence of dark matter comes from the earliest times of the cosmic evolution, when the Universe was very young, dense and hot. In 2016, the Planck Collaboration released the full mission results of the CMB measurements (Planck Collaboration et al., 2016). The fitted power spectrum,

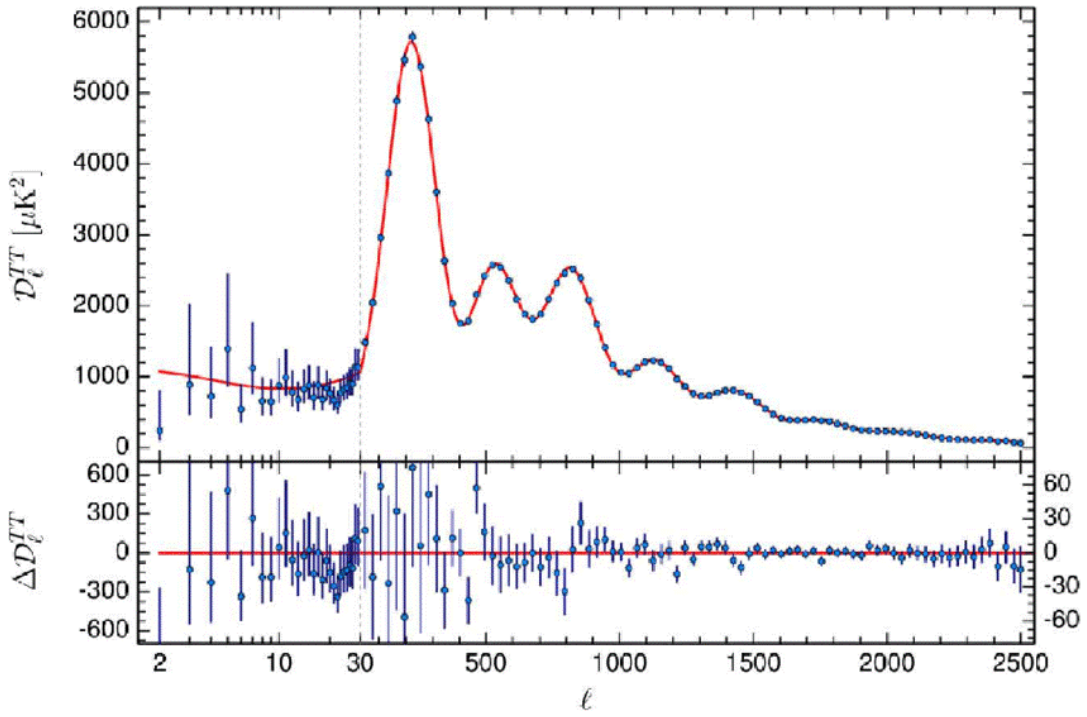


**Figure 1.5:** From Planck Collaboration et al. (2016): the best-fit prediction of ΛCDM theoretical spectrum fitted to the Planck likelihood in the upper panel; residuals with respect to this model are shown in the lower panel. The error bars show $\pm 1\sigma$ uncertainties.

shown in Fig. 1.5, suggests the actual composition of the Universe, its geometry that should be almost flat, and also that the most suitable candidates for the dark matter are non-baryonic particles.

Although these results are probably the most important evidence of the ΛCDM scenario, several aspects are still matter of debate among the scientific community, and many predictions on the evolution of the Universe are strongly model-dependent and based on the nature and physics of dark matter particles.

It is the case of the so-called $H_0$-tension: using the Planck observation of the CMB power spectrum, the predicted value of the Hubble constant results $66.93 \pm 0.62$ km s$^{-1}$ Mpc$^{-1}$ (Planck Collaboration et al., 2016), while the local measurement based on the method of distance ladder gives a result of $H_0 = 73.00 \pm 1.75$ km s$^{-1}$ Mpc$^{-1}$ (Riess et al., 2016), which is $3.3\sigma$ higher than the Planck Collaboration estimate. The $H_0$-tension between these two results has attracted lots of attention of cosmologists because both the distance ladder measurement and the CMB fitting have reduced the uncertainty to 2.4% and less than 1% precision, respectively. Thus, they are in significant - more than $3\sigma$ - tension.

### 1.2.3 Galaxy clusters and gravitational lensing

The CMB measurements seem to be in accordance with the mass discrepancy between baryonic and dark matter that is found in cosmic structures.

Indeed, it is frequently possible to study the matter distribution describing the distribution of light that we observe with telescopes (with some considerations on the emission of photons by the different astrophysical sources and studying the spectra at all wavelengths) and determining the mass-to-luminosity ratio $M/L$. However, the mass can be also determined by measuring the motions of the sources and their kinematical properties. Taking into account the hypothesis of low speed and weak field regime, and comparing the direct dynamical mass with the derived luminous mass estimates, in many cases we can observe a discrepancy between the two distributions: if Newtonian mechanics gives a useful approximation to the dynamics of the systems considered, there should be more matter than the visible one, hence the definition of "dark" matter.

In this context, clusters of galaxies are the largest virialized systems in the Universe and seem to be dominated by this unknown source of gravity. One of the most interesting and most direct hint about the nature of the dark matter is given by the distribution of matter in the Bullet Cluster 1E0657-56 (Clowe, Gonzalez, and Markevitch, 2004; Markevitch et al., 2002; Markevitch et al., 2004), consisting of two colliding clusters of galaxies. In Fig. 1.6 a comparison of this cluster in visible light and X-ray gas emission is shown.

According to ΛCDM, during a merger, the gas motion is impeded by pressure forces since the gas is a collisional fluid (X-ray observations), while the galaxies, observable in visible light, behave as a nearly collisionless fluid. Gravitational lensing allows mapping the matter belonging to the cluster, which seems to be dark matter for the most part. Historically, weak-lensing observations are one of the most significant demonstrations of General Relativity, and in the case of the Bullet Cluster, they demonstrate that the gas does not contribute to the missing matter problem.

Nowadays, the accuracy of the measurements reaches a level at which Newtonian regime might not be sufficient anymore. This is the case of Gaia (Gaia Collaboration et al., 2016) and its data reduction pipeline which considers a fully relativistic inverse ray-tracing methodology in accordance with the local geometrical environment affecting light propagation itself and at the observer's gravitational location, i.e., a correct application of the precepts of the theory of measurement in General Relativity (Crosta, 2019, and references therein). Such corrections are due to the gravitational sources of Solar System

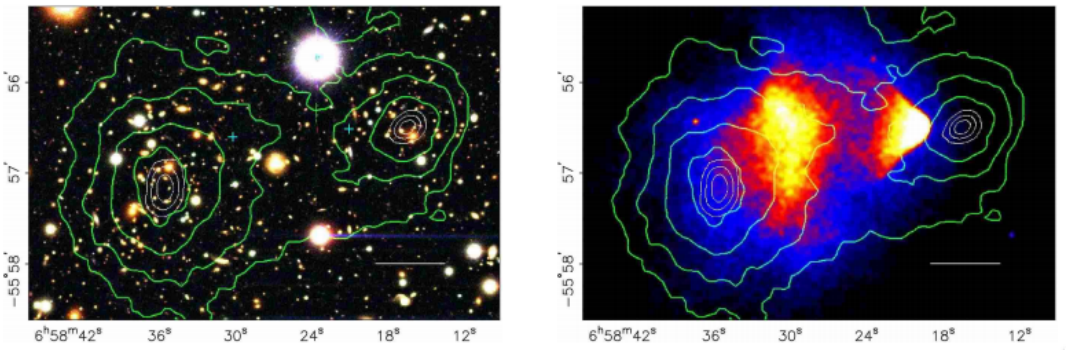


**Figure 1.6:** Images of the merging *bullet* cluster 1E0657-558 (Clowe et al., 2006). The left panel shows a direct image of the cluster obtained with the 6.5-m Magellan telescope in the Las Campanas Observatory, the right panel is a X-ray satellite Chandra image of the cluster. Shock waves of the gas are visible, the gas of the smaller bullet cluster (right) lags behind the cluster galaxies. In both panels green contours are iso-density levels of the gravitational potential of the cluster, found using weak gravitational lensing of distant galaxies. The white bar has 200 kpc/h length at the distance of the cluster. Note that contours of the gravitational potential coincide with the location of visible galaxies, but not with the location of the X-ray gas (the dominant baryonic component of clusters).

bodies and fundamental at the micro-arcsecond level of accuracy (i.e. Earth, Jupiter which effects are of the order of tens $\mu as$, see Crosta and Mignard, 2006, and Fig. 1.7).

Another possible evidence from clusters comes from the redshifts measurements of individual galaxies. This method of analysis was implemented by Fritz Zwicky (Zwicky, 1933) who found that the velocity dispersion of galaxies in the Coma cluster was much greater than expected for a virialized, isolated cluster composed by only the luminous matter. The only way to hold the cluster from rapid expansion is to assume that it contains huge quantities of some "invisible" matter that exceeds the total mass of galaxies at least tenfold.

### 1.2.4 Small-scale problems in cosmological simulations

Also the hierarchical model of galaxies formation show some cracks linked to the Concordance model on galactic and sub-galactic scales, especially in cosmological N-body simulations.

The most relevant challenges are:

- the missing satellites problem (Klypin et al., 1999; Klypin et al., 2015): with respect to Milky Way observations, in simulations there are too

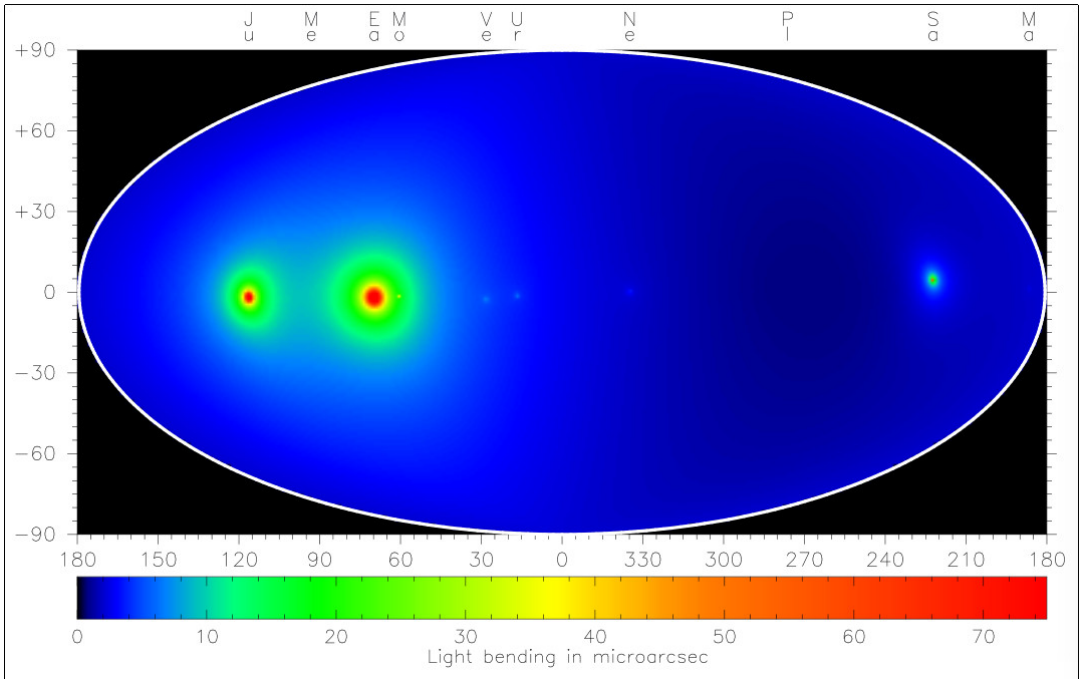


**Figure 1.7:** All-sky map (in ecliptic coordinates, for an L2-based observer) displaying the total amount of post-Newtonian light deflection due to all planets, and the Moon, at 25 May 2014 (two-letter object-name abbreviations appear above the top axis). The Sun has been suppressed because of its immense contribution, extending all over the sky, compared to the other bodies. The colour coding has been chosen such that significant light bending is predicted in all regions of the sky coloured different from blue. Copyright: ESA - Jos de Bruijne.

many sub-halos and dwarf galaxies orbit the central disc galaxies;

- the cusp-core problem (de Blok and McGaugh, 1997; de Blok, 2010): the inner dark matter density profile of low surface brightness and dwarf galaxies seems to be more cored than the cuspy inner region predicted by ΛCDM model. In other words, the model prediction appears to disagree with observations, because dwarf galaxies require a shallower dark matter density profile in their central regions (Carignan and Freeman, 1988; Carignan and Beaulieu, 1989);

- the too-big-to-fail problem (Boylan-Kolchin, Bullock, and Kaplinghat, 2011; Papastergis et al., 2015; Kaplinghat, Valli, and Yu, 2019): observations of dwarf galaxies suggest a deficit of dark matter in the inner region with respect to simulations;

- the diversity problem (Oman et al., 2015): the large variety of shapes of galactic rotation curves;

Most of these problems have been found in dark matter-only simulations, which do not take into account the complex baryonic physics that must be properly modelled. For instance, the energy and mass feedback from supernovae into galactic and extra-galactic medium can modify the inner core profile of galaxies. These small-scale problems have therefore generated significant interest in the exploration of alternative scenarios. For an extensive review see de Martino et al. (2020).

### 1.2.5 Internal galactic dynamics

At galactic scales and inside the Milky Way, the presence of dark matter is of special interest for the internal dynamics of the Galactic disc and in particular the interpretation of rotation curves, namely the graph of circular velocities of stars and gas as a function of their distance from the galactic centre (e.g. Rubin, Ford, and Thonnard, 1980; van Albada and Sancisi, 1986; Balasin and Grumiller, 2008; Iocco, Pato, and Bertone, 2015; Sofue, 2020, and references therein).

Indeed, studying the stellar motions we can determine (according to Newtonian weak-field approximation) the distribution of the mass solving the system between the differential equation $V^2(R) = R(\partial\Phi/\partial R)$ and the Poisson's equation $\nabla^2\Phi = 4\pi G\rho$. On the other hand, from photometric data we can extrapolate the distribution of light, an indirect measurement of baryonic mass distribution. The non-Keplerian trends observed in the external

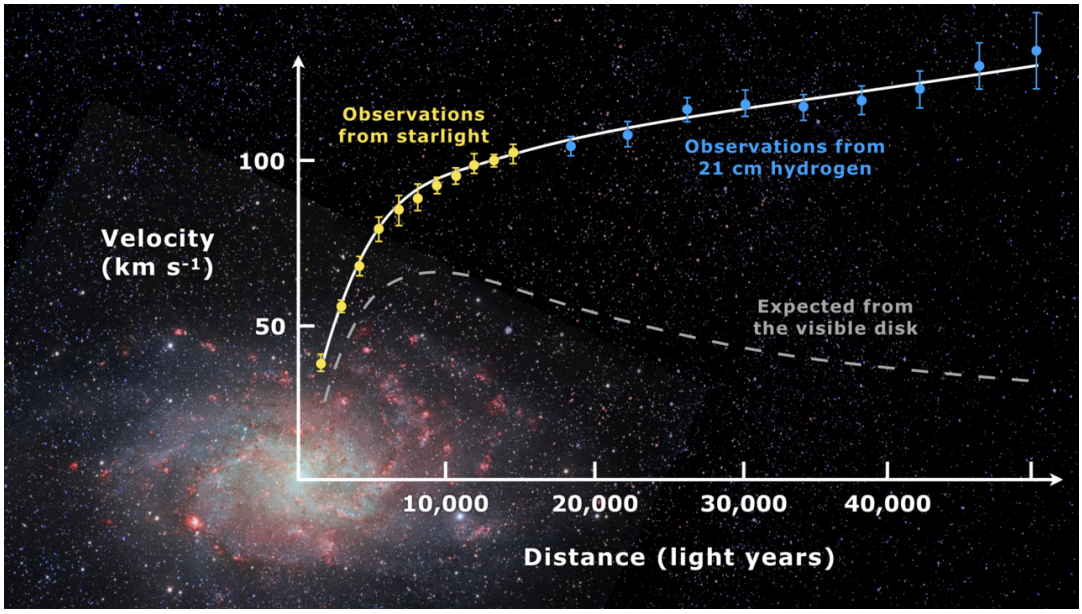


**Figure 1.8:** Rotation curve of spiral galaxy (yellow and blue points with error bars), and a predicted one from distribution of the visible matter (gray line). The discrepancy between the two curves can be accounted for by adding a dark matter halo surrounding the galaxy (Corbelli and Salucci, 2000).

region of disc-like galaxies contradict the simple Newtonian prediction (see Fig. 1.8): in the peripheral region the luminosity of a galaxy drops rather rapidly, thus the expected circular velocity should decrease. In contrast, the rotation speeds of galaxies are almost constant, which can lead to very high local values of mass-to-luminosity ratio $M/L > 200$. This discrepancy is usually interpreted in favour of the presence of the dark matter, that is distributed in large spheroidal volumes according to a density profile that describes the so-called dark halo. The most utilized profiles are the Navarro-Frenk-White (NFWp, Navarro, Frenk, and White, 1996) and the Einasto profile (Ep, Einasto, 1965).

Nevertheless, there are still uncertainties associated with the local density because rotation curves measure the total mass within an orbit, thus the density distributions of the galactic bulge and disc are needed to accurately calculate the eventual dark matter profile. Recently, the data from Gaia DR2 has certainly helped in the characterization of Galactic baryonic structures (determining properties such as radial and vertical scale lengths of the disc, kinematic models and chemical composition) and in the discrimination of theoretical models and profiles (e.g. Eilers et al., 2019; Karukes et al., 2019; de Salas et al., 2019a; Nitschai, Cappellari, and Neumayer, 2020; Crosta et al., 2020, and references therein). This is part of the main topics of this thesis and it is deeply discussed in Chapters 6 and 7.

Another possible analysis is focused on the vertical velocity dispersion of the local stars in the Milky Way disc. The first astronomers who investigated the density due to all stars near the Galactic plane were Jacobus Kapteyn and James Jeans in 1922. Kapteyn (1922) found that the spatial density of known stars is sufficient to explain the vertical motions. In contrast, Jeans (1915) results indicated "the presence of two dark stars to each bright star". The equation used by Jeans can be derived from moments of the collisionless Boltzmann equation in cylindrical coordinates for a steady, axisymmetric stellar tracer component $i$ with density $\rho_i(R, Z)$ (Binney and Tremaine, 2011, Eq. 4.222b, p. 353). For a steady-state potential ($V_k$ = 0 for k = R, Z, i.e. no net flux of stars in R or Z), one obtains

$$\frac{\partial}{\partial Z}\left(\rho_i \sigma^i_{ZZ}\right) + \frac{1}{R}\frac{\partial}{\partial R}\left(R\rho_i \sigma^i_{RZ}\right) - \rho_i g_Z = 0. \tag{1.3}$$

where $\rho_i$ is the density of $i$ sample, $\sigma^i$ is its velocity dispersion component $ZZ$ or $RZ$ and $g_Z$ is the vertical acceleration.

This is an exact description of the connection between the local vertical gravity and the local stellar velocity dispersion within the Newtonian weak-field approximation used to estimate the dark matter density in the Solar neighbourhood. However, the estimates are still poorly constrained, and even recent measurements are compatible within $1\sigma$ with both a null local density (e.g. Moni Bidin et al., 2015) and with a value as high as 37 $M_\odot pc^{-3}$ (Garbari et al., 2012) or 18 $M_\odot pc^{-3}$ (Hagen and Helmi, 2018).

As for the previous rotation curve techniques, local dark matter density estimates from vertical velocity dispersion are affected by different systematic uncertainties. These include uncertainties on baryonic density surface, which depend on the gas mass density with a typical error of about 50%, and the local stellar density although these are typically determined with 10% accuracy or better. Furthermore, the presence of multiple populations and assumptions on their distributions may also affect the conclusions reached.

In their paper, Moni Bidin et al. (2015) report that the calculation of the mass surface density $\Sigma(Z)$ within $\pm$ Z kpc of the Galactic plane by means of the integrated Poisson equation in cylindrical coordinates depends critically on the mass density distribution assumed in the modeling of the Galactic disc. In this way, answering to the critics moved by Bovy and Tremaine (2012), they confirmed their previous result on the mass surface density at the Solar Galactocentric position between 1.5 and 4 kpc from the Galactic plane (Moni Bidin et al., 2012): the local dark matter density they estimated, extrapolating the observed curve of $\Sigma(Z)$, is $\rho_{DM} = 0 \pm 1$ $M_\odot pc^{-3}$ (Fig. 8. of

Moni Bidin et al., 2015).

In recent years, the improvement in quality of the measurements was terrific, and, as already said, the Gaia mission provided kinematics information with unprecedented accuracy. Moreover, reporting Hagen and Helmi (2018) words: "The power of these data increases even further when combined with spectroscopic surveys such as the Radial Velocity Experiment (RAVE), the Apache Point Observatory Galactic Evolution Experiment (APOGEE) and the Large Sky Area Multi-Object Fiber Spectroscopic Telescope (LAMOST), as this provides knowledge of the full phase-space distribution of stars near the Sun [...]".

In 2018, Hagen and Helmi (2018) used TGAS and RAVE data to derive an estimate of the local dark matter density and explore the impact of uncertainties in (some of) the characteristic parameters of the Galactic thin and thick discs. They selected red clump stars' sample and followed a similar procedure as Moni Bidin et al. (2015) and Bovy and Tremaine (2012), determining the vertical force, and found $K_z^{thin} = -2454 \pm 619$ km$^2$ s$^{-2}$ kpc$^{-1}$ and $K_z^{thick} = -2141 \pm 774$ km$^2$ s$^{-2}$ kpc$^{-1}$ at 1.5 kpc away from the Galactic plane for the thin and thick disc samples and for thin and thick disc scale heights of 0.28 kpc and 1.12 kpc, respectively. These measurements can be translated into a local dark matter density $\rho_{DM} = 0.018 \pm 0.002$ M$_\odot$ pc$^{-3}$. The results consider only the internal errors on the dark matter density, as the authors said they do not account for the large systematic uncertainties in the stellar disc parameters (especially the scale heights), the thick-to-thin disc density ratio, the scale lengths of the discs, and the ISM mass. These "extra" sources of uncertainty can lead to a large systematic error on the dark matter density near the Sun, also compatible with $\rho_{DM} \sim 0$ M$_\odot$ pc$^{-3}$ in the Solar Neighbourhood.

### 1.2.6 Direct search for dark matter particles

The determination of the Local dark matter density from the Milky Way rotation curve and the vertical velocity dispersion is a topic of great interest among the community of astrophysicists and astroparticle physicists because it implies important constraints on the lower limit of dark matter particles mass and on the possibility to detect such particles.

Direct searches, for example, look for a scattering process where a dark matter particle in the Milky Way halo interacts with an atomic nucleus of a

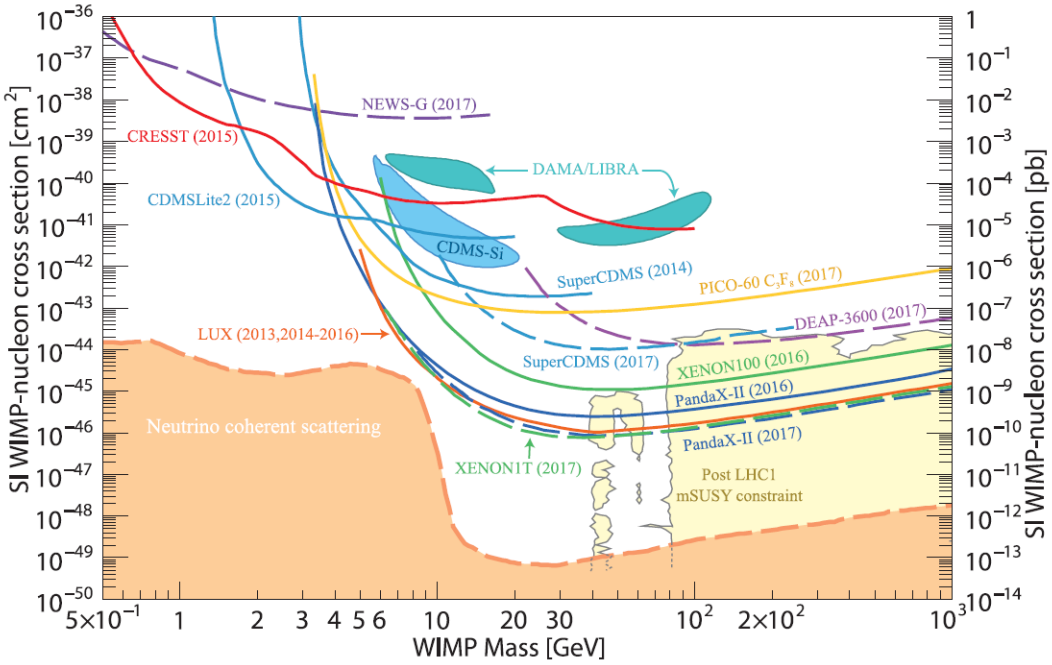


**Figure 1.9:** Upper limits on the spin-independent (SI) elastic DM-nucleon cross-section as a function of mass of the dark matter particle. The figure is reproduced from Tanabashi et al. (2018).

detector whose recoil generates a detectable release of energy. Experiment of this kind is, for example, XENON 1T (Aprile et al., 2011).

Indirect detections of dark matter particles such as WIMPs, one of the possible candidate for dark matter particle, include searches for neutrinos arising from the annihilation in the centre of the Earth or the Sun (see IceCube or Super-K Baur, 2019; Choi et al., 2015), or that can enrich the cosmic rays background (Avrorin et al., 2015).

So far, no experiment has detected a final direct evidence of any dark matter particles. Only the DAMA/LIBRA experiment has been recording an annual fluctuation that might be explained with the detection of WIMP (Bernabei et al., 2014). This result still lacks robust confirmation, because the signal is only consistent with values that are within the regions of the WIMP cross-section-and-mass diagram (see Fig. 1.9) that appear to be excluded by other experiments. For a more recent reviews on dark matter issues the reader can refer to Bertone and Tait (2018), Tanabashi et al. (2018) and Amendola et al. (2018).

## 1.3 Alternatives to ΛCDM and extensions of General Relativity

All the observational clues of dark matter point to the existence of a kind of matter that: (i) it does not absorb or emit light, but it exerts and responds only to the gravity force; (ii) it enters the calculation as extra mass required to justify some deviation from the Newtonian mechanics predictions, i.e. the flat galactic rotational curves (Crosta, Giammaria, Lattanzi, and Poggio, 2020, and references therein).

Historically, the first try to explain the mass discrepancy in cosmic structures and galaxies was to MOdify the Newtonian Dynamics (MOND, Milgrom, 1983) rather than add dark matter. This proposal is based on the introduction of a purely phenomenological acceleration scale, $a_0 \simeq 1.2 \cdot 10^{-10}\mathrm{ms}^{-2}$ below which Newtonian gravity breaks down. The most important problem raises in the formulation of MOND in a covariant form, because, in General Relativity, the acceleration is expressed by a covariant equation and linked to the affine connection $\Gamma^{\mu\nu}_{\lambda}$. Recent models that explicitly attempt to reproduce the MOND phenomenology include, for example, refracted gravity (Cesare et al., 2020).

This latter attempt belongs to the class of alternative solutions aimed to avoid the "dark" components by varying the scalar curvature (or the Ricci scalar), and modify the geometric part of the Einstein equation, like $f(R)$ gravity (Buchdahl, 1970; Starobinsky, 1980; De Felice and Tsujikawa, 2010). Scalar-Vector-Tensor theory of gravity, also called MOdified Gravity or simply MOG extends the Einstein-Hilbert action of gravitational field to more actions (see e.g. Fujii and Maeda, 2003; Capozziello and de Laurentis, 2011).

Citing Crosta, Giammaria, Lattanzi, and Poggio (2020) for example: "Recently, the non-extensive q-statistics1 of the Boltzmann-Gibbs approach (Tsallis, 1988; Tsallis and Gonzalez Arenas, 2014) has been applied in astronomy to describe the velocity distribution function of self gravitating collisionless particles on galactic scales. The rotation curve flatness is considered in the context of Newtonian regime assuming a dark matter halo. Such a non-extensive distribution provides a way to describe dark matter cored haloes from first principles. For example, a set of polytropic, non-Gaussian, Lane-Emden spheres with the central value $q = 0.85$ yielded a successful fitting for all the observed rotation curves of some nearby spiral galaxies (Frigerio Martins, Lima, and Chimenti, 2015, and references therein)."

Most of these attempts are, however, based on peculiar or *ad hoc* physical

assumptions. The dynamics of galaxies is usually considered to be dominated by the Newtonian regime (e.g. solving Poisson's equation in order to derive, for instance, the circular velocity tracing the observed rotation curve) and general relativistic effects are included as corrections.

The weak relativistic regime of Einstein's equation for the dynamics of galaxies has been explored by only a few authors (Cooperstock and Tieu, 2007; Balasin and Grumiller, 2008). These authors formulated models to describe the dynamics of a galactic disc beyond the Newtonian limit, or the spherical mass distribution, considering that the small curvature limit of General Relativity may not coincide with the Newtonian regime, as it is the case of the Lense-Thirring effect (Lense and Thirring, 1918). de Almeida, Piattella, and Rodrigues (2016) compared both these models to fit the rotational curves of some external galaxies for the first time. The investigation of these kind of models are part of the work of this Thesis and is discussed in Chapters 6 and 7.

## 1.4 Motivation and outline of this thesis

It should be clearer at this point that now we are in the era of Local Cosmology: thanks to Gaia, the weak-gravity regime is playing a pivotal role in providing a complementary observational perspective for understanding gravity (Crosta, 2019). There is no doubt that current and future Gaia data releases and the important synergies with spectroscopic ground-based surveys such as APOGEE (Majewski et al., 2017) and GALAH (De Silva et al., 2015) will bring tremendous and fundamental contributions to the studies of Galactic Archaeology on one hand, and to the improvement of cosmological models on the other hand. Moreover, the importance of detailed comparison between high-resolution simulations and observations became mandatory.

Currently, General Relativity is the confirmed standard theory that explains gravity over a range of sixty orders of magnitude. We may certainly assert that the evolution of the Milky Way, and its constituents, is the product of the action of gravity. Nevertheless, the quest nowadays is to push on the use of General Relativity to detail a more complex structure of the Milky Way, pursuing a coherent general relativistic phase-space picture of the Galaxy, our laboratory for Local Cosmology (Crosta, 2019, and references therein), as reconstructed by Gaia.

The main motivations of this thesis are based on two simple but at the same time fundamental points:

1. As stellar astrophysics is based on the Sun, in the era of Local Cosmology the Milky Way is become the keystone for spiral disc-like galaxies and so for cosmology. In other words, the Sun : stars = the Milky Way : spiral galaxies;

2. As General Relativity is required for the data processing and analysis of the Gaia mission, we should apply the precepts of such theory at least at the same order of accuracy for consistency.

In this respect, Gaia represents the perfect conjunction of these two aims: with its second data release, on the one hand we can put several observational constraints on the structure and evolution history of disc-like galaxies. On the other hand, we can trace for the first time the rotation curve of the Galaxy at large radii from its center to evaluate to what extent the Newtonian approximation of Einstein's field equation should be the only one considered in describing the Galactic dynamics.

A General Relativistic picture of the Milky Way can ensure a robust and coherent Local Cosmology Laboratory against which any model of the Galaxy, at first, and then of cosmology can be tested.

## Outline of the thesis

The present introductory Chapter (Part I, Chapter 1) about Local Cosmology and the Concordance model is followed by a brief description of the status and timeline of the Gaia mission, the main concepts of relativistic astrometry (Part II, Chapter 2) and an extensive survey of the Milky Way as seen by Gaia DR2 (Chapter 3. Then, the state-of-the-art of classic (i.e. non-relativistic), N-body simulations is presented with a detailed description of the AqC4 framework, a high-resolution cosmological simulation of a Milky Way-like galaxy (Part III, Chapter 4 and followed by the analysis of such simulation (Chapter 5). The aim is to investigate and disentangle the complex scenario of formation and evolution of our Galaxy, interpreted as a typical cosmological product according to Local Cosmology, and to the first purpose of this thesis. The results here discussed were published in Giammaria et al. (2021). Next, thanks to the exquisite quality of the recently available Gaia DR2 data, a first test of Local Cosmology is discussed in order to push on the use of

General Relativity (Part IV, Chapter 6 and 7): the relativistic kinematics delivered by Gaia is applied to describe the flatness of the Galactic rotation curve at large radii from its center. A classic model that includes a dark matter halo, and a relativistic one based on the full set of Einstein's field equation in the weak field regime and on the representation of the Galactic disc as a relativistic dust, are considered for the analysis that was published in Crosta, Giammaria, Lattanzi, and Poggio (2020). Finally, conclusion remarks and the outline of the future perspectives are summarized (Part V, Chapter 8).

# Part II

# Gaia's Milky Way: the Laboratory of Local Cosmology

# Chapter 2

# Gaia: the billion-star surveyor

Gaia is a cornerstone mission in the science program of the European Space Agency (ESA), an authentic revolution for modern astronomy and, in particular, for Local Cosmology. Indeed, it is the first astrometric mission of this century aimed to map the entire sky down to the visual magnitude $G = 20$ mag, performing with the micro-arcsecond-level astrometry and milli-magnitude-level photometry the deepest and most complete census of our Galaxy (Gaia Collaboration et al., 2016).

It was successfully launched on 19$^{\text{th}}$ December 2013 from the European base of Kourou in French Guyana, and since July 2014 it has been continuously scanning the sky from its vantage position close to the second Lagrange point of the Sun-Earth gravitational system. The Second Data Release (Gaia DR2 Gaia Collaboration et al., 2018b), the first sample of what would be the end-of-mission data set, was released on 25$^{\text{th}}$ April 2018 and is available through the Gaia Archive (*Gaia Archive*). Table 2.1 lists the expected resulting data set at the end of the mission. Currently, an extension until the end of 2020 has been approved and an indicative approval until the end of 2022 has been given. For more than one billion stars, Gaia will collect the five astrometric parameters (right ascension $\alpha$, declination $\delta$, proper motions $\mu_\alpha$ and $\mu_\delta$, and parallax $\varpi$) and photometry in the visual band (i.e. in particular, Gaia will provide the mean $G$ magnitude and the magnitudes $G_{RP}$ and $G_{BP}$ in the red and blue passbands). The complete 6D phase-space, including the radial velocity $RV$ along the line-of-sight, will be produced for $\sim$ 150 million bright objects, and combined with their detailed astrophysical classification and characterisation obtained from the photometry and spectroscopy. The astronomical objects will be observed 70 – 80 times on average, leading a total of more than 150 billion measurements.

In terms of the numbers of objects observed and of measurements accuracy, Gaia is a huge advance on its predecessor, Hipparcos (The HIPPARCOS and TYCHO catalogues; Perryman et al., 1997). Exploiting the same scanning

**Table 2.1:** Expected end-of-mission Gaia performances in comparison to those of Hipparcos (*ESA Web Portal*).

| | Hipparcos | Gaia (end-of-mission) |
|---|---|---|
| Magnitude limit<br>Completeness<br>Bright limit | 12 mag<br>7.3 – 9.0 mag<br>0 mag | 21 mag<br>20 mag<br>3 mag |
| Objects | 120 000 | 47 million to $G = 15$ mag<br>360 million to $G = 18$ mag<br>1 192 million to $G = 20$ mag |
| Distance limit<br>Quasars<br>Galaxies | 1 kpc<br>1 (3C 273)<br>None | 50 kpc<br>500 000<br>1 000 000 |
| Accuracy | 1 milliarcsec | 7 $\mu$arcsec at $G = 10$ mag<br>26 $\mu$arcsec at $G = 15$ mag<br>600 $\mu$arcsec at $G = 20$ mag |
| Photometry<br>Radial Velocity<br>RV mean error<br>Observing | 2-colour (B and V)<br>None<br>–<br>Pre-selected | Low-res. spectra to $G = 20$ mag<br>150 millions objects<br>15 km s$^{-1}$ to $G_{RVS} = 16$ mag<br>Complete and unbiased |

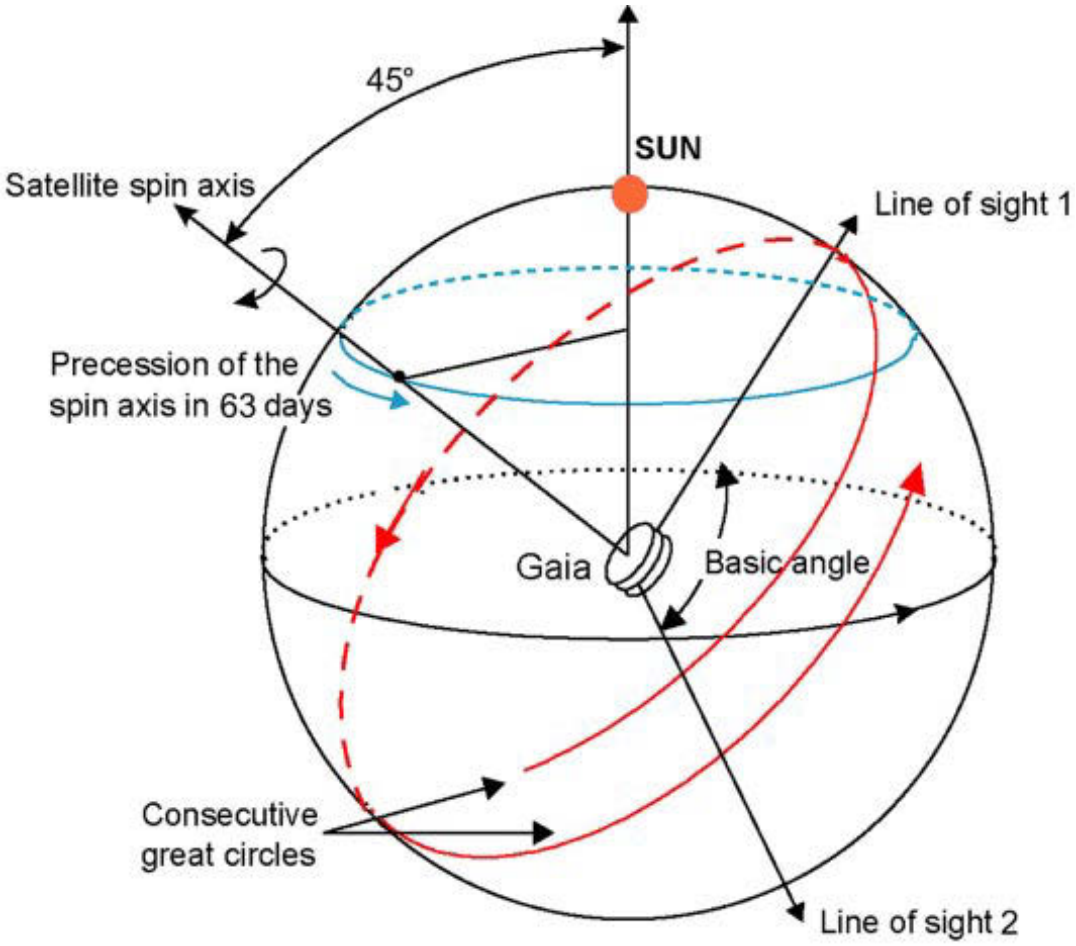


**Figure 2.1:** Gaia scanning law. Credit: ESA.

strategy as Hipparcos (Fig. 2.1), the astrometric accuracies will be extended by 2 – 3 orders of magnitudes and the completeness magnitude limit will be pushed from $\sim$ 7–9 mag to 20 mag. Thanks to the on-board object detection, variable stars, supernovae, burst sources, micro-lensed events, and minor planets will all be detected and catalogued to this faint limit. Further details on the expected performance in *ESA Web Portal* and in Lattanzi (2012), Spagna et al. (2016), and Crosta (2019).

To perform its unique census of stars in the Galaxy, Gaia is using two identical, three-mirror anastigmatic (TMA) telescopes, with apertures of 1.45 m x 0.50 m pointing in directions separated by the basic angle ($\theta = 106.5^{\circ}$). With a scan rate of 60 arcsec $s^{-1}$, equivalent to a 6-hour rotation period, the two telescopes trace great circles on the sky and collect the light to feed the common focal plane. This is a mosaic of 106 CCDs divided into three on-board instruments for astrometry, photometry and spectroscopy. The detection is triggered by the passage of an object through the field of view of the telescopes and the astrometric instruments determine the position of stars and other astronomical sources to unprecedented precision; then from these positions, stellar parallaxes and proper motions are derived. The photometric instrument measures the brightness of all the stars in the Gaia G-band, using a bandpass that covers the visible portion of the spectrum, between 330 and 1050 nm. This band was chosen to optimise the collection of starlight, which in turn maximises the precision of the measurements. Finally, a Radial Velocity Spectrometer (RVS) also shares the same focal plane, providing the radial velocities and high-resolution spectral data in the narrow band 847–874 nm. To cover all the sky, the spin axis is tilted by 45° with respect to the Sun direction and with a precession period of 63.12 days. This represents a good compromise between astrometric performance and system aspects.

The threshold accuracy of Gaia implies the use of General Relativity for the astrometric modelling. The consortium constituted for the data analysis and processing (DPAC) has established the use of two relativistic models: the Gaia RElativity Model as the baseline one (GREM, Klioner, 2003; Klioner, 2004), and the Relativistic Astrometric MODel for the validation (RAMOD, Crosta et al., 2015, and references therein). Both implement two independent sphere solutions that contribute to the definition and materialization of the absolute reference frame used in astronomy, the Barycentric Celestial Reference System (BCRS, Soffel et al., 2003), providing a fully general-relativistic analysis of the inverse ray-tracing problem, from observational data back to the coordinate position of the light-emitting star. The origin of the BCRS is

in the barycentre of the Solar System and its spatial axis are aligned with the International Celestial Reference System (ICRS), while the time coordinate defines the barycentric coordinate time (TCB).

Given these premises, during its mission, Gaia is acquiring an enormous quantity of complex, extremely precise data. The processing of raw data into the final science catalogue is the aim of the Data Processing and Analysis Consortium, or DPAC, a large pan-European team of scientist and software developers, which are sub-divided into nine Coordination Units, or CUs, with a unique set of data processing tasks. The consortium has members from over 20 countries, revelling the international and cooperative spirit of the mission and the ESA itself. As anticipated, Gaia's mission is to create the most accurate map of the Galaxy to date. The science case of the mission is described in Perryman et al. (2001), while a non-exhaustive list of the research fields on which Gaia will have a huge impact is provided in the next section with an outline of the most important Gaia contributions. Further details on the scientific goals can be found in Gaia Collaboration et al. (2016).

## 2.1 Scientific goals

The fundamental target of the mission is the study of the formation, evolution and today structure of the Milky Way through the analysis of the distribution and kinematics of its stellar populations. Despite the Gaia final catalogue will count about 1% of the stars in the Galaxy ($\sim$ 1–2 billion sources), the dynamical range of the Gaia measurements will cover, for the first time, from the outer part of Galactic centre out to the Galactic halo, providing extremely high accuracies in the Galactic disc region and the Solar Neighbourhood (see Fig. 2.2). Moreover, by combining extinction deduced from stars, it is possible to construct the three-dimensional distribution of the interstellar medium (ISM) of the Milky Way.

The important synergies with on-going or proposed large-scale photometric and spectroscopic surveys, both in the visible and in the infrared (e.g. APOGEE, LAMOST, VPHAS, UKIDSS, VVV VISTA, RAVE, Gaia-ESO Survey, etc.) are producing a very homogeneous survey of all the Galactic components (i.e. bulge, disc, and halo) and will bring tremendous and fundamental contributions to unravel the formation history, evolution, and chemo-dynamical properties of the Milky Way in the context of Galactic Archaeology and Local Cosmology.

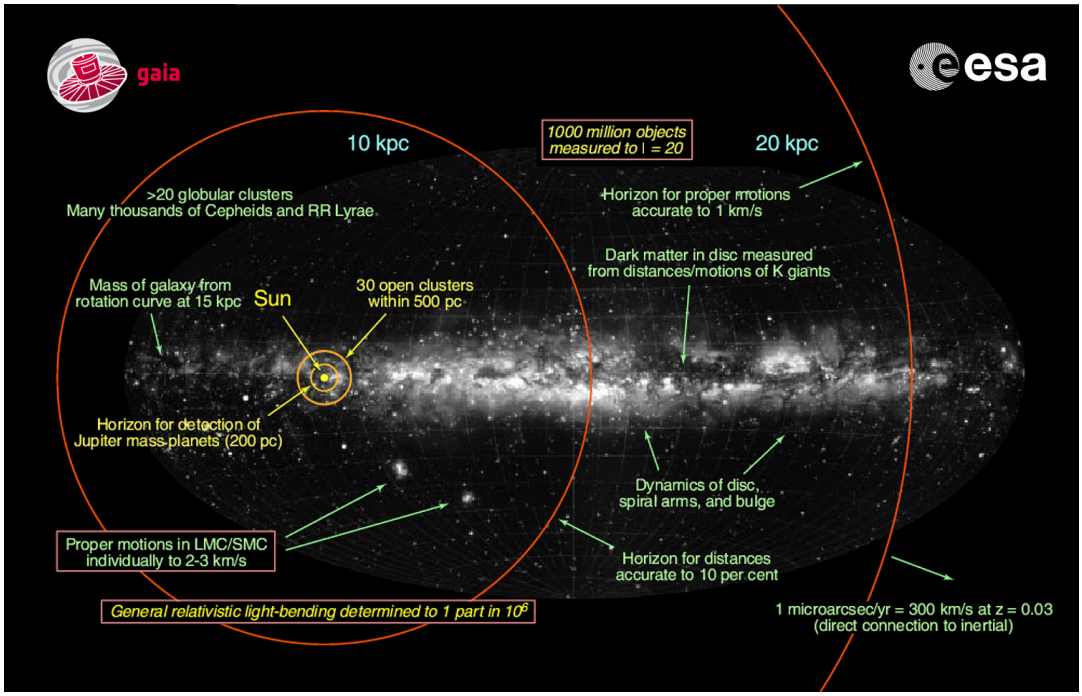


**Figure 2.2:** Illustration of Gaia's range and expected contribution to our knowledge of the Galaxy. Credits: ESA; Background credits: Lund Observatory

The Gaia revolution is in the parallax, the direct measurement of distance using trigonometric observations of any object outside the immediate Solar Neighbourhood. The high-quality colour-magnitude diagrams derived with Gaia represent significant progress in stellar astrophysics and the studies of the many phases of stellar evolution the stellar-mass range, including pre-main sequence stars, white and brown dwarfs and peculiar objects. Moreover, Gaia is a powerful mission to improve our knowledge of multiple stellar systems, helping to answer the fundamental questions of mass distributions and orbital eccentricities among binaries.

Considering that on average each star is will be observed $\sim 70$ times during the five-year nominal operations phase, tens of millions of new variables, including rare objects, pulsating stars such as RR - Lyrae and Cepheids, can easily be discovered. The combination of accurate trigonometric parallaxes and period-luminosity relations will improve the calibration and quality of the cosmic-distance ladder in order to reach Local Cosmological scales.

Although Gaia is designed to detect and observe stars, the on-board instruments can detect and provide a full census of all sources that appear point-like on the sky. The most relevant Solar System object group for Gaia are asteroids, that have smeared images, making them less point-like with respect to the stars. For near-Earth asteroids, the census of these objects is

not going to be very complete, but in those cases where Gaia observations are made, the orbit determination can be very precise.

Gaia will also provide a homogeneous, magnitude-limited sample of unresolved external galaxies, while in tens Local Group galaxies, including the Andromeda galaxy and the Magellanic Clouds, thousands or even millions very bright individual stars will be resolved and observed. These kinds of data may reveal also the impact and the interactions between the Milky Way and its dwarf satellites.

Finally, as relativistic implementations are part of the routine data processing for Gaia, it can be possible to conduct relativity tests in more general fundamental-physics experiments. For example, following the bending of stellar light by the Sun and major planets over the entire celestial sphere, it is possible to directly observe the structure of space-time and determine the parametrised post-Newtonian parameters $\gamma$ and $\beta$ with remarkable precision, or the solar quadrupole moment $J_2$. In this respect, thank Gaia, Astrometry is part of fundamental physics and that of the physics of gravitation in particular (Anton et al., 2012; Crosta et al., 2017).

## 2.2 General Relativity as the core of Gaia

In order to compile the complete census of the Milky Way stellar populations with the exquisite positional precision of Gaia (i.e. the microarcsecond accuracy level to consider the Galaxy as the keystone for disc-like galaxies), the processing, modelling and interpretation of astrometric data demand to be fully compatible with General Relativity since several relativistic effects disturb the light propagation and the detection already at the level of the first post-Newtonian order (Crosta et al., 2017, and references therein).

This is because, according to General Relativity, geometry and physics are joined and a Gaia-like observer is embedded in the ever-present and ever-changing overlapping of the weak local gravitational fields produced by the Solar System bodies. Indeed, the photons' paths passing close to a spherical mass $M$, are deviated in spacetime by an angle

$$\delta\phi = \frac{4GM}{c^2 b} = 1.75'' \left(\frac{M}{M_\odot}\right), \tag{2.1}$$

where $b$ is the distance of closest approach. The deflection increases with the mass of and decreases with the distance from the gravitational body, and

| Perturbing body | Monopole [$\mu$as] | Quadrupole [$\mu$as] |
|---|---|---|
| Sun | 1.75″ (180°) | $\sim 1$ |
| Mercury | 83 (9′) | - |
| Venus | 493 (4.5°) | - |
| Earth | 574 (124°) | 0.6 |
| Moon | 26 (5°) | - |
| Mars | 116 (25′) | 0.2 |
| Jupiter | 16 300 (90°) | 240 (3′) |
| Saturn | 5 800 (18°) | 95 (51″) |
| Uranus | 2 100 (72′) | 25 (6″) |
| Neptune | 2 600 (51′) | 10 (3″) |

**Table 2.2:** Post-Newtonian (pN) effects on the light deflection due to the mass monopole and quadrupole at the order of 1 $\mu$as. The values in parentheses are the maximum angular distances between the perturbing body and photon at which the effect still attains 1 $\mu$as. Values computed in Klioner (2003).

such deviations become relevant locally in angle measurements of Gaia (see Table 2.2). In the static case for example, at the first post-Newtonian approximation order, the deflections of light due to the monopole mass of the planets produce an effect up to the order of several $\mu$as; the contribution to attaining a final accuracy of 1 $\mu$as still be accounted, for example, at 180° from the limb of the Sun and at 90° from that of Jupiter (Klioner, 2003).

Therefore, the Newtonian straight lines description must be avoided and substituted by the null geodesic measurements provided by General Relativity, that describes the trajectory of a photon emitted by a star and detected by an observer through a geometrical environment generated by an n-body distribution of mass that curves the spacetime. Moreover, in the case of the inverse-ray tracing problem also the retarded-time contributions should be taken into account, namely the moment when the gravitational field of the source began to propagate along the incoming light cone. Consequently, to set up an astrometric model, the first step is the identification of the gravitational sources and the background geometry; then, it is possible to fix a reference frame considering an appropriate coordinate system, and describe the light trajectory, the motion of the stars, and that of the observer. This is the framework of modern Relativistic Astrometry that is recently grown as a mature research field (Crosta, 2019).

For Gaia, our relativistic observer, we can assume the Solar System as isolated and the only source of gravity between the observer and the emitting stars. This physical bound system generates a weak gravitational field and is characterized by internal slow motions (Klioner, 2003; de Felice et al., 2004;

de Felice et al., 2006).

Given these premises and according to "The IAU 2000 Resolutions for astrometry, celestial mechanics, and metrology in the relativistic framework" (Soffel et al., 2003), we can adopt a spacetime metric for the background written as a perturbation of the Minkowskian metric, namely,

$$g_{\alpha\beta} = \eta_{\alpha\beta} + h_{\alpha\beta} + \mathcal{O}\left(h^2\right) \tag{2.2}$$

where $\mathcal{O}(h^2)$ collects all nonlinear terms in $h$, the coordinates are $x^0 = ct$, $x^1 = x$, $x^2 = y$, $x^3 = z$, the origin is fixed at the barycenter of the Solar System, and $\eta_{\alpha\beta}$ is the Minkowskian metric. Only first-order terms in the metric perturbation $h$ (or equivalently in the constant $G$ as in the post-Minkowskian approximation) are retained. The $h_{\alpha\beta}$ values describe the effects generated by the bodies of the Solar System. The spatial variations are of the order of $|h_{\alpha\beta}|$, while the time variations are at most of the order $(v/c)|h_{\alpha\beta}|$.

Moreover, the virial theorem requires that the energy density within a bound n-body system must not exceed the maximum amount of the gravitational potential $U$ in it, thus, to reach the micro-arcsecond accuracy level for the Gaia mission, $|h_{\alpha\beta}| \leq U/c^2 \sim v^2/c^2$, where $v$ is the characteristic relative velocity within the system. Then, for a typical velocity $\sim$ 30 km s$^{-1}$, $(v/c)^2 \sim 1$ mas, and also the terms up to $(v/c)^3$ are needed and contribute to the $g_{0i}$ components of the metric, while the even terms in $(v/c)$ to $g_{00}$ and $g_{ij}$ (Crosta et al., 2003).

With these assumptions, at the first post-Newtonian level of approximation, the metric tensor nearby any planet of the Solar System takes the form

$$g_{00} = -1 + h_{00}^{(2)} + \mathcal{O}\left(v^4/c^4\right) \tag{2.3}$$

$$g_{0i} = h_{0i}^{(3)} + \mathcal{O}\left(v^5/c^5\right) \tag{2.4}$$

$$g_{ij} = 1 + h_{00}^{(2)}\delta_{ij} + \mathcal{O}\left(v^4/c^4\right), \tag{2.5}$$

where $h_{00}^{(2)} = 2U/c^2$, $h_{0i}^{(3)} = U^i/c^3$, and $U$ and $U^i$ are, respectively, the gravitational potential and the vector potential generated by all the sources inside the Solar System that can be chosen according to the IAU resolution B1.3 (Soffel et al., 2003).

Inside the Gaia DPAC, the Gaia REativistic Model (GREM Klioner, 2003; Klioner, 2004) is the baseline for the Astrometric Global Iterative Solution (AGIS), while the Relativistic Astrometric MODel (RAMOD de Felice et al.,

2004; de Felice et al., 2006; Crosta et al., 2003) is the one employed for Astrometric Verification Unit (AVU) and the Global Sphere Reconstruction (GSR) at the Italian data center (DPCT). RAMOD conceived to solve the inverse ray-tracing problem in a general relativistic framework not constrained by *a priori* approximation, and is, actually, a family of models of increasing intrinsic accuracy where light propagation is expressed in a general relativistic context, thus not necessarily applied only to astrometry (Crosta, 2019).

Since the quest of this thesis is pursuing a global picture of the Milky Way as a laboratory for Local Cosmology and coherent with General Relativity, it is worth revisiting the level of "smallness" and, therefore, "negligibility" usually applied to Galactic dynamics. Within the Galactic disc, the gravitational potential is usually considered weak and the typical galactocentric rotational velocities of disc stars are small concerning the speed of light, i.e. $v_{\mathrm{Gal}}/c \sim 10^{-3}$. On the other side, the accuracy of Gaia measurements requires that the lowest order takes into account for the metric that describes the weak relativistic regime of the Solar System (SolSys) is $\left(v_{\mathrm{SolSys}}/c\right)^2 \sim 2$ milli-arcsecond (mas). This implies also the off-diagonal term $g_{0i} \sim \left(v_{\mathrm{SolSys}}/c\right)^3 \sim 0.2$ $\mu$as. Hence, applying the virial theorem to a reasonable metric for the Galactic weak fields, the off-diagonal terms is $\sim \left(v_{\mathrm{Gal}}/c\right)^3 \sim 100$ $\mu$as, already within the error level of Gaia's Second Data Release (Crosta, Giammaria, Lattanzi, and Poggio, 2020).

Therefore, from a relativistic point of view, the Gaia catalogue is the representation of the Universe modelled in the BCRS fully compliant with the precepts of General Relativity. Thus, it is perfectly suitable for Local Cosmology.

## 2.3 Gaia Data Release scenario and contents

The Gaia catalogue is released in stages that contain increasing amounts of measurements and observations. The Data Release scenario, constantly updated, is available on the Gaia *ESA Web Portal*. An essential review of the Gaia status and expectations can be found in Pancino (2020).

### 2.3.1 The First Data Release

The first Gaia data release (Gaia DR1, Gaia Collaboration et al., 2016) took place on 14 September 2016 and was based on the data collected during the

first 14 months of Gaia's observations, between 25 July 2014 and 16 September 2015. Since it would require at least 18 months of observations (Lindegren, 2018), not all five astrometric parameters – positions, parallax and proper motions – were successfully estimated for each source. Nevertheless, five-parameter astrometric solution was published for 2 057 050 sources in common between Gaia DR1 (containing 1 142 679 769 sources, Gaia Collaboration et al., 2016) and the two catalogues Hipparcos (containing 117 955 sources, van Leeuwen, 2008) and Tycho-2 (containing 2 539 913 sources, Høg et al., 2000), forming the TGAS catalogue (Tycho-Gaia astrometric solution, Michalik, Lindegren, and Hobbs, 2015).

Gaia DR1 had several limitations also in terms of survey completeness and photometry and did not contain any radial velocities, which instead the second data release included.

### 2.3.2 The Second Data Release

The Second Gaia Data Release (Gaia DR2, Gaia Collaboration et al., 2018b) is based on the data collected during the first 22 months of the nominal mission lifetime and was released on 25 April 2018 and is available through the *Gaia Archive*. Six performance verification papers were published, aimed at demonstrating the scientific potential of the catalogue through a basic examination of some of the key science cases of the Gaia mission.

It represents a major advance concerning Gaia DR1 and provides "high-precision parallax and proper motion catalogue for over 1 billion sources, supplemented by precise and homogeneous multi-band all-sky photometry and a large radial velocity survey at the bright ($G \lesssim 13$) end" (Gaia Collaboration et al., 2018b). For the first time, a very large fraction of the volume of our Galaxy was mapped, well beyond the Solar Neighbourhood. Fig. 2.3 shows how much incredible and fundamental this release is, producing the first high-resolution all-sky view of our Galaxy; instead, Fig. 2.4 summarizes its contents.

The Gaia DR2 provides the five-parameter astrometric solution for 1.3 billion sources down to magnitude $G \sim 21$ mag and a bright limit of $G \approx 3$, enabling the scientific community to derive distances for an unprecedentedly large number of stars. Moreover, the parallaxes and proper motions are based only on Gaia data and do not depend on the Tycho-2 Catalogue as in Gaia DR1. Parallax uncertainties spans from 0.04 mas for sources at $G < 15$, up to the order of 0.7 mas at the faint end $G = 20$. For bright

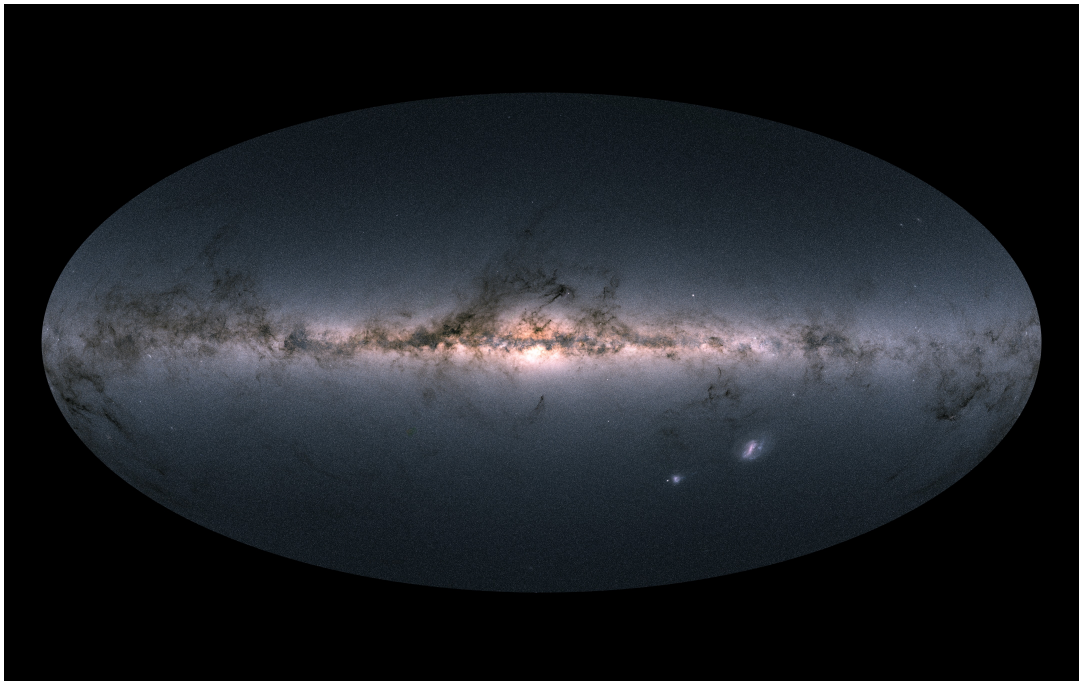

**Figure 2.3:** Gaia's all-sky view of the Milky Way and neighbouring galaxies, based on measurements of nearly 1.7 billion stars. The map shows the total brightness and colour of stars observed in each portion of the sky between July 2014 and May 2016. Credit: ESA/Gaia/DPAC, CC BY-SA 3.0 IGO. Gaia DPAC; A. Moitinho, A. F. Silva, M. Barros, C. Barata, University of Lisbon, Portugal; H. Savietto, Fork Research, Portugal.

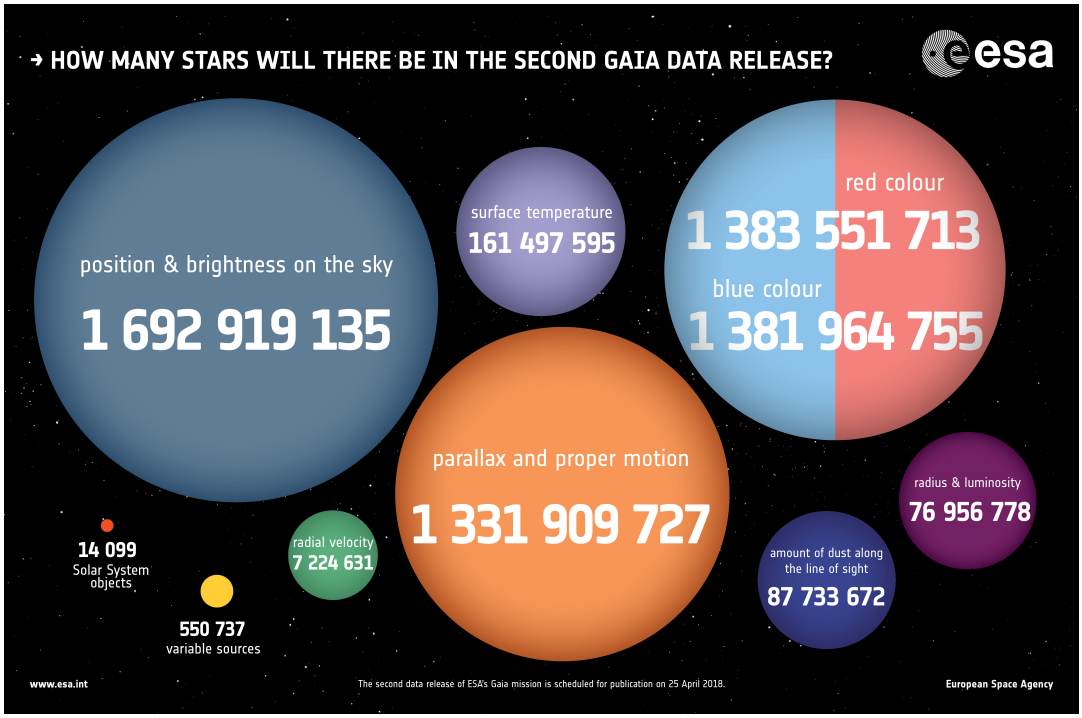


**Figure 2.4:** Gaia DR2 contents based on data collected by the spacecraft spanning a period of 22 months, between 25 July 2014 and 23 May 2016. Credit: ESA, CC BY-SA 3.0 IGO

sources, the typical uncertainties for the proper motions are 0.06 mas yr$^{-1}$, raising to 1.2 mas yr$^{-1}$ for faint stars ($G = 20$ mag).

The release contains median radial velocities (i.e. the median line-of-sight velocities over the epochs) for 7.2 million stars with a mean $G$ magnitude between about 4 and 13 and effective temperature ($T_{eff}$) in the range of about 3550 to 6900 K. This provides a full 6D phase-space reconstruction, all combined with mean $G$ magnitudes, for the largest catalogue ever observed by a single apparatus. The overall precision of the radial velocities at the bright end is in the order of 200 – 300 m s$^{-1}$, while at the faint end the overall precision is approximately 1.2 km s$^{-1}$ for a $T_{eff}$ of 4750 K and about 2.5 km s$^{-1}$ for a $T_{eff}$ of 6500 K.

For more than 1.69 billion sources a two-parameter solution – the positions on the sky ($\alpha$, $\delta$) – combined with the mean $G$ magnitude is available. These sources have a positional uncertainty at $G = 20$ of about 2 mas, at J2015.5, while the $G$ magnitudes precision varies from $\sim$ 1 milli-mag for the brighter stars ($G \leq 13$) to around $\sim$ 20 milli-mag for the faint ones. The photometry in the Blue and Red Passband, $G_{BP}$ and $G_{RP}$ respectively, is available for more than 1.38 billion sources with the same $G$ magnitude precision limits.

The physical parameters are given for a smaller subset of the total catalogue: around 161 million sources brighter than $G \leq 17$ mag have the effective temperature $T_{eff}$ that ranges from 3000 to 10 000 K, and for $\sim$ 76 million sources the luminosity and radius are available as well. Additional 11 million sources also have the line-of-sight extinction $A_G$ and reddening E(BP-RP).

More than 550 000 variable sources were classified in Gaia DR2. They consist in Cepheids, RR-Lyrae, Mira and Semi-Regular Candidates, High-Amplitude Delta Scuti, BY Draconis candidates, SX Phoenicis Candidates and short time scale phenomena.

The Gaia DR2 catalogue is essentially complete between $G = 12$ and $G = 17$, and a list of known issues with the data, such as small systematic effects on parallaxes that yield a bias of 0.025 mas (Lindegren, 2018; Luri et al., 2018), are discussed on the *ESA Web Portal* (i.e. web/gaia/dr2-known-issues). The majority of these critical points are expected to decrease with each upcoming data release because more data are processed and the data reduction pipelines are progressively improved. Nevertheless, with this release, the Galactic census took shape and Local Cosmological scales have become available.

### 2.3.3 Next releases and end-of-mission expectations

Gaia Data Release 3 is split into two steps: the early release called Gaia Early Data Release 3 (Gaia EDR3) has been published on 3 December 2020 at 12:00 CET, while the full Gaia Data Release 3 (Gaia DR3) is expected for the first half of 2022 (*ESA Web Portal*).

Both these catalogues are based on data collected in 34 months of Gaia's routine operational phase, between 25 July 2014 and 28 May 2017 (Gaia DR2 was based on 22 months). The EDR3 contains new astrometry (positions, parallaxes, proper motions) and integrated photometry (integrated $G$, $G_{BP}$, $G_{RP}$) for a larger number of sources that pass the quality filtering in comparison to Gaia DR2, with a limiting magnitude of about $G \approx 21$ and a bright limit of about $G \approx 3$. The errors and the number of sources are close to the expected end-of-mission performances.

New mean radial velocities will be included in the full Gaia DR3 catalogue that will also provide entirely new data, such as mean BP/RP spectra, non-single stars catalogues, results for Quasars and extended objects, variable-star classifications together with the epoch photometry used for the stars, and an additional data set, Gaia Andromeda Photometric Survey, consisting of the photometric time series for all sources located in a 5.5° field centred on the Andromeda galaxy.

The full release for the nominal mission, Gaia DR4, is supposed presumably in 2023 and will be consisting of the full astrometric, photometric, and radial-velocity catalogues at the highest quality level expected at the end of the five-year observations period. All available variable-star, non-single-star solutions and classifications will be included, with also multiple astrophysical parameters (derived from BP/RP, Radial Velocities, and astrometry) for stars, unresolved binaries, galaxies, and quasars. Finally, it is hoped an exoplanet list, and all epoch and transit data for all sources.

A further extension of two more years (up to 2022) has also been preapproved for Gaia mission. The on-board fuel reserve is estimated to be sufficient to operate Gaia at least until 2024, thus more data releases beyond DR4 are in principle possible and to be expected. This would bring the total mission lifetime to 10 years, implying a 40 per cent improvement on the precision of all data products with respect to a five year mission, and a factor of almost three improvement for the proper motions.

# Chapter 3

# The Milky Way as reconstructed by the Gaia DR2

Gaia is, therefore, the fundamental instrument to open the doors of the laboratory of Local Cosmology: the Milky Way. As we know it now, the Galaxy is a gravitationally bound system of stars, gas, dust, characterised by a barred spiral structure, typical of the large disc-like galaxies that today are observed in low-density environments and outer region of large galaxy clusters (Kormendy et al., 2010).

According to ΛCDM, the Galaxy is embedded in a dark matter halo, where most of the mass of the system is located. The current estimate of its mass based on Gaia DR2 data and Galactic rotation curve by Crosta, Giammaria, Lattanzi, and Poggio (2020) gives $M_{vir} \sim 10^{12}$ $M_\odot$ consistent with the range of values quoted in e.g. Bland-Hawthorn and Gerhard (2016), Posti and Helmi (2019a), and Watkins et al. (2019a) and references therein. From cosmological simulations, the density profile of the dark halo is usually modelled according to the Navarro-Frenk-White profile (NFW profile, Navarro, Frenk, and White, 1996), namely,

$$\rho_h^{DM}(r) = \rho_0 \frac{1}{(r/A_h)(1+r/A_h)^2}, \tag{3.1}$$

where $\rho_0$ is the density scale of the dark matter halo and $A_h$ its (spherical) scale radius. For the Milky Way, recent estimete give $A_h \sim 17$ kpc, and $\rho_0 \sim 0.009$ $M_\odot$ pc$^{-3}$, corresponding to $\rho_\odot^{DM} \sim 0.3$ GeV cm$^{-3}$ at the location of the Sun and presuming the halo is spherical (McMillan, 2017; Eilers et al., 2019; Crosta et al., 2020). Alternatively, also the Einasto profile (Einasto, 1965) is often considered. Nevertheless, the correct shape is uncertain and has been the subject of significant debate by the astrophysical community (e.g. Ibata et al., 2001; Johnston, Law, and Majewski, 2005; Koposov, Rix, and Hogg, 2010; Vera-Ciro and Helmi, 2013; Ibata et al., 2013; Bowden, Evans, and Williams,

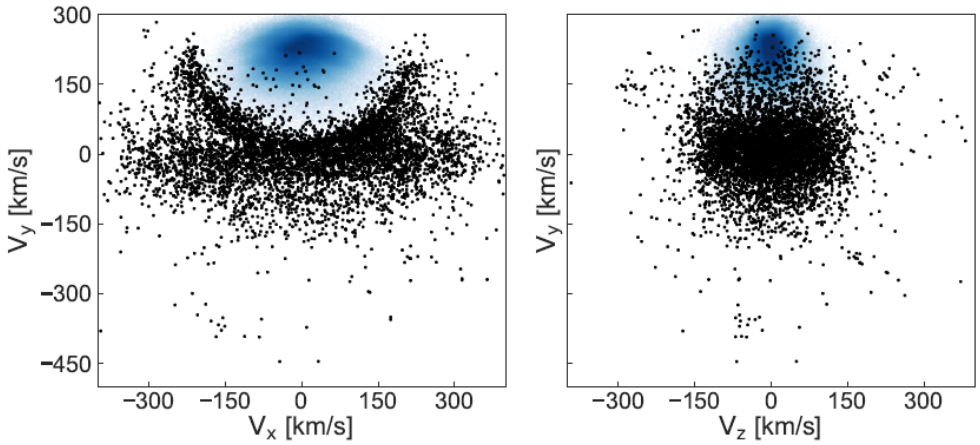


**Figure 3.1:** Velocity distribution of stars in the Solar Neighborhood as determined by Gaia. All these stars have full phase-space information, are located within 1 kpc from the Sun, and only those with relatively accurate parallaxes, i.e. with $\varpi/\sigma_\varpi \geq 5$ have been considered. The nearby halo stars are plotted with black dots and defined as those that satisfy $|V - V_{\rm LSR}| > 210$ km s$^{-1}$, for $V_{\rm LSR} = 232$ km s$^{-1}$. The blue density maps reveal the contribution of the thin and thick discs. The "banana"-shaped structure seen in the left panel reveals an important contribution of "hot" thick disc-like stars to the halo (Koppelman, Helmi, and Veljanoski, 2018).

2016; Posti and Helmi, 2019a; Wegg, Gerhard, and Bieth, 2019). This dark halo should have assembled first in the early stages of Galactic formation and its growth is continuing at present (see for example Helmi, 2020, for a review on the early history of the Milky Way).

On the other hand, the Milky Way baryonic content, the visible component of the Galaxy, is typically dissected in several major structures, which present peculiar characteristics in terms of spatial and kinematical distribution. For instance, Fig. 3.1 shows the kinematical distribution of stars in the Solar Neighborhood as determined by Gaia (Koppelman, Helmi, and Veljanoski, 2018, and their Fig. 2). Of course, also the age and chemical properties of the stellar populations are different and the features of the stellar content in each one of these components are closely related to their origin and timescales during the formation and evolution of the Galaxy. Finally, there are also warm ionized gas in a halo or circum-galactic medium (Richter, 2017; Zheng et al., 2019), and cold gas mostly in the disc. In the next sections, a summary of the main properties of the stellar Galactic components is presented.

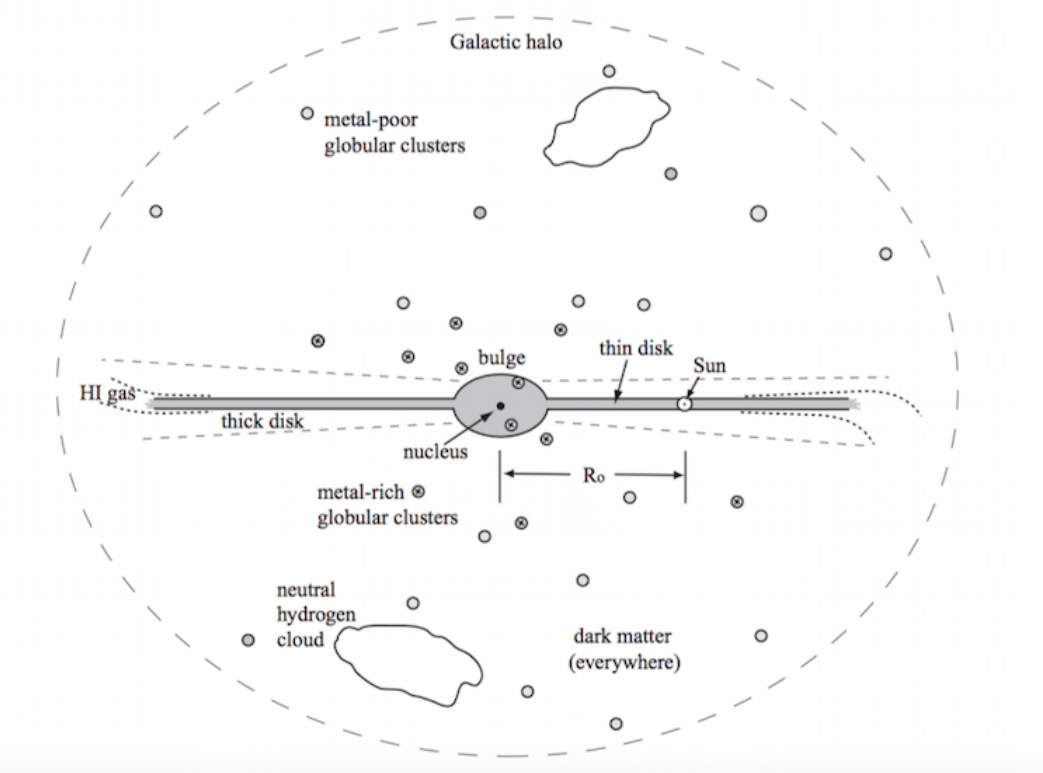


**Figure 3.2:** Schematic diagram of the Milky Way, showing different Galactic components (Sparke and Gallagher, 2006). The Galaxy, according to ΛCDM, is then embedded in a more extended dark matter halo.

## 3.1 Galactic components

The Milky Way has several visible substructures: a central bulge characterised by a bar, a stellar disc separable in a thin and a thick component, and a stellar halo. They are identifiable by eye in Fig. 2.3 and outlined in the schematic diagram of Fig 3.2. See then Table 3.1 for a summary of the main properties and geometric description of the different Galactic components.

### 3.1.1 The bulge

The bulge is the most centrally concentrated component and contains between a third and a quarter of the Milky Way stellar mass. The bulge-over-total stellar mass is estimated to be $B/T \simeq 0.15 - 0.33$ (Bland-Hawthorn and Gerhard, 2016; Belokurov et al., 2018, and references therein), with the upper limit derived from dynamical investigations that usually provide higher values than stellar density profile (see Scannapieco et al., 2010, for a proper definition of the "dynamical" $B/T$). Nevertheless, the bulge stellar mass,

**Table 3.1:** Integrated properties of the Galactic components. The density is in $M_\odot$ $kpc^{-3}$. See Sect. 3.1 for the references.

| | Mass $[10^{10}\ M_\odot]$ | Age [Gyr] | $[Fe/H]$ [dex] | Density profile |
|---|---|---|---|---|
| Bulge | 1 – 2 | $\gtrsim 10$ | $-1.5$ to 0.5 | Boxy-peanut bar<br>$\rho \propto M_b b^2 (r^2 + b^2)^{-5/2}$<br>$b \sim 0.3$ kpc |
| Thin disc | 4 – 5 | $\lesssim 8$ | $-0.6$ to 0.5 | $\rho \propto exp(-R/h_R - \lvert z\rvert/h_Z)$<br>$h_R \sim 2.6$ kpc<br>$h_Z \sim 0.3$ kpc |
| Thick disc | 0.6 – 4 | $\gtrsim 8$ | $-1$ to $\sim 0$ | $\rho \propto exp(-R/h_R - \lvert z\rvert/h_Z)$<br>$h_R \sim 2.0$ kpc<br>$h_Z \sim 0.9$ kpc |
| Stellar halo | $\lesssim 0.2$ | $> 10$ | $\ll -0.5$ | $\rho \propto r^{-\beta}$<br>$r_{break} \sim 25$ kpc<br>$\beta_{in} \sim 2.5$, $\beta_{out} \sim 3.7$ |

$M_b \sim 1 \cdot 10^{10}\ M_\odot$, computed from Galactic rotation curve (Pouliasis, Di Matteo, and Haywood, 2017; Crosta et al., 2020) is in good agreements with what derived by counting red clump stars in the central regions of the Milky Way (Valenti et al., 2016).

Since it is a very dense region of stars and Galactic interstellar medium (ISM), the line of sight to the Galactic centre is heavily obscured, limiting our current understanding of its complex nature. For a long time, the bulge was claimed to have a "classic" spherical shape, a quick formation in the firsts phase of Galactic evolution, supported by the velocity dispersion of its stars. On the other hand, external disc-like galaxies seemed to be characterised by a rotating triaxial structure and possibly an extended rotating bar. Rising interest and significant progress have been made thanks to new surveys in near-infrared wavelength such as APOGEE described in the reviews by Barbuy, Chiappini, and Gerhard (2018) and Zoccali (2019), or the investigation by Queiroz et al. (2020). Recent work suggests a rather long bar (Portail et al., 2015; Wegg, Gerhard, and Portail, 2015), that extends to 2–3 kpc from the centre and with the major axis inclined to the line of sight from 20 to 30 degree. Moreover, McWilliam and Zoccali (2010) and Nataf et al. (2010) evidenced that red clump giants (RCGs) present a bimodal distribution along the line-of-sight and attributed this result to the overlapping of two arms of an X-shaped structure along the direction of their observation. This feature characterises boxy/peanut bulges in barred galaxies (Ness et al., 2012; Wegg, Gerhard, and Portail, 2015) when viewed edge-on as in the case of

our Galaxy. N-body simulations suggest that this boxy/peanut morphology arise naturally because of the secular inwards motion of stars that forms the bar (Athanassoula, 2016).

Spectroscopic studies show a mixture of populations: bulge stars have a wide age distribution (from a few Gyrs up to more than 13 Gyr), with metallicity in range of $-1.5 \leq [Fe/H] \leq +0.5$ dex (Barbuy, Chiappini, and Gerhard, 2018), and some that resemble other Galactic components populations, such as the thick disc and stellar halo. Rojas-Arriagada et al. (2017) with Gaia-ESO data, Schultheis et al. (2017) with APOGEE data and Zoccali et al. (2017), concluded that the metallicity distribution function in the bulge is at least bimodal. Bensby et al. (2017) confirmed that studying microlensed dwarfs and subgiant stars, and identified four peaks corresponding to different star formation episodes occurred 12, 8, 6 and 3 Gyr ago. Many authors (e.g. Renzini et al., 2018; Nogueras-Lara et al., 2018; Bernard et al., 2018) suggest that most of the bulge stars are quite old ($>$ 10 Gyr), and only 10% of bulge stars are younger than 5 Gyr, but this fraction rises to 20–25% in the metal-rich peak. This may imply the existence of relatively young stars in the bulge that can belong to the inner disc as suggested by Haywood et al. (2016). Hence, the observed metal-poor stars may be the product of an early dissipative collapse of a primordial cloud, while the presence of the observed metal-rich stars in the wide metallicity distribution of the bulge can be justified by the (at least partly) disc origin of the Galactic bar due to Lindblad resonance (Lindblad, 1960) and dynamical instabilities (Di Matteo et al., 2014; Bland-Hawthorn and Gerhard, 2016).

From a dynamical point of view, the gravitational potential of the bulge is well described by a Plummer's density profile (Pouliasis, Di Matteo, and Haywood, 2017; Eilers et al., 2019; Crosta et al., 2020):

$$\rho_b(r) = \frac{3b_b^2 M_b}{4\pi(r^2 + b_b^2)^{5/2}} \tag{3.2}$$

where $b_b = 0.3$ kpc is the Plummer radius and $M_b \sim 1 \cdot 10^{10}$ $M_\odot$ the total bulge mass (Pouliasis, Di Matteo, and Haywood, 2017; Crosta et al., 2020). Other possible profiles are a power-law density profile that is exponentially cut-off (Bovy and Rix, 2013) with a power-law exponent of -1.8 and a cut-off radius of 1.9 kpc, or a more complex two components potentials to describe the nuclear stellar cluster, which dominates the potential at $1 \lesssim R[\mathrm{pc}] \lesssim 30$ and the nuclear stellar disc, which dominates the potential at $30 \lesssim R[\mathrm{pc}] \leq 300$ (e.g. Schödel et al., 2014; Gallego-Cano et al., 2020; Sormani et al., 2020).

The innermost regions of the bulge contain a super-massive black hole (SMBH) having a mass of $\approx 4.2 \cdot 10^6$ $M_\odot$ (Ghez et al., 2008; Gillessen et al., 2009a; Gillessen et al., 2009b), and the cited nuclear star cluster with a half-light radius of $\approx 4.2 \pm 0.4$ pc (Schödel et al., 2014). The SMBH is identified by the radio source Sgr A* and usually adopted as the Galactic centre, because it is at rest at the dynamical centre of the Milky Way within the uncertainties (Reid and Brunthaler, 2004; Reid, 2008). By measuring the distance to the Sgr A*, it is possible to determine the position of the Sun with respect to the Galactic centre. The Gravity Collaboration et al. (2018) estimates the radial distance between the Sun and Sgr A* to be $R_\odot = 8.122 \pm 0.033$ kpc.

### 3.1.2 The stellar disc

Since their position within the Milky Way, the Sun and most of the stars in the Solar Neighbourhood belong to the Galactic disc, namely the squashed, more massive, and rotational supported components of the Galaxy. From our perspective, we have a preferential observation point of view to obtain unique and fundamental information about the stellar population embedded to the disc, but since the majority of the gas, atomic and molecular hydrogen, resides here too, extinction effects in the visual band and source crowding make the definition of the disc structure far from trivial. Even if there are some troubles when observing close to the Galactic plane, the use of near and far-infrared data from COBE/DIRBE data (Drimmel and Spergel, 2001) and more recently the important synergies between Gaia and the spectroscopic ground surveys such as GALAH (De Silva et al., 2015) and APOGEE (Majewski et al., 2017) let the three-dimensional structure of the Galaxy being revelled.

The disc is usually described in terms of a thin and a thick component, whose definition was originally based on geometrical properties, as shown by Yoshii (1982) and Gilmore and Reid (1983) from stellar number density profiles. Studies on the stellar ages, kinematics, and chemical abundances have confirmed the existence of two different disc populations.

It is common to describe both discs with a double exponential decay profile (i.e. in the radial and vertical direction), with the thin disc being dominant in terms of stellar density ratio $f = \rho_T/\rho_t = 6 - 12$ per cent (Jurić et al., 2008; Just and Jahreiß, 2010a; Bovy et al., 2015). The radial scale lengths are $h_{\mathrm{Rt}} = 2.6 \pm 0.5$ kpc and $h_{\mathrm{RT}} = 2.0 \pm 0.2$ kpc for the thin and thick

disc respectively, while the vertical scale heights are $h_{Zt} = 300 \pm 50$ pc and $h_{ZT} = 900 \pm 180$ pc (Bland-Hawthorn and Gerhard, 2016).

For dynamical study of the rotation curve is also often used the Miyamoto-Nagai profile to model the Galactic discs (Miyamoto and Nagai, 1975). Their gravitational potential is then determined by the density profile written as

$$\rho(R,Z) = \frac{GM_d b^2}{4\pi} \frac{\left[aR^2 + \left(a + 3\sqrt{Z^2+b^2}\right)\left(a+\sqrt{Z^2+b^2}\right)^2\right]}{\left[R^2\left(a+\sqrt{Z^2+b^2}\right)^2\right]^{5/2}\left(Z^2+b^2\right)^{3/2}} \tag{3.3}$$

where $R$ and $Z$ are the radial and vertical (cylindrical) coordinates, $M_d$ is the (thin or thick) disc mass, and $a$ and $b$ are planar and vertical semi-axis of an highly flattened axisymmetric density distribution. For the thin disc, recent studies estimate $a_t \sim 5.3$ kpc and $b_t \sim 0.25$ kpc, while $a_T \sim 2.6$ kpc and $b_T \sim 0.8$ kpc for the thick disc (Barros, Lépine, and Dias, 2016; Pouliasis, Di Matteo, and Haywood, 2017; Eilers et al., 2019; Crosta et al., 2020). Note, moreover, that this profile can be well approximated by the double exponential decay, and that there is no evidence yet to demonstrate which profile provide a better fit (Pouliasis, Di Matteo, and Haywood, 2017).

The stellar mass contents of the two discs is still a matter of debate because the separation of the two components is not trivial and the distinction based on geometric structure, dynamical contribution or chemistry could provide different results. Recent studies successfully modelled the Galactic rotation curve as reconstructed by Gaia DR2 considering the Miyamoto-Nagai profile to describe two equal massive discs of about $4 \cdot 10^{10}$ $M_\odot$ (Eilers et al., 2019; Crosta et al., 2020, and references therein). On the other hand, Bland-Hawthorn and Gerhard (2016, and references therein) report that the stellar mass of the thin disc is $M_t = 3.5 \pm 1 \cdot 10^{10}$ $M_\odot$ and a lower value for the thick disc, $M_T = 6 \pm 3 \cdot 10^9$ $M_\odot$. The latter values are in good agreement with the surface density ratios and chemical definition of the discs (Bovy et al., 2015).

In terms of kinematics, the thin disc is supported mainly by stellar circular orbits, with small dispersion, $\sigma_{V_\phi} = 26.0 \pm 0.2$ km s$^{-1}$, and mean rotational velocities of the order of 220 km s$^{-1}$ (Spagna et al., 2010; Recio-Blanco et al., 2014; Han et al., 2020); also the thick disc is rotationally supported, although kinematically hotter $\sigma_{V_\phi} = 39.1 \pm 0.3$ km s$^{-1}$ than the thin disc, and with a slower mean rotation of the order of 160 km s$^{-1}$ (Spagna et al., 2010; Recio-Blanco et al., 2014; Han et al., 2020). Combining the Gravity Collaboration et al. (2018) results with the proper motion of Sgr A* from Reid and

Brunthaler (2004), Drimmel and Poggio (2018) found $(V_{R,\odot}, V_{\phi,\odot}, V_{Z,\odot}) = (-12.9 \pm 3.0, 245.6 \pm 1.4, 7.78 \pm 0.09)$ km s$^{-1}$ for the velocity of the Sun with respect to the Galactic centre. Considering the Solar motion by Schönrich, Binney, and Dehnen (2010), the authors confirm also that the Local Standard of Rest (LSR) is in circular motion with a circular velocity of $\sim 233$ km s$^{-1}$.

The majority of the ISM resides in the thin disc, thus it is younger than the thick one, with typical stellar ages $\lesssim 8$ Gyr and $\gtrsim 8$ Gyr respectively (Haywood et al., 2013). The present time Star Formation Rate (SFR) in the Solar Neighbourhood as measured with Gaia is $\sim 1.7$ M$_\odot$ pc$^{-2}$ Gyr$^{-1}$ (Bovy, 2017) compatible with previous estimates by Licquia and Newman (2015). Given this, also the chemical abundances reveal the different nature of the two-disc populations: thick disc stars are more metal-poor and $\alpha$-enhanced than those belonging to the thin disc (Gilmore, Wyse, and Kuijken, 1989; Soubiran, Bienaymé, and Siebert, 2003; Bensby, Feltzing, and Lundström, 2003; Grisoni, Spitoni, and Matteucci, 2018). The stellar metallicities of the thick disc spans from $[Fe/H] \sim -1.0$ dex to approximately solar values, with $[\alpha/Fe]$ systematically higher than those displayed by the thin disc at a given metallicity (Hayden et al., 2015). The metallicity distribution function of the thin disc peeks in the range $-0.6 \leq [Fe/H] \leq +0.5$ dex. Therefore, the two populations define separate chemical sequences as shown in Fig. 3.3 raising the question of how both discs formed and whether or not they share a common formation history. As reported in Giammaria et al. (2021), the "actual origin of the Galactic thick disc is not clear and it is still matters of debate whether it derives mainly from the kinematic heating of the proto-disc, or from a starburst triggered by merging events and feds by the infall of a gas-rich satellites". Helmi et al. (2018) and Gallart et al. (2019) claimed that the thick disc formation was triggered by a major merger with a massive dwarf galaxy, named Gaia-Sausage-Enceladus (GSE) experienced by our Galaxy $\sim 10$ Gyr ago and confirmed by several studies (Belokurov et al., 2018; Helmi et al., 2018; Di Matteo et al., 2019; Vincenzo et al., 2019; Gallart et al., 2019). Many authors support also the global top-down, inside-out scenario for the Galactic disc formation and evolution (e.g. Muñoz-Mateos et al., 2011; González Delgado et al., 2014; Bovy et al., 2016) explaining in this way the signatures of the "dynamically young and perturbed MW disk" found by Antoja et al. (2018) with Gaia DR2.

Finally, the three-dimensional structure of the Milky Way disc presents some inhomogeneities in the density distribution of gas and stars which can be attributed to a spiral structure (for a more recent map of the spiral arms,

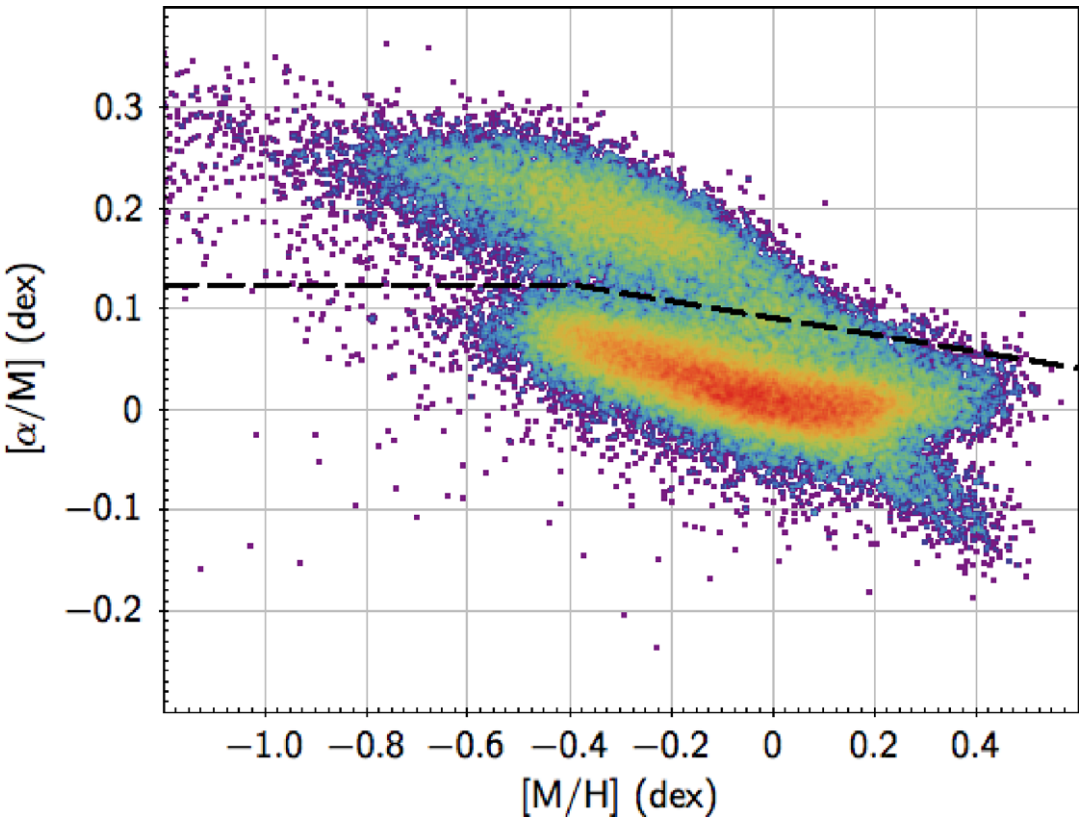


**Figure 3.3:** Chemical distribution, $[\alpha/M]$ versus $[M/H]$, for 67 358 Gaia DR2 and APOGEE DR14 stars from Re Fiorentin, Lattanzi, and Spagna (2019). The stars below the dashed line belongs to the thin disc (below), while those above to the thick disc.

see Reid et al., 2014). The spiral arms are traditionally described as quasi-stationary density waves (Lindblad, 1960; Lin and Shu, 1964), showing the location of star formation fronts in the Galaxy. Moreover, Poggio et al. (2020), using 12 million giant stars from Gaia DR2, show evidence of a dynamically evolving warp in the outer disc, revealing a degree of non-axisymmetry in the structure of the Milky Way disc on large scale.

### 3.1.3 The stellar halo

The stellar halo, distinguished from the dark matter halo which is supposed to surround and dominate the mass content of the Galaxy, is the most extended component but at the same time, it is rather centrally concentrated. It contains approximately 1% of the total Galactic stellar-mass, including globular cluster and field stars (Helmi, 2008). The most recent estimates yield $M^*_{halo} \sim 1.3 \cdot 10^9$ $M_\odot$ (Deason, Belokurov, and Sanders, 2019; Mackereth and Bovy, 2020). The stellar halo contains very metal-poor and old stars, distributed in an extended spheroidal volume, supported by random motions in eccentric orbits and with just a small possible net rotation. All these stars are older than 10 Gyr (Bland-Hawthorn and Gerhard, 2016; Helmi, 2020), and their kinematics and metallicities show evidence of two broadly overlapping components (Carollo et al., 2007): a high-$\alpha$ inner halo with slightly prograde rotation and with typical metallicities $[Fe/H] \approx -1.6$ dex, and a low-$\alpha$ outer halo with retrograde rotation and mean metallicity $[Fe/H] \approx -2.2$ dex (Carollo et al., 2007; Nissen and Schuster, 2010; Hayes et al., 2018). Moreover, the density profile is well-modelled by a broken power-law, i.e. $\rho \propto r^{-\beta}$, defined by the slope parameters $\beta_{in} = 2.5 \pm 0.3$ for the inner halo and $\beta_{out} \sim 3.7 - 5$ for the outer halo, and with a break radius of $r_{break} = 25 \pm 10$ kpc (Bland-Hawthorn and Gerhard, 2016). Various studies based on data reaching down to $R \sim 5$ kpc show that the inner halo is more flattened, $q_{in} = 0.65 \pm 0.05$ (see also Bell et al., 2008; Jurić et al., 2008) with respect to the outer one that is rounder, $q_{out} = 0.8 \pm 0.1$ (Xue et al., 2015; Pila-Díez et al., 2015, that considered RGB and nMSTO, respectively).

In terms of kinematics, the stellar halo shows a velocity ellipsoid whose principal axes align well with spherical coordinates, and with corresponding halo velocity dispersions $(\sigma_{V_R}, \sigma_{V_\phi}, \sigma_{V_Z}) = (141, 75, 85)$ km s$^{-1}$, with a total error in each component of $\sim 5$ km s$^{-1}$ (Spagna et al., 2010; Re Fiorentin et al., 2015; Bland-Hawthorn and Gerhard, 2016).

The "dual" nature of the Galactic stellar halo raises questions on its formation and evolution history. Early works suggested that the halo stars formed during the dissipative collapse of a single gas cloud, which gave rise to the Milky Way (Eggen, Lynden-Bell, and Sandage, 1962), while Searle and Zinn (1978), based on their observation on globular clusters chemical abundances, proposed alternatively that the halo formed from an aggregation of several cloud fragments. Unfortunately, none of these models explained the nature of the two chemo-dynamical populations satisfactorily and the current picture combines these two processes in a more complex scenario for the stellar halo formation. Indeed, most of the halo stars are accreted from smaller galaxies (such as the major mergers Gaia-Sausage-Enceladus claimed by Belokurov et al., 2018; Helmi et al., 2018; Di Matteo et al., 2019; Vincenzo et al., 2019; Gallart et al., 2019) that are then tidally disrupted in the gravitational field (Ibata et al., 1997; Belokurov et al., 2006). On the other hand, a fraction formed in situ (Cooper et al., 2015), during the initial gas collapse (Samland and Gerhard, 2003) and/or was born in the disc but was subsequently scattered on halo orbits (Purcell, Bullock, and Kazantzidis, 2010). In this context, the high-$\alpha$ stars would be formed in-situ in the halo, whereas the low-$\alpha$ stars might correspond to accreted components, explaining the inner/outer halo duality with a different assembly histories (Bonaca et al., 2017). Moreover, the accretion process is continuing nowadays (Helmi, 2008), thus given the low volume density and the long dynamical timescales due to its non-dissipative nature, the stellar halo represents an excellent diagnostic for the Milky Way evolution and an important reservoir of merger debris, which remain observable over Gyrs (see e.g. Helmi, 2008; Re Fiorentin et al., 2015; Re Fiorentin et al., 2021, and references therein). The Sagittarius stream originated from the Sagittarius dwarf galaxy, was the first ongoing accretion event to be discovered in the Milky Way halo (Ibata, Gilmore, and Irwin, 1994), and today a large number of substructures and over-densities have been discovered. In Grillmair and Carlin (2016) can be found a complete list of tidal structures identified in the Milky Way since then.

# Part III

# High-resolution simulations of the Milky Way and the formation of the Galactic disc

# Chapter 4

# Assembling a disc-like galaxy with simulations

In the era of precision astrometry, opened by the impressive improvement given by the Gaia Second Data Release (DR2, Gaia Collaboration et al., 2016), the comparison between observations and high-resolution cosmological simulations of Milky Way-like disc galaxies becomes mandatory to create a coherent laboratory for Local Cosmology studies since many of the chemo-kinematic properties of the Milky Way and nearby galaxies are related to events that occurred a long time ago (e.g. Freeman and Bland-Hawthorn, 2002).

A crucial step in this sense has been given by the advent of supercomputers such as MARCONI at CINECA (*CINECA Web Portal*) and the improvement of high-performance numerical algorithms in the last decades. Thus, it is now possible to investigate the evolution of large cosmic structures and galaxies like the Milky Way throughout the epochs: after the primordial non-linear growth of the density fluctuations of CMB, very complex simulations start running from redshift $z \sim 100$ until the Local scenario at redshift $z = 0$.

The improvements of numerical codes allow us to model a variety of physical processes over an enormous range of time and length scales. Modern standard simulations describe dark matter, dark energy and ordinary baryonic matter in an expanding spacetime starting from well-defined initial conditions. The modelling of ordinary baryonic matter is the most challenging due to the complex interplay of physical processes (e.g. dynamics of collisionless systems, gas flows, star formation, stellar nucleosynthesis, ...) that generated our Galaxy, which represents the Rosetta stone of galaxy evolution.

Cosmological simulations have also proven useful to study alternative cosmological models (i.e. modified gravity as dark matter or dark energy alternatives) and their impact on the galaxy population. Moreover, General

Relativity and its numerical implementation (i.e. numerical relativity) begin to be applied not only for the commonplace use of modelling extreme astrophysical phenomena and compact objects but also to describe cosmological scenarios beyond the Newtonian approximation (see e.g. Bruni, Thomas, and Wands, 2014; Giblin, Mertens, and Starkman, 2016; Adamek et al., 2016; Ames, Andréasson, and Logg, 2016; Macpherson, Price, and Lasky, 2019, and references therein).

In what follows, the state-of-the-art of standard N-body simulation is discussed, providing a focus on the sub-resolution model (MUPPI) of Aquila-C-4 (AqC4 hereafter), the zoomed-in N-body simulation used for the study published in Giammaria et al. (2021).

## 4.1 Classic simulations of galaxy formation

According to the ΛCDM model, dark matter represents the backbone for structures formation and is, therefore, a key ingredient of classic simulations. On top of the power spectrum considered to initialize simulations, and specifying the linear density fluctuation field at some initial time, typically at redshift $z \sim 100$, the initial positions and velocities of dark matter particles are assigned along with baryon density, velocity and temperature fields. Fig. 4.1 from Vogelsberger et al. (2020) summarises the fundamental aspects for galaxies formation implemented in classic cosmological simulations.

The main goal of such kind of simulations is to reconstruct the formation history of our Milky Way. Indeed, as anticipated in the previous chapter, the dark halo of the Galaxy assembled first and its growth continues to the present time (see Helmi, 2020, for an extensive review of the early accretion history of the Milky Way). The stellar inner halo is mainly made up of stellar debris from the accreted satellites and heated disc stars. Moreover, several works have also confirmed that our Galaxy experienced $\sim 10$ Gyr ago a major merger with a massive dwarf galaxy, named Gaia-Sausage-Enceladus (GSE, Belokurov et al., 2018; Helmi et al., 2018; Di Matteo et al., 2019; Vincenzo et al., 2019; Gallart et al., 2019). However, the actual origin of the other structures of the Milky Way is not clear. For example, it is a still matter of debate whether the present thick disc derives mainly from the kinematic heating of the proto-disc, or from a starburst triggered by merging events and fed by the infall of a gas-rich satellite (Brook et al., 2004; Brook et al., 2012).

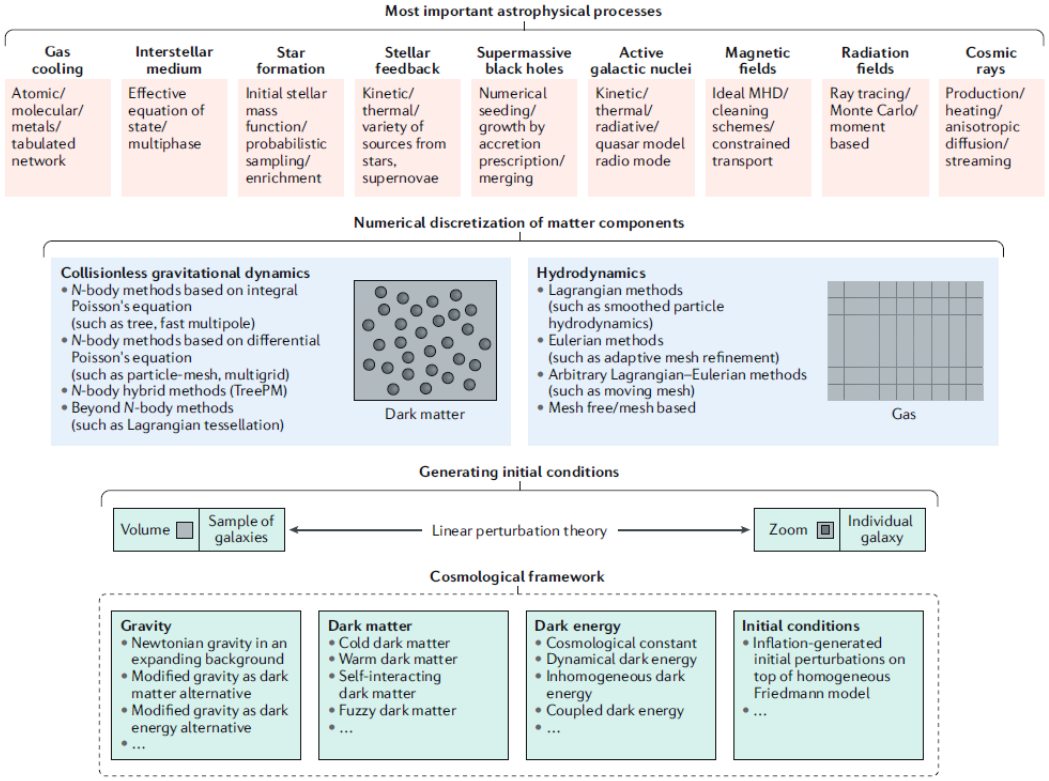


**Figure 4.1:** Overview of the key ingredients of cosmological simulations performed within a given cosmological framework, including physical models for gravity, dark matter, dark energy, baryons and the type of initial conditions. The dark matter component follows the equations of collisionless gravitational dynamics that are in most cases solved through the N-body method. The gas component of baryons is described through the equations of hydrodynamics. Various astrophysical processes must also be considered to achieve a realistic galaxy population. Many of these are implemented through effective sub-resolution models such as MUPPI. Credits: Vogelsberger et al. (2020).

### 4.1.1 Simulating dark matter

Dark matter particles system is described by the collisionless Boltzmann equation coupled to Poisson's equation. This pair of equations should be solved in the expanding background Universe described by the Friedman's equations, which are derived from the field equations of general relativity, but most cosmological simulations use Newtonian rather than relativistic gravity, to reduce the expensive computational cost.

The dynamical evolution is therefore followed with N-body methods, where the phase-space density is sampled by an ensemble of $N$ phase-space points $r_i$, $v_i$, $i = 1 \dots N$ with masses $m_i$. This grained sampling implies that a large number of particles is desirable to reduce Poisson noise and increase the resolution of the simulation, but it is limited, on the other hand, by the computational power. Therefore, a particle can be interpreted as a Monte Carlo estimate of a portion of the total phase-space volume, i.e. a smoothed density field. The main consequence is that the gravitational interactions between nearby particles must be softened on small scales to avoid unphysical two-body scattering. To efficiently solve the collisionless Boltzmann equation and calculate the gravitational forces between particles, several techniques have been developed: (i) particle-mesh method (Hockney and Eastwood, 1981), that considers the differential form of Poisson's equation and calculates the gravitational forces using a fast Fourier transform-based methods in adaptive-mesh-refinement schemes; (ii) the tree-particle approach (Barnes and Hut, 1986), that solves the integral form of Poisson equation with a direct summation of contributions of close particles, while distant ones are approximated by the lowest-order terms of a multipole expansion of the mass distribution; (iii) tree particle-mesh method (Efstathiou et al., 1985; Bode and Ostriker, 2003), a hybrid scheme that combines direct summation-based techniques, for short-range forces, with Fourier transform-based methods, for long-range forces. Finally, some integration tools afford adaptive softening schemes to reduce the softening length in high-density regions to reach higher spatial force resolution (Price and Monaghan, 2007).

### 4.1.2 Simulating baryons and astrophysics

The visible components of galaxies consist of baryons, distributed in gas and stellar populations. Of course, simulating properly these components is mandatory and crucial to making predictions for the visible Universe and Local Cosmology.

In cosmological simulations, baryons initial positions and velocities are usually set using the so-called zoom-in techniques: on top of a low-resolution background realization of the density fields computed with dark matter-only simulation, a region of interest is selected and a high-resolution simulation is reinitialized with the introduction of gas and stellar particles. Some simulations are aimed to mimic the Local Group environment using well-defined constrained initial conditions to reproduce not only a Milky Way-like galaxy but also its formation and evolution history (e.g. Sawala et al., 2016; Carlesi et al., 2016).

If stellar particles can be described, similarly to dark matter ones, as a collisionless fluid, astrophysical gases are typically described as ideal gases and require to include hydrodynamics in cosmological simulations (Lucy, 1977; Springel, 2010; Price, 2012). The hydrodynamical equations can be discretized in different ways, but commonly the Smoothed Particle Hydrodynamics (SPH hereafter) is the most widely used mesh-free technique. It is based on Lagrangian methods "for approximating the continuum dynamics of fluids through the use of sampling particles, which may also be viewed as interpolation points, following the equations of motion derived from the hydrodynamical equations" (Vogelsberger et al., 2020).

These equations have to be complemented by various astrophysical processes that model among others gas cooling, interstellar medium, star formation, stellar and supernovae feedback, chemical enrichment, AGNs, Supermassive Black Holes, magnetic fields, cosmic rays, etc. Most of these processes are implemented through the so-called sub-resolution models, which are necessary due to the limited numerical resolution of simulations. In other words: "every process that is not explicitly resolved in a simulation implementing only fundamental laws of physics is defined to be sub-resolution" (Murante et al., 2015).

### 4.1.3 Gravity in classic N-body simulations

To conclude this brief review, it is not meaningless, according to the main goals of this Thesis, to emphasize once again the gravitational interactions between particles in such classic cosmological simulations. Indeed, the dynamical evolution of classic N-body methods – whether they are based on particle-mesh, tree-particle or hybrid schemes, in other words, whether there are long or short-range gravitational forces – is provided by Newtonian gravity that is smoothed at short ranges introducing a gravitational softening

length $\epsilon$.

Therefore, the evolution of a collisionless self-gravitating system is described by two coupled equations: the collision-less Boltzmann equation (also called Vlasov equation),

$$\frac{\partial f}{\partial t} + \mathbf{v} \cdot \frac{\partial f}{\partial \mathbf{r}} - \nabla\Phi \cdot \frac{\partial f}{\partial \mathbf{v}} = 0, \tag{4.1}$$

where $f = f(\mathbf{r}, \mathbf{v}, t)$ is the one-particle distribution function and $\Phi(\mathbf{r}, t)$ is the gravitational potential, and Poisson's equation,

$$\nabla^2\Phi = 4\pi G\rho = 4\pi G \int d\mathbf{v} f. \tag{4.2}$$

N-body simulations use a Monte-Carlo method to solve these equations. The distribution function is represented by a collection of N particles

$$f(\mathbf{r}, \mathbf{v}, t) = \sum_{i=1}^{N} m_i \delta^3(\mathbf{r} - \mathbf{r}_i(t))\delta^3(\mathbf{v} - \mathbf{v}_i(t)), \tag{4.3}$$

where $m_i$, $\mathbf{r}_i$, and $\mathbf{v}_i$ are the mass, position, and velocity of particle $i$. Over time, particles move along characteristics of 4.1; at each instant, their positions provide the density needed for 4.2.

The best approach to account for gravity is to include it directly into the discretized SPH approach, which has the advantage of also allowing a consistent treatment of variable gravitational softening lengths.

Following Springel (2010), let $\Phi(\mathbf{r}) = G\sum_i m_i \phi(\mathbf{r} - \mathbf{r}_i, \epsilon_i)$ be the gravitational field described by the SPH point set, where $\epsilon_i$ is the gravitational softening length of particle $i$. We then define the total gravitational self-energy of the system of SPH particles as

$$E_{pot} = \frac{1}{2}\sum_i m_i \Phi(\mathbf{r}_i) = \frac{G}{2}\sum_{i,j} m_i m_j \phi(r_{ij}, \epsilon_j). \tag{4.4}$$

As a result, the equation of motion acquires an additional term due to the gravitational forces, given by:

$$m_i \mathbf{a}_i^{\text{grav}} = -\frac{\partial E_{pot}}{\partial \mathbf{r}_i} \tag{4.5}$$

$$= -\sum_j G m_i m_j \frac{\mathbf{r}_{ij}}{r_{ij}} \frac{[\phi'(r_{ij}, \epsilon_i) + \phi'(r_{ij}, \epsilon_j)]}{2} \tag{4.6}$$

$$-\frac{1}{2}\sum_{jk} G m_j m_k \frac{\partial \phi(r_{jk}, \epsilon_i)}{\partial \epsilon} \frac{\partial \epsilon_j}{\partial \mathbf{r}_i}, \tag{4.7}$$

where $\phi'(r,\epsilon) = \partial\phi/\partial r$. The first sum on the right-hand side describes the ordinary gravitational force, where the interaction is symmetrized by averaging the forces in case the softening lengths between an interacting pair are different. The second sum gives an additional force component provides by the adaptive gravitational softening schemes, i.e. when the gravitational softening lengths are a function of the particle coordinates themselves (Price and Monaghan, 2007; Bagla and Khandai, 2009).

In most cosmological SPH codes of structure formation, a fixed gravitational softening is usually used for collisionless dark matter particles and SPH particles alike. Then, the equations of motion integrated into many algorithms are

$$\frac{d\mathbf{r}_i}{dt} = \mathbf{v}_i \tag{4.8}$$

$$\frac{d\mathbf{v}_i}{dt} = \sum_{j\neq i}^{N} G m_j \frac{\mathbf{r}_j - \mathbf{r}_i}{(|\mathbf{r}_j - \mathbf{r}_i|^2 + \epsilon^2)^{3/2}}, \tag{4.9}$$

where $\epsilon$ is the Plummer softening length. Therefore, increasing the force resolution means decreasing the force softening length. This is allowed within regions of high mass resolution where the particle number is enhanced; elsewhere, the force softening length must remain large to avoid collisionality. These equations reduce to the standard Newtonian equations of motion if $\epsilon = 0$. In this sense, softening can also be described as a smoothing operation (i.e. they are mathematically equivalent, see e.g. Hernquist and Barnes, 1990; Barnes, 2012), or a Monte Carlo representation of the density field convolved with the predefined kernel such as Plummer's kernel (as in Eq. 4.9) or other softening prescriptions (e.g. Dehnen, 2001).

Despite most cosmological simulations use Newtonian rather than relativistic gravity, modern galaxy formation simulations are extremely sophisticated and powerful, reproducing numerous observational results (such as galactic structures formation and evolution, chemo-kinematic properties of stellar populations, etc.) and creating virtual universes that are, to first order, close to the real Universe. What follows provides the initial description of Aquila-C-4 (AqC4), a hydrodynamical cosmological simulation of a Milky Way-mass galaxy based on the MUlti Phase Particle Integrator sub-resolution model (MUPPI hereafter Murante et al., 2010; Murante et al., 2015). With this simulation, in the next chapter, the formation history of a Milky Way-like galaxy was investigated and compared to Gaia DR2 data. The results of

this study are published in Giammaria et al. (2021).

## 4.2 The AqC4 simulation framework

Many authors have produced and analysed high-resolution simulations based on different cosmological backgrounds and initial conditions. Some of these projects are listed in Table 4.1 and in Vogelsberger et al. (2020), while detailed chemo-dynamical comparisons are presented by Minchev, Chiappini, and Martig (2013), Stinson et al. (2013), Buck et al. (2019), and Grand et al. (2020).

In Giammaria et al. (2021), we considered the AqC4 simulation, which belongs to the AqCs series that has been presented by Springel et al. (2008) and used, among other works, in the Aquila comparison project (Scannapieco et al., 2012). It consists of a cosmological hydrodynamical simulation that was carried out with the TREEPM+SPH GADGET3 code, a non-public evolution of the GADGET2 code (Springel, 2005). The Initial Conditions (ICs) adopted were introduced by Springel et al. (2008) and based on zoom-in techniques. It is an unconstrained simulation, opposed to constrained ones aimed at perfectly mimicing the Local Group (Sawala et al., 2016; Carlesi et al., 2016). Thus, according to the precepts of Local Cosmology, AqC4 results in a typical cosmological product. It represents a possible realization of the Galaxy, with mass and phase-space properties similar to the Milky Way, and with a merging history comparable to a disc-like galaxy.

### 4.2.1 Cosmological parameters

The cosmological model adopted to compute the simulation is the ΛCDM with the following parameters: $\Omega_{\rm m} = 0.25$, $\Omega_\Lambda = 0.75$, $\Omega_{\rm baryon} = 0.04$, $H_0 = 73$ km s$^{-1}$ Mpc$^{-1}$, $\sigma_8 = 0.9$ and $n_s = 1$. The Plummer softening length for the computation of the gravitational force is $\epsilon_{\rm Pl} = 163\ h^{-1}$ pc, where $h = H_0/100$ represents the reduced Hubble constant. Dark matter particles have a typical mass of $2.7 \cdot 10^5\ h^{-1}\ {\rm M}_\odot$, and the initial mass of gas particles is $5.1 \cdot 10^4\ h^{-1}\ {\rm M}_\odot$. From the dark matter-only, parent simulation, having a cosmological volume of $100\ (h^{-1}\ {\rm Mpc})^3$, a zoomed-in region of interest has been extracted.

In this realization, the ICs provided an isolated dark matter halo at redshift $z = 0$, with a virial mass of $M_{\rm vir} \sim 1.627 \cdot 10^{12}\ {\rm M}_\odot$ within a spherical volume of $r_{\rm vir} = 237.13$ kpc. The virial quantities are those calculated in

**Table 4.1:** Comparison of mass particles and softening limits for recent high resolution zoom-in cosmological simulations.

| Project | mass particle [$M_\odot$] | softening [pc] | reference |
|---|---|---|---|
| Eris | $M_{DM} \sim 1 \cdot 10^5$ | $\epsilon_* \sim 120$ | Guedes et al. (2011) |
| | $M_{gas} \sim 2 \cdot 10^4$ | $\epsilon_{gas} \sim 120$ | |
| Auriga | $M_{DM} \sim 3 \cdot 10^5$ | $\epsilon_{star} \sim 369$ | Grand et al. (2017) |
| | $M_{gas} \sim 5 \cdot 10^4$ | $\epsilon_{gas} \sim 180$ | |
| GIZMO | $M_{DM} \sim 3 \cdot 10^5$ | $\epsilon_{star} \sim 50$ | Ma et al. (2017) |
| | $M_{gas} \sim 6 \cdot 10^4$ | $\epsilon_{gas} \sim 14$ | |
| Illustris | $M_{DM} \sim 7 \cdot 10^6$ | $\epsilon_{star} \sim 740$ | Nelson et al. (2018) |
| TNG100 | $M_{gas} \sim 1 \cdot 10^6$ | $\epsilon_{gas} \gtrsim 185$ | |
| EAGLE | $M_{DM} \sim 1 \cdot 10^6$ | $\epsilon_{star} \sim 700$ | Mackereth et al. (2019) |
| | $M_{gas} \sim 2 \cdot 10^5$ | $\epsilon_{gas} \lesssim 350$ | |
| NIHAO-UHD | $M_{DM} \sim 1 \cdot 10^5$ | $\epsilon_{star} \sim 273$ | Buck et al. (2020) |
| (g7.08e11) | $M_{gas} \sim 2 \cdot 10^4$ | $\epsilon_{gas} \sim 273$ | |
| AqC4 | $M_{DM} \sim 3 \cdot 10^5$ | $\epsilon_{star} \sim 163$ | Giammaria et al. (2021) |
| | $M_{gas} \sim 4 \cdot 10^4$ | $\epsilon_{gas} \sim 163$ | |

a sphere centred on the minimum of the gravitational potential of the halo, which encloses an over-density of 200 times the critical density at present time. The virial mass is consistent with the range of values $0.5 - 2 \cdot 10^{12}$ $M_\odot$ of current Galactic estimates (Bland-Hawthorn and Gerhard, 2016). In particular, the dynamics of globular clusters based on Gaia DR2 data gives $M_{vir} \sim 1.3 \cdot 10^{12}$ $M_\odot$ (Posti and Helmi, 2019b; Watkins et al., 2019b), while studies on the Milky Way rotation curve provide $M_{vir} \sim 1 \cdot 10^{12}$ $M_\odot$ (Eilers et al., 2019; Crosta et al., 2020). The simulation counts a total number of dark matter, gas and stellar particles respectively of 5 518 587, 1 348 120, and 6 919 646 at redshift $z = 0$ within the virial volume.

### 4.2.2 The sub-resolution model MUPPI

As anticipated previously, any SPH cosmological simulation requires a model to describe the sub-resolution evolution of baryons. In AqC4, the model implemented is called MUPPI, accurately presented in Murante et al. (2010) and Murante et al. (2015) and whose validity has been confirmed by several studies (Monaco et al., 2012; Goz et al., 2015; Valentini et al., 2017). Its most relevant features are outlined below.

The MUPPI model describes a multiphase interstellar medium (ISM). A short list of the most important processes implemented is the star formation and stellar feedback, metal cooling and chemical evolution. It accounts for

hot and cold ($T = 300$ K) gas phases in pressure equilibrium utilizing multiphase particles, which are the building blocks of the model. A gas particle enters a multiphase stage if its density increases above a density threshold ($n = 0.01$ cm$^{-3}$) and its temperature drops below a temperature threshold ($T = 10^5$ K).

The mass and energy flows among different components within each multiphase particle (depicted in Fig. 4.2) is described by a set of ordinary differential equations as follows:

$$\dot{M}_\star = \dot{M}_{SF} - \dot{M}_{re} \tag{4.10}$$

$$\dot{M}_c = \dot{M}_{cool} - \dot{M}_{SF} - \dot{M}_{ev} \tag{4.11}$$

$$\dot{M}_h = -\dot{M}_{cool} + \dot{M}_{re} + \dot{M}_{ev} \tag{4.12}$$

$$\dot{E}_h = \dot{E}_{heat,local} - \dot{E}_{cool} + \dot{E}_{hydro} \tag{4.13}$$

where $M_\star$, $M_c$ and $M_h$ are the masses of the hot, cold and stellar components within each SPH particle of mass $M_{SPH}$ (Murante et al., 2015). The mass (or energy) flows are computed as the time derivative of the corresponding quantity and indicated as $\dot{M}_i$ (or $\dot{E}_i$). $\dot{M}_{cool}$ is the cooling flow that moves mass from the hot into the cold phase, while a tiny fraction of the cold gas evaporates due to the destruction of molecular clouds. $\dot{M}_{SF}$ represents the Star Formation Rate (SFR) that increase $M_{star}$ at the expense of $M_c$. $\dot{M}_{ev}$ is the evaporation rate assumed to be proportional to the SFR, while $\dot{M}_{re}$ is the restoration (or recycling) term performed by the chemical evolution code (Tornatore et al., 2007). Finally, $\dot{E}_{heat,local}$ accounts for the contribution of SN energy from stars formed in the same multiphase particle, $\dot{E}_{cool}$ is the energy losses by cooling, and $\dot{E}_{hydro}$ takes into account the energy due to interactions with the neighbour particles.

The phenomenological prescription to estimate the fraction of cold gas which is in the molecular phase and which fuels star formation is provided by Blitz and Rosolowsky (2006). Star formation is then modelled according to the stochastic algorithm introduced by Springel and Hernquist (2003): as a consequence, a multiphase gas particle can generate up to four generations of star particles.

The MUPPI model features stellar feedback both in thermal and kinetic forms (as described in Murante et al., 2015). Besides stellar feedback in energy, star formation and evolution also result in chemical feedback, and galactic outflows generated by supernova (SN) explosions promote the metal

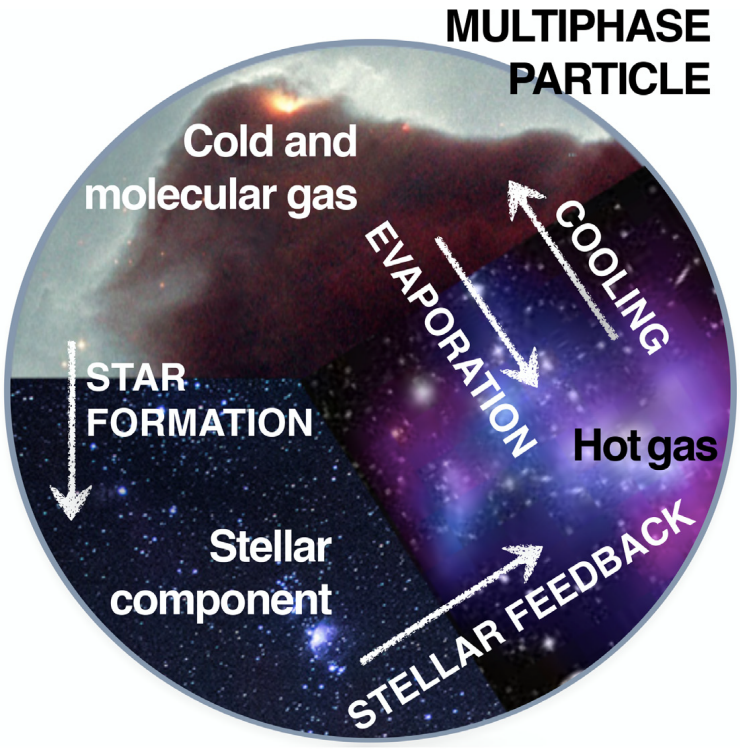


**Figure 4.2:** Cartoon from Valentini et al. (2019) showing the composition of a multiphase gas particle within the MUPPI model. Mass and energy flows among different components are highlighted with arrows.

spread and circulation within the galaxy (Valentini et al., 2017; Valentini et al., 2018). The model accounts for stellar evolution and chemical enrichment following Tornatore et al. (2007), where a thorough description can be found.

According to SPH simulations, each stellar particle should be considered as a simple stellar population. Assuming an initial mass function (Kroupa, Tout, and Gilmore, 1993), as well as predictions for stellar lifetimes (Padovani and Matteucci, 1993) and stellar yields (see Murante et al., 2015, for details), at each time integration step, the number of stars ageing and eventually exploding as SNe, and the amount of metals injected in the ISM is evaluated. Heavy elements released by star particles are distributed to neighbouring gas particles. For each gas particle the code tracks the mass in H, He and in several other chemical species, namely C, Ca, O, N, Ne, Mg, S, Si, Fe, Na, Al, Ar, Ni, synthesized by different sources (namely asymptotic giant branch stars, SNe Ia and SNe II). The chemical evolution is individually followed and the model also features metallicity-dependent radiative cooling (following Wiersma, Schaye, and Smith, 2009) and includes the effect of an ionizing cosmic background (Haardt and Madau, 2001). When a star particle is spawned, its composition is taken as the parent gas particle.

# Chapter 5

# Formation History of the Milky Way disc

*This chapter is a slightly modified version of Giammaria, Spagna, Lattanzi, Murante, Re Fiorentin, and Valentini (2021) published in Monthly Notices of the Royal Astronomical Society, 502, 2, 2251–2265.*

Given the premise of the previous chapter, AqC4 represents a theoretical "error-free" catalogue predicted for a Milky Way-like galaxy. Then, in Giammaria et al. (2021), such simulation was compared to our Galaxy and Gaia DR2 data carrying out the analyses as if it were a real stellar survey. Only the baryonic particles contained in a spherical volume defined by the galactic radius $r_{\rm gal} = 1/10\, r_{\rm vir}$ were considered.

The aim was to investigate a Milky Way-like galaxy as a product of the cosmological evolution according to the predictions of Local Cosmology. To do that, the spatio-kinematic distributions of the stellar disc were characterised in particular in a simulated region representative of the Solar Neighbourhood. Then, the Star Formation History (SFH) of AqC4 in the redshift range $0 < z \lesssim 2$ was also analysed to identify signatures of past and recent merging events that can be used to disentangle the accretion history of our Galaxy.

## 5.1 The spatial distribution of the AqC4 disc

Fig. 5.1 shows the face-on and edge-on projected density of stellar (upper panels) and gas (lower panels) particles. The reference system used is centred in the minimum of the gravitational potential and rotated to be aligned with the angular momentum vector of multiphase gas and stellar particles within 8 kpc from the centre, while the $XY$ plane is orthogonal to it. This reference system has been adopted for the entire analysis

presented here as well as in Giammaria et al. (2021), using cylindrical coordinates $(R, \phi, Z)$, and relative velocity components $(V_R, V_\phi, V_Z)$.

The visual inspection easily reveals the presence of a disc structure both in the stellar and gas distribution dominating the central part of the galactic volume until $R \sim 10$ kpc. The stellar disc is quite symmetric around the $XY$ plane, hereafter the galactic plane. Small stellar over-densities, recalling a spiral pattern, are visible in the outer part of the disc, while the gas distribution exhibits a warped shape at its edge extended till the halo regions. Finally, in the innermost central region, a non-axisymmetric bar structure is visible in both components.

Through the stellar mass distribution as a function of the orbit circularity of all stellar particles within $R_{\rm gal}$ at redshift $z = 0$, it is possible to quantitatively verify that AqC4 is a disc-dominated galaxy like the Milky Way. The circularity of an orbit is defined as $e = J_Z/J_{\rm circ}$, where $J_Z$ is the specific angular momentum in the direction perpendicular to the disc, and $J_{\rm circ}$ is the specific angular momentum of a reference circular orbit at that radius. The results are shown in Fig. 5.2. The prominent peak at $e \sim 1$ demonstrates that AqC4 is characterised by a disc structure, with a bulge component corresponding to the smaller peak at $e \sim 0$.

Scannapieco et al. (2010) defined the "dynamical" ratio of bulge-over-total stellar-mass $B/T$ by doubling the mass of the counter-rotating stars (i.e. those with $e < 0$) within $R_{\rm gal}$, under the hypothesis that the bulge is supported by velocity dispersion and thus has an equal amount of co- and counter-rotating stars. The resulting ratio for AqC4 is $B/T = 0.34$, fairly comparable to the upper limit estimated for the Milky Way, $B/T_{\rm MW} \simeq 0.15 - 0.33$ (see e.g. Bland-Hawthorn and Gerhard, 2016; Bell et al., 2017, and references therein).

### 5.1.1 Radial scale length of the stellar disc

As described in Chapter 3, it is common to divide the stellar disc of the Milky Way in two components, namely the thin and thick disc, characterizing both with a double exponential decay profile in the radial and vertical direction. Bland-Hawthorn and Gerhard (2016) reports that for the Galaxy the radial scale length of thin and thick discs are $h_{\rm Rt} = 2.6 \pm 0.5$ kpc and $h_{\rm RT} = 2.0 \pm 0.2$ kpc, respectively. On the other hand, the thin disc scale height at solar distance from the Galactic center is $h_{\rm Zt} = 300 \pm 50$ pc, while for the thick disc is $h_{\rm ZT} = 900 \pm 180$ pc. Moreover, the relative density normalization $f = \rho_{\rm T}/\rho_{\rm t}$ of the thick disc compared to the thin disc is estimated ranging

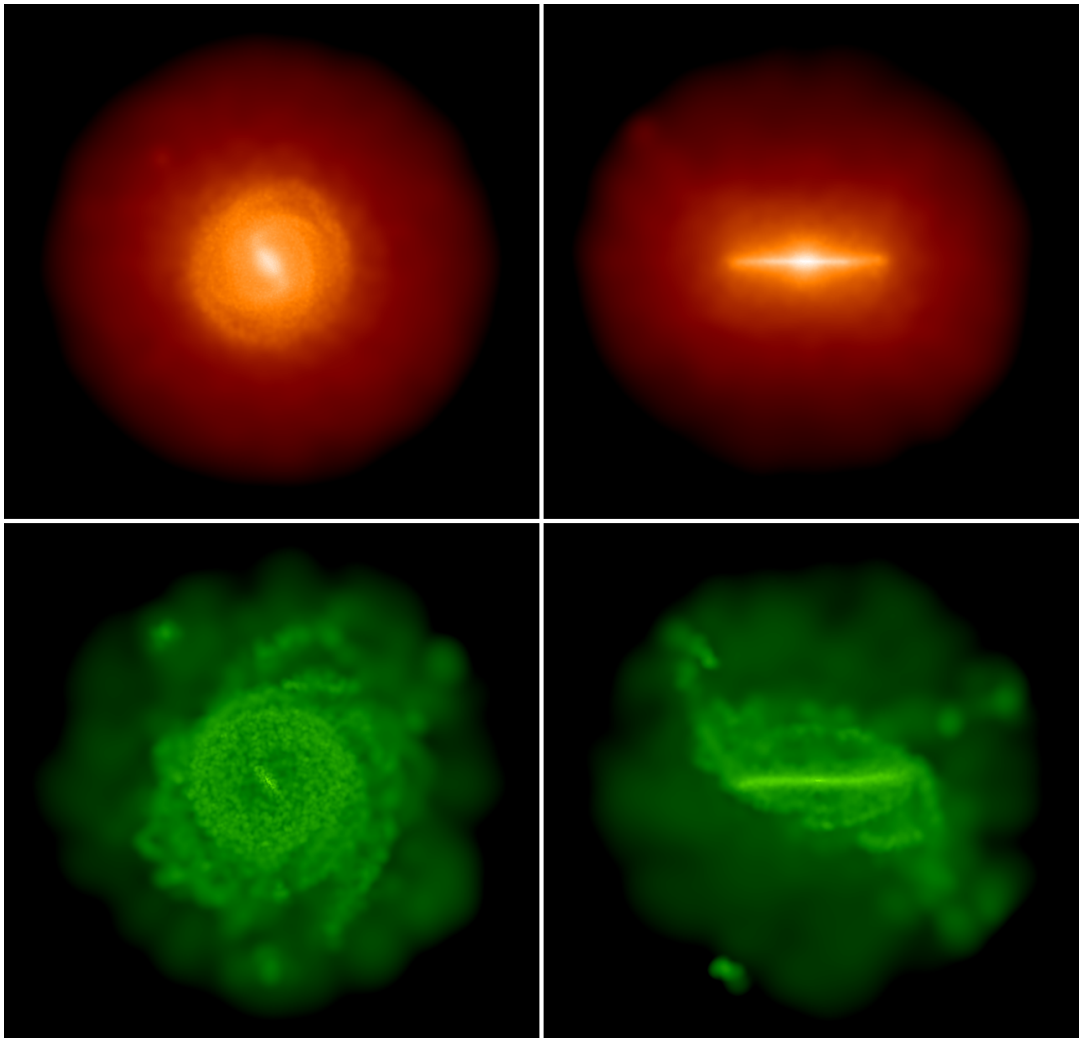

**Figure 5.1:** Stellar (upper panels) and gas (lower panels) projected density for the AqC4 simulation (face-on and edge-on view on left and right panels, respectively). The $Z$-axis of the coordinate system is aligned with the angular momentum vector of multiphase gas and stars enclosed within 8 kpc from the position of the minimum of the gravitational potential. The box is 50 kpc on a side.

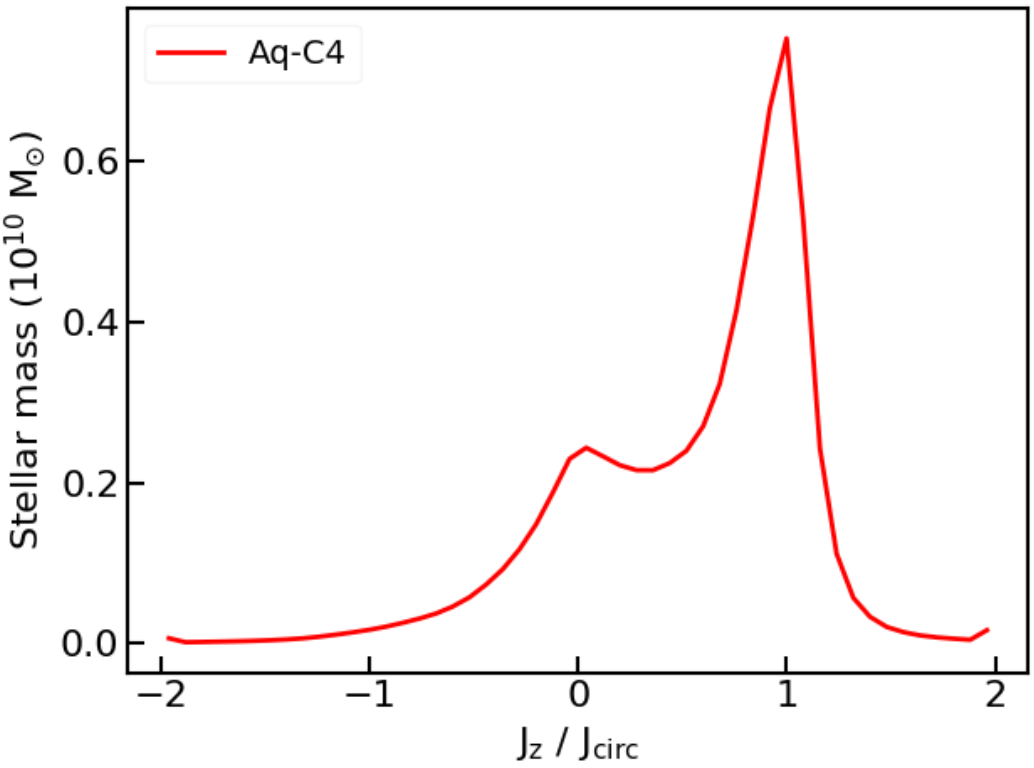


**Figure 5.2:** Distribution of the stellar mass of AqC4 as a function of the orbit circularity $e$ for all stellar particles within $R_{\rm gal}$ at redshift $z = 0$.

from 6 to 12 per cent (e.g. Jurić et al., 2008; Just and Jahreiß, 2010b; Bovy et al., 2015).

In order to disentangle the radial and vertical dependencies of the density, let us focus first on the radial extension of the stellar disc of AqC4. The mass density (in $M_\odot$ pc$^{-3}$) is computed in cylindrical radial bins of $\Delta R = 0.25$ kpc, for all the star particles that lie within a height on the galactic plane $|Z| \leq 1$ kpc, where the thin disc should dominate because of its lower scale height and the relative density normalization $f$. Then, to infer the scale length, we limit the fit in the disc-dominated region between $2.5 \leq R[\text{kpc}] \leq 9$ (solid black lines) as shown in Fig. 5.3 (note the logarithmic scale on the $y$-axis).

By mean of the Python package PyMC3 (Salvatier, Wiecki, and Fonnesbeck, 2016), an MCMC Bayesian algorithm is implemented for this and the following analyses to take into account the mass of single stellar particles, and the Poissonian statistics within each bin. In this way, we verified that the softening resolution limit of the simulation, $\epsilon = 0.163$ kpc, slightly influenced the uncertainties induced by the binning procedure. Setting the Credible Interval (CI) as the $\pm 1\sigma$ equivalent range between the 16$^{\rm th}$ and 84$^{\rm th}$ percentile

of the posterior distribution[1], it results in a very small change, thinner than the best-fit line in the figure.

Unfortunately, the attempt to identify a radial separation between thin and thick disc for AqC4 did not provide significant outcomes, probably due to the resolution of the simulation that limited the radial sampling of the disc. Also, considering a larger vertical cut of $|Z| \leq 2$ –3 kpc does not help, because it increases the contamination by halo stars. Thus, the model selection supports a single-components disc for AqC4 with an estimated radial scale length of $h_{\rm R} = 2.058 \pm 0.002$ kpc. This value is $\sim 21$ per cent smaller than the Milky Way thin disc.

The latter result produces a first important consequence on the economy of the present research work: since one of the main goals is to use the Milky Way as a keystone for disc-like galaxies and Local Cosmology, it is convenient to define a proportionally smaller Simulated Solar Ring (SSR) to reproduce the simulated analogue of the Solar Neighbourhood. For this reason, the SSR was set to $6 \leq R[\text{kpc}] \leq 7$ in Giammaria et al. (2021) with respect to a distance between the Sun and the Galactic center of $R_{\odot} = 8.122 \pm 0.033$ kpc as estimated by the Gravity Collaboration et al. (2018).

### 5.1.2 Vertical distribution of the stellar disc in the SSR

Having defined the SSR as in the previous section, it is now possible to study the vertical mass distribution of the AqC4 disc. In order to reduce the contamination from halo stars, only the 320 354 stellar particles in the SSR within $|Z| \leq 3$ kpc are considered to fit simultaneously a double-component disc described as follows:

$$\rho(Z) = A\left(e^{-\frac{|Z|}{h_1}} + f \cdot e^{-\frac{|Z|}{h_2}}\right), \tag{5.1}$$

where $A$ is the total density normalization, $f$ is the relative density normalization, $h_i$, for $i = 1, 2$, is the scale height of the two components of the disc, and $Z$ is the vertical coordinate. As for the radial scale length, the uncertainties take into account the Poissonian statistic within each bin and are smaller than the size of single data points in the plot of Fig. 5.4. Consequently, the CIs are very narrow and we obtain well-peaked posteriors on the parameters estimates.

[1] the percentage corresponding to a $1\sigma$ range in a Gaussian distribution

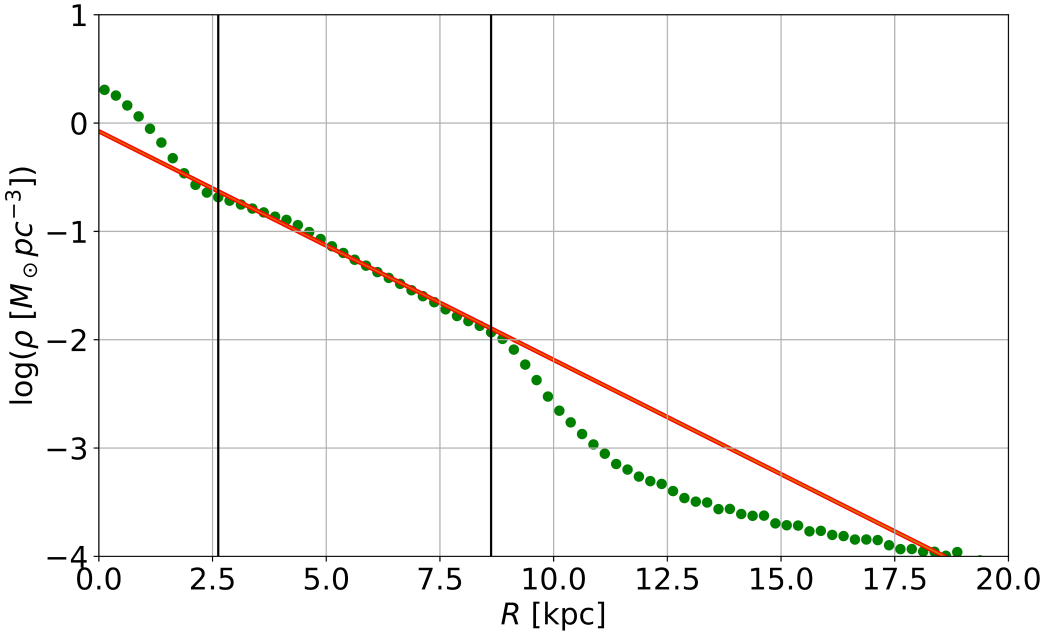


**Figure 5.3:** Radial density distribution (green dots) of stellar particles with $|Z| \leq 1$ kpc from the galactic plane computed in radial bins of $\Delta R = 0.25$ kpc. Error bars are smaller than the size of data point. The red line represents the best fit obtained from the posteriors of the MCMC analysis. The CI is thinner than the best fit red line. The vertical black lines show the radial interval adopted for the fit.

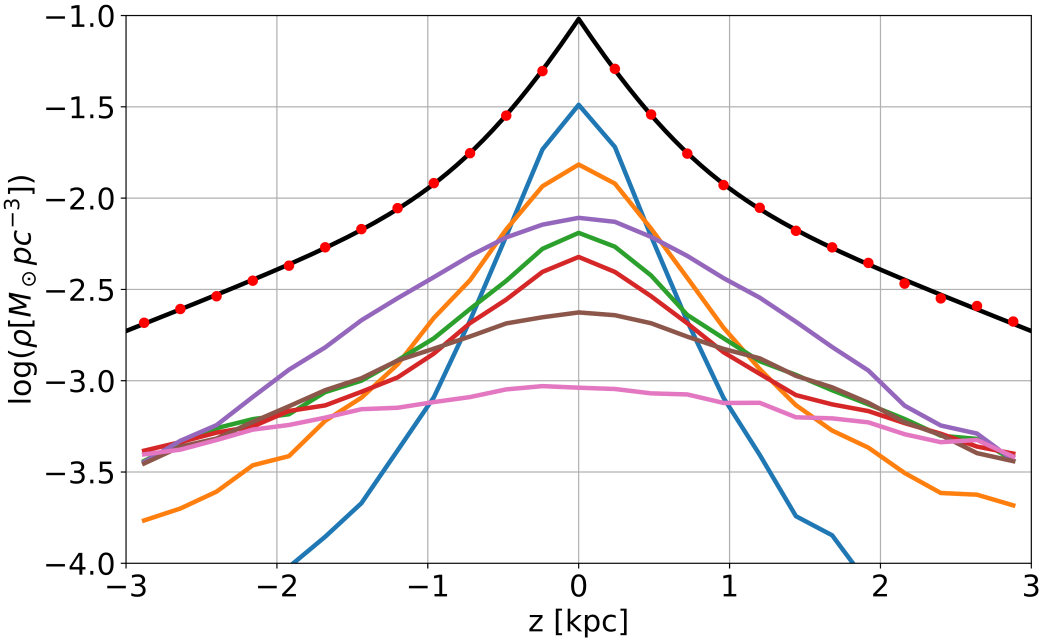


**Figure 5.4:** Vertical density distribution (red dots) of stellar particles in the SSR with $|Z| \leq 3$ kpc computed in vertical bins of $\Delta Z = 0.25$ kpc. The black line represents the best fit obtained from the posteriors of MCMC analysis with a CI thinner than the best-fit line. Colour lines represent mono-age stellar populations divided in bins of 2 Gyr as listed in Table 5.1.

Despite the radial density investigation, it is interesting that here we can distinguish two components of the disc notwithstanding the resolution limit of the simulation. The estimated scale heights are $h_1 = 0.305 \pm 0.005$ kpc that is in good agreement with the Milky Way thin disc, and $h_2 = 1.33 \pm 0.02$ kpc that is $\sim$ 50 per cent larger than what is observed in the Milky Way thick disc. Moreover, the relative density parameter of $f = 22.6 \pm 0.7$ per cent is 2–3 times larger with respect to the Milky Way (Bland-Hawthorn and Gerhard, 2016). The posterior distributions, shown in Fig. 5.5, highlight that $h_1$ and $h_2$ are positively correlated, and they are both negatively correlated with the relative density normalization $f$ indicating the intrinsic physical overlapping of the two disc components.

To improve our understanding of the stellar disc, in Fig. 5.4 we give the distributions, shown as coloured lines, of stellar sub-samples formed in 2 Gyr time bins according to Table 5.1. These bins represent mono-age stellar populations that can be aggregated in four main components:

- the *young disc* (blue and orange lines): the dominating fraction of the stellar population in the SSR (almost 40 per cent of the sample) with

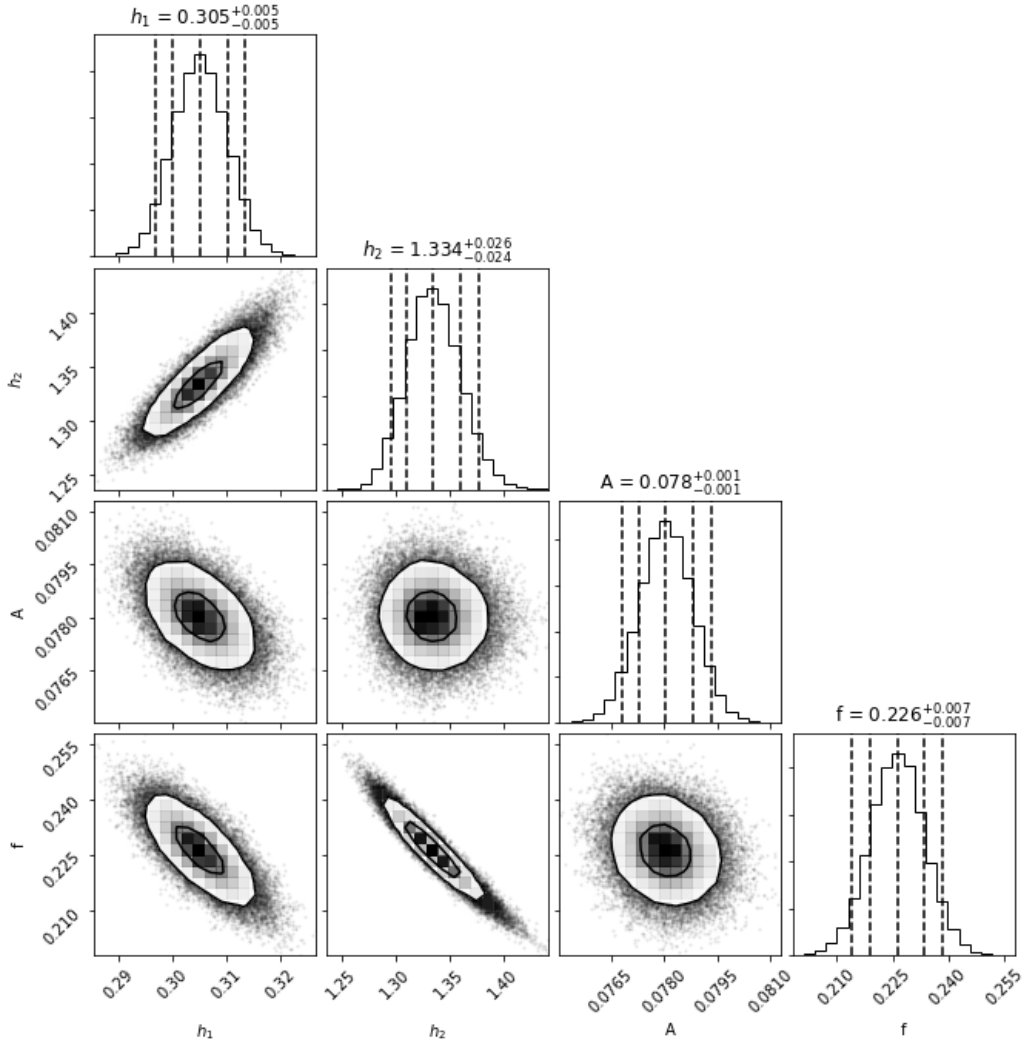


**Figure 5.5:** Posterior distributions of the MCMC analysis for the vertical stellar particles distribution in the SSR. The 1D (histogram) posterior distributions for each parameter are shown on the diagonal, while the other panels represent the 2D (contours) correlations. Dashed lines in each histogram refer to the $10^{\text{th}}$, $16^{\text{th}}$, $50^{\text{th}}$ (i.e. median), $84^{\text{th}}$ and $90^{\text{th}}$ percentiles of the relative distribution, while numbers on top indicate the medians and the $1\sigma$ CIs. Thick black contours indicate the 1 and $2\sigma$ CI of the two-dimensional correlations of the posteriors.

**Table 5.1:** Age and relative weights of the mono-age populations with respect to the total stellar particles ($N_0$) in the SSR ($6 \leq R[\text{kpc}] \leq 7$) within $|Z| \leq 3$ kpc.

| Colour | Age [Gyr] | $N/N_0$ |
|---|---|---|
| blue | 0-2 | 0.22 |
| orange | 2-4 | 0.18 |
| green | 4-6 | 0.12 |
| red | 6-8 | 0.10 |
| purple | 8-10 | 0.22 |
| brown | 10-12 | 0.10 |
| pink | 12-14 | 0.07 |
| black | 0-14 | $N_0$=320 354 |

ages up to 4 Gyr, showing an exponential decreasing from the galactic plane similar to the *thin disc*;

- the *intermediate disc* (green and red lines): 22 per cent of the sample with ages between 4 – 8 Gyr, whose vertical distribution clearly shows the superposition of a thin and a thick component;
- the prominent *thick disc* (purple line): the bulk of the "geometric" thick disc, corresponding to the 22 per cent of the sample with $8 \leq$ Age [Gyr] $\leq 10$;
- the *spheroidal oldest* population (brown and pink lines) with age greater than 10 Gyr that shows a widespread distribution, and includes a large fraction of halo star particles.

The analysis of the scale heights and mono-age distributions reveals an SFH affected by significant changes over time in AqC4 and highlights that the evolution histories experienced by the Milky Way and the simulated galaxy enclose fundamental signatures to understand the origin of Galactic structures. These results are discussed in more detail in Sect. 5.3.

### 5.1.3 The radial disc flaring

Another important spatial feature which stems from the inside-out disc formation scenario is the *disc flaring* (see e.g. Minchev et al., 2017, and references therein). To investigate this property, it is possible to extend the latest study on the vertical distribution of AqC4 stellar particles to the whole radial extension of the disc.

As shown in Fig. 5.6, the star particles with $|Z| \leq 3$ kpc are binned as a function of the cylindrical radial distance in rings of $\Delta R = 1$ kpc. In each ring, the vertical density distribution of the whole stellar sample is fitted with the double exponential model of Eq. (5.1) to determine the variation of $h_1$ and $h_2$ parameters along with the disc. Then, the thickness of each mono-age population listed in Table 5.1 is estimated as the height, $h_Z$, where the density distribution decreases by a factor $e^{-1}$ with respect to the galactic plane $Z = 0$ kpc.

The results reported in Table 5.2 evidence that flaring is present for all mono-age populations and occurs at smaller radii for older populations as expected by the inside-out formation of the disc. In particular, the youngest population (Age $\leq 2$ Gyr) lies close to the galactic plane ($h_Z \lesssim 0.5$ kpc) along the whole disc up to $R \simeq 9$ kpc (cfr. Fig. 5.6), while the *intermediate disc* population ($4 \leq$ Age[Gyr] $\leq 8$) flares already at $R \simeq 6$ kpc with a steep increase towards larger radii. The prominent *thick disc* population (i.e. $8 \leq$ Age[Gyr] $\leq 10$) shows a thickness $h_Z \simeq 1.0 - 1.2$ kpc in the SSR at $R = 6 - 7$ kpc that is pretty close to the scale height $h_2 \simeq 1.33$ kpc previously reported. A radial flaring is already apparent at $R \simeq 4$ kpc, but it shows a milder increase at larger radii than the younger populations.

Recalling that in the SSR the vertical density of stellar particles appears described by a double-component exponential profile (Fig. 5.4), the presence of coeval stars evidences that heterogeneous populations were possibly formed by different progenitors. This is the case of *thick disc* stellar particles that were born in the same period of the starburst at $z \simeq 1.5$ (see Sect. 5.3) and formed the primordial disc. Therefore, the presence of this prominent old population can represent a signature of one of the most important mergers in the accretion history of AqC4 that mimic the GSE event experienced by the Milky Way (Belokurov et al., 2018; Helmi et al., 2018; Di Matteo et al., 2019; Vincenzo et al., 2019; Gallart et al., 2019).

These results support the global top-down and inside-out disc formation model and are consistent with previous observations of the Milky Way (e.g. Muñoz-Mateos et al., 2011; González Delgado et al., 2014; Bovy et al., 2016, where in the latter the authors used mono-abundance populations in the Milky Way instead of mono-age ones) and simulations (Stinson et al., 2013; Grand et al., 2017; Valentini et al., 2019). The analysis confirms what are discussed above: the rigid two-disc decomposition is a "simplified" mathematical description of a more complex physical scenario which implies an overlapping of different mono-age profiles for several stellar generations with

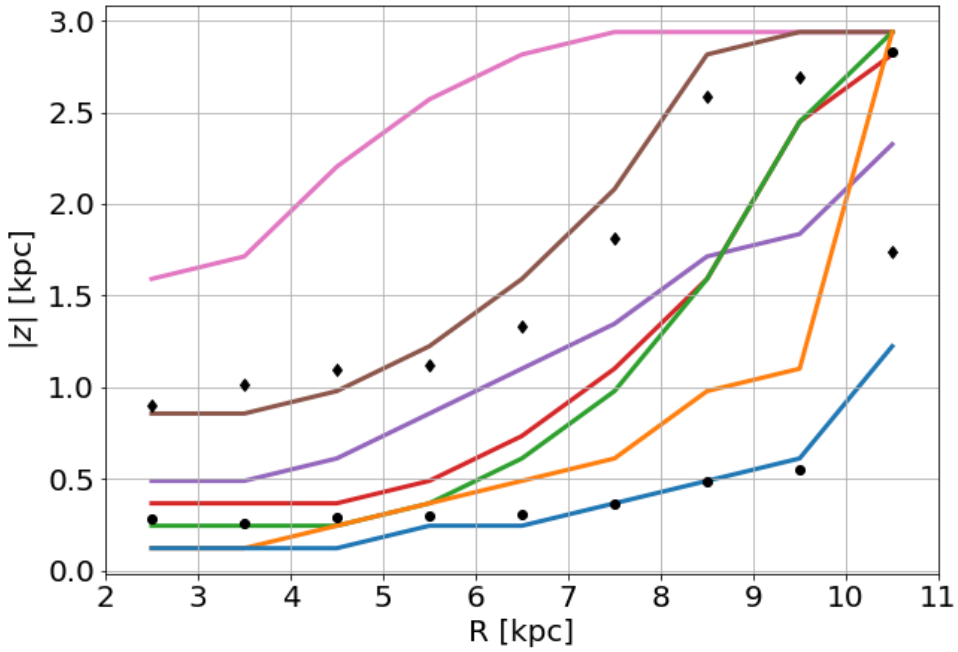


**Figure 5.6:** Variation of stellar height, $|Z|$, with $R$. Flaring is present for all mono-age populations (colour code as in Table 5.1). Solid lines show when the density decays by a factor of $e^{-1}$. The $h_1$ and $h_2$ scale heights for each radial bin integrated over all stellar ages (see Table 5.2) are represented by circles and diamonds, respectively.

possibly different progenitors. Moreover, the peculiar disc formation history of AqC4 highlights the difficulties of distinguishing the different processes that occur during the evolution of a Milky Way-like galaxy, requiring kinematic investigation. It is perhaps superfluous to recall at this point that huge stellar surveys like Gaia are opening the door to this kind of analysis for a large portion of the Galaxy, making available the most important laboratory of Local Cosmology ever.

## 5.2 Kinematic properties of the AqC4 stellar disc

In this section the kinematics of the stellar populations of AqC4 at redshift $z = 0$ is discussed. Again, the *leitmotiv* of the analysis is the comparison with the Milky Way, applying the same methodology used for real stellar surveys. In the following, several investigations on the kinematic structures of the disc in the SSR, the AqC4's rotation curve and the velocity profiles as a function of $R$ of the mono-age stellar populations are presented.

**Table 5.2:** The $h_1$ and $h_2$ scale heights, and relative density normalization $f$ with the $1\sigma$ CI integrated over all the $N_\star$ stellar particles within each radial bin.

| $R$ [kpc] | $h_1$ [kpc] | $h_2$ [kpc] | $f$ [%] | $N_\star$ |
|---|---|---|---|---|
| 2-3 | $0.306^{+0.004}_{-0.003}$ | $0.897^{+0.005}_{-0.005}$ | $35.2^{+0.9}_{-0.9}$ | 767 311 |
| 3-4 | $0.256^{+0.002}_{-0.002}$ | $1.016^{+0.007}_{-0.007}$ | $13.2^{+0.3}_{-0.3}$ | 687 832 |
| 4-5 | $0.288^{+0.002}_{-0.002}$ | $1.09^{+0.02}_{-0.02}$ | $12.2^{+0.4}_{-0.4}$ | 592 207 |
| 5-6 | $0.297^{+0.003}_{-0.003}$ | $1.12^{+0.02}_{-0.02}$ | $21.1^{+0.7}_{-0.5}$ | 436 270 |
| 6-7 | $0.305^{+0.005}_{-0.005}$ | $1.34^{+0.02}_{-0.02}$ | $22.6^{+0.7}_{-0.7}$ | 320 354 |
| 7-8 | $0.362^{+0.007}_{-0.006}$ | $1.81^{+0.05}_{-0.05}$ | $22.0^{+0.9}_{-0.9}$ | 234 454 |
| 8-9 | $0.485^{+0.007}_{-0.007}$ | $2.6^{+0.1}_{-0.1}$ | $19.9^{+1.1}_{-1.1}$ | 171 674 |
| 9-10 | $0.55^{+0.02}_{-0.02}$ | $2.7^{+0.1}_{-0.1}$ | $46^{+2}_{-2}$ | 96 159 |
| 10-11 | $1.7^{+0.2}_{-0.2}$ | $2.8^{+0.7}_{-0.9}$ | $89^{+4}_{-4}$ | 46 019 |

### 5.2.1 Multi-component disc in the SSR

In Sect. 5.1.2 the stellar vertical distribution was modeled with the superposition of a thin disc ($h_1 \simeq 0.305$ kpc) and a thick disc ($h_2 \simeq 1.33$ kpc) that includes a residual contamination of halo star particles. To robustly support this result and extend the characterisation of AqC4 stellar disc beyond the determination of the scale lengths and scale heights, the study of the stellar kinematics in the SSR is now presented. This allows us to properly investigate the complete phase-space of mono-age populations and helps to characterise the different components of the disc.

As usually expected in Galactic surveys, stars belonging to the different Galactic populations have different rotation velocity distributions (see Sect. 3.1 and Bland-Hawthorn and Gerhard, 2016) that are often used to select the thin or thick disc, or inner halo stellar samples in real stellar surveys (Bond et al., 2010; Spagna et al., 2010). Nevertheless, only a few authors have applied such kinematical decomposition to cosmological simulations (see Abadi et al., 2003a; Abadi et al., 2003b; Obreja et al., 2018; Obreja et al., 2019, and references therein), as the required high-resolution level has been only recently achieved.

Before going into the details of the analysis, it is also useful to recall that

one of the most powerful aspects of cosmological simulations is that every quantity of astrophysical interest is known and can be followed throughout the evolution of the system. It is the case of stellar ages, for example, that are considered as a "direct" observable here and in the previous sections of this chapter. From them, the mono-age populations of Table 5.1 were defined However, in real stellar surveys ages are measured indirectly and are strongly dependent upon several factors, such as metallicity, theoretical stellar modelling, population mixing or gas extinction (Sanders and Das, 2018; Gallart et al., 2019; Feuillet et al., 2019; Lian et al., 2020a).

Given these premises, in Giammaria et al. (2021) the 333 616 stellar particles enclosed in the SSR with $|Z| \leq 4$ kpc were selected and divided in velocity bins of $\Delta V = 10$ km s$^{-1}$. Then, the Probability Distribution Function (PDF), $f(V_\phi)$, of the azimuthal velocity was computed by normalizing to 1 the integral of the total sample. A Triple Normal Mixture model (TNM) was applied to the data, according to the equation

$$f(V_\phi) = \sum_{i=1}^{3} w_i \mathcal{N}\left(V_\phi | \langle V_{\phi,i} \rangle, \sigma_{V_{\phi,i}}\right), \tag{5.2}$$

where $0 \leq w_i \leq 1$ is the weight of the $i$-th component in the mixture and $\mathcal{N}$ is a Normal (or Gaussian) distribution with mean $\langle V_{\phi,i} \rangle$ and standard deviation $\sigma_{V_{\phi,i}}$.

This procedure is similar to a *k-means* algorithm in which the sum of squared distances for all cluster pairs, also known as intra-cluster distance or cluster "inertia" is minimized in order to associate each particle to one of the $k$ clusters. The main limitations of $k$-means are the assumptions of cluster convexity and isotropy that, in case of non-regular shaped manifolds and spherical clusters, can bias the results towards equally weighted clusters. A Normal Mixture, instead, is a probabilistic iterative method that results in an assignment of particles to clusters, each particle having a normalized probability to belong to a certain group. This method relaxes the assumption of cluster symmetry, allowing for a fully free covariance matrix to infer the parameters of the Gaussians. Thus, this is a more "natural" choice to describe observed substructures like thin and/or thick discs, classical- and/or pseudo-bulges, and/or stellar haloes, with mass weights that are not constrained to be roughly equal.

For the TNM model the following priors were considered:

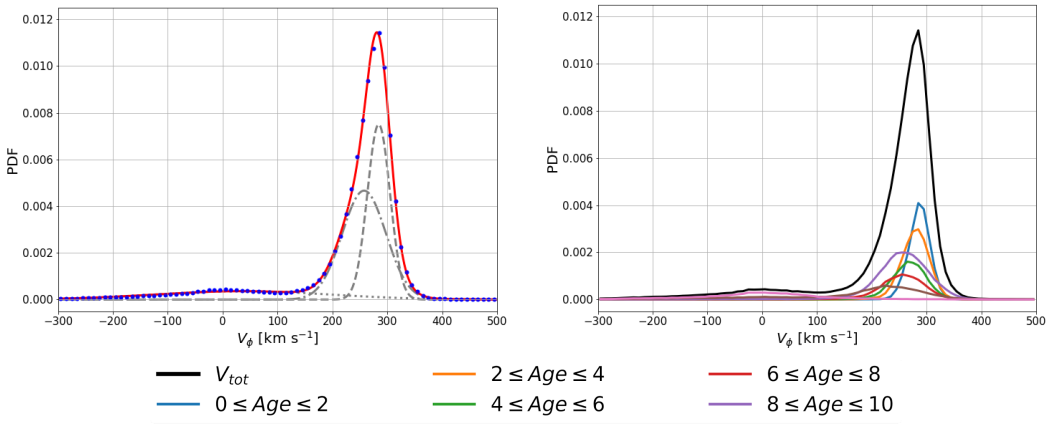


**Figure 5.7:** *Left panel*: kinematical decomposition of the PDF $f(V_{\mathrm{GE}})$ for stellar particles in the SSR with $|Z| \leq 4$ kpc. Binned data are shown as blue dots, while the red line represents the best-fit for the TNM model. *Young disc*, *old disc/thick disc*, and halo structure are shown with dashed, dot-dashed and dotted lines, respectively. *Right panel*: $V_\phi$ distribution for mono-age stellar particles. Colour code as in Table 5.1.

$$\langle V_{\phi,i} \rangle = \mathcal{N}(\mu_i, 10) \tag{5.3}$$

$$\tau_i = \Gamma(1.0, 1.0) \tag{5.4}$$

$$[w_1, w_2, w_3] = Dir([1, 1, 1]) \tag{5.5}$$

where $\mu_i = [300, 220, 10]$ km s$^{-1}$ are the initial guess values for the means of $\mathcal{N}$ in Eq. 5.2, $\tau_i = 1/\sigma^2_{V_{\phi,i}}$ are the precisions of each Gaussian given in terms of the $\Gamma$ conjugate prior, $Dir(\boldsymbol{\alpha})$ is the Dirichlet distribution[2] in order that the total weights of each Gaussian distribution are constrained such that $0 \leq w_i \leq 1$ and $\sum_i w_i = 1$.

The results of the MCMC analysis are listed in Table 5.3 and visualised in Fig. 5.7 (left panel), where the PDF model (red line) appears in good agreement with the observed velocity distribution (blue dots).

The comparison with the mono-age distributions shown in Fig. 5.7 (right panel) confirms that the two disc components represent the superposition of the stellar generations formed in the age intervals 0–4 Gyr and 4–10 Gyr. The *old thin disc* population is much more similar kinematically, to the *thick disc* population, thus they are difficult to distinguish. On the other hand, the

[2]The Dirichlet distribution is a family of continuous multivariate probability distributions parametrized by a vector of positive reals. It is a multivariate generalization of the beta distribution and commonly used as conjugate prior distribution of categorical variables in Bayesian mixture models (Salvatier, Wiecki, and Fonnesbeck, 2016; Kotz, Balakrishnan, and Johnson, 2000).

**Table 5.3:** TNM model parameters: $w_i$ is the mixture weight of the $i$-th component (i.e. young disc, old disc/thick disc, halo), while $\langle V_\phi \rangle$ and $\sigma_{V_\phi}$ are the corresponding mean and the standard deviation of the Normal distribution.

| $i$ | Component | $w$ | $\langle V_\phi \rangle$ [km s$^{-1}$] | $\sigma_{V_\phi}$ [km s$^{-1}$] |
|---|---|---|---|---|
| 1. | young disc | $0.389 \pm 0.006$ | $284.4 \pm 0.2$ | $20.7 \pm 0.2$ |
| 2. | old disc/ thick disc | $0.467 \pm 0.006$ | $257.7 \pm 0.3$ | $39.9 \pm 0.1$ |
| 3. | halo | $0.145 \pm 0.001$ | $35.6 \pm 1.1$ | $159.6 \pm 0.6$ |

residual halo population associated with the *spheroidal oldest* one is easier to separate, validating the larger vertical cut $|Z| \leq 4$ kpc with respect to 3 kpc considered in Sect. 5.1.2. The weights of the two disc components listed in Table 5.3 correspond to the total mass of the *young disc* (Age $\leq$ 4 Gyr) and of the *old disc/thick disc* ($4 \leq$ Age[Gyr] $\leq 10$), respectively (cfr. Table 5.1 considering the different vertical cut applied).

Moreover, the difference between the mean rotation velocity of the AqC4 discs is

$$\Delta V_\phi = 284.4 - 257.7 \simeq 27 \text{ km s}^{-1}, \tag{5.6}$$

that is smaller than what it is observed in the Milky Way, where $\Delta V_{\phi,\text{MW}} = 197.2 - 159.2 = 38$ km s$^{-1}$ (Han et al., 2020). This difference depends on the fact that in AqC4 the two main disc components are associated to the young and the old/thick discs instead of the "geometric" thin disc (comprehending stars with ages $\lesssim 8$ Gyr) and thick disc, as in the Milky Way.

The halo component shows a small prograde rotation as observed in the inner halo of the Milky Way, while its velocity dispersion $\sigma_{V_\phi} \simeq 160$ km s$^{-1}$ is about $70 - 100$ per cent higher than in the Solar Neighbourhood (Re Fiorentin et al., 2015; Bland-Hawthorn and Gerhard, 2016, and references therein).

The probability distributions of the posterior of the TNM model are shown in Fig. 5.8. The means of the posteriors are indicated with a blue square, while the dashed black lines and numbers on top of each histogram have the same meaning as in Fig 5.5. The posteriors are well approximated by a normal distribution, as the means and the medians are similar and the CI are pretty symmetric. The $i = 1, 2$ components, i.e. the two discs components, show the closest correlations between the arrays of the respective parameters. This is again a signature of the intrinsic overlap of the two stellar populations and

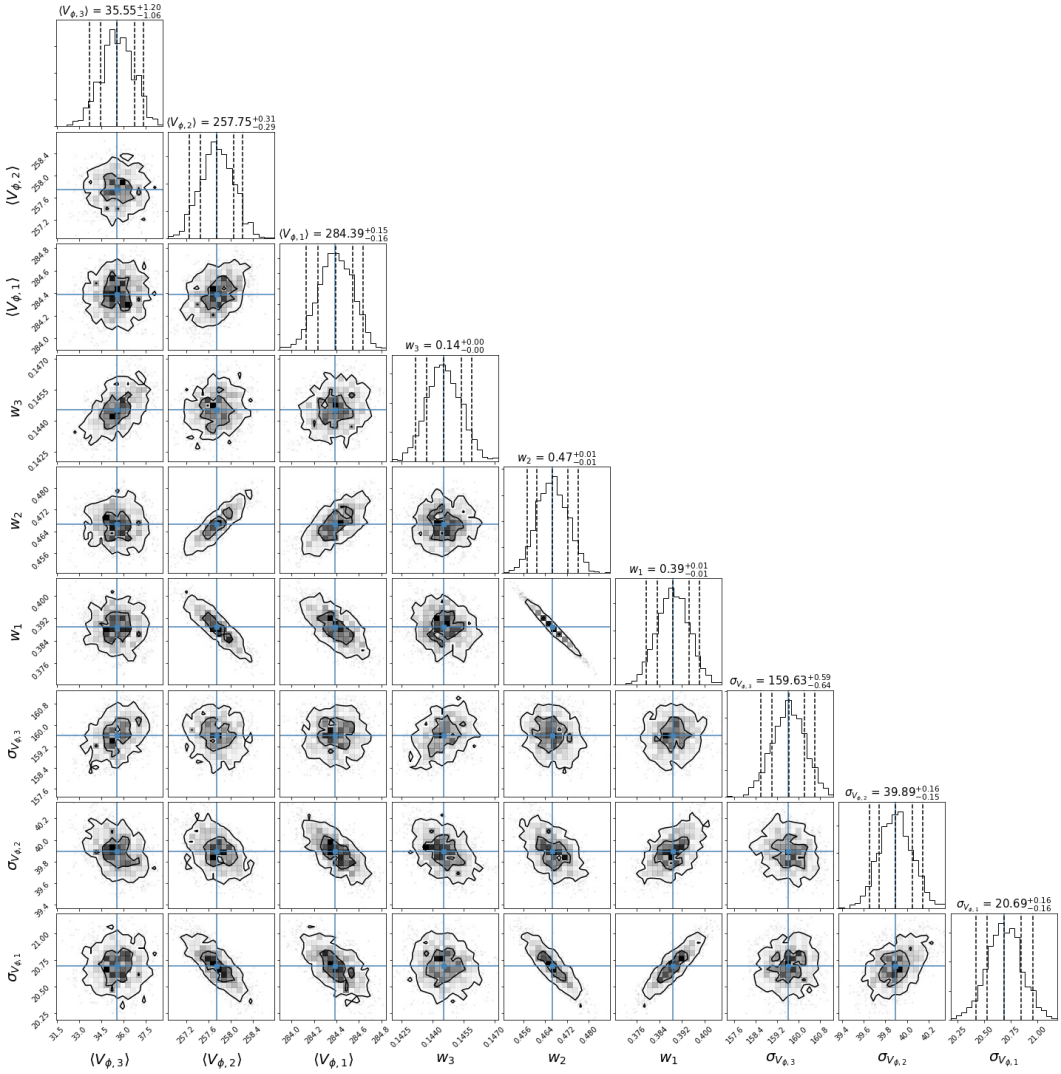


**Figure 5.8:** As in Fig. 5.5 for TNM model parameters according to Eq. 5.2. The blue crosses show the mean value of each posterior distribution.

is similar to what was reported in Sect. 5.1.2. The parameters associated with the residual halo contribution (component $i = 3$) show almost no correlations with the other quantities.

Alternative scenarios with a different number of components were tested, providing fits resulting not in agreement with the data or non-significant improvements of the model. For instance, Fig. 5.9 shows the results for a Double Normal Mixture (DNM) model describing the combination of single disc plus a halo component. Four-component models, aimed as representing additional disc populations, are not statistically different from the TNM model adopted or involve un-physical quantities (e.g. $w_i < 0$ and $\sigma_{V_\phi,i} < 0$).

In summary, in the SSR of AqC4, we can distinguish at least two kinematic disc components which rotate faster than what is measured in the Solar

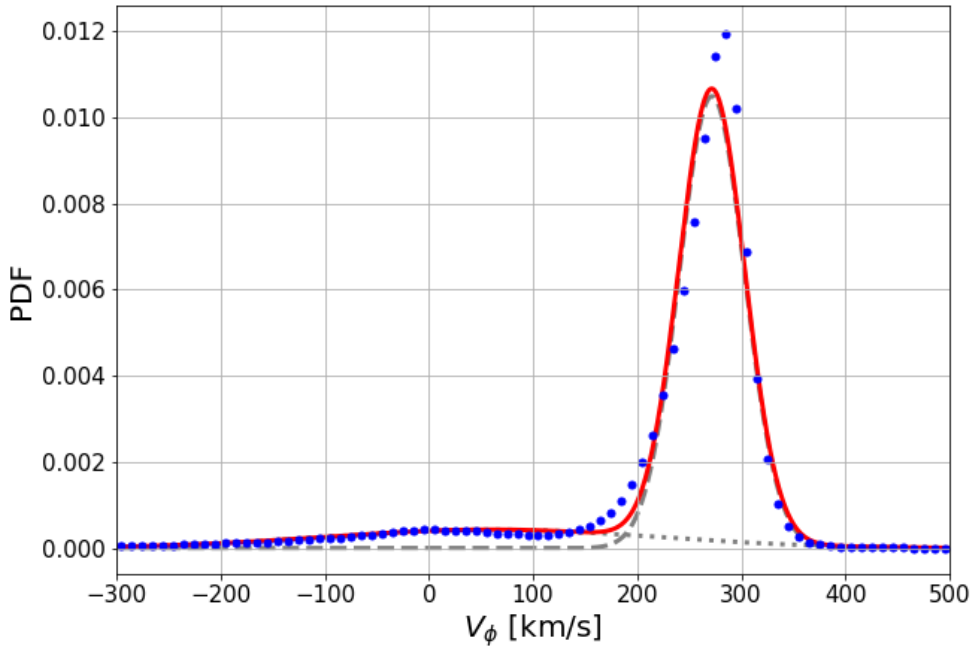


**Figure 5.9:** As in Fig. 5.7 but for a DNM model. The fit results are visually not in agreement with data points.

Neighbourhood of the Milky Way, and with a smaller discrepancy between the mean values.

### 5.2.2 The Rotation Curve

The azimuthal velocity distribution of stellar particles is connected to the Rotation Curve (RC) which constitutes one of the key features that characterise the kinematics of spiral disc galaxies as well as the Milky Way. The next chapters provide a deep investigation on this topic, thus, at this point of the discussion, what is needed to recall is that according to the Newtonian approximation of General Relativity, test particles moving in an axisymmetric gravitational potential $\Phi$, would have a circular velocity $V_c$ given by the equation

$$V_c(R) = \sqrt{\frac{R\partial\Phi}{\partial R}} = \sqrt{\frac{GM(<R)}{R}}. \tag{5.7}$$

where $G$ is the gravitational constant and $M(<R)$ is the total mass inside a particular radius $R$.

The discrepancy existing between the flatness of the empirical curves observed in the outer regions of the discs (e.g. Sofue and Rubin, 2001; Eilers

et al., 2019; Crosta et al., 2020) and the theoretical circular velocity profiles derived from the baryonic mass distribution using Eq. 5.7 represents one of the main lines of evidence of the presence of dark matter in galactic haloes (e.g. Iocco, Pato, and Bertone, 2015; McMillan, 2017; de Salas et al., 2019b).

Fig. 5.10 shows the circular velocity for the total mass (black solid line), and for the individual component of dark matter (grey dashed), stars (grey dot-dashed), gas (grey dotted) particles of AqC4. As expected by ΛCDM model, in the central region ($R \lesssim 5$ kpc) the rotation curve is dominated by the mass of stellar particles, while for $R \gtrsim 5$ kpc the main contribution is due to dark matter responsible for flattening of the curve. Indeed, after a steep linear increase for $R \leq 3$ kpc, the curve has a plateau in the disc-dominated region for $3 \leq R[\mathrm{kpc}] \leq 11$, reaches its peak $V_c = 280.6$ km s$^{-1}$ at $R = 6.25$ kpc, and finally has a smooth decrease for $R \geq 11$ kpc in the halo-dominated region. In the SSR, the circular velocity is 280.1 km s$^{-1}$, which is $\sim$ 20 per cent faster than $V_\phi \simeq 234$ km s$^{-1}$ as estimated by Crosta, Giammaria, Lattanzi, and Poggio (2020) at the Sun position $R_\odot = 8.122$ kpc in the Milky Way. The high rotation velocity of the AqC4 disc is consistent with the more compact structure of AqC4 with respect to the Galactic disc (Sect. 5.1).

In Fig. 5.10, the data from Table 7.1 of Chapter 7, representing the rotation curve of the Milky Way as measured by Crosta, Giammaria, Lattanzi, and Poggio (2020) with Gaia data are plotted as red-star symbols. It is interesting to note that scaling this data to the reduced radial scale length and the higher circular velocity peak of AqC4 keeping *constant* the angular momentum $L_Z$ at the Sun position, the re-scaled Gaia data that describe Galactic disc kinematics (green star symbols in Fig. 5.10) results in good agreement with the rotation curve of AqC4.

Thus, AqC4 appears to be a disc galaxy fairly similar to the Milky Way with a $\sim$ 20 per cent faster-rotating disc and a shorter *pseudo*-solar position location. This emphasizes once again the remarkable results obtained with this unconstrained cosmological simulation that reproduces a disc galaxy very similar to the Milky Way. The scaling factors could be applied in general to all the particles, and it should be applied also to all the particle families (i.e. dark, stellar or gas) in order to maintain the internal consistency of the simulation. This procedure does not change the global results of the simulation, but provides a good testing tool to compare different cosmological simulations produced with different codes, using the Milky Way as a "standard candle" such as the Sun concerning stellar astrophysics.

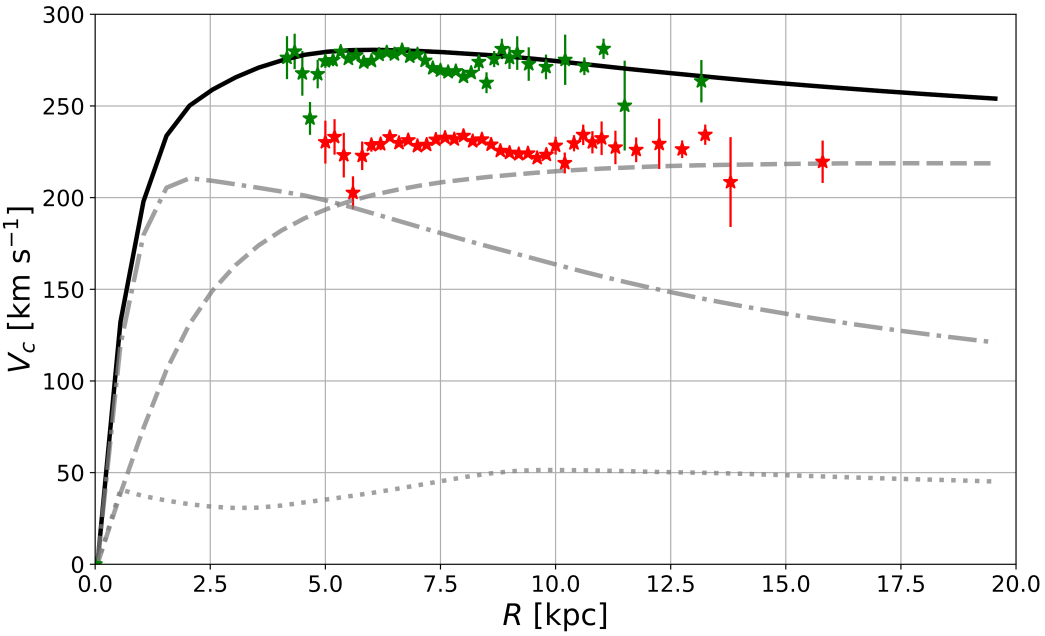


**Figure 5.10:** Rotation curves for AqC4. The solid line shows the total curve, while dashed, dot-dashed and dotted lines show the contribution of the dark matter, stellar and gas component, respectively. Red-star symbols with corresponding uncertainties represent observational data for the Milky Way from Table 7.1. Green star symbols are the same Gaia DR2 data, scaled as described in Sect. 5.2.

### 5.2.3 Kinematics of mono-age populations

Similar to what was done for the disc flaring, where the spatial distribution of mono-age stellar particles was investigated as a function of $R$, Fig. 5.11 shows the medians of the three velocity components $\left(\widetilde{V}_R, \widetilde{V}_\phi, \widetilde{V}_Z\right)$ and the respective dispersions ($\sigma_{V_R}$, $\sigma_{V_\phi}$, $\sigma_{V_Z}$). The values are calculated in annular radial bins of $\Delta R = 0.25$ kpc for the mono-age stellar populations younger than 10 Gyr and with $|Z| \leq 1$ kpc. Error bars are derived via bootstrapping with 100 re-samples.

Based on the different kinematic trends, we can identify three main galactic regions:

- the bulge/bar region for $R \leq 3$ kpc (blue area), characterised by high velocity dispersion and peculiar velocity patterns;
- the region dominated by the disc for $3 \leq R$ [kpc] $\leq 11$ (white area), where we have the lowest dispersions and highest $\widetilde{V}_\phi$;
- the halo region for $R \geq 11$ kpc (grey area) where the velocity dispersions increase and, conversely, the rotation velocity decreases.

A deep investigation of the central region of AqC4 is beyond the aim of this Thesis, since Gaia is limited by gas extinction, when observing the bulge of the Milky Way. However, for the sake of completeness, a few words should be spent about the kinematics of stellar particles within $R \leq 3$ kpc. In this volume, all the mono-age populations show velocity dispersions that are $\sim$ 50 per cent higher than what is measured in the SSR. This is mainly due to the presence of a bar structure, which is easily visible in both the stellar and gas distributions of AqC4 (see left panels of Fig. 5.1). Moreover, as shown in Fig. 5.12, $\widetilde{V}_R$ has an evident non-axisymmetric pattern that is similar to the Milky Way's bar and bulge structure observed by Queiroz et al. (2020, see their Fig. 16), using APOGEE DR16 data to compensate some limitations of Gaia DR2. This "cross" shape reveals a bi-modal distribution of radial velocities that explains the high values of the dispersions.

Moving to the disc-dominated region, the median radial velocity turns out to be negative, i.e. $\widetilde{V}_R = -10 - 0$ km s$^{-1}$, for almost all mono-age populations (see Fig. 5.11, top-left panel). This means that globally more stellar particles move inwards than outwards, in contrast to what is observed in the Milky Way. Despite such zero-point offset in AqC4, the system is out of equilibrium and a "U-shape" with a minimum at about the SSR is visible fairly

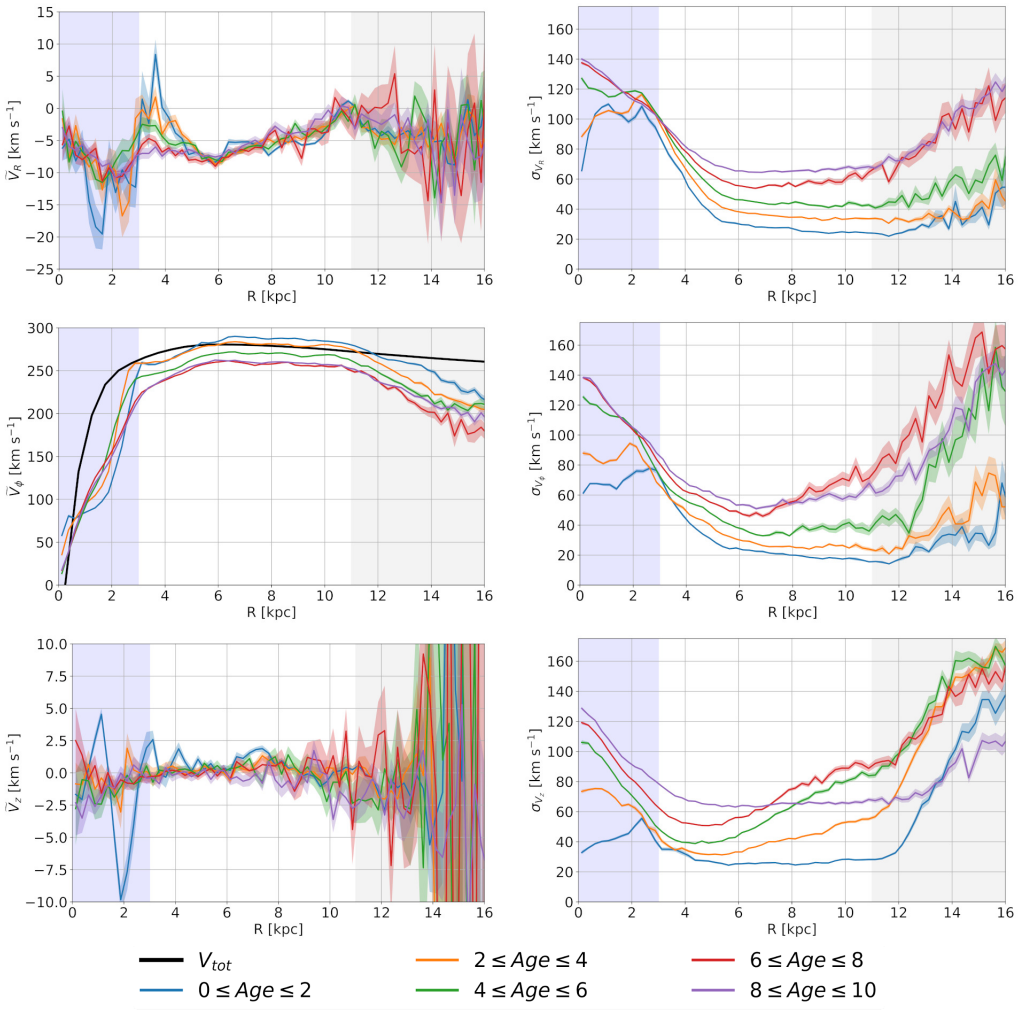


**Figure 5.11:** AqC4 median velocity components $\widetilde{V}_R$, $\widetilde{V}_\phi$, $\widetilde{V}_Z$ (left, from top to bottom), and dispersions $\sigma_{V_R}$, $\sigma_{V_\phi}$, $\sigma_{V_Z}$ (right, from top to bottom), as a function of $R$ for different mono-age stellar populations within $|Z| \leq 1$ kpc (same colour code as in Table 5.1). Blue shadow (for $R \leq 3$ kpc) defines central parts of AqC4, while gray shadow (for $R \geq 11$ kpc) stands for halo region. For $3 \leq R[\text{kpc}] \leq 11$ the disc dominates. Error bars are derived via bootstrapping with 100 re-samples. The *left-middle* panel also shows the total rotation curve as a black solid line.

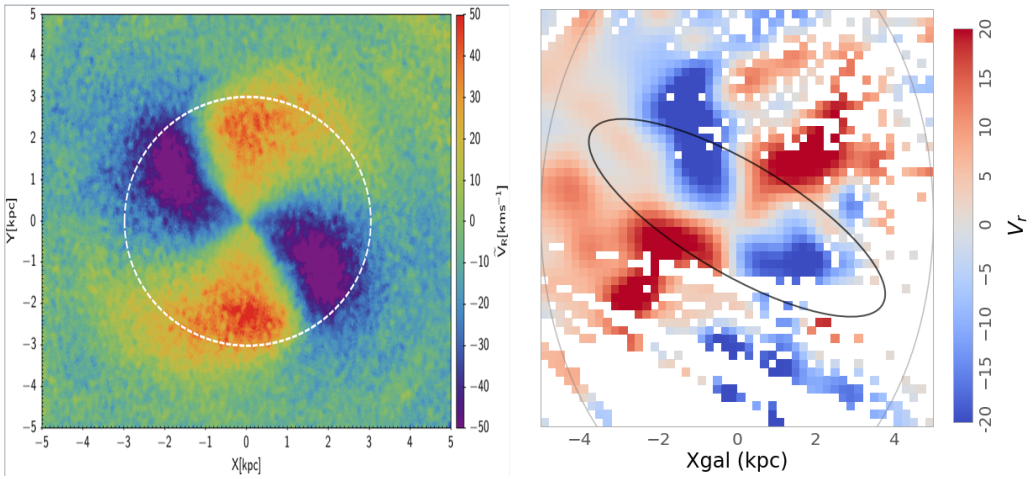


**Figure 5.12:** Cartesian projection of the AqC4 (left panel) and the Milky Way (right panel) innermost 5 kpc region (Queiroz et al., 2020). The white dashed circle in the left panel represents a spherical region of $r = 3$ kpc, while the black solid ellipse shows the size of the bar along both the major and minor axis (Queiroz et al., 2020). The maps are color coded by the radial velocity.

similar to the Milky Way, although the Gaia data samples only a portion of the Galactic disc (Fig. 12 in Gaia Collaboration et al., 2018a).

The last $\sim$ 0.4 Gyr dynamic history of AqC4 reveals that in the previous snapshots of the simulation, $\widetilde{V}_R$ is almost flat around 0 km s$^{-1}$, as commonly expected in the disc region. The negative trend characterises the disc at present only, as shown in Fig. 5.13, but the possibly transitory nature of this trend is not easily investigated because it occurs only in the last snapshot of the simulation. Nevertheless, the disc is not radially oscillating, nor the stellar particles are losing angular momentum, as shown in Appendix A. Moreover, neither an increase of mass in the innermost regions of AqC4, which would have caused an enhancement of the gravitational potential and a contraction of the disc, nor a strong radial inwards migration of stellar particles from the outer regions of the disc, seem to be the possible causes of this phenomena (see Figs. A.3 – A.4 in Appendix A for details). As discussed below in Sect. 5.3, a late impact with a high-velocity and retrograde satellite can explain this feature.

The median rotation velocity $\widetilde{V}_\phi$ is slower for the older stellar generations, as expected from asymmetric drift, as well as to the secular processes (e.g. spiral arms perturbations and bar resonances) and to merging events. In the radial range $6 < R[\text{kpc}] < 11$, the young stellar particles – the most angular-momentum sustained population – rotate faster than $V_c$ (middle-left panel). The reasons for this feature are not clear because of the complex interplay between the variety of dynamical perturbations.

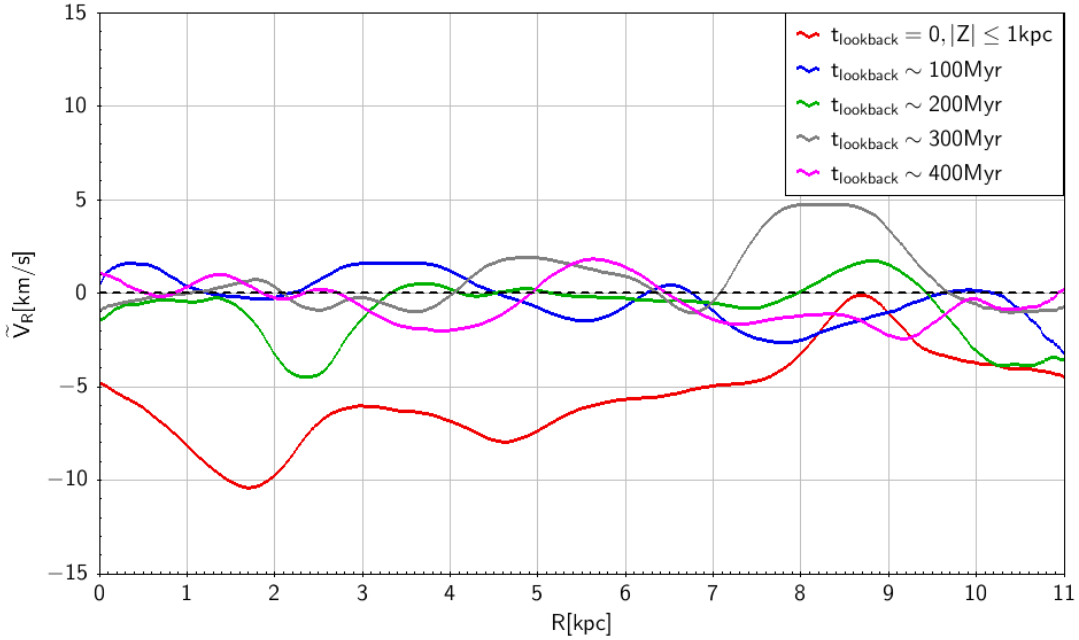


**Figure 5.13:** Evolution of $\widetilde{V}_R$ for stellar particles with $|Z| \leq 1$ kpc. The values are averaged on all stellar ages. Red line corresponds to present time, while other colours sample a time-step of about 100 Myr backwards. There is no significant radial oscillation in the disc region of AqC4 for $t_{lookback} > 100$ Myr.

As expected by the azimuthal averaging, the radial gradient of the vertical velocity is almost flat, with a median value $\widetilde{V}_Z \simeq 0$ km s$^{-1}$ and with larger fluctuations for younger populations (Fig. 5.11, bottom-left panel). On the other hand, in the outer disc of the Milky Way Poggio et al. (2018, Fig. 3) found that the apparent radial increase of the mean vertical velocity, $V_Z$, represents a local signature of the Galactic warp, due to the limited volume sampled by Gaia DR2 and to the peculiar Sun position close to the line of nodes. The difference with the global increase observed in the Milky Way disc arises, therefore, from the peculiar point of view of Gaia that, consequently, can observe a partial region of the Galactic disc "only", i.e. for azimuths $\phi \in [-30°; +30°]$ (Gaia Collaboration et al., 2018a, Fig. 14).

Regarding the velocity dispersions, in the disc region $\sigma_{V_R}$ and $\sigma_{V_\phi}$ decrease from $R \simeq 3$ kpc to $\sim 6$ kpc and then become almost constant until $R \simeq$ 11-12 kpc. The younger populations show stronger gradients $\partial\sigma_V/\partial R$ and cooler isothermal curves than the older populations. These results are consistent with the monotonic radial decrease of the velocity dispersions observed in our Galaxy since the colder and longer-scale-length *young disc* is dominant in the outer part of the disc.

The behaviour of $\sigma_{V_Z}$ in AqC4 is different from the other two components and shows a positive radial gradient for mono-age populations between 2

and 8 Gyr old (i.e. the intermediate *old disc* population), while the youngest and oldest stellar particles are almost isothermal. We argue that this is a cosmological signature of a heating process due to mergers that occurred in the last 7 Gyr of the simulation as discussed below in Sect. 5.3.

In summary, the kinematic analysis reveals that the global inward $\widetilde{V}_R$ systematic motion, the faster rotation $\widetilde{V}_\phi > V_c$ of the youngest stars, and the peculiar velocity dispersions shown by mono-age populations are clear evidence that the stellar disc of AqC4 is still evolving. This is consistent with the recent studies based on Gaia DR2 that have revealed the signatures of a "dynamically young and perturbed Milky Way disk" (Antoja et al., 2018). The kinematical signatures of several past and recent dynamical perturbations and the gas accretion in the external region of the disc (see Fig. 5.1) evidence that the galaxy is still out-of-equilibrium, as discussed in Valentini et al. (2020).

Moreover, the presence of such large reservoir of gas in the extra-galactic regions of AqC4, which sustains the high Star Formation Rate measured at redshift $z = 0$ in the SSR (see following section), represents an interesting starting point for new investigations. A preliminary study of the kinematics of the gas particles is presented in the conclusion of this thesis (Sect. 8.2.2), as a possible future development of the present work.

## 5.3 AqC4 galaxy formation and evolution

The study of the Star Formation History (SFH) is a natural consequence of what discussed so far, since it represents a key to understand the phase-space properties of mono-age populations discussed in Sects. 5.1 and 5.2 and disentangle the origin and evolution of disc-like galaxies and of the Milky Way, as well (Gallart et al., 2019; Helmi, 2020).

This approach is similar to other works on simulated Milky Way-like galaxies (see for example Bignone, Helmi, and Tissera, 2019; Grand et al., 2020) that, according to the precepts of Local Cosmology, contrast the Star Formation Rate (SFR) with the accretion history to study the formation processes of the Galactic disc as a product of the cosmological evolution.

A novel approach to such investigations was proposed in Giammaria et al. (2021) and reported here to conclude the investigation of the AqC4 simulation. In what follows, the spatial and kinematic properties of mono-age stellar particles – namely a synthetic catalogue that mimic the real stellar survey provided by Gaia, discussed in Sects. 5.1 – 5.2 are linked to the whole

accretion history of AqC4. This includes not only ancient merging events such as the GSE experienced by our Galaxy at redshift $z \sim 1.6$ (Helmi et al., 2018), but also the effects of later accretion ones (at redshift $z \leq 0.5$) that influence the out-of-equilibrium state of the stellar disc at redshift $z = 0$. Also, for the first time, the local SFR as inferred from the stellar particles within the SSR is directly confronted with the most recent results derived for the Solar Neighbourhood as observed by Gaia (Mor et al., 2019; Lian et al., 2020b).

### 5.3.1 Star Formation History

Fig. 5.14 shows the evolution of the SFR per unit of surface[3], $M_\odot\ Gyr^{-1}\ pc^{-2}$, for the stellar particles inside two different regions: (i) the red line refers to the whole galactic volume defined by the spherical radius $r_{gal}$; (ii) the blue line is for the SSR limited by a vertical cut $|Z| \leq 3$ kpc. Black symbols with corresponding error bars represent the recent stellar production in the Solar Neighbourhood as estimated by Mor et al. (2019) from Gaia DR2. As specified by the authors, the vertical error bars indicate the 0.16 and 0.84 quantiles of their the posterior estimates, while the horizontal error bars indicate the size of the age bin. On the other hand, the stellar particles subset within the SSR highlights an irregular SFH, quite different from the global SFR evidencing the complex evolution of the local galactic disc.

At redshift $z = 0$, the total SFR for AqC4 is $\sim 2.65\ M_\odot\ yr^{-1}$, which is at least 1.5 times higher than what is measured for our Galaxy by Robitaille and Whitney (2010) and Licquia and Newman (2015), that estimate $SFR = [0.68 \div 1.45]\ M_\odot\ yr^{-1}$ and $SFR = 1.65 \pm 0.19\ M_\odot\ yr^{-1}$, respectively. This indicates that AqC4 is more active and star-forming, at present, than the Milky Way, as also highlighted by the high SFR measured in the SSR.

The apparent peak of the whole SFR at $z > 3.3$ represents the primordial phase of the galaxy formation that builds up the central bulge (as in Murante et al., 2015), while the smooth decrease after redshift $z \sim 2.5$ (i.e. during the last 10 Gyr) describes the disc evolution. Also in the SSR, a starburst is evident at cosmic times $T < 2$ Gyr, clearly indicating that a fraction of the stars formed during the primordial starburst have migrated from the inner galaxy out to $R \simeq 6$–$7$ kpc.

A smaller secondary red peak is visible at redshift $z \sim 1.6$ corresponding to the thick disc formation discussed in Sect. 5.2. At this epoch, the total SFR is approximately $7 - 8\ M_\odot\ yr^{-1}$, which appears more similar to the value of

[3]Note that in this units it is easier to compare the SFR relative to different regions and volume extensions.

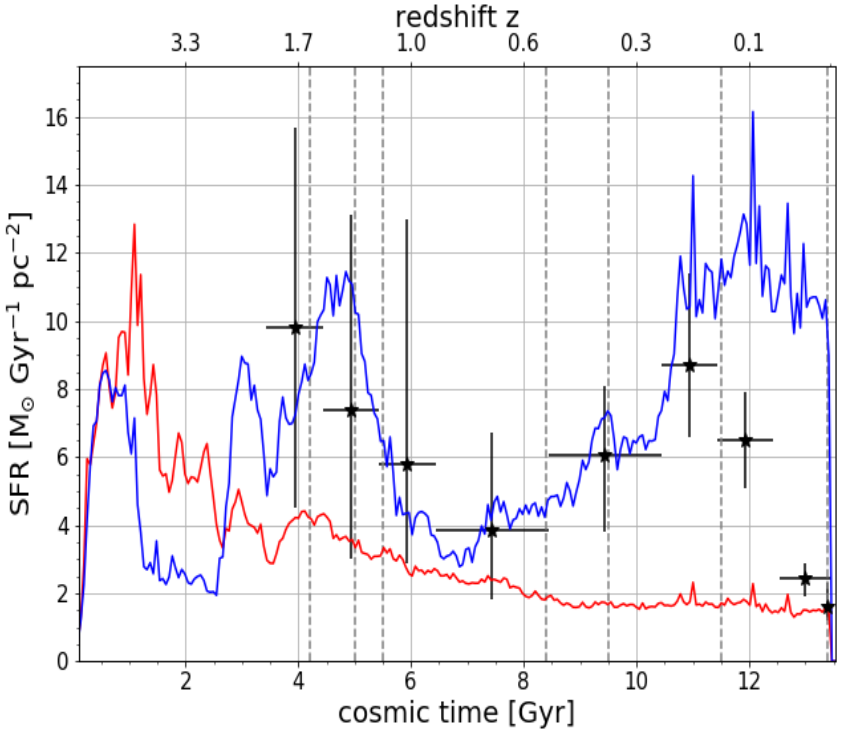


**Figure 5.14:** SFR as a function of cosmic time $T$ in Gyrs for the whole galactic volume (red line) and in the SSR (blue line). Black symbols refer to data from Mor et al. (2019). Vertical dashed lines indicate the redshift/cosmic time of the accreted satellites listed in Table 5.4.

$\sim 6.5\ M_\odot\ yr^{-1}$ found in the EAGLE simulation studied by Bignone, Helmi, and Tissera (2019), than to the much stronger starburst up to $\sim 25\ M_\odot\ yr^{-1}$ resulting from the AURIGA simulation analysed by Grand et al. (2020). The formation of the ancient thick disc is clearer in the SSR, where, after a quenching phase, a double-peak event at redshift $z \sim 2.1$ and $z \sim 1.4$ is evident. This is consistent with the relative weights of the mono-age populations reported in Table 5.1. Indeed, the cosmic time range $T \sim 4 - 6$ Gyr corresponds to stellar ages of 8 – 10 Gyr.

Finally, for $T > 7$ Gyr SFR increases in the SSR, because of the inside-out formation of the disc, as opposed to slightly decreasing trend for the entire AqC4. The very high SFR of $10 - 12\ M_\odot\ Gyr^{-1}\ pc^{-2}$ for $T > 11$ Gyr is forming a massive young disc populations, as already discussed in Sect. 5.1.

Despite the large observational uncertainties especially for ancient epochs, the SFR measured by Mor et al. (2019) in the Solar Neighbourhood results in very good agreement with that of AqC4 in the SSR. Moreover, these authors have hypothesised that the large time-scale (almost 3.5 Gyr) and the large amount of mass indicated by the Milky Way data could be explained by an external factor and simply due to the secular evolution of the disc. This scenario finds here a supporting result: indeed, as already mentioned earlier, a huge amount of gas that is falling from the halo region of AqC4 (lower panels of Fig. 5.1).

Moreover, as shown in the next Section, also the low-redshift merging events may have mediated the recent gas accretion, supporting the hypothesis that the increasing SFR in the Solar Neighbourhood of the Milky Way may be due to the recent merging event claimed by Lian et al. (2020b).

### 5.3.2 The accretion history

The evidence on the SFH discussed above motivates further investigations on the accretion history of AqC4. Giammaria et al. (2021) selected seven snapshots corresponding to some of the main starbursts observed in Fig. 5.14 at redshift $z = 1.637$, 1.314, 1.154, 0.550, 0.401, 0.178 and 0.014. These redshifts do not correspond to the exact epoch at which the merger occurred but they were chosen to identify easily the interacting satellites.

For illustration purpose, Figs. 5.15 – 5.16 show the face-on and edge-on stellar density distributions at these selected redshifts, evidencing the presence of one or more merging satellites.

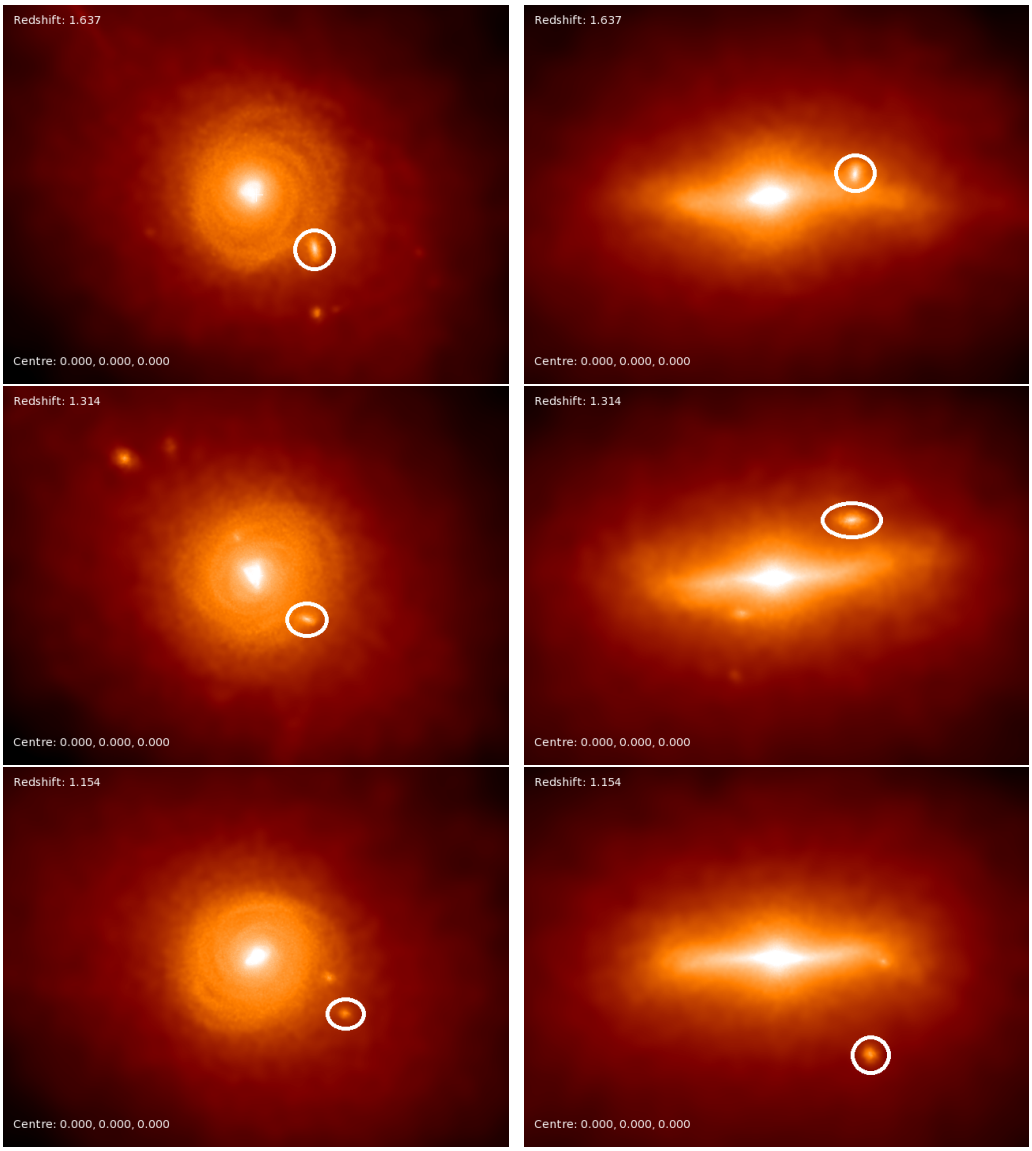


**Figure 5.15:** From top to bottom lines, stellar density maps for the AqC4 simulation at redshift $z = 1.637$, 1.314 and 1.154, respectively. Left-hand panels show face-on projections, while right-hand panels for the edge-on ones. White circles highlight the selected merging satellites.

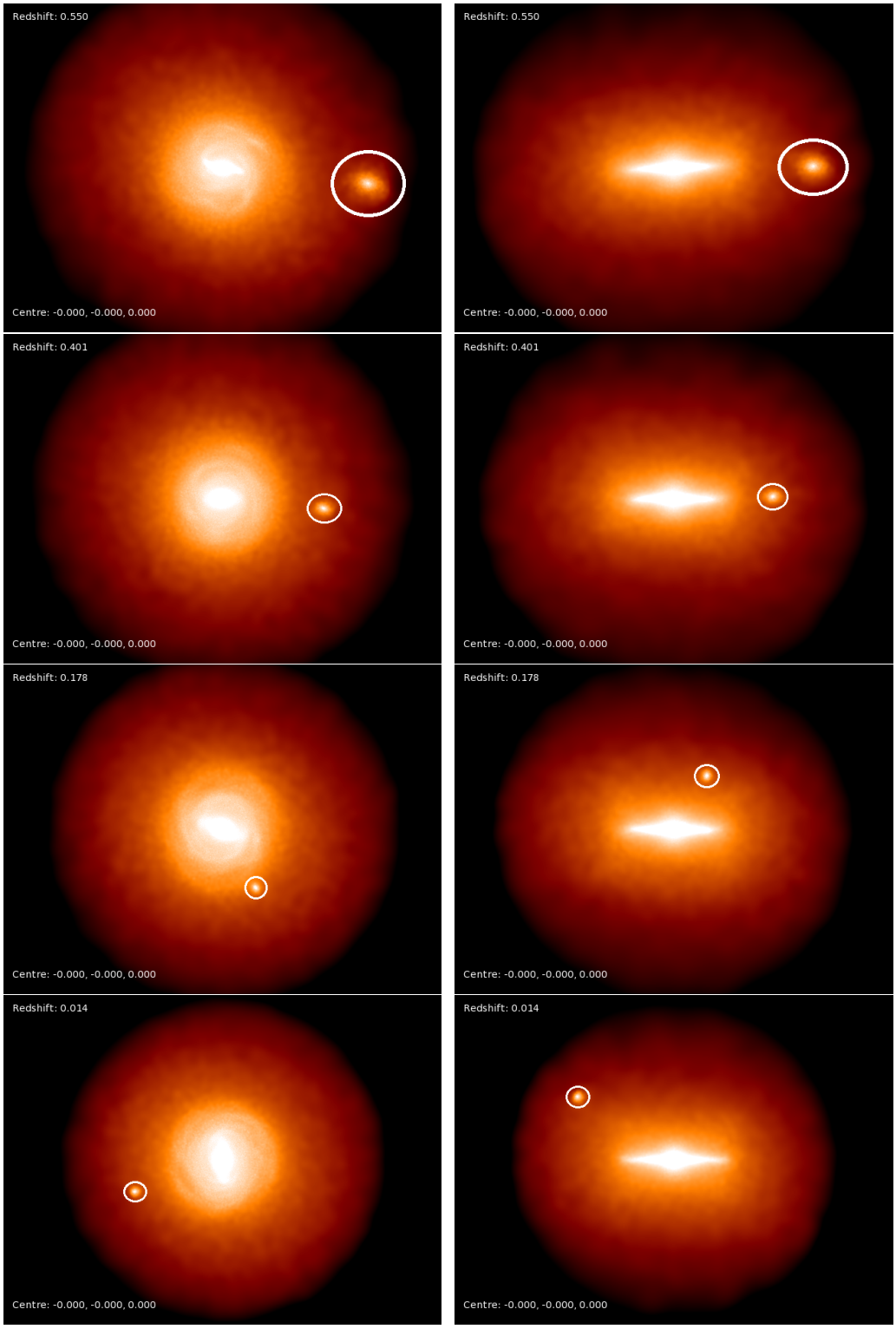


**Figure 5.16:** As Fig. 5.15 but at redshift $z = 0.550$, 0.401, 0.178 and 0.014.

**Table 5.4:** The stellar mass of selected satellite galaxies and the main galactic disc with corresponding stellar mass ratios at different redshift $z$.

| $z$ | $r_{\rm sat}$ [kpc] | $M_\star^{\rm sat}$ [$10^8 {\rm M}_\odot$] | $R_{\rm disc}$ [kpc] | $M_\star^{\rm disc}$ [$10^{10} {\rm M}_\odot$] | $\Delta_\star$ [%] |
|---|---|---|---|---|---|
| 1.637 | 3.0 | 12.0 | 5.0 | 2.2 | 5.5 |
| 1.314 | 2.5 | 4.7 | 5.0 | 2.7 | 1.7 |
| 1.154 | 4.0 | 1.3 | 5.0 | 2.9 | 0.4 |
| 0.550 | 6.0 | 8.8 | 8.0 | 4.5 | 2.1 |
| 0.401 | 3.5 | 5.1 | 8.5 | 4.8 | 1.1 |
| 0.178 | 3.5 | 4.0 | 9.0 | 5.3 | 0.8 |
| 0.014 | 3.5 | 2.6 | 10.0 | 5.7 | 0.4 |

For each snapshot, the main satellite identified is marked with a white circle. For each of them, the total stellar mass, $M_\star^{\rm sat}$, is estimated within a spherical radius, $r_{\rm sat}$ centred on the satellite. Similarly, the mass of the main disc-like galaxy, $M_\star^{\rm disc}$, is calculated considering a cylindrical volume in the reference frame of the main galaxy, defined by $R_{\rm disc}$ for the radial extension of the disc at that epoch and by $|Z| < 2$ kpc for the vertical one. Thus, the stellar mass ratio is computed as

$$\Delta_\star = \frac{M_\star^{\rm sat}}{M_\star^{\rm disc}} \tag{5.8}$$

and the total mass ratio as

$$\Delta_H = \frac{M_H^{\rm sat}}{M_H^{\rm disc}} = \frac{f^{\rm disc}}{f^{\rm sat}} \Delta_\star, \tag{5.9}$$

where $f$ is the ratio of the luminous-to-halo mass of the object, $M_H$ and $M_\star$ denote the halo mass and stellar mass, respectively.

According to McMillan (2017), at the present time, $f^{\rm MW,0} \simeq 0.04$ for the Milky Way, while $f^{\rm sat} \simeq 0.01$ for a typical satellite galaxy involved in a merging such as the Large Magellanic Cloud (van der Marel, Kallivayalil, and Besla, 2009) or the GSE (Helmi et al., 2018). Assuming that the redshift evolution of $f$ between $z = 2$ and $z = 0$ is similar for objects of the scales of the Magellanic Cloud and of the Milky Way (Behroozi, Wechsler, and Conroy, 2013), this implies that $f^{\rm MW}/f^{\rm sat} = f^{\rm MW,0}/f^{\rm sat,0} \simeq 4$. Therefore, by taking a mass of the disc at the time of the merger of $M_\star^{\rm disc} \sim 10^{10}$ M$_\odot$, the typical total mass ratio for the merger is of about 0.24. In the case of AqC4 simulation, $\Delta_\star$ varies from $\sim 0.5$ to 5.5 per cent as listed in Table 5.4.

The oldest satellite at redshift $z = 1.637$ has a stellar mass of $1.2 \cdot 10^9$ $M_\odot$ and is the main merger that can be associated with the starburst between the cosmic time $T = 4 \div 6$ Gyr (see Fig. 5.14). This is pretty similar to what was estimated by Mackereth et al. (2019) and Fattahi et al. (2019) for the GSE progenitor, namely a mass of a few $10^9$ $M_\odot$, assuming a $10^{10}$ $M_\odot$ stellar mass for the thick disc present at the time. This implies a stellar mass ratio $\Delta_\star \sim 5.5$ % which is quite consistent with the value of $\sim 6$ per cent estimated by Helmi et al. (2018) and confirmed by Gallart et al. (2019) for GSE. The long timescales (the last 5 Gyr of the galactic evolution) and the mass involved (in the SSR, the SFR reaches similar during both the thick and the young disc formation) were enough that the kinematically hot and prominent *thick disc* of AqC4 could be produced with kinematic properties similar to the Milky Way.

After this large merger, other accretion events occurred with satellites of mass $M_\star^{\rm sat} \lesssim 10^8$ $M_\odot$ corresponding to $\Delta_\star \leq 2$ per cent. These minor accretions produced the secondary fluctuations of the SFR in the SSR after redshift $z \sim 1.5$ and are consistent with the standard hierarchical formation scenario of the Milky Way (Helmi, 2020, and references therein).

For the accreted satellites detected at $z = 0.550$ and $z = 0.401$, the stellar mass is $M_\star^{\rm sat} \simeq 8.8 \cdot 10^8$ $M_\odot$ and $M_\star^{\rm sat} \simeq 5.1 \cdot 10^8$ $M_\odot$, respectively. These low-redshift, significant mergers have produced a heating of the *old disc* population that can explain the large scale height of the stellar particles with age 4-8 Gyr shown in Fig. 5.6. As I reported in Giammaria et al. (2021), "the presence of merging events during the intermediate phase of the disc formation is consistent with the late-accretion model proposed by Lian et al. (2020b), who suggest that a recent merger event occurred in the Milky Way at 8.2 Gyr in cosmic time (i.e. redshift $z \sim 0.6$). In particular, these authors estimate a mass of $M_\star < 10^9$ $M_\odot$ for the gas-rich dwarf galaxy involved".

Finally, two more satellites at redshift $z = 0.178$ and 0.014 involve a stellar mass of $M_\star^{\rm sat} \simeq 4.0 \cdot 10^8$ $M_\odot$ and $2.6 \cdot 10^8$ $M_\odot$, respectively. These appear to be associated with the increasing SFR in the SSR of AqC4 during the last 2 Gyr.

As anticipated before, the last satellite seems also to be responsible for the various dynamical perturbations experienced by AqC4 and, in particular, of the global inwards motion of stellar particles in the disc-dominated region shown in Sect. 5.2.3.

Fig. 5.17 represents the linear extrapolation of the trajectory of this latest satellite (see also bottom panels of Fig. 5.16). The mean velocity components

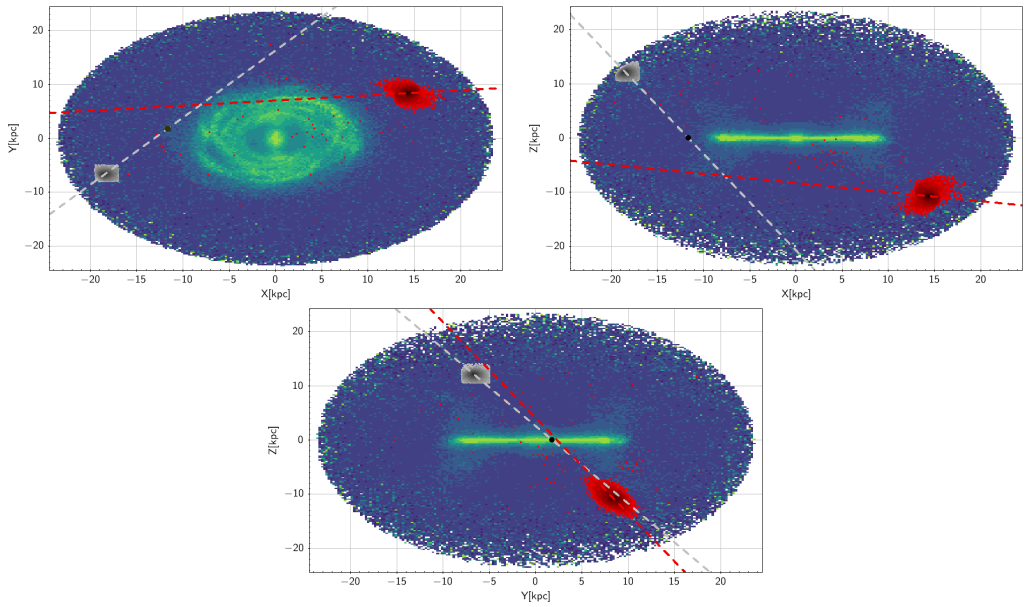


**Figure 5.17:** Projected distributions on the $XY$-, $XZ$- and $YZ$-plane of AqC4 stellar particles at redshift $z = 0.014$. Grey and red colors represent the satellite before and after the impact on the galactic plane, respectively. Dashed lines show the linear extrapolation of the trajectory of the satellite before and after the impact. The black dot indicates approximately where the satellite crosses the galactic plane at $Z = 0$ kpc.

$\langle V_R \rangle, \langle V_\phi \rangle, \langle V_Z \rangle$ of the satellite before and after the impact are of the order of $(-210, -128, -275)$ km s$^{-1}$ and $(350, -163, -65)$ km s$^{-1}$, respectively. The analysis reveals that the high-speed, counter-rotating impact on the galactic plane occurred in the outer region of the disc (i.e. $R \sim 10 \div 12$ kpc) may have produced the dynamic of perturbation of the AqC4 disc affecting all the mono-age populations.

In summary, the SFH and the accretion history of AqC4 are very useful to clarify the formation of the peculiar spatio-kinematic properties observed in the *young disc* and *old disc* mono-age stellar particles populations described in Sects. 5.1 – 5.2. Moreover, the overall formation and evolution of AqC4 appear fairly similar to the Milky Way. The results described in Giammaria et al. (2021) are consistent with both the GSE scenario for the origin of the Galactic *thick disc* (Brook et al., 2012; Stinson et al., 2013; Helmi et al., 2018; Gallart et al., 2019), and with the recent accretion event proposed to explain the increasing SFR in the Solar Neighbourhood (Mor et al., 2019). Finally, the SFR found in AqC4 at redshift $z = 0$ is higher than in the Milky Way and this depends on both the gas contribution from the late accreted satellites and the infall of gas previously expelled by the strong starbursts and supernova explosions that occurred at high redshift.

As discussed in the conclusions of this Thesis (see Chapter 8, Sect. 8.2.2), further investigations including, for example, the Age-Velocity dispersion-Relation (AVR), the study of phase-space distribution of gas particles, or the stellar back-time tracking, are necessary to improve our knowledge of the Galactic thin and thick discs origin and evolution.

# Part IV

# The Galactic Rotation Curve with Gaia DR2 and a first test in the context of Relativistic Astrometry for Local Cosmology

# Chapter 6

# The Rotation Curve and Galactic models

*This chapter is a slightly modified version of Crosta, Giammaria, Lattanzi, and Poggio (2020) published in Monthly Notices of the Royal Astronomical Society, 496, 2, 2107-2122.*

The previous two chapters reveal how fundamental and revolutionary is the combination of high-resolution simulations and very precise observations for Local Cosmology. In this context, Gaia represents a Golden Goose for Galactic astrophysics, but also for Relativistic Astrometry since its few-micro-arcsecond level of measurements requires a fully general-relativistic implementation for the data reduction (see Chapter 2). As already discussed in Chapter 1, the consequence is that the weak gravitational regime is playing a pivotal role in providing a observational perspective for understanding gravity. This requires, in principle, that the data reduction, the modelling of observations and the interpretation of scientific results should be consistent at the same order of approximation.

Indeed, the small curvature limit in General Relativity (GR) may not coincide with the Newtonian regime. It is the case of the Lense-Thirring effect (Lense and Thirring, 1918), for instance. For the advancement of Mercury's perihelion, instead of adding a "dark planet" (Vulcano), General Relativity corrects the dynamics by accounting for the small curvature effects justifying a modification of the Newtonian theory.

Currently, General Relativity is the confirmed standard theory that explains gravity over a range of sixty orders of magnitude, from Planck scales to the observable Universe (Crosta, 2019). Then, according to Local Cosmology, the evolution of the Milky Way and its constituents is the product of the action of gravity as supported, for instance, by the successes of the $\Lambda$CDM model and cosmological simulations. For this reason, within the context of Relativistic Astrometry, one of the aims of this thesis is to push on the use of

General Relativity in galactic dynamics to evaluate to what extent the Newtonian approximation of Einstein's field equation is valid. Nevertheless, only a few exact solutions of Einstein's equation exist, making it even the more difficult to detail a metric for the whole Galaxy, especially if it is made of different structures such as the Milky Way bulge, thin and thick discs, and halo.

With this prospect, this chapter and the next one provide the first attempt to implement a simple relativistic model suitable to represent the Galactic disc as dust in equilibrium at a sufficiently large distance from a (rotating) central body via stationary and axially-symmetric solutions for a Galactic disc metric. After a brief review of the recent investigations on the topic, the two models considered for the analysis of the Milky Way rotation curve as observed by Gaia are presented: the first is a classic representation of the Galaxy according to the Concordance model and includes several baryonic components and a dark matter halo; the second is a relativistic one based on Balasin and Grumiller (2008), derived from the full set of Einstein's field equations in the weak field regime.

## 6.1 The Galactic Rotation Curve

As already mentioned in Chapter 5, the rotation curve is one of the most distinctive features from the observational point of view of disc-like galaxies such as the Milky Way. By definition, a rotation curve is the mean circular velocity, $V_c(R)$, in the Galactocentric rest-frame around the Galactic Centre as a single function of radius. Disc-like galaxies present a flat velocity profile as shown in Fig. 1.8 that has been explained as a deviation from the Newtonian dynamics and an empirical proof of the presence of dark matter (Zwicky, 1937; Rubin, Ford, and Thonnard, 1978) or modified gravity (Milgrom, 1983) and other alternatives already discussed in Chapter 1. Only, a few authors explored the weak relativistic regime of Einstein's equation for the galactic dynamics beyond the Newtonian approximation (see Sect. 6.3 of this thesis)

In the classic framework, the circular velocity curve of the Milky Way can be written as

$$V_c^2(R) = R\frac{\partial \Phi}{\partial R}\Big|_{Z\approx 0} \tag{6.1}$$

where $Z$ denotes the height above the Galactic plane, implying that the spherical radius can be approximated to the cylindrical one, $r = \sqrt{R^2 + Z^2} \simeq R$, since the circular velocity is defined at $Z \simeq 0$ kpc. This means that a test particle would move on circular orbit at radius $R$ in an axisymmetric gravitational potential $\Phi$. Indeed, non-circular streaming motions due to non-axisymmetric gravitational potential components such as spiral arms, bars, and/or expansion/contraction motions are not considered and applied to the result of the observations (Sofue, 2017).

The link between this $V_c(R)$, and in particular its value at the Sun's Galactocentric radius $R_\odot$, and the Galactic potential $\Phi$ provides important constraints on the mass distribution of the Milky Way (e.g. McMillan, 2017; Eilers et al., 2019; Crosta et al., 2020, and references therein). Moreover, the local rotation velocity at the Sun's position, $V_c(R_\odot)$ plays an important role in the cosmological context, for instance, whether it falls onto the Tully-Fisher relation (Klypin, Zhao, and Somerville, 2002).

### 6.1.1 Standard stellar tracers for the Milky Way

From an observational point of view, many are the possible methods and astrophysical objects one can use to trace the rotation velocity profile (see Iocco, Pato, and Bertone, 2015; Sofue, 2017; Sofue, 2020, for reviews of several tracers and data collections). For the inner regions of the Galaxy, the tangent-point method is often considered, based on HI or CO emission lines in the interstellar medium or disc objects, under the assumption of purely circular orbits of the gas (Gunn, Knapp, and Tremaine, 1979; Fich, Blitz, and Stark, 1989; Levine, Heiles, and Blitz, 2008). It is also expected that through gravitational waves (GWs) detected by the Laser Interferometer Space Antenna[1], we would be able to investigate internal regions of the Galaxy that are hardly accessible to electromagnetic observations (Korol, Rossi, and Barausse, 2019). Other measurements from gas kinematics include the thickness of the HI layer (Merrifield, 1992), spectro-photometric distances and radial velocities of HII regions and giant molecular clouds (Fich, Blitz, and Stark, 1989; Brand and Blitz, 1993).

In the outer part of the Galaxy, i.e. for $R \gtrsim R_\odot$, the circular velocity has been measured through the stellar kinematics of planetary nebulae (Schneider and Terzian, 1983), classical cepheids (Pont et al., 1997; Mróz et al., 2019), red giant branch (RGB) and red clump stars in the Galactic disc (Bovy and

[1] LISA is an ESA space mission officially approved in 2017 (Amaro-Seoane et al., 2017) designed to study among other sources ultra-compact Double White Dwarfs (DWDs).

Rix, 2013; Huang et al., 2016; Eilers et al., 2019), masers (Reid et al., 2014; Bobylev, Krisanova, and Bajkova, 2020), RR Lyrae stars (Ablimit and Zhao, 2017; Wegg, Gerhard, and Bieth, 2019), or OB and early-type stars (Bobylev and Bajkova, 2018; Crosta et al., 2020). For the most outer regions (i.e. $R \sim 100 \div 200$ kpc), non-disc tracers such as KG or BHB stars have been considered, to investigate the velocity profile of the Galactic halo (Xue, Rix, and Zhao, 2009; Kafle et al., 2012; Bhattacharjee, Chaudhury, and Kundu, 2014; Huang et al., 2016).

Despite the incredible and crucial improvements that the recent Gaia DR2 (Gaia DR2, Gaia Collaboration et al., 2018b) has produced in terms of observed volume, sample completeness, accuracy and precision of measurements, the reconstruction of the Milky Way rotation curve from the kinematics and proper motions of stars is still a debated topic.

## 6.2 Classic Jeans modelling of the circular velocity

Assuming Newtonian gravity, the non-perfect circular orbits of the stars around the Galactic centre due to out-of-equilibrium perturbations, secular processes such as non-axisymmetric potentials or the asymmetric drift, have to be take in consideration to derive from the stellar azimuthal velocity $V_\phi$ the correct values of $V_c$. The cylindrical form of Jeans' equation (Jeans, 1915; Binney and Tremaine, 2011),

$$\frac{\partial(\rho\langle V_R^2\rangle)}{\partial R} + \frac{\partial(\rho\langle V_R V_Z\rangle)}{\partial Z} + \rho\left(\frac{\langle V_R^2\rangle - \langle V_\phi^2\rangle}{R} + \frac{\partial\Phi}{\partial R}\right) = 0, \tag{6.2}$$

is used to link the moments of the velocity distribution $\langle V_i V_j\rangle$ and the density $\rho$ of a given stellar sample to the gravitational potential $\Phi$ of a stationary and axisymmetric disc. Then, considering Eq. 6.1, with some algebra the circular(ized) velocity is

$$V_c^2(R) = \langle V_\phi^2\rangle - \langle V_R^2\rangle\left(1 + \frac{\partial \ln\rho}{\partial \ln R} + \frac{\partial \ln\langle V_R^2\rangle}{\partial \ln R}\right), \tag{6.3}$$

where the contributions of the vertical gradients were neglected, and $\langle V_i^2\rangle$ represents the averaged squared velocity of the sample at a given radial bin.

The corrections are usually small for typical disc tracers and become less and less important for the most angular-momentum sustained stellar populations. See, for instance, the young mono-age populations in the middle left panel of Fig. 5.11, but also the red-giant disc stars (Fig. 2 of Eilers et al.,

2019), or the early-type stars as discussed in the next chapter and in Crosta, Giammaria, Lattanzi, and Poggio (2020). Moreover, for population I objects and interstellar gases, velocity dispersion is also usually negligible compared to rotational velocity (i.e. $\sigma_{V_\phi}/V_\phi \lesssim 10$ %) and measurement uncertainties, which implies that the dynamical balance between the gravitational and centrifugal forces may be used to calculate the mass with sufficient accuracy (Sofue, 2017).

Note also that in elliptical galaxies the rotation curve analysis is not applicable since their stellar constituents are dominated by thermally hot, scattering motions. Similarly, in the halo regions of disc-like galaxies, the velocity anisotropy of typical halo tracers such as halo K giants (KG) or blue horizontal branch (BHB) stars has to be taken into account to consider the out-of-plane motions and the high-velocity dispersions (Bhattacharjee, Chaudhury, and Kundu, 2014; Huang et al., 2016).

If the total gravitational potential of the Milky Way, $\Phi_{\rm tot}$, is linked to the Galactic rotation curve through Eqs. 6.1 and 6.3, on the other hand, the Poisson equation approximates this potential as a sum of potentials evoked by the baryonic and the dark matter density profiles, as

$$\nabla^2\Phi_{\rm tot} = 4\pi G(\rho_{\rm bar} + \rho_{\rm DM}). \tag{6.4}$$

In summary,

$$\Phi_{\rm tot} = \sum_i \Phi_i \implies V_{\rm tot} = \sqrt{\sum_i V_{\rm i}^2}. \tag{6.5}$$

where $i$ denotes the Galactic components (i.e. the bulge, the discs, the halo etc.) and Eqs. 6.3 and 6.4 are used to fit the velocity profile provided by proper motions, line-of-sight velocities, and parallaxes of stellar samples measured by Gaia for example. With this method, many authors derive important constraints on the mass distribution in our Galaxy and, in particular, on the local dark matter density, $\rho_{\rm DM}(R_\odot)$. In the words of Eilers et al. (2019): "the latter [the local dark matter density] is crucial for interpreting and analyzing any direct as well as indirect detection experiments of dark matter, whereas the shape of the rotation curve is a fundamental parameter for models of the Galactic disc".

Before continuing, note for completeness that Eq. 6.4 is the same as Eq. 4.2, introduced to describe gravity in classic N-body simulations, and can be derived directly from the (Newtonian) weak-field approximation of General Relativity. In fact, when the stress-energy tensor reduces to $T_{00} = \rho c^2$, e.g.

for a pressureless perfect fluid where $T_{00}$ is the energy density and $\rho$ is the mass density, the Einstein field equation 1.2 reduces exactly to Eq. 6.4.

### 6.2.1 The Milky Way Classic model

In the limit of Newtonian approximation of gravity and given the linearity of Eq. 6.4, the Milky Way's gravitational potential can be decomposed in its components as provided in many works that investigate the Galactic rotation curve (see for instance McMillan, 2017; Pouliasis, Di Matteo, and Haywood, 2017; Eilers et al., 2019, among others). Among the various density profiles available in the scientific literature (some of them are reported in Chapter 3), in Crosta, Giammaria, Lattanzi, and Poggio (2020) a model called Milky Way Classic (the *MWC model* hereafter) was defined. This includes a stellar bulge, a thin and thick stellar disc and a dark matter halo.

For the bulge, the Plummer's density profile expressed by Eq. 3.2 (see Chapter 3 of this Thesis and Pouliasis, Di Matteo, and Haywood, 2017; Granados et al., 2021, for supplementary details) was considered. Inserting this profile into the Poisson equation (Eq. 6.4), one obtains Plummer's velocity profile, $V_{\rm bulge}(R)$, as

$$V_{\rm bulge}(R) = \sqrt{GM_{\rm b}\frac{R^2}{(R^2+b_{\rm b}^2)^{3/2}}} \tag{6.6}$$

where $b_{\rm b}$ is the Plummer's radius and $M_{\rm b}$ the total bulge mass.

For the Milky Way stellar disc, a double-component disc modeled as two Miyamoto-Nagai potentials was chosen. The most general description of each single density profile is expressed in the form of Eq. 3.3 (Barros, Lépine, and Dias, 2016; Pouliasis, Di Matteo, and Haywood, 2017; Granados et al., 2021), which provides the Miyamoto-Nagai's velocity contribution, $V_{\rm disc}(R)$,

$$V_{\rm disc}(R) = \sqrt{GM_{\rm d}\frac{R^2}{\left(R^2+(a_{\rm d}+b_{\rm d})^2\right)^{3/2}}}. \tag{6.7}$$

Here, $M_{\rm d}$ is the total (thin or thick) disc mass, and $a_{\rm d}$ and $b_{\rm d}$ are the scale length and scale height, respectively. Alternatively, the density can also be well approximated with a double exponential disc as in McMillan (2017) and Korol, Rossi, and Barausse (2019).

Finally, a standard Navarro-Frank-White (NFW) density, expressed by Eq. 3.1, was considered to describe the dark matter halo as in Navarro, Frenk,

and White (1996), McMillan (2017), and Granados et al. (2021). The consequent velocity profile, $V_{\rm h}(R)$, can be written as

$$V_{\rm h}(R) = \sqrt{\frac{4\pi G \rho_0^{\rm halo} A_{\rm h}^3}{R}\left[\ln\left(1+\frac{R}{A_{\rm h}}\right) - \frac{R/A_{\rm h}}{1+R/A_{\rm h}}\right]} \tag{6.8}$$

where $\rho_0^{\rm halo}$ is the dark matter halo density scale and $A_{\rm h}$ its scale radius. Each contribution to this classical model is calculated by utilizing the GALPY python package (Bovy, 2015).

## 6.3 Relativistic dust modelling of the Galaxy

With the same assumptions of the classical approach, in General Relativity we can assume a pressureless perfect fluid to describe the masses enclosed in a large portion of the Galaxy, far from the central bulge regions, that interact only gravitationally. Such shear-free and expansion-free fluid is defined to be a continuous distribution of matter with stress-energy tensor $T^{\alpha\beta} = \rho u^\alpha u^\beta$ (in geometrized units, Stephani et al., 2009) where the time-like vector field $u^\alpha$ represents the 4-velocity of the fluid and $\rho$ is the mass density. Moreover, the conservation equation implies that the four-velocity motion is geodesic and the mass-energy distribution is conserved. This model defines a relativistic dust, namely the simplest self-gravitating rotating system with no interaction except gravitation. Indeed, as reported in Neugebauer and Meinel (1995) and Neugebauer, Kleinwaechter, and Meinel (1996), a rigidly rotating disc of dust is the universal limit of rigidly rotating perfect fluid configurations, where the ratio of pressure to energy density vanishes. Such a disc may serve as a crude model for galaxies in which the stars are considered as dust grains (Crosta, Giammaria, Lattanzi, and Poggio, 2020).

It is worth recalling here that in cosmological hydrodynamical simulations an ensemble of many particles interacting via gravitational forces alone is represented by a dust system (see Chapter 4). In cosmology, the standard $\Lambda$CDM model is based on the Friedman-Lemaître-Robertson-Walker metric and valid, in the matter-dominated era, for a dust fluid in a homogeneous and isotropic Universe (Wald, 1984). Unfortunately, so far a similar global metric is unknown for the internal galactic dynamics. This is due to the mathematical complexity of coupling the Vlasov equation 4.1 (i.e. the collisionless Boltzmann equations ) with the Einstein field equation 1.2 when considering

the Galaxy as a rotating isolated matter distribution. Recently, some numerical scheme has been proposed by Ames, Andréasson, and Logg (2016, and references therein).

Nevertheless, the dust solution can represent a universal limiting case for the global dynamics of the Galactic disc. Therefore, assuming stars populating the disc as isolated and in equilibrium, meaning that stellar encounters become effective well below the parsec scale, the Galaxy can be considered globally isolated up to around $R \sim 25$ kpc, where the disc flaring effects emerge, indicating the onset of external gravitational perturbations. On the other hand, in the innermost central region, the Gravity Collaboration et al. (2018) limited the dimension of the Galactic nucleus where the stellar orbits are very perturbed (velocities of about $\sim 10^4$ km s$^{-1}$) by the Galactic Super Massive Black Hole, Sgr A$^*$, to less than 1 kpc. Thus, between 5 kpc or more from the Galactic centre up to $\sim 25$ kpc, we can consider that the angular-momentum sustained stellar population traces the Galactic rotation curve, neglecting at first any possible intrinsic streaming motions or tidal forces.

### 6.3.1 The Balasin-Grumiller model

Given the aforementioned considerations, the line element in the cylindrical coordinate $(t, R, \phi, Z)$

$$ds^2 = -dt^2 + 2Nd\phi dt + (R^2 - N^2)d\phi^2 + e^{\nu}(dR^2 + dZ^2) \tag{6.9}$$

where $\nu$ and $N$ are function of $(R, Z)$ and can be used to trace the velocity profiles of disc galaxies in a weakly relativistic scenario away from the central regions. This line element was first chosen by Cooperstock and Tieu (2007, CT hereafter) and then adopted by Balasin and Grumiller (2008, BG) to propose a theoretical description of the rotation curve profile. Additionally, note again that when applying the Jeans correction within the Newtonian dynamics the velocity dispersion is usually "negligibly small compared to rotational velocity, which implies that the pressure term is negligible in the Virial theorem, so that the dynamical balance between the gravitational and centrifugal forces may be used to calculate the mass at sufficient accuracy" (Sofue, 2017).

In the following, I provide the derivation of the velocity of the co-rotating dust particle as measured by an asymptotic observer at rest with respect to the rotation axis as demonstrated in Crosta, Giammaria, Lattanzi, and Poggio

(2020, Sect. 2.2 and Appendix A). Hereafter in this Thesis, this relativistic velocity profile defines the so-called *BG model*.

### The velocity of co-rotating dust particles

In a stationary and axisymmetric space-time described by the line element of Eq. 6.9, a generally spatially circular orbit can be described as a family of time-like observers

$$u^\alpha = \Gamma(\partial_0^\alpha + \beta\partial_\phi^\alpha) \tag{6.10}$$

where $\beta$ is the constant angular velocity w.r.t. to infinity and $\Gamma$ the normalization factor. In particular, in the case of static observers we have $\beta = 0$. Equivalently, the same observer can be expressed with respect to the local frame associated to the Zero-Angular Momentum Observers (ZAMOs) at rest w.r.t. the Galactic Centre. The associated tetrad is: $e_{\hat{0}}^\alpha \equiv Z^\alpha$, $e_{\hat{\phi}}^\alpha \equiv 1/\sqrt{g_{\phi\phi}}\partial_\phi^\alpha$, and $e_{\hat{a}}^\alpha \equiv e^\nu \partial_a^\alpha$ with $a = R, Z$. Thus, we have

$$u^\alpha = \gamma(e_{\hat{0}}^\alpha + \zeta^{\hat{\phi}} e_{\hat{\phi}}^\alpha) \tag{6.11}$$

where $\gamma = -(u|Z)$ is the Lorentz factor[2], $e_{\hat{0}}^\alpha$ is the unit normal to the $t = constant$ hyper-surfaces, and $e_{\hat{\phi}}^\alpha$ the $\phi$ unit direction of the orthonormal frame adapted to the ZAMOs.

With respect to the ZAMOs, the line element 6.9 can be rewritten in terms of the lapse and the shift factor

$$M = r/\sqrt{r^2 - N^2} \tag{6.12}$$

$$M^\phi = N/(r^2 - N^2) \tag{6.13}$$

as

$$ds^2 = -M^2dt^2 + (r^2 - N^2)\left(d\phi + M^\phi dt\right)^2 + e^\nu(dR^2 + dZ^2) \tag{6.14}$$

where $Z^\alpha = (1/M)(\partial_t^\alpha - M^\phi\partial_\phi^\alpha)$. The relationship between $\beta$ and $\zeta^{\hat{\phi}}$ is given by equating the corresponding terms of Eqs. 6.10 and 6.11 with $\gamma = M\Gamma$ de Felice and Clarke (1990) and de Felice and Bini (2010). Therefore,

[2]The symbol $(|)$ stands for the scalar product relative to the chosen metric.

$$\zeta^{\hat{\phi}} = \frac{\sqrt{g_{\phi\phi}}}{M}(\beta + M^{\phi}), \tag{6.15}$$

where the index $\alpha$ was dropped to simplify the reading.

Using Eqs. 6.12 and 6.13 in Eq. 6.15 for a static observer (i.e. $\beta = 0$), the velocity of the co-rotating dust particle as measured by an asymptotic observer at rest with respect to the rotation axis reduces to

$$\zeta^{\hat{\phi}} = \frac{\sqrt{R^2 - N^2}}{(R/\sqrt{R^2 - N^2})}\left(\frac{N}{R^2 - N^2}\right) = \frac{N(R,Z)}{R} \equiv V^{\mathrm{BG}}. \tag{6.16}$$

This turns out to be proportional to the off-diagonal term $g_{t\phi}$ of the metric (6.9), i.e. the background geometry (Crosta, Giammaria, Lattanzi, and Poggio, 2020), and can be related to the gravitational dragging (de Felice and Clarke, 1990).

The above framework can be applied to the Gaia context since its observables are developed with respect to the static observer $u^{\alpha} = (1/\sqrt{-g_{tt}})\partial_t^{\alpha}$, locally at rest relative to the BCRS. As mentioned in Chapter 2, this coordinates frame takes into account the gravitational fields within the Solar System and $u^{\alpha}$ reduces to be $\propto \partial_t^{\alpha}$ far away from the Sun, i.e. at Galactic scales (Crosta et al., 2017).

### The analytic expression of the relativistic velocity profile

The function $N(R,Z)$ in Eq. 6.16 was constrained by Balasin and Grumiller (2008) assuming a separability *ansatz*, $N(R,Z) = \mathcal{G}(R)\,\mathcal{F}(Z)$, and the reflection symmetry around the Galactic plane (Balasin and Grumiller, 2008, Eq. 25). The final expression is

$$\begin{aligned} N(R,Z) = {} & V_0(R_{\mathrm{out}} - r_{\mathrm{in}}) + \\ & \frac{V_0}{2}\sum_{\pm}\left(\sqrt{(Z \pm r_{\mathrm{in}})^2 + R^2} - \sqrt{(Z \pm R_{\mathrm{out}})^2 + R^2)}\right), \end{aligned} \tag{6.17}$$

which provides, on the equatorial plane $Z = 0$, the relativistic velocity profile for the Galactic rotation curve

$$V^{\mathrm{BG}}(R) = \frac{V_0}{R}\left(R_{\mathrm{out}} - r_{\mathrm{in}} + \sqrt{r_{\mathrm{in}}^2 + R^2} - \sqrt{R_{\mathrm{out}}^2 + R^2}\right). \tag{6.18}$$

Here, the unknown parameters $V_0$, $R_{\mathrm{out}}$, $r_{\mathrm{in}}$ represent, respectively, the velocity in the flat regime of the rotation curve, the extension of the Milky Way

disc and the bulge radius. The original expression of Balasin and Grumiller (2008) is recovered by setting $R \equiv r$, $R_{\text{out}} \equiv R_0$, and $r_{\text{in}} \equiv r_0$.

Balasin and Grumiller (2008) solve for $N(R, Z)$ by avoiding values that could prevent a physical solution or violate the weak energy condition and the assumption of vanishing pressure. These features occurred instead in Cooperstock and Tieu (2007), where localized exotic matter emerges in the energy-momentum tensor (see appendix B of Balasin and Grumiller, 2008, and references therein, for example, Zingg, Aste & Trautmann, 2007)). Such flaws persist in the recent publications of Carrick and Cooperstock (2012) and Magalhaes and Cooperstock (2017), where the mass density profile is estimated.

Both models assume the *ansatz* that the metric function $N$ is separable, $N(R, Z) = \mathcal{G}(R)\,\mathcal{F}(Z)$, and the reflection symmetry around the Galactic plane, which implies four solutions for $\mathcal{F}(Z)$: $e^{\pm k|Z|}$, $\cos kZ$, $\cosh kZ$. With the further restriction that the rotation velocity, and thus $N(R, Z)$, should not blow up as $Z$ becomes large, this leaves two possibilities: the negative exponential and the cosine functions. Cooperstock and Tieu (2007) use $\mathcal{F}(Z) = e^{-k|Z|}$ (not smooth at $Z = 0$, see Appendix B of Balasin and Grumiller, 2008) and write the velocity as a linear superposition of Bessel function of the first kind to get a good fit to the data. In Balasin and Grumiller (2008), instead, $\mathcal{F}(Z) = \cos kZ$ is adopted. This led to a solution involving modified Bessel functions, which can be integrated over all possible modes to obtain expression 6.17.

The solution for $N$ allows one to obtain a Minkowskian metric far from the centre of the Galaxy (Neill, Wiltshire, and Mattsson, 2011, private communication to M. Crosta). However, it still presents some limitations at $R = 0$, where the model lacks an appropriate physical boundary for $R \ll N$ and the metric is not defined (Grumiller, Balasin, and Preis, 2009), and for $|Z| > r_{\text{in}}$, because of the separability *ansatz* applied by Balasin and Grumiller (2008) to solve the metric function $N = N(R, Z)$. Similar behaviour can be found in the solution proposed by Cooperstock and Tieu (2007) in which, moreover, the metric approaches the flat space metric far from the galaxy in the vertical direction but not in the radial direction (Neill, Wiltshire, and Mattsson, 2011, private communication to M. Crosta).

Even though it is based on tailored assumptions and with some limitations (e.g. for $R \ll N$ and for $|Z| > r_{\text{in}}$, see Sect. 8.2.3 for details on these issues which will need to be addressed in future developments), Eq. 6.18 represents one of the first attempts at deriving a suitable General Relativity

velocity profile for the Galactic rotation curve. This is worth testing as a first case-study, before pushing for more reliable and complex solutions (Crosta, Giammaria, Lattanzi, and Poggio, 2020).

# Chapter 7

# Fits to the Galactic models with Gaia-DR2 data

*This chapter is a slightly modified version of Crosta, Giammaria, Lattanzi, and Poggio (2020) published in Monthly Notices of the Royal Astronomical Society, 496, 2, 2107-2122.*

In what follows, the models presented in the previous chapter, namely the MWC and BG models, are fitted to the best data of the Milky Way rotation curve obtain only from the Gaia DR2. These data are model-independent and can be used to confirm or not the validity of these models.

## 7.1 Sample Selection

Having defined the two theoretical models to describe the Galactic rotation curve, the next step is to select the most suitable stellar sample tracing the velocity profile as a function of the radial distance from the Galactic Centre. In Crosta, Giammaria, Lattanzi, and Poggio (2020), we fixed the following strict criteria to extract the complete set of stellar data needed from Gaia DR2 archive (*Gaia Archive*):

1. availability of the complete astrometric parameters with corresponding errors and covariance matrix, i.e. right ascension $\alpha$ and declination $\delta$, proper motions $\mu_\alpha^* = \mu_\alpha cos\delta$ and $\mu_\delta$, and parallax $\varpi$;
2. availability of the Gaia-measured velocity along the line of sight, $RV$, and its error;
3. parallaxes good to 20%, i.e. $\varpi/\sigma_\varpi \geq 5$;
4. availability of a cross-matched entry in the 2MASS catalogue (Skrutskie et al., 2006), i.e. the magnitudes in the Gaia $G$-band and the infrared $H$, $J$, and $K$ bands;

The first two requirements are necessary for the proper 6-dimensional reconstruction of the phase-space location occupied by each star as derived by the same observer. The third one ensures a quasi-Gaussian statistics when transforming the stellar parallaxes into distances, as discussed in Smith and Eichhorn (1996, and references therein), and the validity of coordinates transformations shown in Sect. 7.1.1. The last criterium is necessary for the actual materialization of the dataset: indeed, the most suitable stellar sample is constituted by the early-type stars since they are relatively young and, therefore, represent the most angular-momentum sustained stellar sample in the Galactic disc, as demonstrated in Sect. 5.2.3.

Following Poggio et al. (2018), we can combine the three near-infrared magnitudes $H$, $J$, and $K$ from the 2MASS survey (Skrutskie et al., 2006) with the $G$-band magnitude from Gaia DR2 and determine the following photometric colour selection:

$$\begin{aligned} (J-H) &< 0.14(G-K)+0.02 \\ (J-K) &< 0.23(G-K) \end{aligned} \tag{7.1}$$

These criteria select from the Gaia catalogue a stellar sub-population based on their colours and absolute magnitudes. Such stars belong to upper main sequence (see also Re Fiorentin, Lattanzi, and Spagna, 2019).

The most important limitation is linked to the Gaia-measured $RV$. As mentioned in Chapter 2, Gaia provides velocity along the line of sight for stars with estimated effective temperatures between 3 550 and 6 900 K only (Gaia Collaboration et al., 2018b). For this reason, the total 1.6 billion samples in the DR2 reduces to $\sim$ 7.2 million objects with full 6D astrometric solution, which can be used to reconstruct the phase-space location occupied by each star, as derived by the same observer in the relativistic sense. This issue implies that a large fraction, if not all of the OB stars initially contained in the 2MASS cross-matched sample, drops out of it because of the $RV$ requirement, leaving mainly A, and some F, early-type stars. This bias will be greatly mitigated with the forthcoming Gaia releases starting from the third Data Release (Gaia DR3, see Sect. 8.2.1 in Chapter 8), or through synergy with spectro-photometric ground-based surveys such as APOGEE.

The selection process just described allows us to select a very homogeneous sample of 5 277 early-type stars, to whom 325 classical type I Cepheids are added as classified by the Gaia pipelines (Clementini et al., 2019) and considering only the first three requirements above. This is the largest stellar

sample of this kind available at the time of this analysis and is suitable to study the Galactic rotation curve.

### 7.1.1 Coordinates transformation with covariance

As reported in Chapter 2, in Gaia the astrometric parameters of the sources and the ephemerides refer to the BCRS. This reference system has its origin at the solar-system barycentre (typically within two solar radii of the Sun's position) and its axes are kinematically non-rotating with respect to objects at cosmological distances, coinciding with those of the International Celestial Reference Frame (ICRS; Arias et al., 1995).

For Galactic study purpose, the quantities extracted from the *Gaia Archive* are expressed in the ICRS reference system and have to be transformed from their original values – namely $\alpha$, $\delta$, $\varpi$, $\mu_\alpha^*$, $\mu_\delta$, $RV$ where the superscript $*$ stands for $\mu_\alpha^* = \mu_\alpha \cos\delta$ – to their cylindrical Galactocentric counterparts, i.e. $(R, \phi, Z)$ for the Galactocentric spatial coordinates and $(V_R, V_\phi, V_Z)$ for the corresponding velocities. Although these or similar transformations are standard, the corresponding transformation of covariances is usually neglected. The procedure here reported follows that described in the Gaia DR2 Documentation (van Leeuwen et al., 2018) and The HIPPARCOS and TYCHO catalogues and includes the correct error propagation due to the availability of the correlation matrix of the parameters.

First, let $s \equiv \begin{pmatrix} b_x & b_y & b_z & v_x & v_y & v_z \end{pmatrix}$ be the position-velocity column vector of the star in the BCRS. The barycentric position measured in parsec and the barycentric space velocity measured in km s$^{-1}$ are

$$b = \begin{pmatrix} b_x \\ b_y \\ b_z \end{pmatrix} = T \begin{pmatrix} 0 \\ 0 \\ A_p/\varpi \end{pmatrix} \tag{7.2}$$

and

$$v = \begin{pmatrix} v_x \\ v_y \\ v_z \end{pmatrix} = T \begin{pmatrix} k\mu_\alpha^* A_v/\varpi \\ k\mu_\delta A_v/\varpi \\ kRV \end{pmatrix} \tag{7.3}$$

where $T$ is the $3 \times 3$ ortho-normal matrix

$$T = \begin{pmatrix} p_x & q_x & r_x \\ p_y & q_y & r_y \\ p_z & q_z & r_z \end{pmatrix} = \begin{pmatrix} -\sin\alpha & -\sin\delta\cos\alpha & \cos\delta\cos\alpha \\ \cos\alpha & -\sin\delta\sin\alpha & \cos\delta\sin\alpha \\ 0 & \cos\delta & \sin\alpha \end{pmatrix} \tag{7.4}$$

including the components of the normal triad $\begin{bmatrix} p & q & r \end{bmatrix}$ that converts the spherical equatorial coordinates into their Cartesian counterparts, and $A_p = 10^3$ mas pc and $A_v = 4.74047$ km yr s$^{-1}$ are constants that convert mas to parsec and mas yr$^{-1}$ to km s$^{-1}$. The parameter $k = (1 - RV/c)^{-1}$ is the Doppler factor linked to the velocity along the line of sight. Thus, in the Galactic heliocentric system the components of the position-velocity vector are given by the $6 \times 1$ matrix $s = \begin{pmatrix} x & y & z & v_x & v_y & v_z \end{pmatrix} = G\,s$, in the helio-centric coordinates and where

$$G = \begin{pmatrix} A_G^T & 0_{33} \\ 0_{33} & A_G^T \end{pmatrix}. \tag{7.5}$$

Here, $0_{mn}$ is the $m \times n$ matrix of zeros and

$$A_G^T = R_z(-l_\Omega)\, R_x(90^\circ - \delta_{\rm NGP})\, R_z(\alpha_{\rm NGP} + 90^\circ) = \begin{pmatrix} -0.0548755604162154 & -0.8734370902348850 & -0.4838350155487132 \\ +0.4941094278755837 & 0.4448296299600112 & +0.7469822444972189 \\ -0.8676661490190047 & 0.1980763734312015 & +0.4559837761750669 \end{pmatrix} \tag{7.6}$$

is the transpose of the fixed orthogonal matrix $A_G$ defined in The HIPPARCOS and TYCHO catalogues that rotates the coordinates from the equatorial system to the Galactic one. $R_i(\theta)$ represents the $3 \times 3$ rotation matrix of the coordinate frame by the angle $\theta$ about axis $i$, while $(\alpha_{\rm NGP}, \delta_{\rm NGP}) = (192.85948^\circ, +27.12825^\circ)$ are the coordinates of the North Galactic Pole with respect to the equatorial system and $l_\Omega = 32.93192^\circ$ is the galactic longitude of the first intersection of the galactic plane with the celestial equator.

The statistical errors associated with the astrometric parameters are given by the standard uncertainties $\sigma_i$ together with the correlation coefficients $\rho(i,j)$ with $i \neq j$. Note that the $RV$ measurements are computed by a different on-board instrument with respect to the other astrometric parameters (see Chapter 2), therefore the corresponding correlation coefficients are null,

i.e. $\rho(RV, i) = 0$, with $i = \alpha, \delta, \varpi, \mu^*_\alpha, \mu_\delta$. The $6 \times 6$ covariance matrix of the vector $s$ is

$$Cov(s) = J \begin{pmatrix} C & 0_{51} \\ 0_{51} & \sigma^2_{RV} \end{pmatrix} J^T \tag{7.7}$$

where $C$ is the $5 \times 5$ covariance matrix of the astrometric parameters provided by Gaia observations[1], $\sigma^2_{RV}$ the standard error of the velocity along the line of sight $RV$, and

$$J = \begin{pmatrix} A_p p_x/\varpi & A_p q_x/\varpi & -A_p r_x/\varpi^2 & 0 & 0 & 0 \\ A_p p_y/\varpi & A_p q_y/\varpi & -A_p r_y/\varpi^2 & 0 & 0 & 0 \\ A_p p_z/\varpi & A_p q_z/\varpi & -A_p r_z/\varpi^2 & 0 & 0 & 0 \\ 0 & 0 & -(p_x\mu^*_\alpha + q_x\mu_\delta)A_v/\varpi^2 & p_x A_v/\varpi & q_x A_v/\varpi & r_x \\ 0 & 0 & -(p_y\mu^*_\alpha + q_y\mu_\delta)A_v/\varpi^2 & p_y A_v/\varpi & q_y A_v/\varpi & r_y \\ 0 & 0 & -(p_z\mu^*_\alpha + q_z\mu_\delta)A_v/\varpi^2 & p_z A_v/\varpi & q_z A_v/\varpi & r_z \end{pmatrix} \tag{7.8}$$

is the Jacobian matrix of the transformation from astrometric parameter vector to $s$[2]. The associated covariance matrix in the galactic system is therefore

$$Cov(Gs) = G\,J \begin{pmatrix} C & 0_{51} \\ 0_{51} & \sigma^2_{RV} \end{pmatrix} J^T\,G^T \tag{7.9}$$

Finally, we need to translate from such heliocentric coordinates to the Galactocentric system taking into account the height of the Sun above the Galactic plane. The full transformation for the position is then

$$P_{GC} = H(P - R_\odot \hat{x}_{GC}) = \begin{pmatrix} \cos\theta & 0 & \sin\theta \\ 0 & 1 & 0 \\ -\sin\theta & 0 & \cos\theta \end{pmatrix} \begin{pmatrix} x - R_\odot \\ y \\ z \end{pmatrix} \tag{7.10}$$

where $P = (\,x\ y\ z\,)$, $R_\odot = 8.122$ kpc is the distance between the Sun and the

[1] With the diagonal elements $C_{ii} = \sigma^2_i$ and off-diagonal elements $V_{ij} = \sigma_i \sigma_j \rho_{ij}$ (with $\rho_{ji} = \rho_{ij}$).

[2] The Doppler factor $k$ has been neglected for the calculation of the partial derivatives.

Galactic Centre which is purely along the $x$-axis with unit vector $\hat{x}_{GC}$ (Gravity Collaboration et al., 2018), and $\theta = sin^{-1}(Z_\odot/R_\odot)$ specifies the height, $Z_\odot \sim 25$ pc, of the Sun above the Galactic plane. For the velocity, the procedure is similar but accounting for the solar reflex motion $(U_\odot, V_\odot, W_\odot) = (12.9, 245.6, 7.8)$ km s$^{-1}$ in the Galactocentric reference frame, as derived by Drimmel and Poggio (2018) from the proper motion of Sgr A$^*$ adopted as the Galactic Centre. In this way, the final coordinates are independent from the Local Standard of Rest.

### 7.1.2 Spatial and kinematical analysis

Having transformed the data from their original ICRS coordinates to Galactocentric system, it is now possible to compute both spatial and kinematical tests to ensure that the selected stellar sample traces the Milky Way disc and its kinematics.

The 99.4 per cent of the 5 566 stars are within $4.9 \leq R[\text{kpc}] \leq 15.8$, a range of $\sim 11$ kpc along the Galactic disc, and with $|Z| \leq 1$ kpc from the Galactic plane in according to the characteristic scale height for the validity of the BG model (see Sect. 3.1 of Balasin and Grumiller, 2008). Table 7.1 lists the binned data in cylindrical rings delimited by $[R - \Delta R, R + \Delta R]$ as a function of $R$. The Robust Scatter Estimate (RSE) has been adopted as a robust measure of the dispersion of a distribution within each bin and estimate the "warmth" of a stellar population. It is defined as $(2\sqrt{2}\,erf^{-1}(4/5))^{-1} \simeq 0.390152$ times the difference between the 90$^{\text{th}}$ and 10$^{\text{th}}$ percentiles (the interdecile range) and, for a normal distribution, it equals the standard deviation (Lindegren et al., 2018).

The median heights from the mid-plane spans between $\widetilde{Z}_{max} = 0.496$ kpc and $\widetilde{Z}_{min} = -0.234$ kpc, with a total average of $\langle \widetilde{Z} \rangle = -0.027$ kpc; the average vertical dispersion is 0.206 kpc. The weighted average of the median azimuthal velocity $V_\phi$ across the bins is $\langle \widetilde{V}_\phi \rangle \sim 224$ km s$^{-1}$, while the RSE is always below 41.4 km s$^{-1}$, with a typical (i.e. mean) value of 21.1 km s$^{-1}$ as expected for a young thin disc stellar population; it results always larger than the uncertainty on the medians, $\sigma_{V_\phi}$, computed via bootstrapping with 100 re-samples of the bin population. Therefore, the $|\widetilde{Z}|$ and the $\widetilde{V}_\phi$ are quite compatible with those expected for a population belonging to the Milky Way young disc and confirm, in turn, the effectiveness of the procedure we adopted for extracting stars from the upper main sequence.

**Table 7.1:** Properties of the binned data for the stellar sample extracted from the Gaia DR2 data. $\Delta R$ is the bin size of the cylindrical rings $[R - \Delta R, R + \Delta R]$. Medians and RSE are used as robust estimates of the population in each bin.

| $\Delta R$ [kpc] | $R$ [kpc] | # of stars | $\widetilde{Z}$ [kpc] | $\widetilde{V}_\phi$ [km s$^{-1}$] | $\sigma_{V_\phi}$ [km s$^{-1}$] | $RSE$ [km s$^{-1}$] |
|---|---|---|---|---|---|---|
| 0.2 | 5.0 | 3 | -0.234 | 230 | 12 | 10.9 |
| | 5.2 | 7 | -0.077 | 233 | 8 | 14.9 |
| | 5.4 | 13 | -0.162 | 223 | 12 | 34.2 |
| | 5.6 | 14 | -0.069 | 203 | 8 | 21.4 |
| | 5.8 | 30 | -0.122 | 220 | 8 | 41.4 |
| | 6.0 | 40 | -0.112 | 229 | 3 | 37.4 |
| | 6.2 | 71 | -0.125 | 229 | 3 | 23.3 |
| | 6.4 | 102 | -0.124 | 234 | 3 | 19.8 |
| | 6.6 | 156 | -0.078 | 229 | 2 | 19.3 |
| | 6.8 | 244 | -0.036 | 231 | 2 | 19.8 |
| | 7.0 | 273 | -0.014 | 228 | 1 | 19.2 |
| | 7.2 | 364 | 0.007 | 229 | 1 | 20.2 |
| | 7.4 | 392 | 0.016 | 232 | 1 | 20.1 |
| | 7.6 | 428 | 0.023 | 233 | 1 | 18.7 |
| | 7.8 | 366 | 0.007 | 231 | 2 | 20.4 |
| | 8.0 | 368 | 0.010 | 234 | 1 | 19.7 |
| | 8.2 | 342 | -0.010 | 231 | 2 | 20.9 |
| | 8.4 | 380 | 0.009 | 232 | 1 | 22.4 |
| | 8.6 | 368 | -0.011 | 229 | 1 | 23.0 |
| | 8.8 | 343 | -0.055 | 226 | 1 | 17.2 |
| | 9.0 | 296 | -0.054 | 224 | 2 | 17.8 |
| | 9.2 | 219 | -0.044 | 224 | 1 | 18.1 |
| | 9.4 | 202 | -0.019 | 224 | 1 | 19.6 |
| | 9.6 | 155 | -0.039 | 222 | 2 | 21.0 |
| | 9.8 | 105 | -0.049 | 225 | 2 | 20.3 |
| | 10.0 | 77 | -0.012 | 228 | 4 | 23.1 |
| | 10.2 | 51 | 0.007 | 219 | 6 | 32.9 |
| | 10.4 | 27 | -0.067 | 230 | 2 | 21.1 |
| | 10.6 | 25 | -0.032 | 234 | 5 | 22.5 |
| | 10.8 | 20 | -0.031 | 230 | 6 | 32.3 |
| | 11.0 | 13 | -0.103 | 232 | 8 | 15.0 |
| 0.4 | 11.3 | 19 | -0.030 | 227 | 9 | 27.8 |
| 0.5 | 11.75 | 18 | 0.031 | 226 | 6 | 23.5 |
| | 12.25 | 20 | 0.061 | 229 | 14 | 21.3 |
| | 12.75 | 11 | -0.039 | 227 | 5 | 18.8 |
| | 13.25 | 7 | 0.001 | 234 | 10 | 8.2 |
| 1 | 13.8 | 4 | 0.496 | 208 | 24 | 32.9 |
| 1.5 | 15.8 | 2 | 0.043 | 220 | 12 | 9.2 |

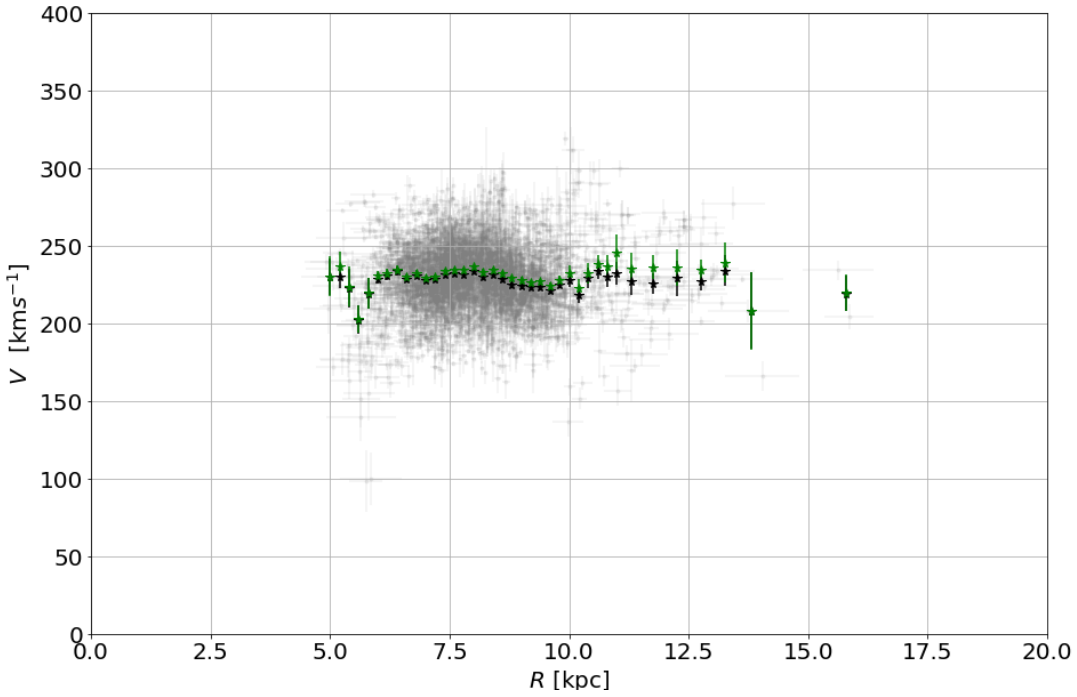


**Figure 7.1:** Comparison between the azimuthal velocity, $\widetilde{V}_\phi$ (black star symbols), and circular(ized) velocity, $V_c$ (green star symbols). The corresponding error bars are computed via bootstrapping by means of the bin population or Eq. 6.3, respectively. The grey dots represent the total sample of 5 566 stars with their measured uncertainties.

The calculation of the circular(ized) velocity through Eq. 6.2 represents a final robust and consistent test for the analysis. As already described in Chapter. 6, the circular(ized) velocity, $V_c$, is described by Eq. 6.3 where the contributions of the vertical gradients in Eq. 6.2 were neglected, and $\langle V_i^2 \rangle$ represents the averaged squared velocity of the velocity matrix in each bin.

Following Eilers et al. (2019), the radial density profile is approximated as $\rho(R) \propto exp(-R/h_r)$ with $h_r = 3$ kpc, while the radial gradient of $\langle V_R^2 \rangle$ – last term in the parenthesis of Eq. 6.3 – is close to zero in the radial range covered by data. The corresponding uncertainties, $\sigma_{V_c}$, are computed via bootstrapping with 100 re-samples on the individual values of the azimuthal velocities, accounting for the possible systematic errors (estimated within 5 per cent) that the approximations mentioned above could introduce. Fig. 7.1 shows the comparison between $\widetilde{V}_\phi$ and $V_c$. There is a slight positive gradient towards larger radial distances, as naturally expected by Jeans analysis, but the corrections due to the circularization procedure are always well below 10% and up to $\sim$ 10 km s$^{-1}$ throughout the radial range probed by the data. They are smaller than the RSEs and fairly consistent with the increasing uncertainties within each bin population.

In view of these results, in Crosta, Giammaria, Lattanzi, and Poggio (2020) we decided to use the observed and *model-independent* azimuthal velocity profile to test the two models of the Galactic rotation curve because this "preserves the internal consistency of our work since the Jeans analysis assumes Newtonian gravity and not a complete relativistic description". In fact, so far a relativistic generalization of the Jeans' analysis had not been implemented yet, due to the high level of complexity of the Einstein Field Equations. The only early attempts were the numerical computations by Ames, Andréasson, and Logg (2016) for Einstein-Vlasov self-gravitating systems, or by Nazari et al. (2017), for a post-Newtonian approximation.

Nevertheless, the implementation of the Jeans correction has no significant effect since the two series of data are consistent within their uncertainties and, as reported below in Tables 7.4 and 7.5, the fit results are compatible within the statistically Credible Interval of the posteriors for the two cases. This is because the selected stellar sample is the most suitable to ensure the effective applicability of a pressureless perfect fluid model to the Galaxy. As a further proof of this hypothesis note that in Table 7.1 the RSEs, equivalent to a pressure term in the Jeans analysis, is on average less than 10 per cent compared to the $\widetilde{V}_\phi$ in each bin.

## 7.2 The Galactic rotation curve velocity profile

The two models presented in the previous chapter are now fitted to the Gaia DR2 $\widetilde{V}_\phi(R_i)$ data of Table 7.1, accounting for the corresponding uncertainties, to infer the best-fit results. For the MWC model, we have a vector of parameters, $\theta$, including seven free parameters, namely the bulge mass $M_\mathrm{b}$, the masses and the scale lengths of the thin and thick discs, $M_\mathrm{td}$, $M_\mathrm{Td}$, $a_\mathrm{td}$, $a_\mathrm{Td}$, the scale-density and the radial scale length of the dark matter halo, $\rho_0^\mathrm{halo}$, $A_h$. Instead, for the BG model, we have a total of four free parameters: the normalization of the velocity in the flat regime, $V_0$, the lower and upper radial limits of the model representing the bulge radial scale length and the Galactic radius, $r_\mathrm{in}$ and $R_\mathrm{out}$, and the estimated dimensionless value characterizing the conformal factor function in the line element 6.9, $e^{\nu_0}$, inferred at $R_\odot$ and assumed constant elsewhere.

In Crosta, Giammaria, Lattanzi, and Poggio (2020), I implemented a Bayesian analysis with a Markov Chain Monte Carlo (MCMC) method to fit the data with the following log-likelihood function

$$\begin{aligned}\log\mathcal{L} &= -\frac{1}{2}\sum_i\left(\frac{[\widetilde{V}_\phi(R_i)-V_\phi^{\exp}(R_i|\theta)]^2}{\sigma^2_{V_\phi}}+\log\left(\sigma^2_{V_\phi}\right)\right)\\ &- \frac{1}{2}\left(\frac{[\rho(R_\odot)-\rho^{\exp}(R_\odot|\theta)]^2}{\sigma^2_{\rho_\odot}}+\log\left(\sigma^2_{\rho_\odot}\right)\right).\end{aligned} \tag{7.11}$$

Here, the first term fits the expected velocity value, $V_\phi^{\exp}(R_i|\theta)$, evaluated from the two theoretical models at each $R_i$ given the corresponding vector of parameters, $\theta$; the second term, instead, considers the expected model values of the baryonic matter density at the Sun position, $\rho^{exp}(R_\odot|\theta)$.

Note that in the classic framework the velocity profile is totally determined by the density profile via the Poisson equation (Eq. 6.4), hence the second term in Eq. 7.11 would not be necessary. Contrary to the MWC case, the use of the expected density profile, $\rho^{exp}(R_\odot|\theta)$, in the likelihood is mandatory for the BG model since the parameter $e^{\nu_0}$ can not be estimate with Eq. 6.18 only. For the relativistic model, such component is calculated via the 00-term of Einstein field equation reported in Appendix B (see Sect. 7.3 below for further details), while for the MWC model $\rho^{\exp}(R_\odot|\theta) = \rho_{\rm b}(R=R_\odot, Z=0)+\rho_{\rm td}(R=R_\odot, Z=0)+\rho_{\rm Td}(R=R_\odot, Z=0)$ from Eqs. 3.2 and 3.3. Unfortunately, direct observations of the baryonic matter density are limited to regions very close to the Sun. We have therefore the equivalent of a single data point with respect to the radial extension of the kinematic data to constrain this second term. McKee, Parravano, and Hollenbach (2015) provide the most recent "observed" estimate for the local baryonic matter density corresponding to $\rho(R_\odot) = 0.084 \pm 0.012\ \mathrm{M_\odot\ pc^{-3}}$.

### 7.2.1 On the parameters and priors of the fit

Since the parameter space is too large to be explored with a simple non-linear fit, the exploration of the full probability distribution functions of the unknown parameters and their uncertainties is conducted with an MCMC method using the python package *PYMC3* (Salvatier, Wiecki, and Fonnesbeck, 2016) with the No-U-Turn-Sampler algorithms (NUTS) for the step selection. Such sampler is used for continuous variables and automatically tunes the step size and the number of steps per sample. A detailed description can be found in Hoffman and Gelman (2014).

Since this is the first time that the BG model is fitted to Milky way data and there is no previous knowledge of its parameter distributions, the following uniform priors

- Uniform for $V_0 \in [150, 300]$ km s$^{-1}$;
- Uniform for $R_{\rm out} \in [10, 100]$ kpc;
- Uniform for $r_{\rm in} \in [0, 2]$ kpc;
- Uniform for $e^{\nu_0}[\cdot 10^{-7}] \in [0.001, 10]$;

are adopted to explore and determine the corresponding posteriors. On the other hand, for the MWC model normal-distributed priors are considered, in order to compare the Bayesian analysis results to the most recent observational estimates from Iocco, Pato, and Bertone (2015), Bovy (2015), Moni Bidin et al. (2015), McMillan (2017), Pouliasis, Di Matteo, and Haywood (2017), and Korol, Rossi, and Barausse (2019). In this case the priors are the following:

- $P(M_{\rm b}) = \mathcal{N}(\mu = 1.067, \sigma = 0.5) \cdot 10^{10}$ M$_\odot$;
- $P(M_{\rm td}) = \mathcal{N}(\mu = 3.944, \sigma = 0.5) \cdot 10^{10}$ M$_\odot$;
- $P(M_{\rm Td}) = \mathcal{N}(\mu = 3.944, \sigma = 0.5) \cdot 10^{10}$ M$_\odot$;
- $P(a_{\rm td}) = \mathcal{N}(\mu = 5.3, \sigma = 0.5)$ kpc;
- $P(a_{\rm Td}) = \mathcal{N}(\mu = 2.6, \sigma = 0.5)$ kpc;
- $P(\rho_0^{\rm halo}) = \mathcal{N}(\mu = 0.01, \sigma = 0.005)$ M$_\odot$ pc$^{-3}$;
- $P(A_h) = \mathcal{N}(\mu = 19.6, \sigma = 4.9)$ kpc.

Besides, the bulge radial scale length is fixed to $b_{\rm b} = 0.3$ kpc, following Pouliasis, Di Matteo, and Haywood (2017), since our data do not explore the Galactic central region where the bulge dominates. At the same time, the vertical scale heights of the thin and thick discs are also fixed at $b_{\rm td} = 0.25$ kpc and $b_{\rm td} = 0.8$ kpc (Pouliasis, Di Matteo, and Haywood, 2017) since the rotation curve profile depends only on the radial coordinate and the vertical distribution of the data can not be probed. With these precautions, any possible correlations with the free parameters posteriors are compensated.

It is worth mentioning here that de Almeida, Piattella, and Rodrigues (2016) already tried to fit the BG model (and the other relativistic model by

**Table 7.2:** The bets-fit results for the BG model. $\theta$ represents the medians, while $\sigma_\theta^-$ and $\sigma_\theta^+$ are the $1\sigma$ Credible Intervals of the parameters posteriors.

| BG model | $\theta$ | $\sigma_\theta^-$ | $\sigma_\theta^+$ |
|---|---|---|---|
| $r_{\rm in}$ [kpc] | 0.39 | -0.25 | +0.36 |
| $R_{\rm out}$[kpc] | 47.87 | -14.80 | +23.96 |
| $V_0$ [km s$^{-1}$] | 263.10 | -16.44 | +25.93 |
| $e^{\nu_0}$ [$\cdot 10^{-7}$] | 3.59 | -0.47 | +0.65 |

Cooperstock and Tieu, 2007, CT model) to the observed rotation curves for some external galaxies. They converted the data set into an effective analogue called "effective Newtonian" velocity profile, $V_{\rm eN}$, in order to define a method to compare non-Newtonian gravity models with or without the implementation of a dark matter halo. Fitting a Newtonian velocity profile to such effective Newtonian curve and solving Poisson-like equations, the authors claimed that both CT and BG approaches have strong problems fitting galactic rotation curves without dark matter. However, they considered a $\chi^2$ minimization procedure for the fit, a statistical technique that could be insufficient to explore the whole parameter space as discussed below in Sect. 7.2.2. In fact, some of their results do not appear suitable for a consistent representation of the BG model: for example, for some of the galaxies these authors investigated, a galactic radius of $R \sim 10^7$ kpc is provided (see de Almeida, Piattella, and Rodrigues, 2016, Table 3); these values are out of the range given by the BG solution and galaxies cannot be considered isolated at such distances.

### 7.2.2 The resulting parameters and the goodness of the fit

The best-fit results for the two models are listed in Tables 7.2 and 7.3 and shown in Fig. 7.2. The star-like symbols show the medians $\widetilde{V}_\phi$ versus $R$ from Table 7.1. The errors due to the Bayesian inference are at least one order of magnitude lower than the resulting uncertainties on the parameters.

The two estimated velocity profiles are both fairly good representations of the data as confirmed by the Widely Applicable Information Criterion (WAIC, Watanabe and Opper, 2010), which is a fully Bayesian criterion for estimating the out-of-sample expectation and measures the *poorness* of the fit. By definition, the preferred model is the one with the minimum WAIC

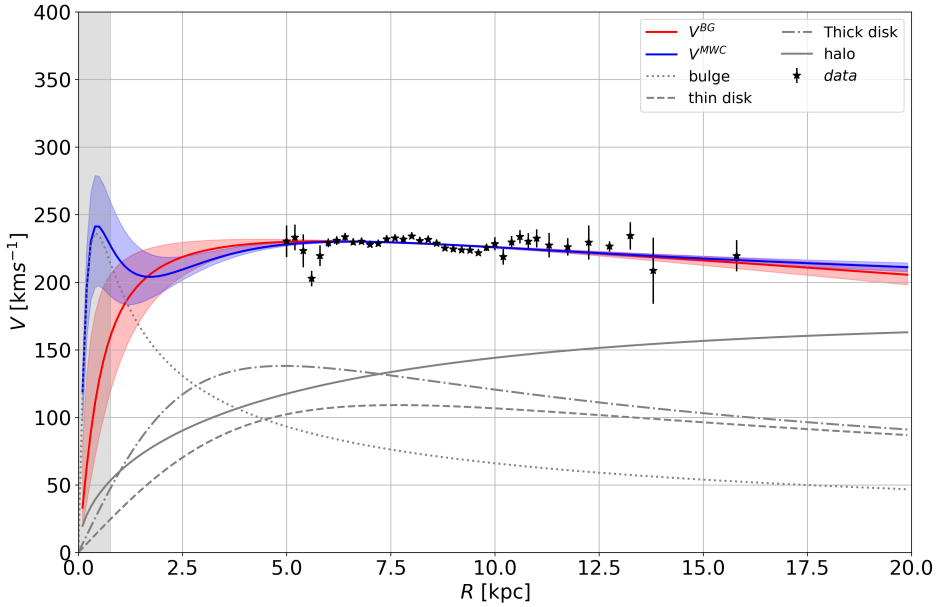


**Figure 7.2:** Velocity profiles of the Milky Way rotation curve derived from the disc tracers sample. The black starred symbols represent the median values of binned data of Table 7.1 with the corresponding error bars. The red and blue curves show the best-fit to the BG and MWC models, respectively, with the corresponding Credible Intervals as the shadow coloured areas. The grey curves represent the separated kinematic contributions to the MWC model: dotted line for the bulge, dashed and dot-dashed lines for thin and thick discs, and solid line for the dark matter halo. The grey vertical band on the left represents twice the value of $r_{\rm in}$ estimated by the BG model.

**Table 7.3:** As Table 7.2 but for the free parameters of the MWC model.

| MWC model | $\theta$ | $\sigma_\theta^-$ | $\sigma_\theta^+$ |
|---|---|---|---|
| $M_{\rm b}[10^{10}{\rm M}_\odot]$ | 1.0 | -0.4 | +0.4 |
| $M_{\rm td}[10^{10}{\rm M}_\odot]$ | 3.9 | -0.4 | +0.4 |
| $M_{\rm Td}[10^{10}{\rm M}_\odot]$ | 4.0 | -0.5 | +0.5 |
| $a_{\rm td}$ [kpc] | 5.2 | -0.5 | +0.5 |
| $a_{\rm Td}$ [kpc] | 2.7 | -0.4 | +0.4 |
| $\rho_0^{\rm halo}[{\rm M}_\odot{\rm pc}^{-3}]$ | 0.009 | -0.003 | +0.004 |
| $A_h$ [kpc] | 17 | -3 | +4 |

value discouraging, at the same time, overfitting with a penalty factor related to the number of estimated parameters[3]. Given this, the two models appear almost identically consistent with the data with WAIC = 288.8 and 282.6 for the BG and MWC models, respectively.

For the MWC model, the estimated parameters are consistent within the uncertainties of the most recent literature estimates (Iocco, Pato, and Bertone, 2015; Bovy, 2015; Moni Bidin et al., 2015; McMillan, 2017; Pouliasis, Di Matteo, and Haywood, 2017; Korol, Rossi, and Barausse, 2019). Because of the relatively "narrow" range covered by the Gaia DR2 data, the largest contributions to the $1\sigma$ credible interval come from $M_{\rm b}$ and $A_h$ uncertainties, which are the most difficult parameters to be constrained.

For the BG model, the least constrained parameter is the "upper" radial limit, $R_{\rm out}$, for similar reasons, while an interesting result is obtained on the "lower" limit parameter, $r_{\rm in}$: remarkably, the fitted value $r_{\rm in} = 0.39$ kpc in Table 7.2 is quite close to the value of $b_{\rm b} = 0.3$ kpc adopted for the Plummer's scale length of the bulge in the MWC model (see Eq. 3.2 in Sect. 6.2.1). According to Balasin and Grumiller (2008), as $r_{\rm in}$ "determines the transition between the linear ($r \ll r_{\rm in}$) and the flat ($r_{\rm in} \leq r \leq R_{\rm out}$) regime of the velocity profile", the size of the bulge "may be predicted from the velocity profile". This provides an independent measurement of the radial size of the Milky Way bulge directly from the Galactic rotation curve, despite the already discussed existence of the critical region at $|Z| > 0.39$ kpc that limits the physical validity of the BG model and prevents it from describing large parts of the actual Galaxy. However, we can highlight here an important experimental result: the selected stellar population is spatially constrained to small distances from the Galactic plane with an average median height $\langle \widetilde{Z} \rangle \simeq -0.03$ kpc and a corresponding average dispersion of 0.2 kpc (see Table 7.1), thus, in turn, $\langle \widetilde{Z} \rangle \leq r_{\rm in}$ virtually everywhere across the radial range spanned by the Gaia rotational velocity data. This confirms the back-compatibility of the model with the data considered.

The posterior distributions of the parameters for the MWC model and the BG model are shown in Figs. 7.3 and 7.4, respectively. For both models, the mean values and the medians are both good estimates of the distribution for each posterior. The strongest correlation in the MWC model is between the scale-density, $\rho_0^{\rm halo}$, and the radial scale length, $A_h$, of the dark matter halo, similarly to what was found by McMillan (2017). There are smoother

[3] This is desired because increasing the number of parameters in the model almost always improves the goodness of the fit resulting in a loss of generalization of the model itself.

**Table 7.4:** Posterior estimates for the BG model using $V_\phi$ and $V_c$ data. Hpd stands for Highest Posterior Density and is the minimum width Bayesian Credible Interval computed by the PYMC3 algorithm.

| BG model $V_\phi$ | $V_0$ [km s$^{-1}$] | $R_{out}$ [kpc] | $r_{in}$ [kpc] | $e^{\nu_0}$ [$10^{-7}$] |
|---|---|---|---|---|
| hpd 0.16 | 246.67 | 33.07 | 0.13 | 3.12 |
| median | 263.10 | 47.87 | 0.39 | 3.59 |
| hpd 0.84 | 289.04 | 71.84 | 0.74 | 4.24 |
| BG model $V_c$ | $V_0$ [km s$^{-1}$] | $R_{out}$ [kpc] | $r_{in}$ [kpc] | $e^{\nu_0}$ [$10^{-7}$] |
| hpd 0.16 | 250.48 | 38.33 | 0.27 | 3.37 |
| median | 269.22 | 53.28 | 0.55 | 3.88 |
| hpd 0.84 | 289.21 | 92.83 | 0.81 | 4.60 |

**Table 7.5:** As Table 7.4 but for the MWC model. Note the different units of $\rho_0^{halo}$ with respect to Table 7.3.

| MCW model $V_\phi$ | $M_b$ [$M_\odot$] | $M_{td}$ [$M_\odot$] | $M_{Td}$ [$M_\odot$] | $a_{td}$ [kpc] | $a_{Td}$ [kpc] | $\rho_0^{halo}$ [$10^2$ $M_\odot$ pc$^{-3}$] | $A_h$ [kpc] |
|---|---|---|---|---|---|---|---|
| hpd 0.16 | 0.65 | 3.49 | 3.56 | 4.70 | 2.30 | 0.61 | 13.61 |
| median | 1.01 | 3.89 | 4.01 | 5.16 | 2.68 | 0.87 | 16.75 |
| hpd 0.84 | 1.37 | 4.28 | 4.47 | 5.63 | 3.08 | 1.23 | 20.74 |
| MCW model $V_c$ | $M_b$ [$M_\odot$] | $M_{td}$ [$M_\odot$] | $M_{Td}$ [$M_\odot$] | $a_{td}$ [kpc] | $a_{Td}$ [kpc] | $\rho_0^{halo}$ [$10^2$ $M_\odot$ pc$^{-3}$] | $A_h$ [kpc] |
| hpd 0.16 | 0.54 | 3.49 | 3.52 | 4.79 | 2.40 | 0.69 | 14.05 |
| median | 0.90 | 3.88 | 3.98 | 5.25 | 2.79 | 0.95 | 17.02 |
| hpd 0.84 | 1.25 | 4.27 | 4.43 | 5.71 | 3.19 | 1.32 | 20.75 |

correlations between all other parameters. On the other hand, for the BG model the velocity normalization parameter, $V_0$, appears strongly correlated and anti-correlated with the two radial parameters, $r_{in}$ and $R_{out}$, respectively, as expected by their definitions (see Sect. 6.3.1). The conformal factor, $e^{\nu_0}$, seems to be less correlated to all other parameters, because of the single data point available to constrain the baryonic density.

Finally, the numerical evidence that the implementation of the Jeans correction discussed in Sect. 7.1.2 has no strong influence on the posteriors estimates is demonstrated by the results listed in Tables 7.4 and 7.5 for $V_\phi$ and $V_c$, respectively.

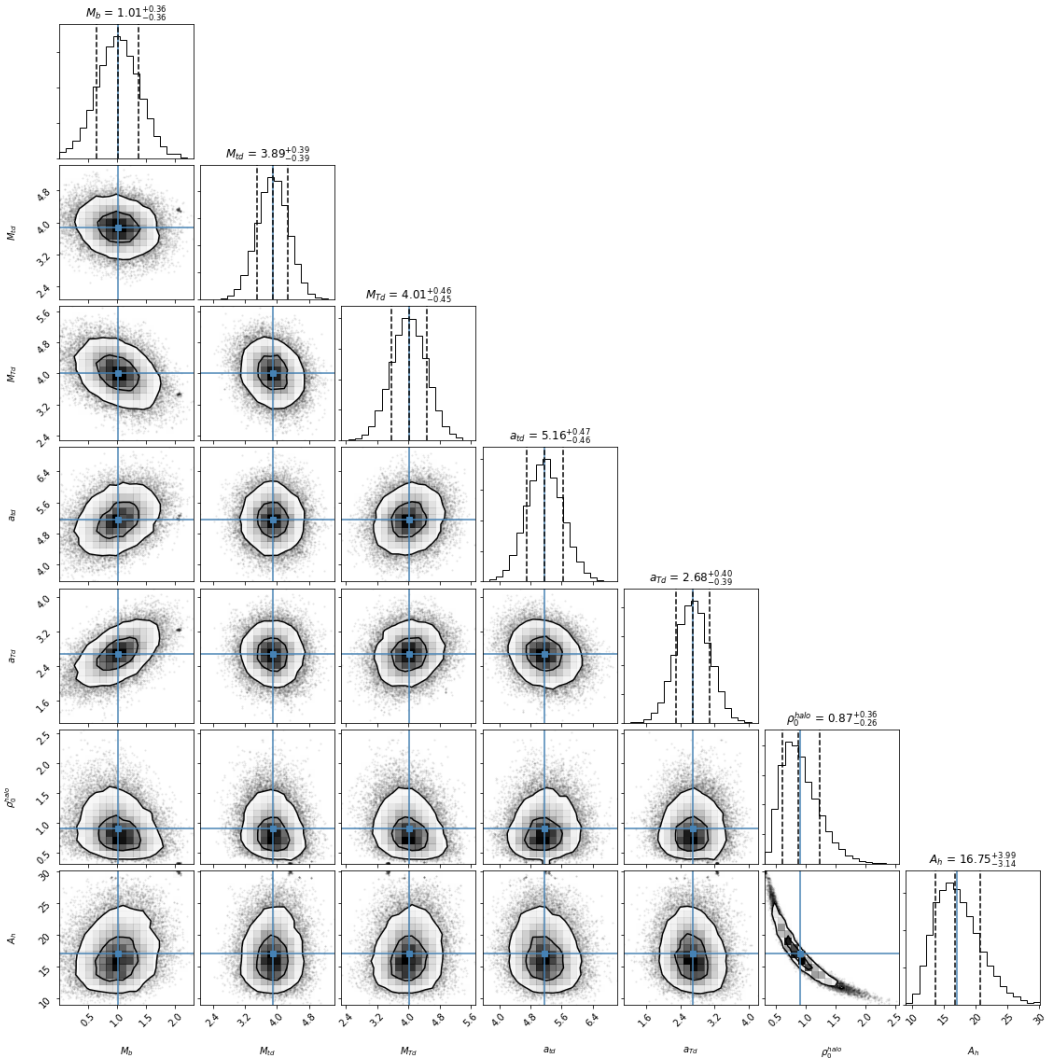


**Figure 7.3:** MWC parameters corner plot. On the diagonal, the histograms represent the 1D posterior distributions of each parameter, and the other panels represent the 2D correlations. The black thick contours indicate the $1\sigma$ and $2\sigma$ credible levels, while the blue crossing lines represent the mean values. The black dashed vertical lines mark the $16^{\text{th}}$, $50^{\text{th}}$ (i.e. median), and $84^{\text{th}}$ percentiles of the posteriors. Finally, the average values and their corresponding $16^{\text{th}}$ and $84^{\text{th}}$ percentiles are shown on top of the histograms. Note that $\rho_0^{\text{halo}}$ is in unit of $10^2$ $M_\odot$ $pc^{-3}$.

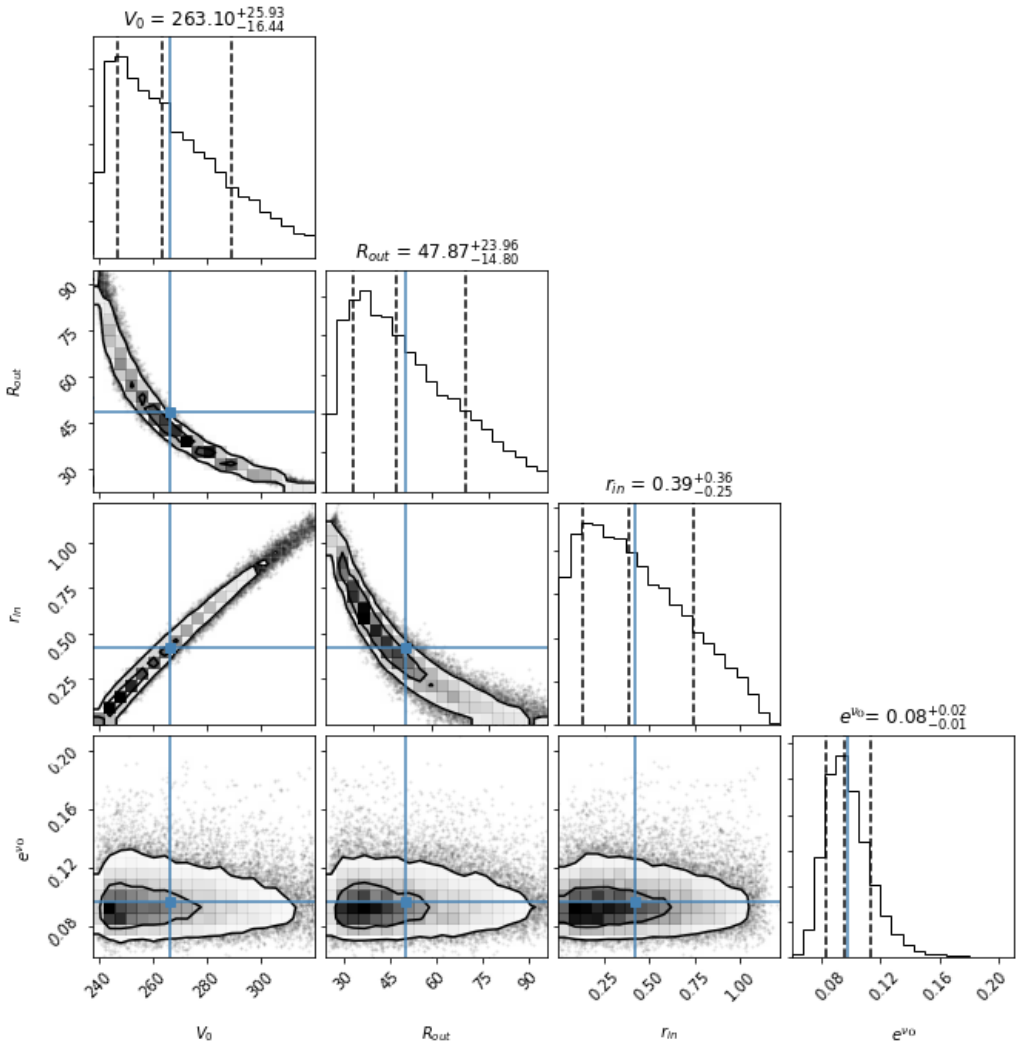


**Figure 7.4:** As Fig. 7.3 but for the BG parameters.

## 7.3 The mass density profile

Given the line element 6.9 and the metric function of Eq. 6.17, the 00-term of the Einstein field equation (see last Eq. B.5 in Appendix B) provides the matter density profile written as

$$\rho^{\mathrm{BG}}(R,Z) = \frac{(\partial_R N(R,Z))^2 + (\partial_Z N(R,Z))^2}{8G\pi R^2 e^{\nu(R,Z)}} \tag{7.12}$$

where $\rho^{\mathrm{BG}}(R,Z)$ is the mass density at $(R,Z)$ and $e^{\nu(R,Z)}$ is the dimensionless conformal factor defined in Sect. 6.3. With $R$ and $Z$ in kpc, the estimated model parameters as in Table 7.2, and $G = 4.3 \cdot 10^{-6}$ kpc km$^{-2}$ s$^{-2}$ M$_\odot^{-1}$, this equation yields the density in M$_\odot$ pc$^{-3}$. Despite the already mentioned inadequacy of the BG model to represent our Galaxy for regions above $|Z| = r_{\mathrm{in}} = 0.39$ kpc (see previous chapter), the density approaches zero for $R \to \infty$ and $Z \to \infty$, as physically required and demonstrated later on in Sect. 8.2.3.

### 7.3.1 The relativistic mass density at Sun position

Using the best-fit values of Table 7.2 in Eq. 7.12, the local baryonic matter density is, therefore, $\rho(R = R_\odot, Z = 0) \equiv \rho_\odot = 0.083 \pm 0.006$ M$_\odot$ pc$^{-3}$, which is in agreement with current independent estimates of $0.098^{+0.006}_{-0.014}$ M$_\odot$ pc$^{-3}$, $0.077 \pm 0.007$ M$_\odot$ pc$^{-3}$, or $0.084 \pm 0.012$ M$_\odot$ pc$^{-3}$ provided by Garbari et al. (2012), Bienaymé et al. (2014), and McKee, Parravano, and Hollenbach (2015), respectively. Notice that the latter is the most recent determination of $\rho(R = R_\odot)$ and was considered to fit the likelihood function of Eq. 7.11. Nevertheless, such local baryonic density estimate is the true result of the fit procedure given the prior distributions of Sect. 7.2.1 and the crude assumption that the conformal metric factor is constant with $R$, i.e. $e^{\nu}(R, Z = 0) \simeq e^{\nu_0}$.

The aforementioned procedure is a generalization of and conceptually different than what was proposed by Balasin and Grumiller (2008), Cooperstock and Tieu (2007) or Magalhaes and Cooperstock (2017). Instead of an a priori approximation of $e^{\nu}$ to compare the mass density to the Newtonian regime (see Sects. 3.2 and 3.3 of Balasin and Grumiller, 2008), in the likelihood function 7.11 the functional dependence of the conformal factor upon the $\rho^{\mathrm{exp}}$ term is directly computed. On one side, the results are somewhat "forced" to consider the single observed density value available at $R = R_\odot$ and a constant $e^{\nu}$, leading to the dimensionless estimate $e^{\nu_0} = 0.083$ (Table 7.2). On the other hand, the MCMC fit procedure allows $e^{\nu_0}$ to vary freely and uniformly

distributed as for the rest of the BG model parameters: at variance with previous works, it varies by 4 orders of magnitude within the interval $[0.001, 10]$. For instance, Magalhaes and Cooperstock (2017) considered a fixed $e^{\nu} = 1$ in their model.

Of course, in Newtonian dynamics the case is much different (and in some way "simpler"), since the rotational velocity data alone suffice to fit all of the parameters needed to define the different contributions to the Galaxy density functions via Eqs. 3.1, 3.2, and 3.3.

### 7.3.2 The mass density in the Galactic plane

To extend the analysis to the whole Galactic plane, Eq. 7.12 can be evaluated as a function of $R$ at $Z = 0$ using best-fit values listed in Tables 7.2 and 7.3. In this case, the term $\partial_Z N(R, Z)$ goes to zero everywhere and the two density profiles are shown in Fig. 7.5 with red and blue lines for the BG and the MWC models, respectively.

For the MWC model, the result comprising the baryonic and the dark matter is compatible with what shown in McMillan (2017), Pouliasis, Di Matteo, and Haywood (2017), and Eilers et al. (2019), confirming the goodness of our "classical" analysis. As expected, in the Galactic plane the dominant matter component is the baryonic one, with a value of $\rho_{\rm bar} \sim 0.08 - 0.10\ \mathrm{M}_\odot\ \mathrm{pc}^{-3}$ at $R_\odot$, while for the dark matter the analysis yields $\rho_{\rm DM} \sim 0.01\ \mathrm{M}_\odot\ \mathrm{pc}^{-3}$. This is not surprising since the stars and gas, i.e. the baryonic matter, are mainly concentrated in the Galactic disc, while the dark matter is distributed in a far larger spherical volume surrounding the Galaxy, i.e. the dark matter halo, resulting in a low average density. As a consequence, integrating to different radii, the total amount of baryonic mass (the sum of the bulge, thin, and thick discs contributions) is mainly enclosed within a spherical volume of $r = 30$ kpc and totals $M_{\rm bar} \sim 7 \cdot 10^{10}\ \mathrm{M}_\odot$, while the dark matter halo has a virial mass of $M_{\rm DM} \sim 1 \cdot 10^{12}\ \mathrm{M}_\odot$. This is similar to McMillan (2017), which reports for the Milky Way a total stellar mass of $(5.43 \pm 0.57) \cdot 10^{10}\ \mathrm{M}_\odot$ and a total virial mass of $(1.30 \pm 0.30) \cdot 10^{12}\ \mathrm{M}_\odot$, composed mainly of dark matter. On the other hand, Magalhaes and Cooperstock (2017), using the CT model obtained a mass of $9.3 \cdot 10^{10}\ \mathrm{M}_\odot$ for the Galaxy.

Fig. 7.5 shows also that the two solid lines representing the baryonic MWC profile and its BG analogue are almost coincident for $R > 4$ kpc and predict a very similar baryonic mass distribution in the Galactic plane for the radial

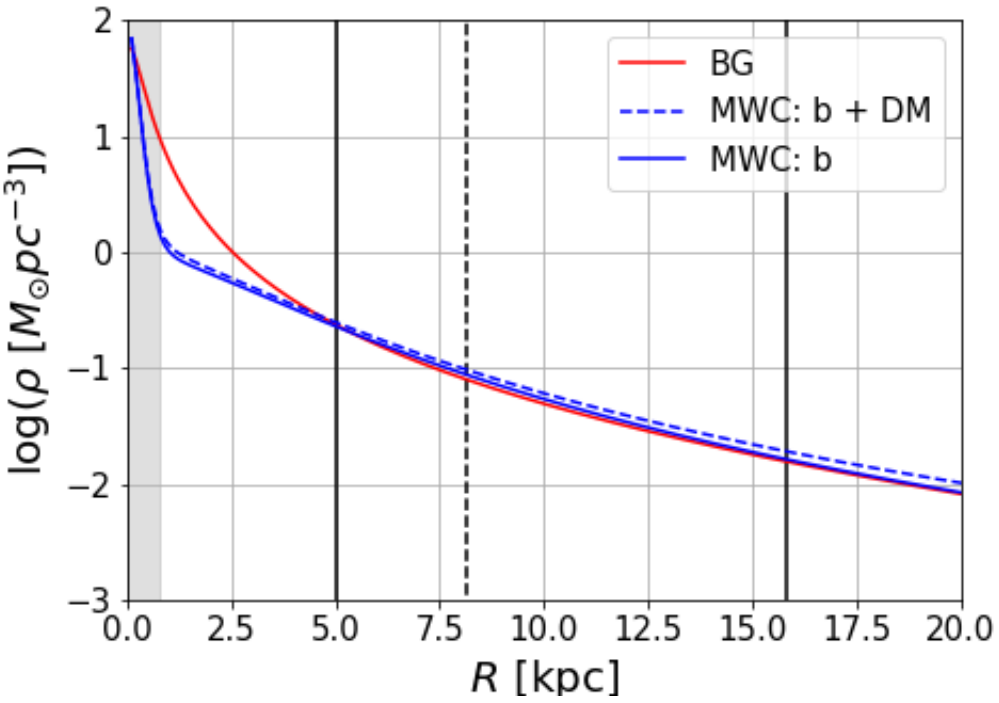


**Figure 7.5:** The density profile of the Milky Way at $Z = 0$ derived from 100 random draws from the distributions of the posteriors. As in Fig. 7.2, the red solid line is the BG model, while the blue solid line shows the contribution of the baryonic matter-only for the MWC model and the blue dashed line the total matter contribution including the dark matter. The vertical black solid lines limit the range of the Gaia data, while the vertical black dashed line indicates the Sun position in the Galaxy. The grey vertical band represents twice the value of $r_{\rm in}$ estimated with the BG model.

range $5 \leq R[\text{kpc}] \leq 16$ probed by Gaia data. This confirms *a posteriori* the assumption of a constant value for $e^{\nu}$ at the Sun position.

On the other hand, the two profiles differ for $R \leq 4$ kpc, i.e. inside the Milky Way bulge regions. The BG mass density at $R \sim 0.8$ kpc (by assumption, only baryonic) requires more than 10 times the mass provided by the density components of the MWC model including the dark halo. This promote the question of whether the BG model simply moves the necessity of more mass from the outer regions of the Galaxy to a very concentrated central distribution. However, this is not the case. In fact, in the MWC case the baryonic mass results to be $3.5 \cdot 10^{10}$ $M_{\odot}$, integrating the baryonic density for the two discs in the region limited respectively, by boundaries [$r \leq 4$ kpc; $|Z| \leq 10$ kpc]. The value of 10 kpc is more than 10 times the scale height adopted for the thick disc, while the spherical radius of $r \leq 4$ kpc is more than 10 times the $b_{\text{b}}$ radial scale length of the Plummer bulge considered. This value compares quite favourably with the $4.8 \cdot 10^{10}$ $M_{\odot}$ derived from integrating the BG mass density in the region $\epsilon \ll R \leq 4$ kpc, with $\epsilon \ll 1$ kpc, and $|Z| \leq |Z|_{\text{eff}} = 0.215$ kpc. Here, $|Z|_{\text{eff}}$ represents the effective half-thickness of the BG Milky Way disc, as derived in the next section. It is worth mentioning at this point that its value is below $r_{\text{in}}$, as it should be, given by the theoretical assumptions of the BG model. On the other side, $\epsilon$ represents an extremely small region, very close to the $Z$-axis where the BG model is not defined and arises inconsistent velocities only when $|Z| \geq r_{\text{in}}$ (see Sect. 6.3.1. This appears to be the upper limit of the forbidden region where $R < N(R, Z)$ starts deviating significantly from $R = 0$ (see Sect. 6.3 of this Thesis and Grumiller, Balasin, and Preis, 2009, for further details).

## 7.4 Gravitational dragging and dark halo contributions to the Milky Way rotation curve

The aforementioned effective half-thickness of the Galactic disc, $|Z|_{\text{eff}}$, was defined in Crosta, Giammaria, Lattanzi, and Poggio (2020) starting from Eq. 16 of de Almeida, Piattella, and Rodrigues (2016, Sect. 3.2).

Using the relativistic density computed with Eq. 7.12, the effective Newtonian circular velocity profile, $V_{\text{eN}}^{\text{BG}}$, can be calculated at any given point along $R$ by solving the Poisson equation $\nabla^2\Phi(R, Z, \theta) = 4\pi G\rho(R, Z, \theta)$, and using $V^2(R, \theta) = R\partial_R\Phi(R, \theta)$, where $\theta$ is the best-fit parameters vector used

to evaluate the density. In particular, the expression for $V_{\rm eN}^{\rm BG}$ can be directly evaluated with the relation

$$\begin{aligned} V_{\rm eN}^{\rm BG\,2}(R,\theta) &= R\partial_R\Phi(R,Z=0,\theta) \\ &= -GR\partial_R\int_{-\pi}^{\pi}d\phi'\int_{-\infty}^{\infty}dZ'\int_0^{\infty}dR' \\ &\times\frac{\rho^{\rm BG}(R',Z',\theta)}{\sqrt{R^2+R'^2+Z'^2-2RR'\cos\phi'}}R' \\ &= -2GR\int_0^{\infty}dZ'\int_0^{\infty}dR'\rho^{\rm BG}(R',Z',\theta)\partial_R\left[\frac{4K\left(\frac{4RR'}{(R+R')^2+Z'^2}\right)}{\sqrt{(R+R')^2+Z'^2}}\right]R' \end{aligned} \tag{7.13}$$

where $K$ is the complete elliptic integral defined by

$$K(x)=F(\pi/2,x)=\int_0^{\pi/2}d\alpha(1-x\sin^2\alpha)^{-1/2}. \tag{7.14}$$

and considering that the extension of the integration along the direction perpendicular to the Galactic plane in the equation above must be restricted to the region of validity of the BG model, i.e. $|Z|\leq r_{\rm in}=0.39$ kpc. For further details, see Binney and Tremaine (2011, Chapters 2 and 4 and Appendix C), and Eqs. 16-17 of de Almeida, Piattella, and Rodrigues (2016), noting that the authors did not fit the $e^{\nu_0}$ parameter and, therefore, they mistakenly integrated along the whole $z$-axis, neglecting the limit of applicability of the BG model.

With this definition of $V_{\rm eN}^{\rm BG}$, we can evaluate the amount of rotational velocity at $Z=0$ due to gravitational dragging, $V_{\rm drag}^{\rm BG}$, which has no a Newtonian counterpart, and then compare it with the dark matter contribution to $V^{\rm MWC}$ as follows.

As we did in Crosta, Giammaria, Lattanzi, and Poggio (2020), given the Newtonian baryonic velocity profile derived from the MWC model

$$V_{\rm eN}^{\rm MWC}=\sqrt{V_{\rm bulge}^2+V_{\rm td}^2+V_{\rm Td}^2} \tag{7.15}$$

where $V_{\rm bulge}$, $V_{\rm td}$, and $V_{\rm Td}$ are the circular velocities due to the Milky Way bulge, thin, and thick discs, respectively (i.e. the dashed lines shown in Fig. 7.2), the quantity

$$\Delta V_{BG-MWC}=(V_{\rm eN}^{\rm BG}(R_i,k)-V_{\rm eN}^{\rm MWC}(R_i))^2 \tag{7.16}$$

is the square of the differences between the relativistic effective Newtonian rotational velocity at $R_i$ and its pure Newtonian analogue, $V_{\rm eN}^{\rm MWC}(R_i)$. Let us then consider the quadratic form

$$\frac{\sum_{i=1}^{N}(V_{\rm eN}^{\rm BG}(R_i,k)-V_{\rm eN}^{\rm MWC}(R_i))^2}{N} \tag{7.17}$$

where $N$ is the total number of $R_i$'s utilized in the radial domain of the experimental velocity data, spacing from $R_1 = 5$ kpc to $R_{N_{max}} = 20$ kpc with $R_N = ((N-1)\cdot\Delta R_{\rm step}+5)$ kpc and $\Delta R_{\rm step} = 0.1$ kpc. The second index $k$ identifies the half-thickness, $|Z|_k \leq r_{\rm in}$, of the $k$-th BG disc used in the vertical integral of Eq. 7.13 to compute numerically each effective Newtonian circular velocity value, as the index $i$ runs from 1 to $N_{max}$.

By minimizing the quadratic form 7.17 as a function of the relativistic disc half-thickness $|Z|_k = k\cdot\Delta Z_{\rm step}$, with $k = 1,\ldots,M$, $\Delta Z_{\rm step} = 0.005$ kpc and $|Z|_M \leq r_{\rm in}$, the two effective Newtonian velocity profiles are made as similar as possible in the radial range explored by Gaia data. Finally, the amount of rotational velocity across the Milky Way plane due to gravitational dragging can be calculated as the square root of the quadratic difference between the BG velocity profile from Eq. 6.18, and the effective Newtonian circular velocity, as computed for the disc half-thickness $|Z|_{\rm eff}$ provided by the minimization procedure, namely

$$V_{\rm drag}^{\rm BG}(R,|Z|_{\rm eff}) = \sqrt{(V^{\rm BG}(R))^2-(V_{\rm eN}^{\rm BG}(R,|Z|_{\rm eff}))^2}. \tag{7.18}$$

For the effective BG disc, the minimization process yields a half-thickness $|Z|_{\rm eff} = 0.215$ kpc. Smaller radial and/or vertical steps changes only the non-significant digits of the $|Z|_{\rm eff}$ value, while as $|Z|_k$ increases to the physical limit of 0.39 kpc, the BG effective Newtonian circular profile grows to unrealistic rotational velocities, well above the $V^{\rm BG}(R)$ profile itself, for even larger portions of the Galactic plane. Indeed, for $|Z|_{\rm eff} = 0.39$ kpc, $V_{\rm drag}^{\rm BG}$ (R) is already unrealistically higher than the $V^{\rm BG}(R)$ curve throughout the whole radial interval.

In Fig. 7.6 the results of the above computation are shown. The red solid line represents the $V_{\rm eN}^{\rm BG}(R,|Z|_{\rm eff})$ that the minimization procedure finds closest to $V_{\rm eN}^{\rm MWC}(R)$, the blue solid line in the chart. The $V_{\rm drag}^{\rm BG}(R,|Z|_{\rm eff})$ profile is shown by the red dashed line and can be compared to the contribution of the dark matter halo alone, the blue dashed curve $V_{\rm DM}^{\rm MWC}$, namely the grey solid line in Fig. 7.2).

The gravitational dragging curve is close to zero at $R \sim 4.5$ kpc, where

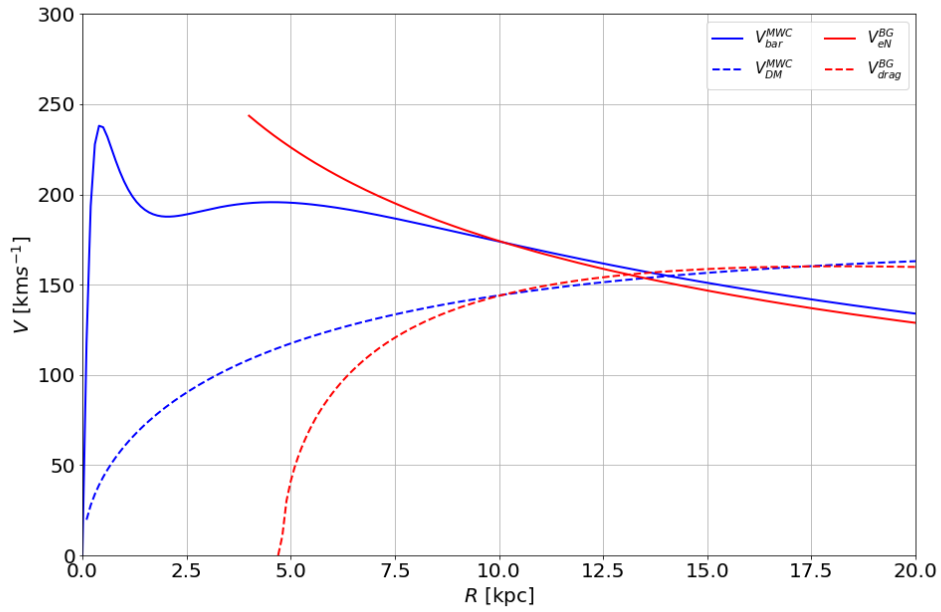


**Figure 7.6:** The colours code refer again to the BG and MWC model, respectively. Solid lines represent the relativistic effective Newtonian rotation curve, $V^{\rm BG}_{\rm eN}$, and its analogue for the MWC model for the total baryonic mass-only. The dashed lines show the MWC halo component alone, and the gravitational dragging contribution, $V^{\rm BG}_{\rm drag}$, to the $V^{\rm BG}$ itself.

$V^{\rm BG}_{\rm eN}(R, |Z|_{\rm eff}) \sim V^{\rm BG}(R)$, and then grows sharply within 2.5 kpc outwards to resemble the dark matter curve for most of the range up to $R = 20$ kpc. As reported in Crosta, Giammaria, Lattanzi, and Poggio (2020): "This shows quantitatively that gravitational dragging can plausibly compensate for the need of a dark halo to sustain the flat velocity profile at large radii from the Galactic Centre as long as $|Z|_{\rm eff} = 0.215$ kpc is used in the context of the BG model".

The limit of the applicability of the effective Newtonian velocity in combination with a density model, $\rho^{\rm BG}$, becomes evident for $R \leq 5$ kpc in the regions were Gaia can not observe and investigate yet. Here, the two effective Newtonian velocities differ sharply, to the point that, for $R \lesssim 4.5$ kpc, $V^{\rm BG}_{\rm eN}(R)$ grows unrealistically above $V^{\rm BG}(R)$ itself. However, this could be also an indication of the fact that the representation with just a disc component of the BG model – an axisymmetric distribution of rotating stellar particle system – is unsuited to describe the complex structure of the Milky Way, especially towards its central regions. More data and much improved mathematical models are necessary before such a scenario can be confirmed.

# Part V

# Conclusion

# Chapter 8

# Conclusions and future developments

The aim of this thesis is to consider the Milky Way as the fundamental keystone for the study of formation and evolution of disc-like galaxies, pushing at the same time on the use of General Relativity in this context. The realization of the largest laboratory of Local Cosmology at our disposal is made available by Gaia DR2 data and next releases that are fundamental to pursue these goals. To recall what said at the beginning of this manuscript (Sect. 1.4): a General Relativistic picture of the Milky Way can ensure a strong and coherent Laboratory of Local Cosmology against which any model, for the Galaxy first and and then for cosmology, can be fully tested. In this last chapter, the main results exposed in this Thesis are summarised and some possible future developments based upon the next Gaia Data Releases, are proposed.

## 8.1 Summary of the main results

With the revolutionary improvement given by the Astrometric observations of *Gaia* (Gaia Collaboration et al., 2016) and the new generations of large-scale spectroscopic surveys such as *APOGEE* (Majewski et al., 2017) and *GALAH* (Hayden et al., 2020), the doors to the largest and most important laboratory available nowadays for galactic studies are now open and we are in the era of Local Cosmology. At the same time, thanks to high-resolution cosmological simulations, we can extensively test our models for the formation history of the Galaxy. In the following, the main results of this Thesis are listed.

### 8.1.1 The Formation of the Milky Way disc from AqC4 simulation

In Chapters 4 and 5, the spatial and kinematical properties of stellar particles of the Milky Way-like galaxy AqC4 has been analysed in details. This investigation was published in Giammaria, Spagna, Lattanzi, Murante, Re Fiorentin, and Valentini (2021).

The innovative approach of this work was to consider such a simulation as a real survey of the stellar contents of our Galaxy, and, therefore, the methods implemented are the same usually applied to real stellar catalogues. The aim was to study the Star Formation History and the accretion history of AqC4 in comparison to the Milky Way. With the identification of cosmological signatures enclosed in the mono-age stellar populations, defined as coeval particles sub-samples of 2 Gyr age bins, we were able to contrast their phase-space properties with the spatial-kinematical distributions of the Milky Way stellar populations. Moreover, the focus of the investigation was on an annular region within $6 < R[\mathrm{kpc}] < 7$ defined as Simulated Solar Ring (SSR). Such region corresponds approximately to the Solar Neighbourhood located in our Galaxy at $R_\odot \sim 8$ kpc from the Galactic centre, given the $\sim 20$ per cent smaller radial scale length of the thin disc of AqC4 with respect to the Milky Way ($h_\mathrm{R} \simeq 2.1$ kpc wrt. 2.6 kpc). In this way, it was possible to compute a more proper and direct comparison with Gaia data.

The suite of the high-resolution cosmological simulation considered is based on the "Aquila-C" framework presented by Springel et al. (2008) and the MUPPI algorithm to model the sub-resolution baryonic physics (see Murante et al., 2010; Murante et al., 2015, for more details). It consists in an unconstrained simulation, hence not aimed to perfectly mimic the Local Group environment, but to reproduce a main disc-like galaxy that should be interpreted as a typical realization of the cosmological evolution of a Milky Way-like object with a similar mass, $M_\mathrm{vir} \sim 1.627 \cdot 10^{12}\ \mathrm{M}_\odot$, and phase-space properties. The Plummer-equivalent softening length for the computation of the gravitational force is $\epsilon_\mathrm{Pl} = 163\, h^{-1}$ pc and, at redshift $z = 0$, it includes within the virial volume 5 518 587, 1 348 120, and 6 919 646 dark matter, gas and stellar particles, respectively.

In the SSR, the presence of at least two disc components characterized by a density profile with a double exponential decrease from the galactic plane is found (see Sect. 5.1). Their estimated scale heights are $h_1 \sim 0.3$ kpc, which is in good agreement with the Milky Way thin disc, and $h_2 \sim 1.33$ kpc, which

is $\sim$ 50 per cent larger than the Milky Way thick disc (Bland-Hawthorn and Gerhard, 2016). The AqC4 thick disc is also more massive, corresponding to a relative density parameter $f = 22.6 \pm 0.7$ %, i.e. 2 – 3 times larger than the Milky Way (Bland-Hawthorn and Gerhard, 2016).

Moreover, the vertical distribution of the mono-age stellar particles in the SSR reveals that the thin disc of AqC4 is mainly formed by a *young disc* population with age $\leq$ 4 Gyr and an height, $h_Z$ where the density distribution decreases by a factor $e^{-1}$ with respect to the galactic plane $Z = 0$ kpc of about $\sim$ 250 – 500 pc. Another *old disc* component has an age between 4 and 8 Gyr, with intermediate thickness, $h_Z \sim$ 500 – 1000 pc, while a prominent *thick disc* population with age 8-10 Gyr has $h_Z \sim$ 1200 pc (Fig. 5.6).

The vertical scale heights and weights of the mono-age populations are strictly correlated with the SFH of AqC4. In particular, the large scale heights of the stellar particles in the SSR with age 4-8 Gyr cannot be explained by the secular disc evolution only, but they may be due by the low-redshift mergers shown in Fig. 5.14 that have triggered a disc heating process.

The kinematical analysis described in Sect. 5.2 suggests that the stellar particles in the SSR have an azimuthal velocity distribution corresponding to two main kinematic disc components (i.e. the young disc and the old/thick disc), plus a slightly prograde inner halo. Given that the AqC4 discs rotate faster than the Milky Way, , $\langle V_{\phi,1} \rangle \simeq 284.4$ km s$^{-1}$ and $\langle V_{\phi,2} \rangle \simeq 257.7$ km s$^{-1}$ wrt. $\langle V_{\phi,1} \rangle \simeq 230$ km s$^{-1}$ and $\langle V_{\phi,2} \rangle \simeq 160$ km s$^{-1}$ (Bland-Hawthorn and Gerhard, 2016; Han et al., 2020), and with a smaller velocity difference, these results are consistent with the more compact structure of AqC4 with respect to the Milky Way.

However, the median $\widetilde{V}_R$ and $\widetilde{V}_\phi$ components of mono-age stellar particles and their relative dispersions revealed that similar to what happens for the Milky Way, the stellar disc of AqC4 is out of equilibrium and shows the dynamical signatures of perturbations due to both recent mergers and gas accretion. In particular, in the disc region at $3 \leq R[\mathrm{kpc}] \leq 11$ of Fig. 5.11, a systematic inward motion for all the mono-age populations is evident, while younger stars show a higher median $\widetilde{V}_\phi$ than older ones, and also rotate faster than the circular velocity.

These kinematical features are consistent with the recent studies based on Gaia DR2 data such as the "dynamically young and perturbed Milky Way disk" described by Antoja et al. (2018) and agree with the inside-out, top-down scenario of Galactic disc formation. Moreover, they suggest that the accretion history is one the keys to understanding the origin of the ancient

Milky Way thick disc and inner halo, as proposed by Stinson et al. (e.g. 2013), Helmi et al. (2018), and Gallart et al. (2019).

Supported by these findings, the possible links between the phase-space distribution of the mono-age populations and the Star Formation and accretion events occurred to AqC4 were investigated in Sect. 5.3.

The prominent AqC4 *thick disc* population seems to have been generated by the accretion of the major satellite detected at redshift $z \sim 1.6$. Such merging event is associated to the starburst at redshift $1 < z < 2$ shown in Fig. 5.14, which attains a total SFR of $\sim 7 - 8$ $M_\odot$ $yr^{-1}$. This scenario is consistent with the Gaia-Sausage-Enceladus event observed by Gallart et al. (2019) in the Solar Neighbourhood. Moreover, also Bignone, Helmi, and Tissera (2019) and Grand et al. (2020) proposed a similar model for the origin of Galactic thick disc, analysing independent cosmological simulations of Milky Way-like galaxies selected from the EAGLE and Auriga projects, respectively. Although such simulations show SFH's quite different from AqC4, all these studies suggest a significant increase in the SFR triggered by a galaxy merger experienced by the Milky Way at redshift $z \sim 1.5$. This highlights also that the formation models of the Galactic thick disc are not completely defined and need to be further investigated, given the difficulties of confronting different simulated Milky Way-like galaxies and compare them with real galactic observations.

Another significant result is provided by the investigation of the late SFH of AqC4 discussed in Sect. 5.3. This represents a novel approach to the study of Galactic disc evolution since estimates obtained in the SSR are directly compared with recent Gaia observations. In fact, at redshift $1 < z < 2$, an evident starburst matches quite well the high SFR ($\sim 10$ $M_\odot$ $Gyr^{-1}$ $pc^{-2}$) recently derived at the same epoch by Mor et al. (2019) in the Milky Way till $z \simeq 0.2$. The comparison with the accretion history of AqC4 supports the hypothesis that the increase of the SFR occurred $2 - 4$ Gyr ago in the Milky Way Solar Neighbourhood may be due to a late merging event as claimed at $z \sim 0.6$ by Lian et al. (2020b). The higher SFR revealed in the SSR concerning the Milky Way after $z \simeq 0.2$ may depend on a greater gas contribution from the last satellites accreted at low redshift, as well as from the delayed infall of the gas outflows triggered by the strong starbursts at high redshift.

In general, this work sheds light on the complex scenario of the origin and evolution of the Galactic disc, supporting the global top-down, inside-out disc formation model and implying an overlap of several stellar generations closely correlated with the accretion history of the Galaxy. The comparison

between the SSR, namely "a theoretical prediction", and the Solar Neighborhood provides a novel approach to relate the present-time phase-space properties of coeval stellar populations with past and recent signatures of merging events enclosed in the SFH.

### 8.1.2 The Galactic rotation curve from Gaia DR2

The results discussed in Chapters 6 and 7, which were published in Crosta, Giammaria, Lattanzi, and Poggio (2020) could represent a breaking point for the application to real data of a theoretical model of the galactic rotation curve that is fully compliant with the precepts of General Relativity.

In fact, galaxy rotation curves represent by definition the mean circular velocity profile of disc-like galaxies around their centre as a single function of radius. Their flatness has usually been interpreted as a deviation from Newtonian dynamics and one of the most important empirical evidence of the presence of dark matter (Zwicky, 1937; Rubin, Ford, and Thonnard, 1978) or modified gravity (Milgrom, 1983). Part of my Thesis was then focused on the investigations of this observational property that characterises the disc of the Milky Way.

The study was made possible thanks to the exquisite Gaia DR2 data. From these, I selected the largest stellar ensemble ever observed by a single apparatus, i.e. a single observer in a relativistic framework. According to very precise requirements listed in Sect. 7.1, the most angular-momentum sustained population was extracted from the Gaia archive, representing the most suitable stars to trace the Galactic rotation curve.

The velocity profile was then fitted to two different models presented in Sects. 6.2.1 and 6.3: (i) the so-called *MWC model*, a classical Newtonian representation of the Galaxy as composed by a central bulge, a thin and thick discs, surrounded by a dark matter halo; (ii) and the *BG model*, a "simple" General Relativistic model that approximates galactic dynamics adopting an axisymmetric stationary metric as solution of the Einstein field equations, to describe the stellar disc population with a relativistic rotating dust. The first one is the usual model generally used to describe the galactic dynamics in the standard dark matter scenario. The second is based on the model for the metric proposed by Balasin and Grumiller (2008) and has received little attention so far. This provides a first possible step towards a fully-relativistic description to the Milky Way rotation curve, an approach pursued by de Almeida, Piattella, and Rodrigues (2016) for external galaxies. Despite that, the fact

that the densities inferred with the model by Balasin and Grumiller (2008, BG model) or the one by (Cooperstock and Tieu, 2007, CT model) do not fit the effective Newtonian velocity, $V_{\rm eN}$ (see Sect. 7.2.1), in the absence of dark matter indicates that off-diagonal terms, not analysed in de Almeida, Piattella, and Rodrigues (2016), may account for the contribution that flattens the observed rotation curves.

The results of Sect. 7.2 (see Fig. 7.2) show that both models are almost identically consistent with the highly accurate Gaia data. The classical MWC model attains results (Table 7.3), in line with the most recent derivations from fits to independent data different from the Gaia sample such as Iocco, Pato, and Bertone (2015), Bovy (2015), Moni Bidin et al. (2015), McMillan (2017), Pouliasis, Di Matteo, and Haywood (2017), Korol, Rossi, and Barausse (2019), and Eilers et al. (2019). At the same time, despite the limitations of the BG model, the results listed in Table 7.2 show that such a relativistic framework can reproduce the flat rotation curve, with the off-diagonal term in the line element 6.9 mimicking the dark matter effect.

Moreover, using the best-fit values of the BG model and Eq. 7.12, the local baryonic matter density is estimated as $\rho(R = R_\odot, Z = 0) \equiv \rho_\odot = 0.083 \pm 0.006$ $\mathrm{M}_\odot$ $\mathrm{pc}^{-3}$ (Fig. 7.5), which is in agreement with current estimates provided in independent studies by Garbari et al. (2012), Bienaymé et al. (2014), and McKee, Parravano, and Hollenbach (2015). For the MWC model, the dominant component in the Galactic plane is also the baryonic matter with a smaller content of dark matter, as expected from other works (e.g. McMillan, 2017; Pouliasis, Di Matteo, and Haywood, 2017; Eilers et al., 2019). The BG model predicts a very similar baryonic mass distribution in the Galactic plane for the radial range $5 \leq R[\mathrm{kpc}] \leq 16$ probed by Gaia data and the results shown in Fig. 7.6 suggest that gravitational dragging-like effect could sustain the Galactic rotation curve with rather significant consequences on the application of an axisymmetric stationary metric to the Einstein field equations to describe the dynamics of the Galactic disc.

All observational evidences of dark matter point to the existence of a cosmic component that does not absorb or emit light but interacts only via its gravitational force, entering the calculations as extra mass required to justify for example the flatness of the galactic rotation curve. The relativistic *ansatz* proved in Crosta, Giammaria, Lattanzi, and Poggio (2020) and discussed in this Thesis, highlights that geometry, as a manifestation of gravity according to Einstein's theory, can mimic the perceived effect of dark matter and may be responsible for such a flatness at large radii via a gravitational dragging-like

effect, which has no Newtonian counterpart.

Thus, there would be nothing new in saying that General Relativity is the standard theory of gravity, but the results described in this Thesis show that a General Relativistic "dust", namely pure matter made only of the non-collisional baryonic particles in the disc, recovers the local energy-mass density with no need of extra unknown matter within the 11-kpc range covered by the Gaia sample. Although these are initial results based on a tailored physical solution of the Einstein field equations,, it appears that the application of General Relativity to more physically appropriate metrics, along with adequate solutions, may yield an explanation to the rotation curve flatness problem at least in our Galaxy, without the need for dark matter.

## 8.2 Future prospects

There is no doubt that current and future Gaia data releases and the important synergies with ground-based spectroscopic surveys such as APOGEE (Majewski et al., 2017) and GALAH (De Silva et al., 2015) and detailed comparison with ever improving numerical simulations will bring tremendous and fundamental contributions to Local Cosmology. Also, the combination of high-resolution simulation in more General Relativistic frameworks will be surely helpful to understand how our Galaxy and our local universe was formed and evolve. In the following, a list of future possible improvements of these investigations is proposed.

### 8.2.1 The Third Gaia release: EDR3 and DR3

On 3 December 2020, the Gaia's Early Data Release 3 (Gaia EDR3 Gaia Collaboration et al., 2020) has been made public and available through the *Gaia Archive*. Although it is an intermediate part of the full Data Release 3 planned for the first half of 2022, it represents a significant improvement in both the precision and accuracy of the astrometry and broad-band photometry. The data, collected during the first 34 months of the mission, yields a factor two improvement in proper motion precision and photometry that is much more homogeneous over the sky, as well as over source brightness and colour, with no systematics above the 1 per cent level with respect to the Second Data Release (Gaia Collaboration et al., 2018b).

**Table 8.1:** Overview of the sources in Gaia Early Data Release 3 (Gaia EDR3). For user convenience, Gaia Data Release 2 radial velocities are provided for Gaia EDR3 sources with an internal cross-match. CRF stands for Celestial Reference Frame representing extra-galactic sources to provide a reference frame for measuring "absolute" positions and motions.

| Sources | in Gaia EDR3 | in Gaia DR2 | in Gaia DR1 |
|---|---|---|---|
| Total | 1 811 709 771 | 1 692 919 135 | 1 142 679 769 |
| 5-parameters | 585 416 709 | 1 331 909 727 | 2 057 050 |
| 6-parameters | 882 328 109 | | |
| 2-parameter | 343 964 953 | 361 009 408 | 1 140 622 719 |
| mean $G$ mag | 1 806 254 432 | 1 692 919 135 | 1 142 679 769 |
| mean $G_{BP}$ mag | 1 542 033 472 | 1 381 964 755 | - |
| mean $G_{RP}$ mag | 1 554 997 939 | 1 383 551 713 | - |
| Gaia-CRF | 1 614 173 | 556 869 | 2 191 |
| Radial velocities | 7 209 831 from DR2 | 7 224 631 | - |
| Variable sources | in DR3 / see DR2 | 550 737 | 3 194 |
| $T_{eff}$ | in DR3 / see DR2 | 161 497 595 | - |
| $A_G$ & E(BP-RP) | in DR3 / see DR2 | 87 733 672 | - |
| Radius & luminosity | in DR3 / see DR2 | 76 956 778 | - |

As listed in Table 8.1 and depicted in Fig. 8.1, Gaia EDR3[1] contains detailed information on more than 1.8 billion sources (more than 100 million sources over Gaia DR2) and an increase of about 200 million sources for a total around 1.5 billion colour information. The Gaia EDR3 catalogue is essentially complete between $G = 12$ and $G = 17$ with parallax uncertainties of $0.02 \div 0.03$ mas for $G < 15$, 0.07 mas at $G = 17$, 0.5 mas at $G = 20$, and 1.3 mas and at $G = 21$ mag. Similar values but in mas yr$^{-1}$ for the proper motions uncertainties. Moreover, the systematic errors have been reduced with a parallax zero-point of about $-17$ $\mu$as. Unfortunately, Gaia EDR3 does not comprehend new sources with radial velocities, but the archive is complemented with a set of Gaia DR2 radial velocities through an internal cross-match operation. External cross matches will be made available after 3 December 2020 with other catalogues such as GSC 2.3, APASS DR9, RAVE DR5, TMASS PSC XSC, and allWISE.

The performance verification papers already give an idea of the science potential of this new early release. For example, Gaia Collaboration et al. (2021) shows that the gain in EDR3 for the number of sources with $\varpi/\sigma_\varpi > 3$ compared to DR2 at large radii is very significant and notably more stars are available at almost all radii. The median errors in $R$ remain lower than 1 kpc up to $R < 14$ kpc and the velocity uncertainties are smaller than $2 \div 5$ km s$^{-1}$

[1]Table from https://www.cosmos.esa.int/web/gaia/earlydr3

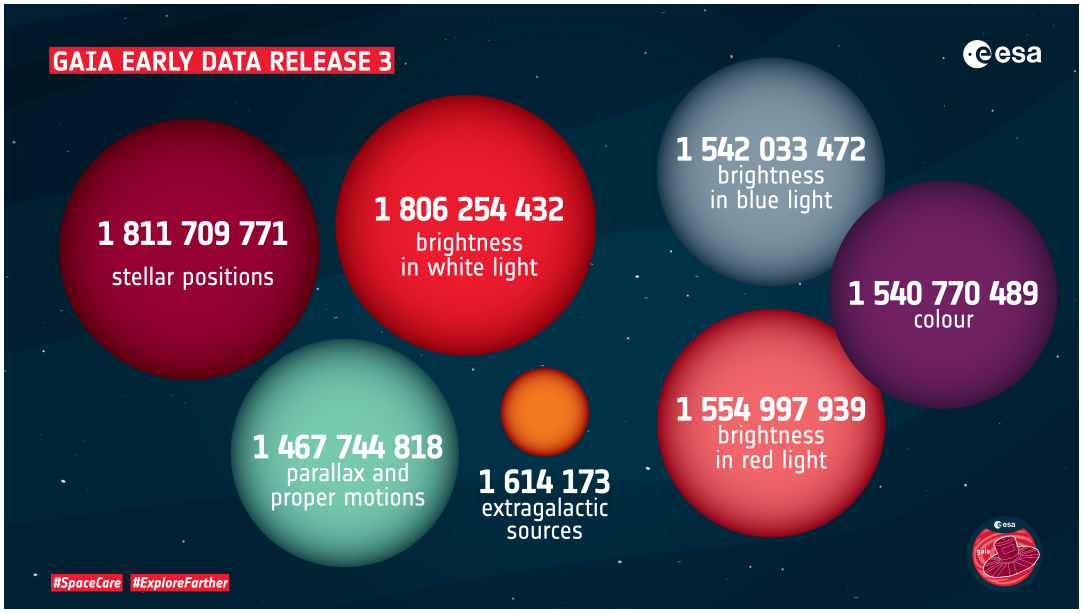


**Figure 8.1:** Gaia's Early Data Release 3 in numbers. Credits: ESA, CC BY-SA 3.0 IGO.

for most of the radii probed.

As discussed in the next sections, the improvements that the new release will bring could provide a more complete census of the stellar content of the Milky Way. This will increase our knowledge of several populations belonging to the Galactic thin and thick discs or Galactic halo, helping in the studies on the Star Formation History and the origin of the Milky Way. Moreover, the detailed determination of the mass-luminosity relation will allows us to estimate the density of the baryonic matter in the Solar Neighbourhood more precisely, hopefully up to a few kpcs from the Sun. These estimates, with the possible extension of the radial range for which the Galactic rotation curve can be traced and investigated by another 1-2 kpc, will be significant to constrain the total mass of the Milky Way and its dynamics.

### 8.2.2 Chemo-dynamics in classic Milky Way simulations

Given the new Gaia data releases, the fine structure of the Galactic disc and the phase-space distributions of mono-age populations can be further studied including chemo-dynamical analysis of mono-abundance stellar populations.

Cosmological simulations like AqC4 and future higher-resolution realisations could be used to investigate the *in-situ/ex-situ* star formation contributions and stellar back-time tracking in order to select halo streams and identify common progenitors to study the Galactic halo. This will improve

our knowledge of the Milky Way thin and thick discs origin and evolution with also the use of constrained simulation (e.g. Carlesi et al., 2016) that can be very promising.

### Age-Velocity dispersion Relation

Given the results reported in Sect. 8.1.1, the negative median $\widetilde{V}_R$ trends represents an interesting starting point for future studies. As discussed in Chapter 5, this feature should be produced by the interaction between the main galaxy and a minor, external satellite. To confirm this scenario, however, it is necessary to further investigate the Age-Velocity dispersion Relation (AVR) of stellar particles within the SSR.

This relation has been observed in the Solar Neighbourhood by many authors (e.g. Wielen, 1977; Casagrande et al., 2011; Yu and Liu, 2018) and also studied in N-body simulations (e.g. Aumer, Binney, and Schönrich, 2016). Table 8.2 lists the values of mean velocity, dispersions and their ratios computed for the mono-age stellar populations in the SSR within $|Z| \leq 1$ kpc. Comparing these results with recent estimates measured by Yu and Liu (2018, in particular Table 2 in the paper) for the Solar Neighbourhood, it is noticeable that AqC4 is kinematically hotter than the Milky Way, confirming what I discussed in Sect. 5.2.3. On average, $\sigma_{V_\phi} \sim 0.8\sigma_{V_R}$ and $\sigma_{V_\phi} \sim 0.6\sigma_{V_Z}$ for stellar particles with $4 \leq$ Age [Gyr] $\leq 6$, compared to $\sigma_{V_\phi} \sim \sigma_{V_Z} \sim 0.5\sigma_{V_R}$ for the same range of ages in the Galaxy.

These discrepancies should be due to the slightly different accretions history experienced by AqC4 and the Milky Way, as reported in Sect. 5.3.2. In particular, the merging events with an high mass ratios, $\Delta$, and a different amount of gas contents at very low redshift, can have heated the intermediate populations[2] more than what has happened in the Galaxy.

Fig. 8.2 shows, interestingly, that in the SSR of AqC4, stellar particles provide significant and positive AVR for all the velocity components, similar to what was observed by Yu and Liu (2018). AqC4 stellar particles seem to trace well the Age-$\sigma_{V_R}$ relation of Milky Way stars, while for the other two velocity components the situation appears largely different, with several oscillations and peaks that characterise the simulated catalogue.

[2]stellar particles which were born before or during the specific accretion events at the time

**Table 8.2:** Kinematic features for mono-age stellar particles populations in the SSR within $|Z| \leq 1$ kpc.

| Age [Gyr] | $\langle V_R \rangle$ [km s$^{-1}$] | $\langle V_\phi \rangle$ [km s$^{-1}$] | $\langle V_Z \rangle$ [km s$^{-1}$] | $\sigma_{V_R}$ [km s$^{-1}$] | $\sigma_{V_\phi}$ [km s$^{-1}$] | $\sigma_{V_Z}$ [km s$^{-1}$] | $\sigma_{V_R}/\sigma_{V_\phi}$ | $\sigma_{V_R}/\sigma_{V_Z}$ | $\sigma_{V_\phi}/\sigma_{V_Z}$ |
|---|---|---|---|---|---|---|---|---|---|
| 0–2 | -5.6 $\pm$ 0.1 | 286.75 $\pm$ 0.07 | 0.7 $\pm$ 0.1 | 26.4 $\pm$ 0.1 | 19.7 $\pm$ 0.2 | 25.1 $\pm$ 0.2 | 1.34 | 1.05 | 0.79 |
| 2–4 | -4.8 $\pm$ 0.1 | 280.3 $\pm$ 0.1 | 0.5 $\pm$ 0.2 | 34.5 $\pm$ 0.1 | 25.2 $\pm$ 0.2 | 42.5 $\pm$ 0.3 | 1.37 | 0.81 | 0.59 |
| 4–6 | -5.0 $\pm$ 0.2 | 268.4 $\pm$ 0.2 | 0.4 $\pm$ 0.4 | 43.9 $\pm$ 0.3 | 35.9 $\pm$ 0.6 | 64.2 $\pm$ 0.5 | 1.22 | 0.68 | 0.56 |
| 6–8 | -4.4 $\pm$ 0.3 | 253.4 $\pm$ 0.4 | -0.2 $\pm$ 0.4 | 56.5 $\pm$ 0.5 | 57.2 $\pm$ 1.2 | 74.9 $\pm$ 0.5 | 0.99 | 0.75 | 0.76 |
| 8–10 | -4.4 $\pm$ 0.3 | 256.9 $\pm$ 0.3 | -0.2 $\pm$ 0.3 | 65.4 $\pm$ 0.3 | 55.8 $\pm$ 0.6 | 65.6 $\pm$ 0.4 | 1.17 | 1.00 | 0.85 |

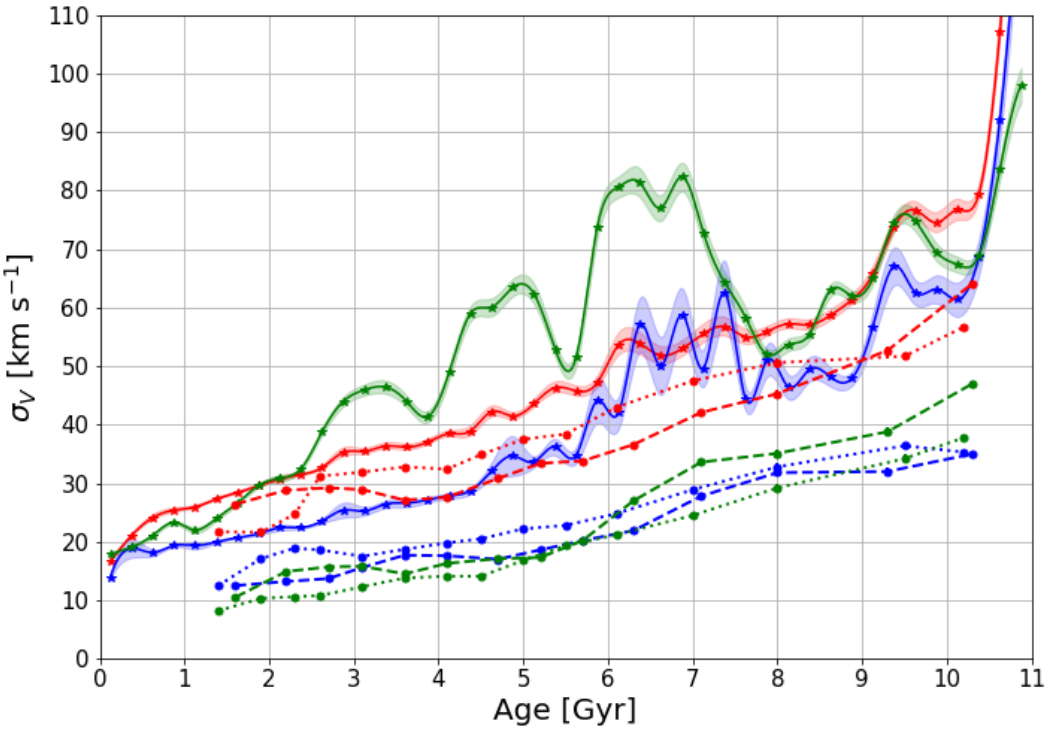


**Figure 8.2:** AVR for stellar particles in the SSR of AqC4 simulation with $|Z| \leq 0.5$ kpc (solid lines with relative Credible Intervals). Dashed and dotted lines represent data from Yu and Liu (2018) for stars in the Milky Way Solar Neighbourhood with $|Z| > 0.270$ kpc and $|Z| < 0.270$ kpc, respectively. Red, blue and green colours correspond to radial, azimuthal and vertical velocity dispersion components, respectively.

#### Kinematics of gas particles in AqC4

In parallel, to study the SFH and the star-forming regions in AqC4, the investigation of gas kinematics is very important. Figs. 8.3, 8.4 and 8.5 show the evolution during the last $\sim$ 0.4 Gyr of the radial and vertical velocity distributions of gas particles in the galactic volume, projected on the $XY$, $XZ$ and $YZ$ plane, respectively.

The presence of several minor mergers can be notice in each panel, on top of very interesting and significant gas in- and out-flows, revealing once more the goldmine of information hidden in the fine structure of phase-space distributions of the Galaxy.

### 8.2.3 Milky Way relativistic models and simulations

The results discussed in Sect. 8.1.2 for the Galactic rotation curve, comparing the MWC and BG models with the Gaia DR2 measurements, open several scenarios and possible future developments.

Recalling once more that the rotation curve describes the velocity profile as a function of the radial coordinate only, I remark that is not possible to obtain a complete 3D description of the Galactic disc structure using kinematic data only, but one needs to consider also the density distribution of the stars. This is obvious in the classic Newtonian description, since the velocity profile is totally defined by the density profile through the Poisson equation, but it is made even more evident in the BG model since we need to directly take into account the local baryonic mass to constrain one of its free parameters, $e^{\nu_0}$.

A first step to extend the analysis to other kinds of stellar populations, less angular-momentum sustained and more "virilized", to increase for instance our tracers sample, or to extend the radial range probed using the new Gaia data releases requires to include in any kind of model the velocity dispersion of the other velocity components, as done for the Jeans analysis. Indeed, if $|Z|$ and $R$ increases, the tilt of the Local Velocity Ellipsoid must be taken into account (Everall et al., 2019).

#### The Galactic rotation curve in the outer regions

Several classical studies such as Huang et al. (2016) and Bhattacharjee, Chaudhury, and Kundu (2014) have started to consider non-disc tracers relating the number density, the radial and transverse velocity dispersions as well as the velocity anisotropy $\beta$ of the tracers at radius $R$ to the circular velocity $V_c$ at

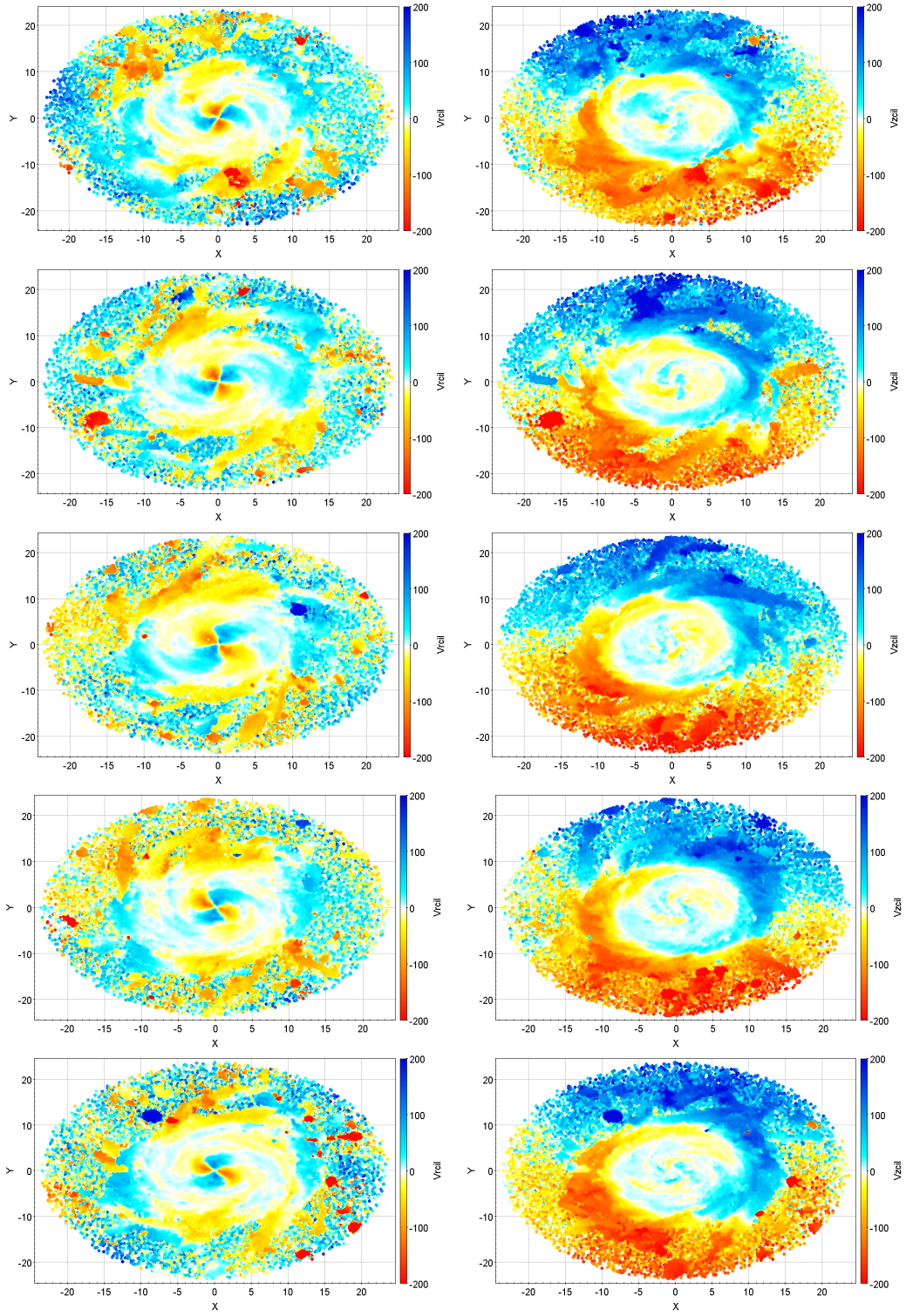


**Figure 8.3:** Radial ($V_R$, on the left) and vertical ($V_Z$, on the right) velocity distributions on the $XY$-plane projection of AqC4 gas particles. From top to bottom, each row represents a temporal snapshot showing the last $\sim$ 0.4 Gyr evolution history of the simulation.

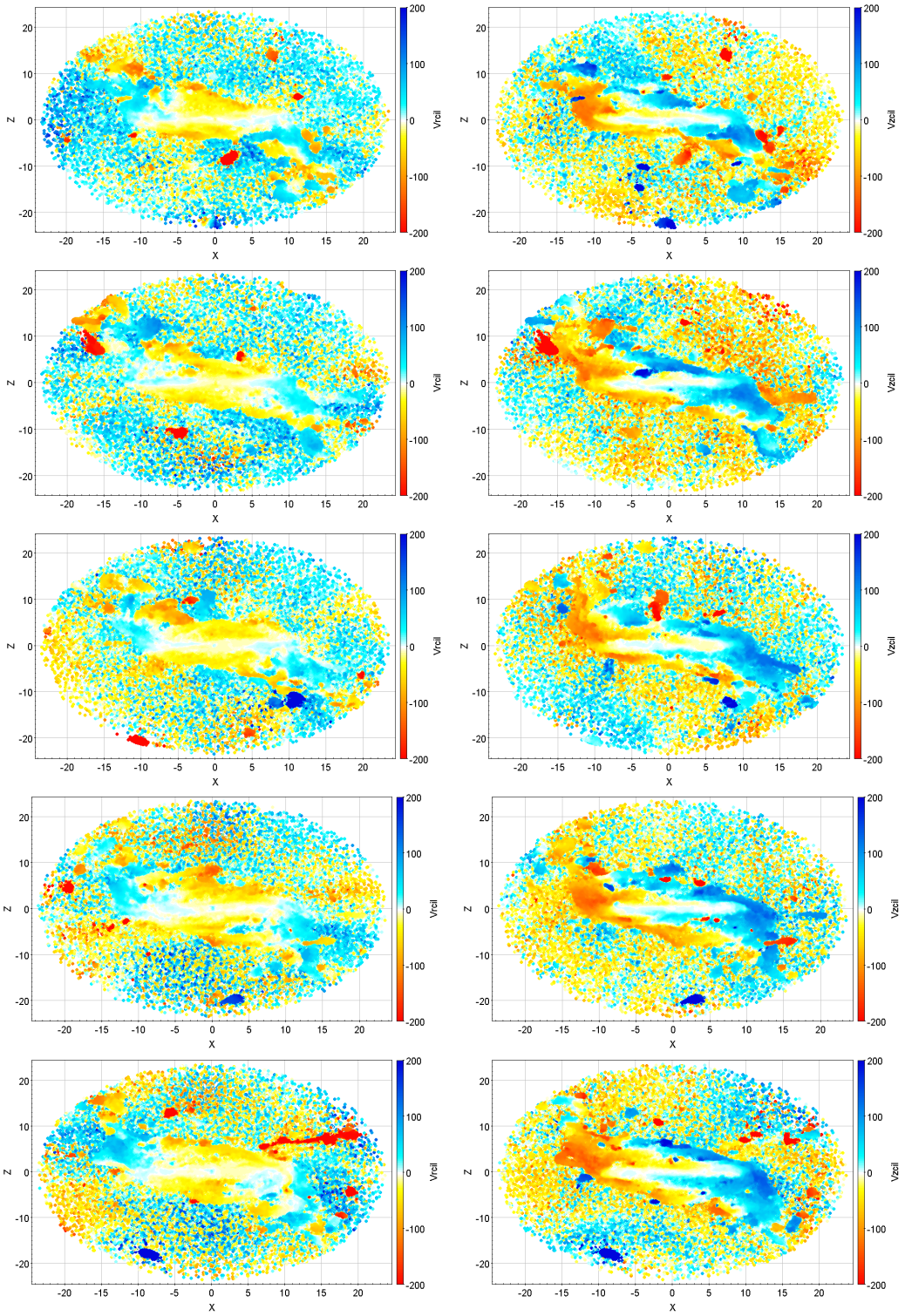


**Figure 8.4:** As for Fig. 8.3 but for $XZ$-plane projection.

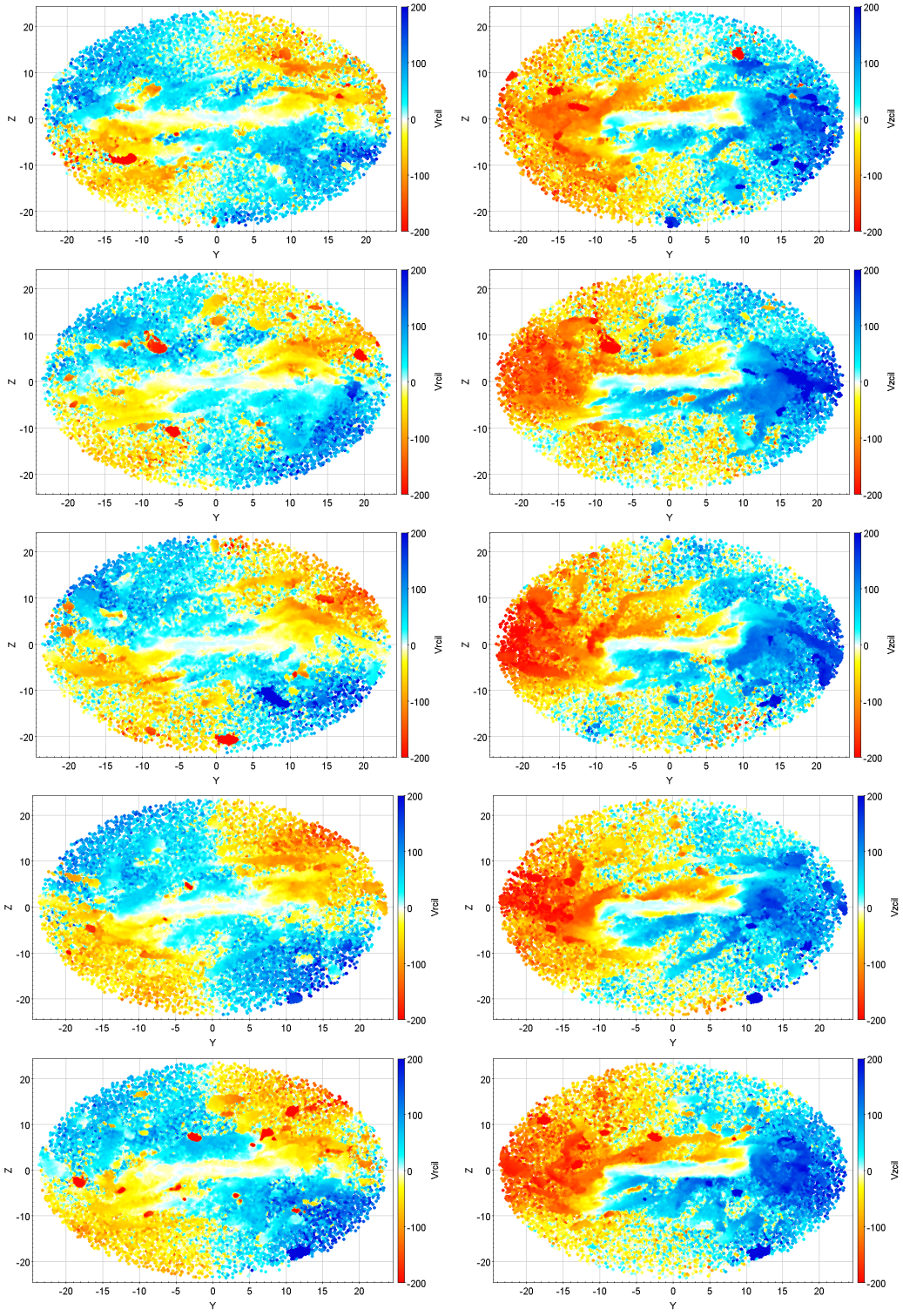


**Figure 8.5:** As for Fig. 8.3 but for $YZ$-plane projection.

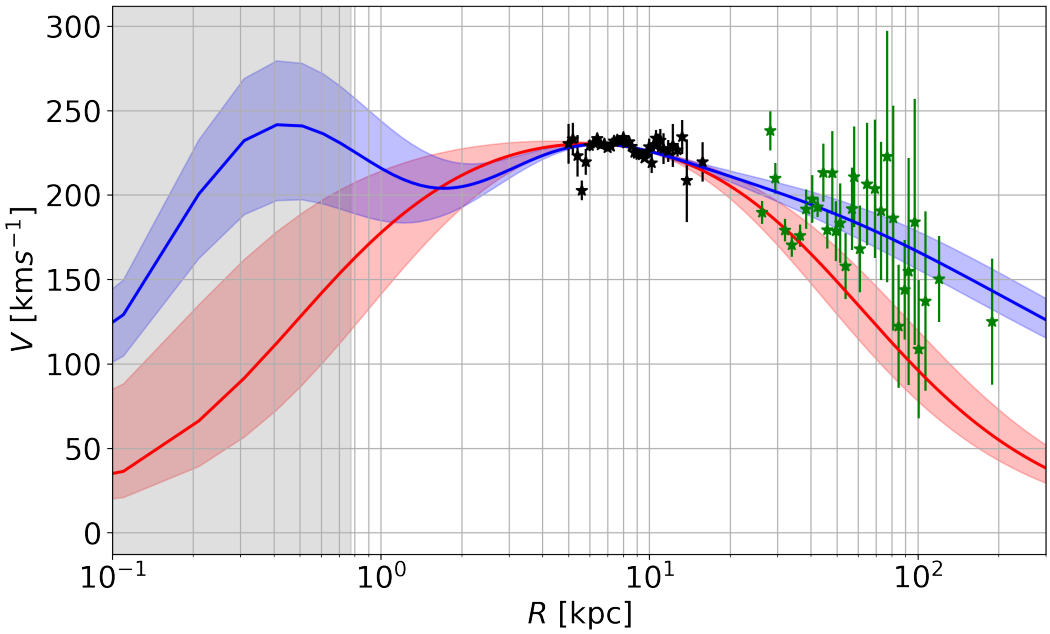


**Figure 8.6:** The Galactic rotation curve up to 300 kpc. The blue and red lines with corresponding CIs refer to the MWC and BG models best-fit results (Tables 7.2 and 7.3. Black star symbols are the Gaia DR2 data from Table 7.1, while the green ones are from Bhattacharjee, Chaudhury, and Kundu (2014) derived with Blue Horizontal Branch and K-Giant (KG) star samples.

the same radius. Such kind of analysis implements not only the asymmetric drift corrections to compute the circularization of the $V_\phi$s through Eq. 6.2, but also considers the Jeans equation for spherical systems.

In this respect, Fig. 8.6 shows the Galactic rotation curve in a logarithmic radial scale. The black star symbols refer to the Gaia DR2 data from Table 7.1, while the best-fit parameters for the MWC and the BG models were used to trace the blue and red lines with corresponding Credible Intervals up to 300 kpc. On top of this, the rotation curve data derived by Bhattacharjee, Chaudhury, and Kundu (2014) using Blue Horizontal Branch (BHB) and K-Giant (KG) stars, as non-disc tracers for the rotation curve, are plotted.

Notice how the velocity profile of the BG model decreases more quickly than the one provided by the MWC model in the outer region of the Galaxy because of the presence of the dark matter halo in the latter one. Although it is not a fit, a visual inspection suggests that the classic model appears to trace better the non-disc data than the relativistic one, which is however compatible with the data within the margins of uncertainties.

As the BG model implements a dust solution, the separability *ansatz* assumed to derive the function $N(R, Z)$ of Eq. 6.16 can affect the following aspects: (i) the pressure-less condition can be broken in the central region,

and (ii) the older stellar populations, which mainly populate the Milky Way thick disc, acquire a higher intrinsic scatter in the three velocity components. Therefore, a more complex scenario should be considered in order to take into account perfect fluid solutions with non-vanishing pressure (Andréasson, 2011).

Future studies should focus on appropriate mathematical solutions for a global metric, suitable to account for the multi-component Milky Way structure. This is a very compelling task, since it implies to solve Einstein equations accordingly. However, the implementation of the relativistic velocity profile should be still consistent with Eq. 6.16, while the Gaia-like data will provide new constraints on the values of the corresponding metric functions.

**Developments of the BG model density profile**

Another significant starting point for a more suitable relativistic description of the Milky Way rotation curve, is provided by the central Galactic regions for which we might need to abandon the separability *ansatz* in the solution for $N(R,Z)$, as well as to find a more general solution for $e^{\nu}(R,Z)$.

For instance from Eq. 7.12 (i.e. the last of the Einstein field equations in Appendix B), and since $e^{\nu} \to 1$ at infinity (Neill, Wiltshire, and Mattsson, 2011), the BG density profile becomes

$$\rho \approx \frac{2}{R^2} \sum_{\pm} \left[ 1 - \frac{R^2 + (Z \pm r_{\rm in})(Z \pm R_{\rm out})}{\sqrt{((Z \pm r_{\rm in})^2 + R^2)((Z \pm R_{\rm out})^2 + R^2)}} \right] \tag{8.1}$$

The Taylor series expansion about $x = 1/Z = 0$ of $\rho(R,x)$ and about $y = 1/R = 0$ of $\rho(y,Z)$, provided by using the software MATHEMATICA (Wolfram Research Inc., 2012), demonstrates that the fraction in the square brackets becomes 1 as $R$ or $Z$ tends to infinity, thus the density approaches zero with the following asymptotic behaviours

$$\rho(R,Z) \approx \frac{1}{R^4} \tag{8.2}$$

$$\rho(R,Z) \approx \frac{1}{Z^4} \tag{8.3}$$

$$\tag{8.4}$$

which are not the exponential falloff usually expected for the Galactic baryonic matter density at large $R$ and $Z$ (see e.g. Chapter 3, Sect. 3.1 or Chapter 5, Sect. 5.1).

The density in the BG relativistic model can be estimated only through its direct use in the likelihood function 7.11. As already mentioned, we need more direct baryonic-mass density measurements to extend throughout the Galactic plane the method presented in this Thesis to determine a more general function for the density and the conformal factor of the metric, $e^{\nu(R,Z\sim 0)}$. This can, in turn, verify the overall consistency of the BG model and can be used to test more general ones, as they become available.

The tremendous improvement provided by the Gaia DR3 suggests that future data releases can solve some of the systematic biases and observational limitations found in Gaia Collaboration et al. (2018b). The evaluation of the observed density profile with the forthcoming Gaia data, using, for example, mass-luminosity ratios, may allow extending the investigations provided by McKee, Parravano, and Hollenbach (2015) beyond the Solar Neighbourhood, especially from $R \sim 5$ kpc inward.

**Relativistic cosmological simulations**

A very interesting future development of the present work – and a possible point of conjunction of the two main topics of this Thesis – can be represented by the implementation of more relativistic frameworks in cosmological simulations of galaxy formation. In fact, in the most advanced simulations nowadays, General Relativity is only partially considered. With the words of Coley and Wiltshire (2017): "Friedman tells space how to curve and Newton tells mass how to move".

Indeed, standards ΛCDM cosmology assumes an average FLRW evolution background while the growth of cosmic structures is treated by Newtonian N-body simulations since the full General Relativity computational cosmology is an immense technical challenge that has hitherto been simply too computationally expensive. Recently, first investigations have begun (see e.g. Bruni, Thomas, and Wands, 2014; Giblin, Mertens, and Starkman, 2016; Adamek et al., 2016; Ames, Andréasson, and Logg, 2016; Macpherson, Price, and Lasky, 2019, and references therein), opening what we could consider will become a major frontier for General Relativity for decades to come.

So far, only a few very advanced codes implement numerical relativity to investigate whether or not general relativistic effects on the surrounding spacetime could affect the formation of large-scale structures. A comparison between Newtonian and fully general-relativistic simulations found sub-percent differences within the weak-field regime (East, Wojtak, and Abel, 2018), in agreement with post-Friedmannian N-body calculations (Adamek

et al., 2013; Adamek, Durrer, and Kunz, 2014). Despite these effects are not expected to be a dominant contribution to either the dynamics of our Universe or the propagation of information through it, simulating such a physical system nevertheless provides us with a way to explore to what extent the applicability of traditional Newtonian simulations to cosmology and galaxies formation in a weak-field limit remain valid.

Currently, the most studied relativistic codes are *g*EVOLUTION (Adamek et al., 2016), GRAMSES (Barrera-Hinojosa and Li, 2020), the EINSTEIN TOOLKIT (ET, Loffler et al., 2012), and COSMOGRAPH (Mertens, Giblin, and Starkman, 2016) employing a different approaches to solve relativistic equations. See Adamek et al. (2020) for a comparison review of these algorithms. Unfortunately, all these frameworks are used to investigate relativistic effects at cosmological scales or in the strong-field regime, while much further work needed to obtain "realistic" simulations at Galactic scales and compare them with Newtonian N-body counterparts and observations.

Other works consider self-gravitating Einstein-Vlasov system to describe galaxies and cosmic structures as particles distributions with perfect fluid assumption (Ames, Andréasson, and Logg, 2016). This approach is based on the *ansatz* that the Vlasov distribution depends on the phase-space coordinates only through a function of the two classical integrals of motion, and solve numerically for the spatial density and the metric fields. This appears as a valid alternative and a generalization of the Jeans analysis, implementing off-diagonal terms of the background spacetime metric to accurately model galaxies.

## 8.3 Final remarks

In this final section, I would like to report a few concluding remarks (and short personal considerations) on this Thesis as a brief global discussion of the present research project.

Once again, the two main aims of the project were to consider the Milky Way as a keystone for disc-like galaxies and, thus, for Local Cosmology and to push on the use of General Relativity, regardless of how difficult this might be, to detail a more complex Galactic structure. Pursuing a more relativistic picture of the Milky Way can ensure a coherent Laboratory of Local Cosmology as mentioned many times (for example see the motivation of this Thesis in Sect. 1.4). The present and future Gaia data releases are offering the unique opportunity to trace the Galactic potential star by star from within the Solar

System gravitational fields and will allow us to find the signatures of the origin and evolution of Milky Way-like galaxies and, at the same time, to establish to what extent can General Relativity account for dark matter or if we need alternatives solutions at least for the rotation curve.

The outcomes presented here seem to suggest that the detailed investigation of the fine structure of mono-age stellar populations represents the most promising step to reconstruct the formation history of the Galactic disc. As stated in Crosta, Giammaria, Lattanzi, and Poggio (2020), on the other hand, the new relativistic interpretations of the rotation curve is suggestive of a Milky Way mostly shaped by the bulky central rotating mass source and the global dynamics could be dominated by spacetime, whereas Newtonian approximation is valid only locally (although also the Solar System is not Newtonian as Gaia and the GREM and RAMOD model highlight!). The implementation and availability of methods of experimental gravity, both theoretical and numerical, are more necessary than ever today, especially in the weak-gravity regime. Dragging-like effects could be further enhanced by similar sources distributed in the Galactic disc (see e.g. Liu et al., 2019).

In general, the implementation of purely relativistic effects in cosmological simulations of large-scale structures and galaxies formation can be one fundamental step to improve our knowledge of the Universe since General Relativity is still untested at both ends of the distance scale.

At this point, a very good question could be "Why should we doubt of a cosmological model such as the Concordance Model that is extremely successful in explaining many astrophysical observations?". Despite its success, many open problems are still unsolved and, in many ways, General Relativity is not fully utilized in cosmology and modern physical theories. Consider, for example, the fitting problem (Ellis and Stoeger, 1987) namely, how does one coarse grain matter and geometry on a given scale fit into an effective geometry on larger scales? This problem remains one of the most important unsolved ones in mathematical cosmology (see e.g. Wiltshire, 2011; Coley and Wiltshire, 2017). Answering this kind of questions is very complicated since cosmological measurements of the evolution of large-scale structure depend strongly on the underlying cosmological model and the $\Lambda$CDM solution leads to the very problematic issues of non-baryonic dark matter and dark energy which have not been directly detected, and whose origin remains a mystery.

However, this Thesis was motivated by the existence of relativistic astrometry, namely the fact that, once a relativistic model for the data reduction

has been implemented, any subsequent scientific exploitation should be consistent with the precepts of the theory underlying such a model. Therefore, rather than abandoning General Relativity or any other alternative theory, in my opinion, a better question may be "Why we should not doubt?". George Mallory once said: "Because it is there." answering the question "Why do you want to climb Mt. Everest?". Simply, the aim is our basic curiosity that pushes on thinking harder about the fundamental and scientific principles in order to tackle the cosmic mysteries.

Future developments of this work, theoretical and observational, may confirm this scenario, but the path to Local Cosmology investigations using more sophisticated General Relativistic frameworks is traced. Until there: "Fatti non foste a viver come bruti, ma per seguir virtute e canoscenza" (Dante Alighieri, Inferno, canto XXVI, verso 119).

# Appendix A

# AqC4 extended analysis and details

As discussed in Chapter 5, the medians radial velocity $\widetilde{V}_R$ of mono-age populations in the disc region of AqC4 show a global inward motion.

The radial distribution of the stellar particles that at the present time are located in the SSR (i.e. $6 \leq R[\text{kpc}] \leq 7$) with $|Z| \leq 1$ kpc change in last $\sim 0.4$ Gyr as shown in Fig. A.1. It is noticeable that the original distributions are not centred with respect to the actual SSR and that most of the stellar particles come from slightly inner regions. Moreover, Fig. A.2 shows that the same stellar sample does not keep losing angular momentum. Hence, it appears that the disc is not radially oscillating.

Within the spherical volume of radius $r = 11$ kpc, the variation of the total mass contents results at the sub-percent level as shown in Fig. A.3, therefore it is not possible that the global inward motion was produced by an increase of the gravitational potential in the innermost regions of AqC4.

The investigation of the stellar radial migration presented in Fig. A.4 confirms that more than the 80 per cent of the stellar particles that today are within the SSR have $\Delta R = R_f - R_i > 0$ kpc, thus have migrated outwards (most of them by less than 1 kpc), hence, it seems that also radial migration can not explain the negative radial velocity trends, $V_R < 0$ km s$^{-1}$, but further analysis on this specific topic are necessary.

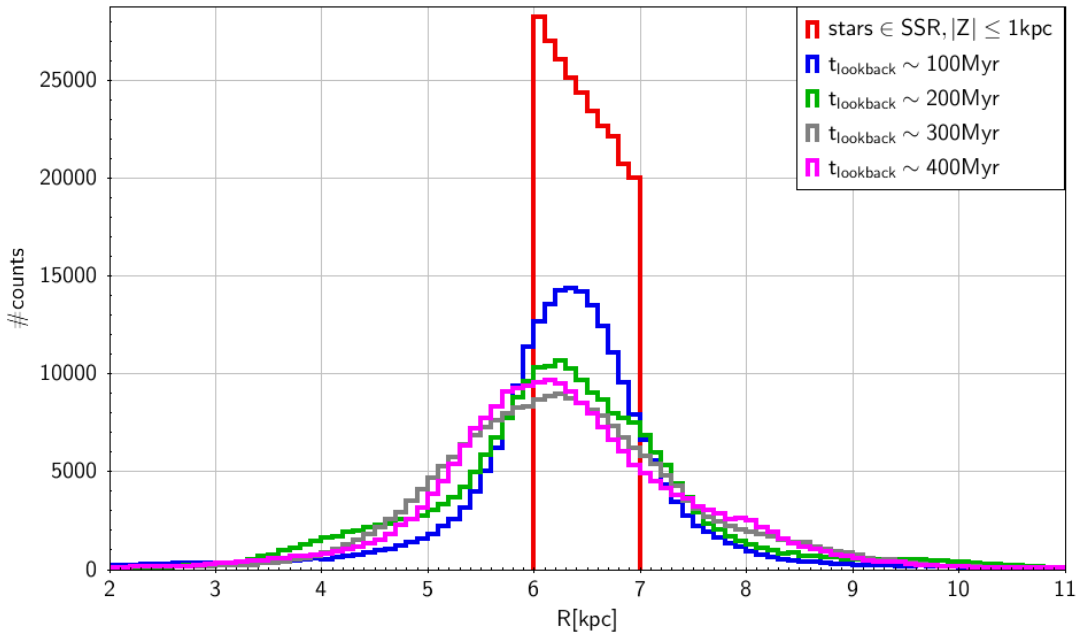


**Figure A.1:** Radial distribution of stellar particles that belong to the SSR with $|Z| \leq 1$ kpc at present time. Red line corresponds to present time, while other colours sample a time-step of about 100 Myr backwards.

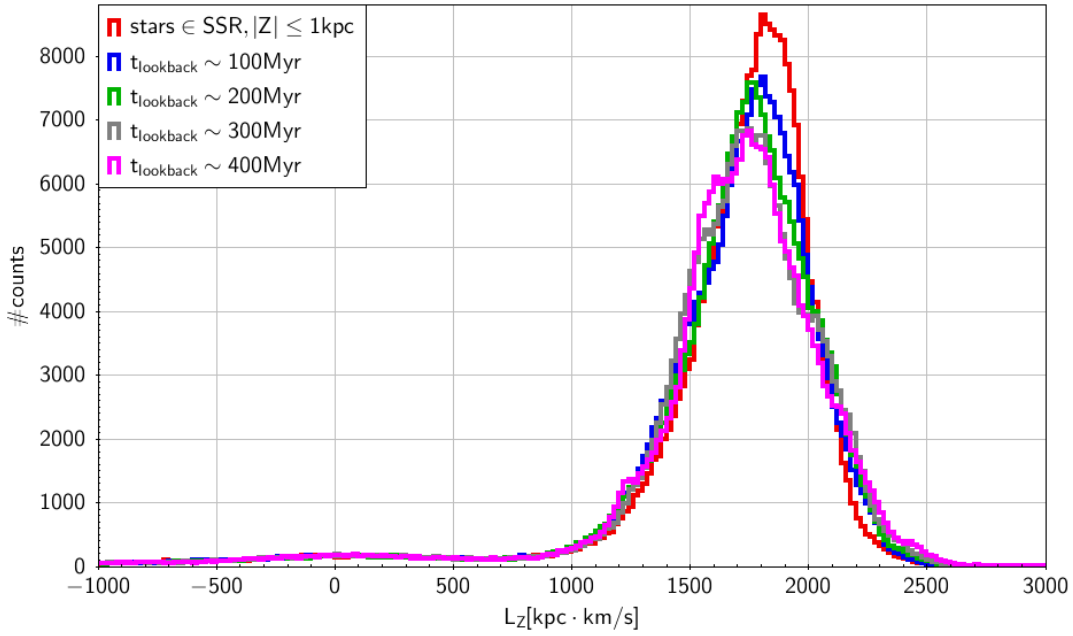


**Figure A.2:** As Fig. A.1 but for the distribution of vertical angular momentum, $L_Z$.

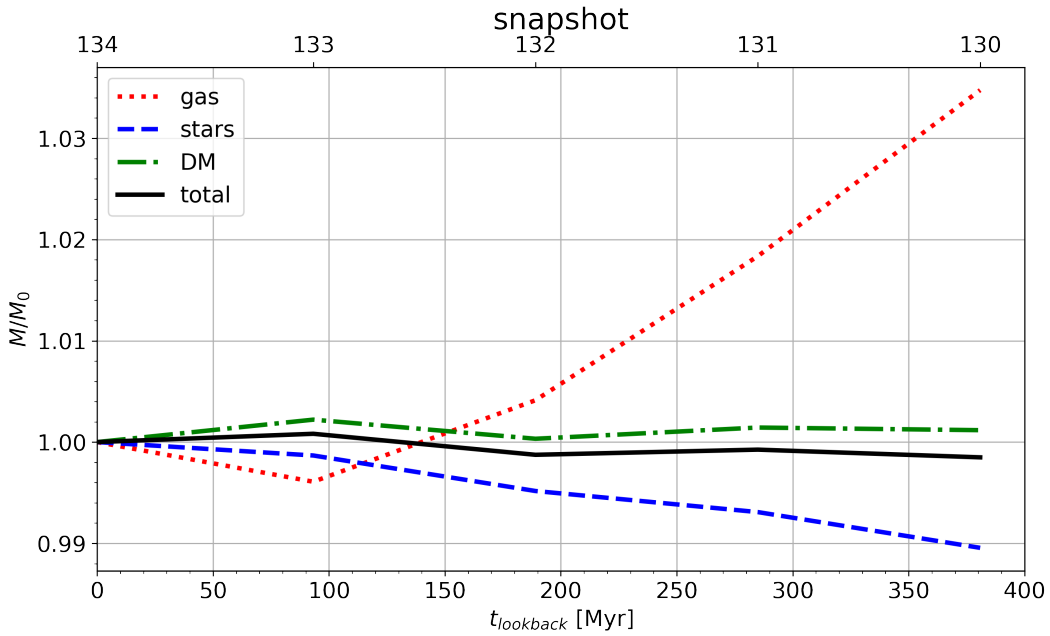


**Figure A.3:** Evolution of the mass contents in the spherical volume of $r = 11$ kpc normalized to the present amounts for the different particle families.

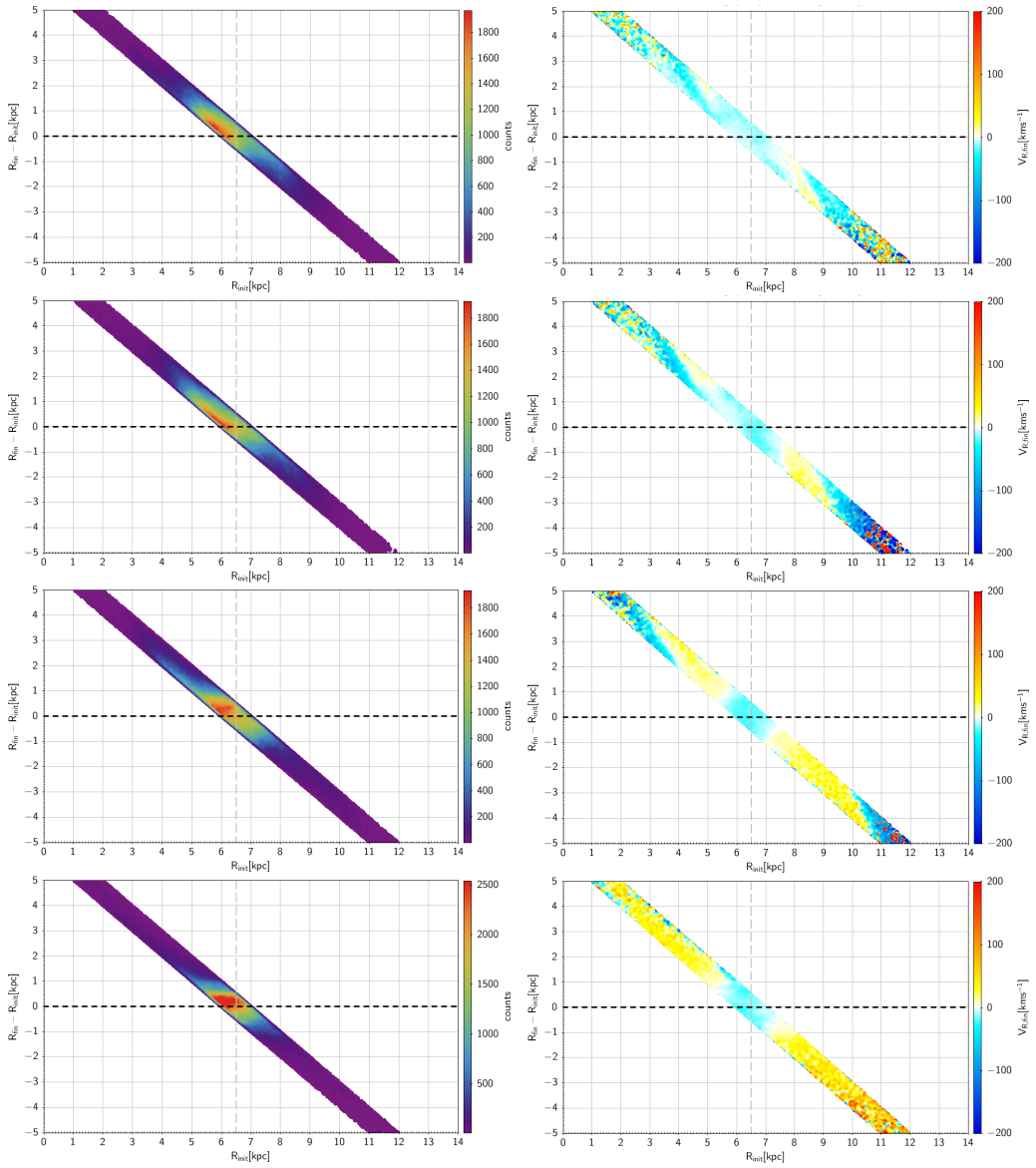


**Figure A.4:** Radial migration of stellar particles in the SSR. From top to bottom, each row represents a temporal snapshot of the evolution for the last $\sim$ 0.4 Gyr. The left column shows the stellar counts, while the right column depicts the final radial velocity $V_{R,\mathrm{fin}}$ that the stellar particles have at the present time. The black dashed lines correspond to zero radial migration.

# Appendix B

# Details of the BG model

## B.1 The Einstein field equations for the BG model

Solving Einstein's field equation translates into solving a system of coupled nonlinear partial differential equations (PDE). For this reason, there exists no general method to obtain all of the solutions.

For the BG model, the line element of Eq. 6.9 and the energy-momentum tensor $T_{\alpha\beta} = \rho g_{\alpha\mu} g_{\beta\tau} u^{\mu} u^{\tau}$ are considered. In virtue of the definition of $T_{\alpha\beta}$, and in the limit of small density, $u^{\alpha}$ results geodetic, and one obtains the following expressions for the Einstein field equations:

$$R\partial_Z \nu + \partial_R N \partial_Z N = 0 \tag{B.1}$$

$$2R\partial_R \nu + (\partial_R N)^2 - (\partial_Z N)^2 = 0 \tag{B.2}$$

$$2R^2(\partial_R \partial_R \nu + \partial_Z \partial_Z \nu) + (\partial_R N)^2 + (\partial_Z N)^2 = 0 \tag{B.3}$$

$$R(\partial_R \partial_R N + \partial_Z \partial_Z N) - \partial_R N = 0 \tag{B.4}$$

$$(\partial_R N)^2 + (\partial_Z N)^2 = kR^2 \rho e^{\nu} \tag{B.5}$$

By solving this system of PDE's one recovers the functions $N(R, Z)$, $\nu(R, Z)$ of the BG model (see Sects. 2.3 and 2.4 of Balasin and Grumiller, 2008), while via Eq. B.5 one can compute the local mass density provided in Sect. 7.3.

# Bibliography


Abadi, Mario G. et al. (July 2003a).
"Simulations of Galaxy Formation in a Λ Cold Dark Matter Universe. I. Dynamical and Photometric Properties of a Simulated Disk Galaxy".
In: *The Astrophysical Journal* 591.2, pp. 499–514. DOI: 10.1086/375512.
arXiv: astro-ph/0211331 [astro-ph].

— (Nov. 2003b). "Simulations of Galaxy Formation in a Λ Cold Dark Matter Universe. II. The Fine Structure of Simulated Galactic Disks".
In: *The Astrophysical Journal* 597.1, pp. 21–34. DOI: 10.1086/378316.
arXiv: astro-ph/0212282 [astro-ph].

Ablimit, Iminhaji and Gang Zhao (Sept. 2017).
"The Milky Way's Circular Velocity Curve and Its Constraint on the Galactic Mass with RR Lyrae Stars".
In: *The Astrophysical Journal* 846.1, 10, p. 10.
DOI: 10.3847/1538-4357/aa83b2. arXiv: 1708.00170 [astro-ph.GA].

Adamek, J., R. Durrer, and M. Kunz (Nov. 2014).
"N-body methods for relativistic cosmology".
In: *Classical and Quantum Gravity* 31.23, p. 234006.
DOI: 10.1088/0264-9381/31/23/234006.
URL: https://doi.org/10.1088/0264-9381/31/23/234006.

Adamek, J. et al. (Nov. 2013).
"General relativistic N-body simulations in the weak field limit".
In: *Physical Review D* 88 (10), p. 103527.
DOI: 10.1103/PhysRevD.88.103527.
URL: https://link.aps.org/doi/10.1103/PhysRevD.88.103527.

Adamek, Julian et al. (July 2016).
"gevolution: a cosmological N-body code based on General Relativity".
In: *Journal of Cosmology and Astroparticle Physics* 2016.7, 053, p. 053.
DOI: 10.1088/1475-7516/2016/07/053. arXiv: 1604.06065 [astro-ph.CO].

Adamek, Julian et al. (Aug. 2020). "Numerical solutions to Einstein's equations in a shearing-dust universe: a code comparison".
In: *Classical and Quantum Gravity* 37.15, 154001, p. 154001.
DOI: 10.1088/1361-6382/ab939b. arXiv: 2003.08014 [astro-ph.CO].

Amaro-Seoane, Pau et al. (Feb. 2017).
"Laser Interferometer Space Antenna".
In: *arXiv e-prints*, arXiv:1702.00786, arXiv:1702.00786.
arXiv: 1702.00786 [astro-ph.IM].

Amendola, Luca et al. (Apr. 2018).
"Cosmology and fundamental physics with the Euclid satellite".
In: *Living Reviews in Relativity* 21.1, 2, p. 2.
DOI: 10.1007/s41114-017-0010-3. arXiv: 1606.00180 [astro-ph.CO].

Ames, Ellery, Håkan Andréasson, and Anders Logg (Aug. 2016).
"On axisymmetric and stationary solutions of the self-gravitating Vlasov system". In: *Classical and Quantum Gravity* 33.15, 155008, p. 155008.
DOI: 10.1088/0264-9381/33/15/155008. arXiv: 1603.05404 [gr-qc].

Andréasson, Håkan (May 2011).
"The Einstein-Vlasov System/Kinetic Theory".
In: *Living Reviews in Relativity* 14.1, 4, p. 4. DOI: 10.12942/lrr-2011-4.
arXiv: 1106.1367 [gr-qc].

Antoja, T. et al. (Sept. 2018).
"A dynamically young and perturbed Milky Way disk".
In: *Nature Physics* 561.7723, pp. 360–362. DOI: 10.1038/s41586-018-0510-7.
arXiv: 1804.10196 [astro-ph.GA].

Anton, S. et al. (Jan. 2012). "QSO astrophysics, fundamental physics, and astrometric cosmology in the Gaia era".
In: *Memorie della Societá Astronomica Italiana* 83, p. 901.

Aprile, E. et al. (Sept. 2011).
"Dark Matter Results from 100 Live Days of XENON100 Data".
In: *Physical Review Letters* 107.13, 131302, p. 131302.
DOI: 10.1103/PhysRevLett.107.131302. arXiv: 1104.2549 [astro-ph.CO].

Arias, E. F. et al. (Nov. 1995). "The extragalactic reference system of the International Earth Rotation Service, ICRS."
In: *Astronomy & Astrophysics* 303, pp. 604–608.

Athanassoula, E. (2016). "Boxy/Peanut/X Bulges, Barlenses and the Thick Part of Galactic Bars: What Are They and How Did They Form?" In: *Galactic Bulges*.
Ed. by Eija Laurikainen, Reynier Peletier, and Dimitri Gadotti. Vol. 418. Astrophysics and Space Science Library, p. 391.
DOI: 10.1007/978-3-319-19378-6_14.

Aumer, Michael, James Binney, and Ralph Schönrich (Oct. 2016).
"Age-velocity dispersion relations and heating histories in disc galaxies".

In: *Monthly Notices of the Royal Astronomical Society* 462.2, pp. 1697–1713. DOI: 10.1093/mnras/stw1639. arXiv: 1607.01972 [astro-ph.GA].

Avrorin, A. D. et al. (Mar. 2015). "Search for neutrino emission from relic dark matter in the sun with the Baikal NT200 detector". In: *Astroparticle Physics* 62, pp. 12–20. DOI: 10.1016/j.astropartphys.2014.07.006. arXiv: 1405.3551 [astro-ph.HE].

Bagla, J. S. and Nishikanta Khandai (July 2009). "The Adaptive TreePM: an adaptive resolution code for cosmological N-body simulations". In: *Monthly Notices of the Royal Astronomical Society* 396.4, pp. 2211–2227. DOI: 10.1111/j.1365-2966.2009.14880.x. arXiv: 0811.4228 [astro-ph].

Balasin, H. and D. Grumiller (Jan. 2008). "Non-Newtonian Behavior in Weak Field General Relativity for Extended Rotating Sources". In: *International Journal of Modern Physics D* 17.3-04, pp. 475–488. DOI: 10.1142/S0218271808012140. arXiv: astro-ph/0602519 [astro-ph].

Barbuy, Beatriz, Cristina Chiappini, and Ortwin Gerhard (Sept. 2018). "Chemodynamical History of the Galactic Bulge". In: *Annual Review of Astronomy and Astrophysics* 56, pp. 223–276. DOI: 10.1146/annurev-astro-081817-051826. arXiv: 1805.01142 [astro-ph.GA].

Barnes, Josh and Piet Hut (Dec. 1986). "A hierarchical O(N log N) force-calculation algorithm". In: *Nature* 324.6096, pp. 446–449. DOI: 10.1038/324446a0.

Barnes, Joshua E. (Sept. 2012). "Gravitational softening as a smoothing operation". In: *Monthly Notices of the Royal Astronomical Society* 425.2, pp. 1104–1120. DOI: 10.1111/j.1365-2966.2012.21462.x. arXiv: 1205.2729 [astro-ph.CO].

Barrera-Hinojosa, C. and B. Li (Jan. 2020). "GRAMSES: a new route to general relativistic N-body simulations in cosmology. Part I. Methodology and code description". In: *Journal of Cosmology and Astroparticle Physics* 2020.01, pp. 007–007. DOI: 10.1088/1475-7516/2020/01/007. URL: https://doi.org/10.1088/1475-7516/2020/01/007.

Barros, D. A., J. R. D. Lépine, and W. S. Dias (Sept. 2016). "Models for the 3D axisymmetric gravitational potential of the Milky Way galaxy. A detailed modelling of the Galactic disk". In: *Astronomy & Astrophysics* 593, A108, A108. DOI: 10.1051/0004-6361/201527535. arXiv: 1607.02541 [astro-ph.GA].

Baur, S. (July 2019). "Dark Matter Searches with the IceCube Upgrade". In: *36th International Cosmic Ray Conference (ICRC2019)*. Vol. 36. International Cosmic Ray Conference, p. 506. arXiv: 1908.08236 [astro-ph.HE].

Behroozi, Peter S., Risa H. Wechsler, and Charlie Conroy (June 2013). "The Average Star Formation Histories of Galaxies in Dark Matter Halos from z = 0-8". In: *The Astrophysical Journal* 770.1, 57, p. 57. DOI: 10.1088/0004-637X/770/1/57. arXiv: 1207.6105 [astro-ph.CO].

Bell, Eric F. et al. (June 2008). "The Accretion Origin of the Milky Way's Stellar Halo". In: *The Astrophysical Journal* 680.1, pp. 295–311. DOI: 10.1086/588032. arXiv: 0706.0004 [astro-ph].

Bell, Eric F. et al. (Mar. 2017). "Galaxies Grow Their Bulges and Black Holes in Diverse Ways". In: *The Astrophysical Journal Letters* 837.1, L8, p. L8. DOI: 10.3847/2041-8213/aa6158. arXiv: 1702.06116 [astro-ph.GA].

Belokurov, V. et al. (May 2006). "The Field of Streams: Sagittarius and Its Siblings". In: *The Astrophysical Journal Letters* 642.2, pp. L137–L140. DOI: 10.1086/504797. arXiv: astro-ph/0605025 [astro-ph].

Belokurov, V. et al. (July 2018). "Co-formation of the disc and the stellar halo". In: *Monthly Notices of the Royal Astronomical Society* 478.1, pp. 611–619. DOI: 10.1093/mnras/sty982. arXiv: 1802.03414 [astro-ph.GA].

Bensby, T., S. Feltzing, and I. Lundström (Nov. 2003). "Elemental abundance trends in the Galactic thin and thick disks as traced by nearby F and G dwarf stars". In: *Astronomy & Astrophysics* 410, pp. 527–551. DOI: 10.1051/0004-6361:20031213.

Bensby, T. et al. (Sept. 2017). "Chemical evolution of the Galactic bulge as traced by microlensed dwarf and subgiant stars. VI. Age and abundance structure of the stellar populations in the central sub-kpc of the Milky Way". In: *Astronomy & Astrophysics* 605, A89, A89. DOI: 10.1051/0004-6361/201730560. arXiv: 1702.02971 [astro-ph.GA].

Bernabei, R. et al. (Apr. 2014). "The Dark Matter annual modulation results from DAMA/LIBRA". In: *European Physical Journal Web of Conferences*. Vol. 70.

European Physical Journal Web of Conferences, p. 00043.
DOI: 10.1051/epjconf/20147000043.

Bernard, Edouard J. et al. (July 2018). "Star formation history of the Galactic bulge from deep HST imaging of low reddening windows".
In: *Monthly Notices of the Royal Astronomical Society* 477.3, pp. 3507–3519.
DOI: 10.1093/mnras/sty902. arXiv: 1801.01426 [astro-ph.GA].

Bertone, Gianfranco and Tim M. P. Tait (Oct. 2018).
"A new era in the search for dark matter". In: *Nature* 562.7725, pp. 51–56.
DOI: 10.1038/s41586-018-0542-z. arXiv: 1810.01668 [astro-ph.CO].

Bhattacharjee, Pijushpani, Soumini Chaudhury, and Susmita Kundu (Apr. 2014). "Rotation Curve of the Milky Way out to ~200 kpc".
In: *The Astrophysical Journal* 785.1, 63, p. 63.
DOI: 10.1088/0004-637X/785/1/63. arXiv: 1310.2659 [astro-ph.GA].

Bienaymé, O. et al. (Nov. 2014).
"Weighing the local dark matter with RAVE red clump stars".
In: *Astronomy & Astrophysics* 571, A92, A92.
DOI: 10.1051/0004-6361/201424478. arXiv: 1406.6896 [astro-ph.GA].

Bignone, Lucas A., Amina Helmi, and Patricia B. Tissera (Sept. 2019).
"A Gaia-Enceladus Analog in the EAGLE Simulation: Insights into the Early Evolution of the Milky Way".
In: *The Astrophysical Journal Letters* 883.1, L5, p. L5.
DOI: 10.3847/2041-8213/ab3e0e. arXiv: 1908.07080 [astro-ph.GA].

Binney, J. and S. Tremaine (2011). *Galactic Dynamics: Second Edition*.
Princeton Series in Astrophysics. Princeton University Press.
ISBN: 978-1-4008-2872-2.

Bland-Hawthorn, Joss, Ken Freeman, and Francesca Matteucci (Jan. 2014).
*The Origin of the Galaxy and Local Group*. Saas-Fee Advanced Course.
DOI: 10.1007/978-3-642-41720-7.

Bland-Hawthorn, Joss and Ortwin Gerhard (Sept. 2016). "The Galaxy in Context: Structural, Kinematic, and Integrated Properties".
In: *Annual Review of Astronomy and Astrophysics* 54, pp. 529–596.
DOI: 10.1146/annurev-astro-081915-023441.
arXiv: 1602.07702 [astro-ph.GA].

Blitz, L. and E. Rosolowsky (Oct. 2006).
"The Role of Pressure in GMC Formation II: The $H_2$-Pressure Relation".
In: *The Astrophysical Journal* 650, pp. 933–944. DOI: 10.1086/505417.
eprint: astro-ph/0605035.

Bobylev, V. V. and A. T. Bajkova (Nov. 2018). "Kinematics of the Galaxy from OB Stars with Data from the Gaia DR2 Catalogue".
In: *Astronomy Letters* 44.11, pp. 676–687.
DOI: 10.1134/S1063773718110026. arXiv: 1809.10512 [astro-ph.GA].

Bobylev, V. V., O. I. Krisanova, and A. T. Bajkova (Nov. 2020).
"Study of the Galactic Rotation Based on Masers and Radio Stars with VLBI Measurements of Their Parallaxes".
In: *Astronomy Letters* 46.7, pp. 439–448. DOI: 10.1134/S1063773720070038.
arXiv: 2009.04261 [astro-ph.GA].

Bode, Paul and Jeremiah P. Ostriker (Mar. 2003).
"Tree Particle-Mesh: An Adaptive, Efficient, and Parallel Code for Collisionless Cosmological Simulation".
In: *The Astrophysical Journal Supplement Series* 145.1, pp. 1–13.
DOI: 10.1086/345538. arXiv: astro-ph/0302065 [astro-ph].

Bonaca, Ana et al. (Aug. 2017).
"Gaia Reveals a Metal-rich, in situ Component of the Local Stellar Halo".
In: *The Astrophysical Journal* 845.2, 101, p. 101.
DOI: 10.3847/1538-4357/aa7d0c. arXiv: 1704.05463 [astro-ph.GA].

Bond, Nicholas A. et al. (June 2010).
"The Milky Way Tomography with SDSS. III. Stellar Kinematics".
In: *The Astrophysical Journal* 716.1, pp. 1–29.
DOI: 10.1088/0004-637X/716/1/1. arXiv: 0909.0013 [astro-ph.GA].

Bovy, Jo (Feb. 2015). "galpy: A python Library for Galactic Dynamics".
In: *The Astrophysical Journal Supplement Series* 216.2, 29, p. 29.
DOI: 10.1088/0067-0049/216/2/29. arXiv: 1412.3451 [astro-ph.GA].

— (Sept. 2017).
"Stellar inventory of the solar neighbourhood using Gaia DR1".
In: *Monthly Notices of the Royal Astronomical Society* 470.2, pp. 1360–1387.
DOI: 10.1093/mnras/stx1277. arXiv: 1704.05063 [astro-ph.GA].

Bovy, Jo and Hans-Walter Rix (Dec. 2013). "A Direct Dynamical Measurement of the Milky Way's Disk Surface Density Profile, Disk Scale Length, and Dark Matter Profile at 4 kpc < R < 9 kpc".
In: *The Astrophysical Journal* 779.2, 115, p. 115.
DOI: 10.1088/0004-637X/779/2/115. arXiv: 1309.0809 [astro-ph.GA].

Bovy, Jo and Scott Tremaine (Sept. 2012).
"On the Local Dark Matter Density".
In: *The Astrophysical Journal* 756.1, 89, p. 89.
DOI: 10.1088/0004-637X/756/1/89. arXiv: 1205.4033 [astro-ph.GA].

Bovy, Jo et al. (Feb. 2015). "The Power Spectrum of the Milky Way: Velocity Fluctuations in the Galactic Disk".
In: *Astrophysical Journal* 800.2, 83, p. 83.
DOI: 10.1088/0004-637X/800/2/83. arXiv: 1410.8135 [astro-ph.GA].

Bovy, Jo et al. (May 2016).
"The Stellar Population Structure of the Galactic Disk".
In: *The Astrophysical Journal* 823.1, 30, p. 30.
DOI: 10.3847/0004-637X/823/1/30. arXiv: 1509.05796 [astro-ph.GA].

Bowden, A., N. W. Evans, and A. A. Williams (July 2016).
"Is the dark halo of the Milky Way prolate?"
In: *Monthly Notices of the Royal Astronomical Society* 460.1, pp. 329–337.
DOI: 10.1093/mnras/stw994. arXiv: 1604.06885 [astro-ph.GA].

Boylan-Kolchin, Michael, James S. Bullock, and Manoj Kaplinghat (July 2011). "Too big to fail? The puzzling darkness of massive Milky Way subhaloes".
In: *Monthly Notices of the Royal Astronomical Society* 415.1, pp. L40–L44.
DOI: 10.1111/j.1745-3933.2011.01074.x. arXiv: 1103.0007 [astro-ph.CO].

Brand, J. and L. Blitz (Aug. 1993). "The velocity field of the outer galaxy."
In: *Astronomy & Astrophysics* 275, pp. 67–90.

Brook, C. B. et al. (Oct. 2012).
"Thin disc, thick disc and halo in a simulated galaxy".
In: *Monthly Notices of the Royal Astronomical Society* 426.1, pp. 690–700.
DOI: 10.1111/j.1365-2966.2012.21738.x. arXiv: 1206.0740 [astro-ph.GA].

Brook, Chris B. et al. (Sept. 2004).
"The Emergence of the Thick Disk in a Cold Dark Matter Universe".
In: *The Astrophysical Journal* 612.2, pp. 894–899. DOI: 10.1086/422709.
arXiv: astro-ph/0405306 [astro-ph].

Bruni, Marco, Daniel B. Thomas, and David Wands (Feb. 2014).
"Computing general-relativistic effects from Newtonian N-body simulations: Frame dragging in the post-Friedmann approach".
In: *Physical Review D* 89.4, 044010, p. 044010.
DOI: 10.1103/PhysRevD.89.044010. arXiv: 1306.1562 [astro-ph.CO].

Buchdahl, H. A. (Jan. 1970).
"Non-linear Lagrangians and cosmological theory".
In: *Monthly Notices of the Royal Astronomical Society* 150, p. 1.
DOI: 10.1093/mnras/150.1.1.

Buck, Tobias et al. (Feb. 2019). "NIHAO XV: the environmental impact of the host galaxy on galactic satellite and field dwarf galaxies".

In: *Monthly Notices of the Royal Astronomical Society* 483.1, pp. 1314–1341. DOI: 10.1093/mnras/sty2913. arXiv: 1804.04667 [astro-ph.GA].

Buck, Tobias et al. (Jan. 2020). "NIHAO-UHD: the properties of MW-like stellar discs in high-resolution cosmological simulations". In: *Monthly Notices of the Royal Astronomical Society* 491.3, pp. 3461–3478. DOI: 10.1093/mnras/stz3241. arXiv: 1909.05864 [astro-ph.GA].

Bullock, James S. and Michael Boylan-Kolchin (Aug. 2017). "Small-Scale Challenges to the ΛCDM Paradigm". In: *Annual Review of Astronomy and Astrophysics* 55.1, pp. 343–387. DOI: 10.1146/annurev-astro-091916-055313. arXiv: 1707.04256 [astro-ph.CO].

Buser, R. (Jan. 2000). "The formation and early evolution of the Milky Way galaxy." In: *Science* 287, pp. 69–74. DOI: 10.1126/science.287.5450.69.

Capozziello, Salvatore and Mariafelicia de Laurentis (Dec. 2011). "Extended Theories of Gravity". In: *Physics Reports* 509.4, pp. 167–321. DOI: 10.1016/j.physrep.2011.09.003. arXiv: 1108.6266 [gr-qc].

Carignan, Claude and Sylvie Beaulieu (Dec. 1989). "Optical and H i Studies of the "Gas-rich" Dwarf Irregular Galaxy DDO 154". In: *The Astrophysical Journal* 347, p. 760. DOI: 10.1086/168167.

Carignan, Claude and Kenneth C. Freeman (Sept. 1988). "DDO 154: A "Dark" Galaxy?" In: *The Astrophysical Journal Letters* 332, p. L33. DOI: 10.1086/185260.

Carlesi, Edoardo et al. (May 2016). "Constrained Local UniversE Simulations: a Local Group factory". In: *Monthly Notices of the Royal Astronomical Society* 458.1, pp. 900–911. DOI: 10.1093/mnras/stw357. arXiv: 1602.03919 [astro-ph.CO].

Carollo, Daniela et al. (Dec. 2007). "Two stellar components in the halo of the Milky Way". In: *Nature* 450.7172, pp. 1020–1025. DOI: 10.1038/nature06460. arXiv: 0706.3005 [astro-ph].

Carrick, J. D. and F. I. Cooperstock (Jan. 2012). "General relativistic dynamics applied to the rotation curves of galaxies". In: *Astrophysics and Space Science* 337.1, pp. 321–329. DOI: 10.1007/s10509-011-0854-z. arXiv: 1101.3224 [astro-ph.GA].

Casagrande, L. et al. (June 2011). "New constraints on the chemical evolution of the solar neighbourhood and Galactic disc(s). Improved astrophysical parameters for the Geneva-Copenhagen Survey".

In: *Astronomy & Astrophysics* 530, A138, A138.
DOI: 10.1051/0004-6361/201016276. arXiv: 1103.4651 [astro-ph.GA].

Cesare, V. et al. (May 2020).
"Dynamics of DiskMass Survey galaxies in refracted gravity".
In: *Astronomy & Astrophysics* 637, A70, A70.
DOI: 10.1051/0004-6361/201935950. arXiv: 2003.07377 [astro-ph.GA].

Choi, K. et al. (Apr. 2015).
"Search for Neutrinos from Annihilation of Captured Low-Mass Dark Matter Particles in the Sun by Super-Kamiokande".
In: *Physical Review Letters* 114.14, 141301, p. 141301.
DOI: 10.1103/PhysRevLett.114.141301.

*CINECA Web Portal*. Website.
URL: https://www.hpc.cineca.it/content/hardware.

Clementini, G. et al. (Feb. 2019). "Gaia Data Release 2. Specific characterisation and validation of all-sky Cepheids and RR Lyrae stars".
In: *Astronomy & Astrophysics* 622, A60, A60.
DOI: 10.1051/0004-6361/201833374. arXiv: 1805.02079 [astro-ph.SR].

Clowe, Douglas, Anthony Gonzalez, and Maxim Markevitch (Apr. 2004).
"Weak-Lensing Mass Reconstruction of the Interacting Cluster 1E 0657-558: Direct Evidence for the Existence of Dark Matter".
In: *The Astrophysical Journal* 604.2, pp. 596–603. DOI: 10.1086/381970.
arXiv: astro-ph/0312273 [astro-ph].

Clowe, Douglas et al. (Sept. 2006).
"A Direct Empirical Proof of the Existence of Dark Matter".
In: *The Astrophysical Journal Letters* 648.2, pp. L109–L113.
DOI: 10.1086/508162. arXiv: astro-ph/0608407 [astro-ph].

Coley, Alan A. and David L. Wiltshire (May 2017).
"What is general relativity?" In: *Physica Scripta* 92.5, 053001, p. 053001.
DOI: 10.1088/1402-4896/aa6857. arXiv: 1612.09309 [gr-qc].

Cooper, Andrew P. et al. (Dec. 2015).
"Formation of in situ stellar haloes in Milky Way-mass galaxies".
In: *Monthly Notices of the Royal Astronomical Society* 454.3, pp. 3185–3199.
DOI: 10.1093/mnras/stv2057. arXiv: 1501.04630 [astro-ph.GA].

Cooperstock, F. I. and S. Tieu (May 2007). "Galactic Dynamics via General Relativity: a Compilation and New Developments".
In: *International Journal of Modern Physics A* 22.13, pp. 2293–2325.
DOI: 10.1142/S0217751X0703666X. arXiv: astro-ph/0610370 [astro-ph].

Corbelli, Edvige and Paolo Salucci (Jan. 2000).
"The extended rotation curve and the dark matter halo of M33".
In: *Monthly Notices of the Royal Astronomical Society* 311.2, pp. 441–447.
DOI: 10.1046/j.1365-8711.2000.03075.x.
arXiv: astro-ph/9909252 [astro-ph].

Croft, Rupert A. C. et al. (Dec. 2002). "Toward a Precise Measurement of Matter Clustering: Ly$\alpha$ Forest Data at Redshifts 2-4".
In: *The Astrophysical Journal* 581.1, pp. 20–52. DOI: 10.1086/344099.
arXiv: astro-ph/0012324 [astro-ph].

Crosta, M. et al. (Aug. 2015). "The ray tracing analytical solution within the RAMOD framework. The case of a Gaia-like observer".
In: *Classical and Quantum Gravity* 32.16, 165008, p. 165008.
DOI: 10.1088/0264-9381/32/16/165008. arXiv: 1501.03705 [gr-qc].

Crosta, M. T. and F. Mignard (Aug. 2006).
"Microarcsecond light bending by Jupiter".
In: *Classical and Quantum Gravity* 23.15, pp. 4853–4871.
DOI: 10.1088/0264-9381/23/15/006.
arXiv: astro-ph/0512359 [astro-ph].

Crosta, M. T. et al. (Sept. 2003).
"Some Aspects of Relativistic Astrometry from Within the Solar System".
In: *Celestial Mechanics and Dynamical Astronomy* 87.1, pp. 209–218.
arXiv: astro-ph/0305399 [astro-ph].

Crosta, Mariateresa (Oct. 2019).
"Astrometry in the 21st century. From Hipparchus to Einstein".
In: *Rivista del Nuovo Cimento* 42.10, pp. 443–510.
DOI: 10.1393/ncr/i2019-10164-2.

Crosta, Mariateresa et al. (Nov. 2017). "General relativistic observable for gravitational astrometry in the context of the Gaia mission and beyond".
In: *Physical Review D* 96.10, 104030, p. 104030.
DOI: 10.1103/PhysRevD.96.104030.

Crosta, Mariateresa et al. (Apr. 2019).
"Shedding light on the Milky Way rotation curve with Gaia DR2".
In: *The Gaia Universe*, p. 63. DOI: 10.5281/zenodo.3237518.

Crosta, Mariateresa et al. (June 2020). "On testing CDM and geometry-driven Milky Way rotation curve models with Gaia DR2".
In: *Monthly Notices of the Royal Astronomical Society* 496.2, pp. 2107–2122.
DOI: 10.1093/mnras/staa1511. arXiv: 1810.04445 [astro-ph.GA].

de Almeida, Álefe O. F., Oliver F. Piattella, and Davi C. Rodrigues (Nov. 2016). "A method for evaluating models that use galaxy rotation curves to derive the density profiles".
In: *Monthly Notices of the Royal Astronomical Society* 462.3, pp. 2706–2714. DOI: 10.1093/mnras/stw1844. arXiv: 1605.04269 [astro-ph.GA].

de Blok, W. J. G. (Jan. 2010). "The Core-Cusp Problem".
In: *Advances in Astronomy* 2010, 789293, p. 789293. DOI: 10.1155/2010/789293. arXiv: 0910.3538 [astro-ph.CO].

de Blok, W. J. G. and S. S. McGaugh (Sept. 1997). "The dark and visible matter content of low surface brightness disc galaxies".
In: *Monthly Notices of the Royal Astronomical Society* 290.3, pp. 533–552. DOI: 10.1093/mnras/290.3.533. arXiv: astro-ph/9704274 [astro-ph].

De Felice, Antonio and Shinji Tsujikawa (June 2010). "f( R) Theories".
In: *Living Reviews in Relativity* 13.1, 3, p. 3. DOI: 10.12942/lrr-2010-3. arXiv: 1002.4928 [gr-qc].

de Felice, F. and C. J. S. Clarke (1990). *Relativity on Curved Manifolds*.

de Felice, F. et al. (May 2004). "A General Relativistic Model of Light Propagation in the Gravitational Field of the Solar System: The Static Case".
In: *The Astrophysical Journal* 607.1, pp. 580–595. DOI: 10.1086/383244. arXiv: astro-ph/0401637 [astro-ph].

de Felice, F. et al. (Dec. 2006). "A General Relativistic Model of Light Propagation in the Gravitational Field of the Solar System: The Dynamical Case".
In: *The Astrophysical Journal* 653.2, pp. 1552–1565. DOI: 10.1086/508701. arXiv: astro-ph/0609073 [astro-ph].

de Felice, Fernando and Donato Bini (2010). *Classical Measurements in Curved Space-Times*.

de Martino, Ivan et al. (July 2020). "Dark matters on the scale of galaxies".
In: *arXiv e-prints*, arXiv:2007.15539, arXiv:2007.15539. arXiv: 2007.15539 [astro-ph.CO].

de Salas, P. F. et al. (Oct. 2019a). "On the estimation of the local dark matter density using the rotation curve of the Milky Way".
In: *Journal of Cosmology and Astroparticle Physics* 2019.10, 037, p. 037. DOI: 10.1088/1475-7516/2019/10/037. arXiv: 1906.06133 [astro-ph.GA].

— (Oct. 2019b). "On the estimation of the local dark matter density using the rotation curve of the Milky Way".

In: *Journal of Cosmology and Astroparticle Physics* 2019.10, 037, p. 037. DOI: 10.1088/1475-7516/2019/10/037. arXiv: 1906.06133 [astro-ph.GA].

De Silva, G. M. et al. (May 2015). "The GALAH survey: scientific motivation". In: *Monthly Notices of the Royal Astronomical Society* 449.3, pp. 2604–2617. DOI: 10.1093/mnras/stv327. arXiv: 1502.04767 [astro-ph.GA].

Deason, Alis J., Vasily Belokurov, and Jason L. Sanders (Dec. 2019). "The total stellar halo mass of the Milky Way". In: *Monthly Notices of the Royal Astronomical Society* 490.3, pp. 3426–3439. DOI: 10.1093/mnras/stz2793. arXiv: 1908.02763 [astro-ph.GA].

Dehnen, Walter (June 2001). "Towards optimal softening in three-dimensional N-body codes - I. Minimizing the force error". In: *Monthly Notices of the Royal Astronomical Society* 324.2, pp. 273–291. DOI: 10.1046/j.1365-8711.2001.04237.x. arXiv: astro-ph/0011568 [astro-ph].

Di Matteo, P. et al. (July 2014). "Mapping a stellar disk into a boxy bulge: The outside-in part of the Milky Way bulge formation". In: *Astronomy & Astrophysics* 567, A122, A122. DOI: 10.1051/0004-6361/201322958. arXiv: 1404.0304 [astro-ph.GA].

Di Matteo, P. et al. (Dec. 2019). "The Milky Way has no in-situ halo other than the heated thick disc. Composition of the stellar halo and age-dating the last significant merger with Gaia DR2 and APOGEE". In: *Astronomy & Astrophysics* 632, A4, A4. DOI: 10.1051/0004-6361/201834929. arXiv: 1812.08232 [astro-ph.GA].

Drimmel, Ronald and Eloisa Poggio (Nov. 2018). "On the Solar Velocity". In: *Research Notes of the American Astronomical Society* 2.4, 210, p. 210. DOI: 10.3847/2515-5172/aaef8b.

Drimmel, Ronald and David N. Spergel (July 2001). "Three-dimensional Structure of the Milky Way Disk: The Distribution of Stars and Dust beyond 0.35 $R_{solar}$". In: *The Astrophysical Journal* 556.1, pp. 181–202. DOI: 10.1086/321556. arXiv: astro-ph/0101259 [astro-ph].

East, W. E., R. Wojtak, and Tom Abel (Feb. 2018). "Comparing fully general relativistic and Newtonian calculations of structure formation". In: *Physical Review D* 97 (4), p. 043509. DOI: 10.1103/PhysRevD.97.043509. URL: https://link.aps.org/doi/10.1103/PhysRevD.97.043509.

Efstathiou, G. et al. (Feb. 1985). "Numerical techniques for large cosmological N-body simulations".

In: *The Astrophysical Journal Supplement Series* 57, pp. 241–260. DOI: 10.1086/191003.

Eggen, O. J., D. Lynden-Bell, and A. R. Sandage (Nov. 1962). "Evidence from the motions of old stars that the Galaxy collapsed." In: *The Astrophysical Journal* 136, p. 748. DOI: 10.1086/147433.

Eilers, Anna-Christina et al. (Jan. 2019). "The Circular Velocity Curve of the Milky Way from 5 to 25 kpc". In: *The Astrophysical Journal* 871.1, 120, p. 120. DOI: 10.3847/1538-4357/aaf648. arXiv: 1810.09466 [astro-ph.GA].

Einasto, J. (Jan. 1965). "On the Construction of a Composite Model for the Galaxy and on the Determination of the System of Galactic Parameters". In: *Trudy Astrofizicheskogo Instituta Alma-Ata* 5, pp. 87–100.

Einstein, Albert (Jan. 1917). "Kosmologische Betrachtungen zur allgemeinen Relativitätstheorie". In: *Sitzungsberichte der Königlich Preußischen Akademie der Wissenschaften (Berlin*, pp. 142–152.

Ellis, G. F. R. and W. Stoeger (Nov. 1987). "The "fitting problem" in cosmology". In: *Classical and Quantum Gravity* 4.6, pp. 1697–1729. DOI: 10.1088/0264-9381/4/6/025. URL: https://doi.org/10.1088/0264-9381/4/6/025.

*ESA Web Portal*. Website. URL: https://www.cosmos.esa.int/web/gaia.

Everall, A. et al. (Oct. 2019). "The tilt of the local velocity ellipsoid as seen by Gaia". In: *Monthly Notices of the Royal Astronomical Society* 489.1, pp. 910–918. DOI: 10.1093/mnras/stz2217. arXiv: 1904.08460 [astro-ph.GA].

Fattahi, Azadeh et al. (Apr. 2019). "The origin of galactic metal-rich stellar halo components with highly eccentric orbits". In: *Monthly Notices of the Royal Astronomical Society* 484.4, pp. 4471–4483. DOI: 10.1093/mnras/stz159. arXiv: 1810.07779 [astro-ph.GA].

Feuillet, Diane K. et al. (Oct. 2019). "Spatial variations in the Milky Way disc metallicity-age relation". In: *Monthly Notices of the Royal Astronomical Society* 489.2, pp. 1742–1752. DOI: 10.1093/mnras/stz2221. arXiv: 1908.02772 [astro-ph.GA].

Fich, Michel, Leo Blitz, and Antony A. Stark (July 1989). "The Rotation Curve of the Milky Way to 2R 0". In: *The Astrophysical Journal* 342, p. 272. DOI: 10.1086/167591.

Foreman-Mackey, Daniel (2016). "corner.py: Scatterplot matrices in Python". In: *The Journal of Open Source Software* 1.2, p. 24. DOI: 10.21105/joss.00024. URL: https://doi.org/10.21105/joss.00024.

Freeman, Ken and Joss Bland-Hawthorn (Jan. 2002). "The New Galaxy: Signatures of Its Formation". In: *Annual Review of Astronomy and Astrophysics* 40, pp. 487–537. DOI: 10.1146/annurev.astro.40.060401.093840. arXiv: astro-ph/0208106 [astro-ph].

Frigerio Martins, C., J. A. S. Lima, and P. Chimenti (June 2015). "Galaxy rotation curves and nonextensive statistics". In: *Monthly Notices of the Royal Astronomical Society* 449.4, pp. 3645–3650. DOI: 10.1093/mnras/stu2583. arXiv: 1409.6367 [astro-ph.GA].

Fujii, Y. and K. Maeda (2003). *The Scalar-Tensor Theory of Gravitation*. Cambridge Monographs on Mathematical Physics. Cambridge University Press. DOI: 10.1017/CBO9780511535093.

*Gaia Archive*. Website. URL: https://gea.esac.esa.int/archive/.

Gaia Collaboration et al. (Nov. 2016). "The Gaia mission". In: *Astronomy & Astrophysics* 595, A1, A1. DOI: 10.1051/0004-6361/201629272. arXiv: 1609.04153 [astro-ph.IM].

Gaia Collaboration et al. (Aug. 2018a). "Gaia Data Release 2. Mapping the Milky Way disc kinematics". In: *Astronomy & Astrophysics* 616, A11, A11. DOI: 10.1051/0004-6361/201832865. arXiv: 1804.09380 [astro-ph.GA].

Gaia Collaboration et al. (Aug. 2018b). "Gaia Data Release 2. Summary of the contents and survey properties". In: *Astronomy & Astrophysics* 616, A1, A1. DOI: 10.1051/0004-6361/201833051. arXiv: 1804.09365 [astro-ph.GA].

Gaia Collaboration et al. (Dec. 2020). "Gaia Early Data Release 3: Summary of the contents and survey properties". In: *arXiv e-prints*, arXiv:2012.01533, arXiv:2012.01533. arXiv: 2012.01533 [astro-ph.GA].

Gaia Collaboration et al. (Jan. 2021). "Gaia Early Data Release 3: The Galactic anticentre". In: *arXiv e-prints*, arXiv:2101.05811, arXiv:2101.05811. arXiv: 2101.05811 [astro-ph.GA].

*Gaia DPAC*. Website. URL: https://www.cosmos.esa.int/web/gaia/dpac/consortium.

Gallart, Carme et al. (July 2019). "Uncovering the birth of the Milky Way through accurate stellar ages with Gaia".
In: *Nature Astronomy* 3, pp. 932–939. DOI: 10.1038/s41550-019-0829-5. arXiv: 1901.02900 [astro-ph.GA].

Gallego-Cano, E. et al. (Feb. 2020).
"New constraints on the structure of the nuclear stellar cluster of the Milky Way from star counts and MIR imaging".
In: *Astronomy & Astrophysics* 634, A71, A71.
DOI: 10.1051/0004-6361/201935303. arXiv: 2001.08182 [astro-ph.GA].

Garbari, Silvia et al. (Sept. 2012). "A new determination of the local dark matter density from the kinematics of K dwarfs".
In: *Monthly Notices of the Royal Astronomical Society* 425.2, pp. 1445–1458.
DOI: 10.1111/j.1365-2966.2012.21608.x. arXiv: 1206.0015 [astro-ph.GA].

Ghez, A. M. et al. (Dec. 2008). "Measuring Distance and Properties of the Milky Way's Central Supermassive Black Hole with Stellar Orbits".
In: *The Astrophysical Journal* 689.2, pp. 1044–1062. DOI: 10.1086/592738. arXiv: 0808.2870 [astro-ph].

Giammaria, Marco et al. (Apr. 2021). "The formation history of the Milky Way disc with high-resolution cosmological simulations".
In: *Monthly Notices of the Royal Astronomical Society* 502.2, pp. 2251–2265.
DOI: 10.1093/mnras/stab136. arXiv: 2102.02652 [astro-ph.GA].

Giblin, John T., James B. Mertens, and Glenn D. Starkman (June 2016). "Departures from the Friedmann-Lemaitre-Robertston-Walker Cosmological Model in an Inhomogeneous Universe: A Numerical Examination". In: *Physical Review Letters* 116.25, 251301, p. 251301.
DOI: 10.1103/PhysRevLett.116.251301. arXiv: 1511.01105 [gr-qc].

Gillessen, S. et al. (Feb. 2009a). "Monitoring Stellar Orbits Around the Massive Black Hole in the Galactic Center".
In: *The Astrophysical Journal* 692.2, pp. 1075–1109.
DOI: 10.1088/0004-637X/692/2/1075. arXiv: 0810.4674 [astro-ph].

Gillessen, S. et al. (Dec. 2009b). "The Orbit of the Star S2 Around SGR A* from Very Large Telescope and Keck Data".
In: *The Astrophysical Journal Letters* 707.2, pp. L114–L117.
DOI: 10.1088/0004-637X/707/2/L114. arXiv: 0910.3069 [astro-ph.GA].

Gilmore, G. and N. Reid (Mar. 1983). "New light on faint stars - III. Galactic structure towards the South Pole and the Galactic thick disc."
In: *Monthly Notices of the Royal Astronomical Society* 202, pp. 1025–1047.
DOI: 10.1093/mnras/202.4.1025.

Gilmore, Gerard, Rosemary F. G. Wyse, and Konrad Kuijken (Jan. 1989). "Kinematics, chemistry, and structure of the Galaxy." In: *Annual Review of Astronomy and Astrophysics* 27, pp. 555–627. DOI: 10.1146/annurev.aa.27.090189.003011.

González Delgado, R. M. et al. (Feb. 2014). "The star formation history of CALIFA galaxies: Radial structures". In: *Astronomy & Astrophysics* 562, A47, A47. DOI: 10.1051/0004-6361/201322011. arXiv: 1310.5517 [astro-ph.CO].

Goz, David et al. (Feb. 2015). "Properties of barred spiral discs in hydrodynamical cosmological simulations". In: *Monthly Notices of the Royal Astronomical Society* 447.2, pp. 1774–1788. DOI: 10.1093/mnras/stu2557.

Granados, Andrés et al. (Jan. 2021). "GalRotpy: a tool to parametrize the gravitational potential of disc-like galaxies". In: *New Astronomy* 82, 101456, p. 101456. DOI: 10.1016/j.newast.2020.101456.

Grand, Robert J. J. et al. (May 2017). "The Auriga Project: the properties and formation mechanisms of disc galaxies across cosmic time". In: *Monthly Notices of the Royal Astronomical Society* 467.1, pp. 179–207. DOI: 10.1093/mnras/stx071. arXiv: 1610.01159 [astro-ph.GA].

Grand, Robert J. J. et al. (Jan. 2020). "Sausage & Mash: the dual origin of the Galactic thick disc and halo from the gas-rich Gaia-Enceladus-Sausage merger". In: *arXiv e-prints*, arXiv:2001.06009, arXiv:2001.06009. arXiv: 2001.06009 [astro-ph.GA].

Gravity Collaboration et al. (July 2018). "Detection of the gravitational redshift in the orbit of the star S2 near the Galactic centre massive black hole". In: *Astronomy & Astrophysics* 615, L15, p. L15. DOI: 10.1051/0004-6361/201833718. arXiv: 1807.09409 [astro-ph.GA].

Grillmair, Carl J. and Jeffrey L. Carlin (2016). "Stellar Streams and Clouds in the Galactic Halo". In: *Tidal Streams in the Local Group and Beyond*. Ed. by Heidi Jo Newberg and Jeffrey L. Carlin. Vol. 420. Astrophysics and Space Science Library, p. 87. DOI: 10.1007/978-3-319-19336-6_4.

Grisoni, V., E. Spitoni, and F. Matteucci (Dec. 2018). "Abundance gradients along the Galactic disc from chemical evolution models".

In: *Monthly Notices of the Royal Astronomical Society* 481.2, pp. 2570–2580. DOI: 10.1093/mnras/sty2444. arXiv: 1805.11415 [astro-ph.GA].

Grumiller, D., H. Balasin, and F. Preis (2009). "Non-Perturbative Effects in Complex Gravitationally Bound Systems". In:

Guedes, Javiera et al. (Dec. 2011). "Forming Realistic Late-type Spirals in a ΛCDM Universe: The Eris Simulation". In: *The Astrophysical Journal* 742.2, 76, p. 76. DOI: 10.1088/0004-637X/742/2/76. arXiv: 1103.6030 [astro-ph.CO].

Gunn, J. E., G. R. Knapp, and S. D. Tremaine (Aug. 1979). "The global properties of the Galaxy. II. The galactic rotation parameters from 21-cm H I observations." In: *The Astronomical Journal* 84, pp. 1181–1188. DOI: 10.1086/112525.

Guo, Hong et al. (July 2016). "Modelling galaxy clustering: halo occupation distribution versus subhalo matching". In: *Monthly Notices of the Royal Astronomical Society* 459.3, pp. 3040–3058. DOI: 10.1093/mnras/stw845. arXiv: 1508.07012 [astro-ph.CO].

Haardt, F. and P. Madau (2001). "Modelling the UV/X-ray cosmic background with CUBA". In: *Clusters of Galaxies and the High Redshift Universe Observed in X-rays. CEA, Saclay, p.64*. Ed. by D. M. Neumann and J. T. V. Tran. eprint: astro-ph/0106018.

Hagen, Jorrit H. J. and Amina Helmi (July 2018). "The vertical force in the solar neighbourhood using red clump stars in TGAS and RAVE. Constraints on the local dark matter density". In: *Astronomy & Astrophysics* 615, A99, A99. DOI: 10.1051/0004-6361/201832903. arXiv: 1802.09291 [astro-ph.GA].

Han, Doo Ri et al. (June 2020). "Insights into the Formation and Evolution History of the Galactic Disk System". In: *Astrophysical Journal* 896.1, 14, p. 14. DOI: 10.3847/1538-4357/ab919a. arXiv: 2005.04866 [astro-ph.GA].

Hayden, Michael R. et al. (Aug. 2015). "Chemical Cartography with APOGEE: Metallicity Distribution Functions and the Chemical Structure of the Milky Way Disk". In: *The Astrophysical Journal* 808.2, 132, p. 132. DOI: 10.1088/0004-637X/808/2/132. arXiv: 1503.02110 [astro-ph.GA].

Hayden, Michael R. et al. (Apr. 2020). "The GALAH survey: chemodynamics of the solar neighbourhood".

In: *Monthly Notices of the Royal Astronomical Society* 493.2, pp. 2952–2964. DOI: 10.1093/mnras/staa335. arXiv: 1901.07565 [astro-ph.GA].

Hayes, Christian R. et al. (Jan. 2018). "Disentangling the Galactic Halo with APOGEE. I. Chemical and Kinematical Investigation of Distinct Metal-poor Populations". In: *The Astrophysical Journal* 852.1, 49, p. 49. DOI: 10.3847/1538-4357/aa9cec. arXiv: 1711.05781 [astro-ph.GA].

Haywood, M. et al. (Sept. 2016). "Hiding its age: the case for a younger bulge". In: *Astronomy & Astrophysics* 593, A82, A82. DOI: 10.1051/0004-6361/201628816. arXiv: 1606.04092 [astro-ph.GA].

Haywood, Misha et al. (Dec. 2013). "The age structure of stellar populations in the solar vicinity. Clues of a two-phase formation history of the Milky Way disk". In: *Astronomy & Astrophysics* 560, A109, A109. DOI: 10.1051/0004-6361/201321397. arXiv: 1305.4663 [astro-ph.GA].

Helmi, Amina (June 2008). "The stellar halo of the Galaxy". In: *The Astronomy and Astrophysics Review* 15.3, pp. 145–188. DOI: 10.1007/s00159-008-0009-6. arXiv: 0804.0019 [astro-ph].

— (Feb. 2020). "Streams, substructures and the early history of the Milky Way". In: *arXiv e-prints*, arXiv:2002.04340, arXiv:2002.04340. arXiv: 2002.04340 [astro-ph.GA].

Helmi, Amina et al. (Oct. 2018). "The merger that led to the formation of the Milky Way's inner stellar halo and thick disk". In: *Nature Physics* 563.7729, pp. 85–88. DOI: 10.1038/s41586-018-0625-x. arXiv: 1806.06038 [astro-ph.GA].

Hernquist, Lars and Joshua E. Barnes (Feb. 1990). "Are Some N-Body Algorithms Intrinsically Less Collisional than Others?" In: *The Astrophysical Journal* 349, p. 562. DOI: 10.1086/168343.

Hockney, R. W. and J. W. Eastwood (1981). *Computer Simulation Using Particles*.

Hoffman, Matthew D. and Andrew Gelman (Apr. 2014). "The No-U-Turn Sampler: Adaptively Setting Path Lengths in Hamiltonian Monte Carlo". In: *Journal of Machine Learning Research* 15, arXiv:1111.4246, arXiv:1111.4246. arXiv: 1111.4246 [stat.CO].

Høg, E. et al. (Mar. 2000).
"The Tycho-2 catalogue of the 2.5 million brightest stars".
In: *Astronomy & Astrophysics* 355, pp. L27–L30.

Huang, Y. et al. (Dec. 2016). "The Milky Way's rotation curve out to 100 kpc and its constraint on the Galactic mass distribution".
In: *Monthly Notices of the Royal Astronomical Society* 463.3, pp. 2623–2639. DOI: 10.1093/mnras/stw2096. arXiv: 1604.01216 [astro-ph.GA].

Ibata, R. et al. (Mar. 2013). "Does the Sagittarius Stream Constrain the Milky Way Halo to be Triaxial?"
In: *The Astrophysical Journal Letters* 765.1, L15, p. L15.
DOI: 10.1088/2041-8205/765/1/L15. arXiv: 1212.4958 [astro-ph.GA].

Ibata, R. A., G. Gilmore, and M. J. Irwin (July 1994).
"A dwarf satellite galaxy in Sagittarius".
In: *Nature* 370.6486, pp. 194–196. DOI: 10.1038/370194a0.

Ibata, Rodrigo et al. (Apr. 2001). "Great Circle Tidal Streams: Evidence for a Nearly Spherical Massive Dark Halo around the Milky Way".
In: *The Astrophysical Journal* 551.1, pp. 294–311. DOI: 10.1086/320060.
arXiv: astro-ph/0004011 [astro-ph].

Ibata, Rodrigo A. et al. (Feb. 1997). "The Kinematics, Orbit, and Survival of the Sagittarius Dwarf Spheroidal Galaxy".
In: *The Astronomical Journal* 113, pp. 634–655. DOI: 10.1086/118283.
arXiv: astro-ph/9612025 [astro-ph].

Iocco, Fabio, Miguel Pato, and Gianfranco Bertone (Mar. 2015).
"Evidence for dark matter in the inner Milky Way".
In: *Nature Physics* 11.3, pp. 245–248. DOI: 10.1038/nphys3237.
arXiv: 1502.03821 [astro-ph.GA].

Jeans, J. H. (Dec. 1915).
"On the theory of star-streaming and the structure of the universe".
In: *Monthly Notices of the Royal Astronomical Society* 76, pp. 70–84.
DOI: 10.1093/mnras/76.2.70.

Johnston, Kathryn V., David R. Law, and Steven R. Majewski (Feb. 2005).
"A Two Micron All Sky Survey View of the Sagittarius Dwarf Galaxy. III. Constraints on the Flattening of the Galactic Halo".
In: *The Astrophysical Journal* 619.2, pp. 800–806. DOI: 10.1086/426777.
arXiv: astro-ph/0407565 [astro-ph].

Jurić, Mario et al. (Feb. 2008). "The Milky Way Tomography with SDSS. I. Stellar Number Density Distribution".

In: *Astrophysical Journal* 673.2, pp. 864–914. DOI: 10.1086/523619. arXiv: astro-ph/0510520 [astro-ph].

Just, A. and H. Jahreiß (Feb. 2010a). "Towards a fully consistent Milky Way disc model - I. The local model based on kinematic and photometric data". In: *Monthly Notices of the Royal Astronomical Society* 402.1, pp. 461–478. DOI: 10.1111/j.1365-2966.2009.15893.x. arXiv: 0910.3481 [astro-ph.GA].

— (Feb. 2010b). "Towards a fully consistent Milky Way disc model - I. The local model based on kinematic and photometric data". In: *Monthly Notices of the Royal Astronomical Society* 402.1, pp. 461–478. DOI: 10.1111/j.1365-2966.2009.15893.x. arXiv: 0910.3481 [astro-ph.GA].

Kafle, Prajwal R. et al. (Dec. 2012). "Kinematics of the Stellar Halo and the Mass Distribution of the Milky Way Using Blue Horizontal Branch Stars". In: *The Astrophysical Journal* 761.2, 98, p. 98. DOI: 10.1088/0004-637X/761/2/98. arXiv: 1210.7527 [astro-ph.GA].

Kaplinghat, Manoj, Mauro Valli, and Hai-Bo Yu (Nov. 2019). "Too big to fail in light of Gaia". In: *Monthly Notices of the Royal Astronomical Society* 490.1, pp. 231–242. DOI: 10.1093/mnras/stz2511. arXiv: 1904.04939 [astro-ph.GA].

Kapteyn, J. C. (May 1922). "First Attempt at a Theory of the Arrangement and Motion of the Sidereal System". In: *The Astrophysical Journal* 55, p. 302. DOI: 10.1086/142670.

Karukes, E. V. et al. (Sept. 2019). "Bayesian reconstruction of the Milky Way dark matter distribution". In: *Journal of Cosmology and Astroparticle Physics* 2019.9, 046, p. 046. DOI: 10.1088/1475-7516/2019/09/046. arXiv: 1901.02463 [astro-ph.GA].

Klioner, Sergei A. (Mar. 2003). "A Practical Relativistic Model for Microarcsecond Astrometry in Space". In: *The Astronomical Journal* 125.3, pp. 1580–1597. DOI: 10.1086/367593.

— (June 2004). "Physically adequate proper reference system of a test observer and relativistic description of the GAIA attitude". In: *Physical Review D* 69.12, 124001, p. 124001. DOI: 10.1103/PhysRevD.69.124001. arXiv: astro-ph/0311540 [astro-ph].

Klypin, Anatoly, HongSheng Zhao, and Rachel S. Somerville (July 2002). "ΛCDM-based Models for the Milky Way and M31. I. Dynamical Models". In: *The Astrophysical Journal* 573.2, pp. 597–613. DOI: 10.1086/340656. arXiv: astro-ph/0110390 [astro-ph].

Klypin, Anatoly et al. (Sept. 1999).
"Where Are the Missing Galactic Satellites?"
In: *The Astrophysical Journal* 522.1, pp. 82–92. DOI: 10.1086/307643.
arXiv: astro-ph/9901240 [astro-ph].

Klypin, Anatoly et al. (Dec. 2015). "Abundance of field galaxies".
In: *Monthly Notices of the Royal Astronomical Society* 454.2, pp. 1798–1810.
DOI: 10.1093/mnras/stv2040. arXiv: 1405.4523 [astro-ph.CO].

Koposov, Sergey E., Hans-Walter Rix, and David W. Hogg (Mar. 2010).
"Constraining the Milky Way Potential with a Six-Dimensional
Phase-Space Map of the GD-1 Stellar Stream".
In: *The Astrophysical Journal* 712.1, pp. 260–273.
DOI: 10.1088/0004-637X/712/1/260. arXiv: 0907.1085 [astro-ph.GA].

Koppelman, Helmer, Amina Helmi, and Jovan Veljanoski (June 2018).
"One Large Blob and Many Streams Frosting the nearby Stellar Halo in
Gaia DR2". In: *The Astrophysical Journal Letters* 860.1, L11, p. L11.
DOI: 10.3847/2041-8213/aac882. arXiv: 1804.11347 [astro-ph.GA].

Kormendy, John et al. (Nov. 2010). "Bulgeless Giant Galaxies Challenge Our
Picture of Galaxy Formation by Hierarchical Clustering".
In: *The Astrophysical Journal* 723.1, pp. 54–80.
DOI: 10.1088/0004-637X/723/1/54. arXiv: 1009.3015 [astro-ph.GA].

Korol, Valeriya, Elena M. Rossi, and Enrico Barausse (Mar. 2019).
"A multimessenger study of the Milky Way's stellar disc and bulge with
LISA, Gaia, and LSST".
In: *Monthly Notices of the Royal Astronomical Society* 483.4, pp. 5518–5533.
DOI: 10.1093/mnras/sty3440. arXiv: 1806.03306 [astro-ph.GA].

Kotz, Samuel, Narayanaswamy Balakrishnan, and Norman Johnson (Jan.
2000). *Continuous Multivariate Distributions: Models and Applications,
Volume 1, Second Edition*. Vol. 1, p. 735. ISBN: 9780471183877.
DOI: 10.1002/0471722065.

Kroupa, P., C. A. Tout, and G. Gilmore (June 1993).
"The distribution of low-mass stars in the Galactic disc".
In: *Monthly Notices of the Royal Astronomical Society* 262, pp. 545–587.
DOI: 10.1093/mnras/262.3.545.

Lacey, Cedric and Shaun Cole (June 1993).
"Merger rates in hierarchical models of galaxy formation".
In: *Monthly Notices of the Royal Astronomical Society* 262.3, pp. 627–649.
DOI: 10.1093/mnras/262.3.627.

Lattanzi, M. G. (Jan. 2012). "Astrometric cosmology".
In: *Memorie della S. A. It.* 83, p. 1033.

Leavitt, Henrietta S. and Edward C. Pickering (Mar. 1912).
"Periods of 25 Variable Stars in the Small Magellanic Cloud."
In: *Harvard College Observatory Circular* 173, pp. 1–3.

Lense, Josef and Hans Thirring (Jan. 1918). "Über den Einfluß der Eigenrotation der Zentralkörper auf die Bewegung der Planeten und Monde nach der Einsteinschen Gravitationstheorie".
In: *Physikalische Zeitschrift* 19, p. 156.

Levine, E. S., Carl Heiles, and Leo Blitz (June 2008). "The Milky Way Rotation Curve and Its Vertical Derivatives: Inside the Solar Circle".
In: *The Astrophysical Journal* 679.2, pp. 1288–1298. DOI: 10.1086/587444. arXiv: 0802.2714 [astro-ph].

Lian, Jianhui et al. (July 2020a). "The age-chemical abundance structure of the Galactic disc - II. $\alpha$-dichotomy and thick disc formation".
In: *Monthly Notices of the Royal Astronomical Society* 497.2, pp. 2371–2384. DOI: 10.1093/mnras/staa2078. arXiv: 2007.03687 [astro-ph.GA].

Lian, Jianhui et al. (Apr. 2020b).
"The age-chemical abundance structure of the Galaxy I: evidence for a late-accretion event in the outer disc at z $\sim$ 0.6".
In: *Monthly Notices of the Royal Astronomical Society* 494.2, pp. 2561–2575. DOI: 10.1093/mnras/staa867. arXiv: 2003.11549 [astro-ph.GA].

Licquia, Timothy C. and Jeffrey A. Newman (June 2015).
"Improved Estimates of the Milky Way's Stellar Mass and Star Formation Rate from Hierarchical Bayesian Meta-Analysis".
In: *Astrophysical Journal* 806.1, 96, p. 96.
DOI: 10.1088/0004-637X/806/1/96. arXiv: 1407.1078 [astro-ph.GA].

Liddle, Andrew R. and David H. Lyth (2000).
*Cosmological Inflation and Large-Scale Structure*.

Lin, C. C. and Frank H. Shu (Aug. 1964).
"On the Spiral Structure of Disk Galaxies."
In: *The Astrophysical Journal* 140, p. 646. DOI: 10.1086/147955.

Lindblad, B. (Feb. 1960).
"The importance of methods of electronic photography for certain problems concerning the structure and dynamics of galaxies".
In: *Annales d'Astrophysique* 23, p. 373.

Lindegren, L. et al. (Aug. 2018).
"Gaia Data Release 2. The astrometric solution".

In: *Astronomy & Astrophysics* 616, A2, A2.
DOI: 10.1051/0004-6361/201832727. arXiv: 1804.09366 [astro-ph.IM].

Lindegren, Lennart (Apr. 2018). "The Tycho-Gaia Astrometric Solution".
In: *Astrometry and Astrophysics in the Gaia Sky*.
Ed. by A. Recio-Blanco et al. Vol. 330. IAU Symposium, pp. 41–48.
DOI: 10.1017/S1743921317005919.

Liu, Jifeng et al. (Nov. 2019). "A wide star-black-hole binary system from radial-velocity measurements". In: *Nature* 575.7784, pp. 618–621.
DOI: 10.1038/s41586-019-1766-2. arXiv: 1911.11989 [astro-ph.SR].

Loffler, F. et al. (May 2012). "The Einstein Toolkit: a community computational infrastructure for relativistic astrophysics".
In: *Classical and Quantum Gravity* 29.11, p. 115001.
DOI: 10.1088/0264-9381/29/11/115001.
URL: https://doi.org/10.1088/0264-9381/29/11/115001.

Lucy, L. B. (Dec. 1977).
"A numerical approach to the testing of the fission hypothesis."
In: *The Astronomical Journal* 82, pp. 1013–1024. DOI: 10.1086/112164.

Luri, X. et al. (Aug. 2018). "Gaia Data Release 2. Using Gaia parallaxes".
In: *Astronomy & Astrophysics* 616, A9, A9.
DOI: 10.1051/0004-6361/201832964. arXiv: 1804.09376 [astro-ph.IM].

Ma, Xiangcheng et al. (May 2017). "The structure and dynamical evolution of the stellar disc of a simulated Milky Way-mass galaxy".
In: *Monthly Notices of the Royal Astronomical Society* 467.2, pp. 2430–2444.
DOI: 10.1093/mnras/stx273. arXiv: 1608.04133 [astro-ph.GA].

Mackereth, J. Ted and Jo Bovy (Mar. 2020). "Weighing the stellar constituents of the galactic halo with APOGEE red giant stars".
In: *Monthly Notices of the Royal Astronomical Society* 492.3, pp. 3631–3646.
DOI: 10.1093/mnras/staa047. arXiv: 1910.03590 [astro-ph.GA].

Mackereth, J. Ted et al. (Jan. 2019).
"The origin of accreted stellar halo populations in the Milky Way using APOGEE, Gaia, and the EAGLE simulations".
In: *Monthly Notices of the Royal Astronomical Society* 482.3, pp. 3426–3442.
DOI: 10.1093/mnras/sty2955. arXiv: 1808.00968 [astro-ph.GA].

Macpherson, Hayley J., Daniel J. Price, and Paul D. Lasky (Mar. 2019).
"Einstein's Universe: Cosmological structure formation in numerical relativity". In: *Physical Review D* 99.6, 063522, p. 063522.
DOI: 10.1103/PhysRevD.99.063522. arXiv: 1807.01711 [astro-ph.CO].

Magalhaes, N. and F. Cooperstock (Oct. 2017). "Mass density and size estimates for spiral galaxies using general relativity". In: *Astrophysics and Space Science* 362, p. 210. DOI: 10.1007/s10509-017-3179-8.

Majewski, Steven R. et al. (Sept. 2017). "The Apache Point Observatory Galactic Evolution Experiment (APOGEE)". In: *The Astronomical Journal* 154.3, 94, p. 94. DOI: 10.3847/1538-3881/aa784d. arXiv: 1509.05420 [astro-ph.IM].

Markevitch, M. et al. (Mar. 2002). "A Textbook Example of a Bow Shock in the Merging Galaxy Cluster 1E 0657-56". In: *The Astrophysical Journal Letters* 567.1, pp. L27–L31. DOI: 10.1086/339619. arXiv: astro-ph/0110468 [astro-ph].

Markevitch, M. et al. (May 2004). "Direct Constraints on the Dark Matter Self-Interaction Cross Section from the Merging Galaxy Cluster 1E 0657-56". In: *The Astrophysical Journal* 606.2, pp. 819–824. DOI: 10.1086/383178. arXiv: astro-ph/0309303 [astro-ph].

McKee, Christopher F., Antonio Parravano, and David J. Hollenbach (Nov. 2015). "Stars, Gas, and Dark Matter in the Solar Neighborhood". In: *The Astrophysical Journal* 814.1, 13, p. 13. DOI: 10.1088/0004-637X/814/1/13. arXiv: 1509.05334 [astro-ph.GA].

McMillan, Paul J. (Feb. 2017). "The mass distribution and gravitational potential of the Milky Way". In: *Monthly Notices of the Royal Astronomical Society* 465.1, pp. 76–94. DOI: 10.1093/mnras/stw2759. arXiv: 1608.00971 [astro-ph.GA].

McWilliam, Andrew and Manuela Zoccali (Dec. 2010). "Two Red Clumps and the X-shaped Milky Way Bulge". In: *The Astrophysical Journal* 724.2, pp. 1491–1502. DOI: 10.1088/0004-637X/724/2/1491. arXiv: 1008.0519 [astro-ph.GA].

Merrifield, Michael R. (May 1992). "The Rotation Curve of the Milky Way to 2.5 R/o From the Thickness of the HI Layer". In: *The Astronomical Journal* 103, p. 1552. DOI: 10.1086/116168.

Mertens, J. B., J. T. Giblin, and G. D. Starkman (June 2016). "Integration of inhomogeneous cosmological spacetimes in the BSSN formalism". In: *Physical Review D* 93 (12), p. 124059. DOI: 10.1103/PhysRevD.93.124059. URL: https://link.aps.org/doi/10.1103/PhysRevD.93.124059.

Michalik, Daniel, Lennart Lindegren, and David Hobbs (Feb. 2015). "The Tycho-Gaia astrometric solution . How to get 2.5 million parallaxes with less than one year of Gaia data". In: *Astronomy & Astrophysics* 574, A115, A115. DOI: 10.1051/0004-6361/201425310. arXiv: 1412.8770 [astro-ph.IM].

Milgrom, M. (July 1983). "A modification of the newtonian dynamics : implications for galaxy systems." In: *The Astrophysical Journal* 270, pp. 384–389. DOI: 10.1086/161132.

Minchev, I., C. Chiappini, and M. Martig (Oct. 2013). "Chemodynamical evolution of the Milky Way disk. I. The solar vicinity". In: *Astronomy & Astrophysics* 558, A9, A9. DOI: 10.1051/0004-6361/201220189. arXiv: 1208.1506 [astro-ph.GA].

Minchev, I. et al. (Jan. 2017). "The Relationship between Mono-abundance and Mono-age Stellar Populations in the Milky Way Disk". In: *Astrophysical Journal* 834.1, 27, p. 27. DOI: 10.3847/1538-4357/834/1/27. arXiv: 1608.04737 [astro-ph.GA].

Miyamoto, M. and R. Nagai (Jan. 1975). "Three-dimensional models for the distribution of mass in galaxies." In: *Publications of the Astronomical Society of Japan* 27, pp. 533–543.

Monaco, Pierluigi et al. (Apr. 2012). "Schmidt-Kennicutt relations in SPH simulations of disc galaxies with effective thermal feedback from supernovae". In: *Monthly Notices of the Royal Astronomical Society* 421.3, pp. 2485–2497. DOI: 10.1111/j.1365-2966.2012.20482.x. arXiv: 1109.0484 [astro-ph.CO].

Moni Bidin, C. et al. (May 2012). "Kinematical and Chemical Vertical Structure of the Galactic Thick Disk. II. A Lack of Dark Matter in the Solar Neighborhood". In: *The Astrophysical Journal* 751.1, 30, p. 30. DOI: 10.1088/0004-637X/751/1/30. arXiv: 1204.3924 [astro-ph.GA].

Moni Bidin, C. et al. (Jan. 2015). "On the local dark matter density". In: *Astronomy & Astrophysics* 573, A91, A91. DOI: 10.1051/0004-6361/201424675.

Mor, R. et al. (Apr. 2019). "Gaia DR2 reveals a star formation burst in the disc 2-3 Gyr ago". In: *Astronomy & Astrophysics* 624, L1, p. L1. DOI: 10.1051/0004-6361/201935105. arXiv: 1901.07564 [astro-ph.GA].

Mróz, Przemek et al. (Jan. 2019). "Rotation Curve of the Milky Way from Classical Cepheids".

In: *The Astrophysical Journal Letters* 870.1, L10, p. L10.
DOI: 10.3847/2041-8213/aaf73f. arXiv: 1810.02131 [astro-ph.GA].

Muñoz-Mateos, J. C. et al. (Apr. 2011).
"Radial Distribution of Stars, Gas, and Dust in SINGS Galaxies. III. Modeling the Evolution of the Stellar Component in Galaxy Disks".
In: *The Astrophysical Journal* 731.1, 10, p. 10.
DOI: 10.1088/0004-637X/731/1/10. arXiv: 1102.1724 [astro-ph.CO].

Murante, Giuseppe et al. (July 2010).
"A subresolution multiphase interstellar medium model of star formation and supernova energy feedback".
In: *Monthly Notices of the Royal Astronomical Society* 405.3, pp. 1491–1512.
DOI: 10.1111/j.1365-2966.2010.16567.x. arXiv: 1002.4122 [astro-ph.CO].

Murante, Giuseppe et al. (Feb. 2015). "Simulating realistic disc galaxies with a novel sub-resolution ISM model".
In: *Monthly Notices of the Royal Astronomical Society* 447.1, pp. 178–201.
DOI: 10.1093/mnras/stu2400.

Nataf, D. M. et al. (Sept. 2010).
"The Split Red Clump of the Galactic Bulge from OGLE-III".
In: *The Astrophysical Journal Letters* 721.1, pp. L28–L32.
DOI: 10.1088/2041-8205/721/1/L28. arXiv: 1007.5065 [astro-ph.GA].

Navarro, Julio F., Carlos S. Frenk, and Simon D. M. White (May 1996).
"The Structure of Cold Dark Matter Halos".
In: *The Astrophysical Journal* 462, p. 563. DOI: 10.1086/177173.
arXiv: astro-ph/9508025 [astro-ph].

Nazari, Elham et al. (Apr. 2017). "Post-Newtonian Jeans Analysis".
In: *The Astrophysical Journal* 839.2, 75, p. 75.
DOI: 10.3847/1538-4357/aa68e0. arXiv: 1703.07714 [astro-ph.HE].

Neill, C., David L. Wiltshire, and Teppo Mattsson (2011).
*General Relativistic Galaxy Models*. private communication to M. Crosta.

Nelson, Dylan et al. (Mar. 2018). "First results from the IllustrisTNG simulations: the galaxy colour bimodality".
In: *Monthly Notices of the Royal Astronomical Society* 475.1, pp. 624–647.
DOI: 10.1093/mnras/stx3040. arXiv: 1707.03395 [astro-ph.GA].

Ness, M. et al. (Sept. 2012). "The Origin of the Split Red Clump in the Galactic Bulge of the Milky Way".
In: *The Astrophysical Journal* 756.1, 22, p. 22.
DOI: 10.1088/0004-637X/756/1/22. arXiv: 1207.0888 [astro-ph.GA].

Neugebauer, G., A. Kleinwaechter, and R. Meinel (Nov. 1996). "Relativistically rotating dust." In: *Helvetica Physica Acta* 69.4, pp. 472–489. arXiv: gr-qc/0301107 [gr-qc].

Neugebauer, G. and R. Meinel (Oct. 1995). "General Relativistic Gravitational Field of a Rigidly Rotating Disk of Dust: Solution in Terms of Ultraelliptic Functions". In: *Physical Review Letters* 75.17, pp. 3046–3047. DOI: 10.1103/PhysRevLett.75.3046. arXiv: gr-qc/0302060 [gr-qc].

Nissen, P. E. and W. J. Schuster (Feb. 2010). "Two distinct halo populations in the solar neighborhood. Evidence from stellar abundance ratios and kinematics". In: *Astronomy & Astrophysics* 511, L10, p. L10. DOI: 10.1051/0004-6361/200913877. arXiv: 1002.4514 [astro-ph.GA].

Nitschai, Maria Selina, Michele Cappellari, and Nadine Neumayer (Apr. 2020). "First Gaia dynamical model of the Milky Way disc with six phase space coordinates: a test for galaxy dynamics". In: *Monthly Notices of the Royal Astronomical Society* 494.4, pp. 6001–6011. DOI: 10.1093/mnras/staa1128. arXiv: 1909.05269 [astro-ph.GA].

Nogueras-Lara, F. et al. (Dec. 2018). "Star formation history and metallicity in the Galactic inner bulge revealed by the red giant branch bump". In: *Astronomy & Astrophysics* 620, A83, A83. DOI: 10.1051/0004-6361/201833518. arXiv: 1809.07627 [astro-ph.GA].

Obreja, Aura et al. (July 2018). "Introducing galactic structure finder: the multiple stellar kinematic structures of a simulated Milky Way mass galaxy". In: *Monthly Notices of the Royal Astronomical Society* 477.4, pp. 4915–4930. DOI: 10.1093/mnras/sty1022. arXiv: 1804.05576 [astro-ph.GA].

Obreja, Aura et al. (Aug. 2019). "NIHAO XVI: the properties and evolution of kinematically selected discs, bulges, and stellar haloes". In: *Monthly Notices of the Royal Astronomical Society* 487.3, pp. 4424–4456. DOI: 10.1093/mnras/stz1563. arXiv: 1804.06635 [astro-ph.GA].

Oman, Kyle A. et al. (Oct. 2015). "The unexpected diversity of dwarf galaxy rotation curves". In: *Monthly Notices of the Royal Astronomical Society* 452.4, pp. 3650–3665. DOI: 10.1093/mnras/stv1504. arXiv: 1504.01437 [astro-ph.GA].

Padovani, P. and F. Matteucci (Oct. 1993). "Stellar Mass Loss in Elliptical Galaxies and the Fueling of Active Galactic Nuclei".
In: *The Astrophysical Journal* 416, p. 26. DOI: 10.1086/173212.

Pancino, Elena (Jan. 2020).
"Gaia: The Galaxy in six (and more) dimensions".
In: *Advances in Space Research* 65.1, pp. 1–10.
DOI: 10.1016/j.asr.2019.11.007. arXiv: 1912.09233 [astro-ph.SR].

Papastergis, E. et al. (Feb. 2015).
"Is there a "too big to fail" problem in the field?"
In: *Astronomy & Astrophysics* 574, A113, A113.
DOI: 10.1051/0004-6361/201424909. arXiv: 1407.4665 [astro-ph.GA].

Penzias, A. A. and R. W. Wilson (July 1965).
"A Measurement of Excess Antenna Temperature at 4080 Mc/s."
In: *The Astrophysical Journal* 142, pp. 419–421. DOI: 10.1086/148307.

Perryman, M. A. C. et al. (July 1997). "The Hipparcos Catalogue."
In: *Astronomy & Astrophysics* 500, pp. 501–504.

Perryman, M. A. C. et al. (Apr. 2001).
"GAIA: Composition, formation and evolution of the Galaxy".
In: *Astronomy & Astrophysics* 369, pp. 339–363.
DOI: 10.1051/0004-6361:20010085. arXiv: astro-ph/0101235 [astro-ph].

Pila-Díez, B. et al. (July 2015). "A skewer survey of the Galactic halo from deep CFHT and INT images".
In: *Astronomy & Astrophysics* 579, A38, A38.
DOI: 10.1051/0004-6361/201425457. arXiv: 1502.02460 [astro-ph.GA].

Planck Collaboration et al. (Sept. 2016).
"Planck 2015 results. I. Overview of products and scientific results".
In: *Astronomy and Astrophysics* 594, A1, A1.
DOI: 10.1051/0004-6361/201527101. arXiv: 1502.01582 [astro-ph.CO].

Poggio, E. et al. (Nov. 2018).
"The Galactic warp revealed by Gaia DR2 kinematics".
In: *Monthly Notices of the Royal Astronomical Society* 481.1, pp. L21–L25.
DOI: 10.1093/mnrasl/sly148. arXiv: 1805.03171 [astro-ph.GA].

Poggio, E. et al. (Mar. 2020).
"Evidence of a dynamically evolving Galactic warp".
In: *Nature Astronomy* 4, pp. 590–596. DOI: 10.1038/s41550-020-1017-3.
arXiv: 1912.10471 [astro-ph.GA].

Pont, F. et al. (Feb. 1997).
"Rotation of the outer disc from classical cepheids."
In: *Astronomy & Astrophysics* 318, pp. 416–428.

Portail, M. et al. (Mar. 2015). "Made-to-measure models of the Galactic box/peanut bulge: stellar and total mass in the bulge region".
In: *Monthly Notices of the Royal Astronomical Society* 448.1, pp. 713–731.
DOI: 10.1093/mnras/stv058. arXiv: 1502.00633 [astro-ph.GA].

Posti, Lorenzo and Amina Helmi (Jan. 2019a). "Mass and shape of the Milky Way's dark matter halo with globular clusters from Gaia and Hubble".
In: *Astronomy & Astrophysics* 621, A56, A56.
DOI: 10.1051/0004-6361/201833355. arXiv: 1805.01408 [astro-ph.GA].

— (Jan. 2019b). "Mass and shape of the Milky Way's dark matter halo with globular clusters from Gaia and Hubble".
In: *Astronomy & Astrophysics* 621, A56, A56.
DOI: 10.1051/0004-6361/201833355. arXiv: 1805.01408 [astro-ph.GA].

Pouliasis, E., P. Di Matteo, and M. Haywood (Feb. 2017).
"A Milky Way with a massive, centrally concentrated thick disc: new Galactic mass models for orbit computations".
In: *Astronomy & Astrophysics* 598, A66, A66.
DOI: 10.1051/0004-6361/201527346. arXiv: 1611.07979 [astro-ph.GA].

Price, D. J. and J. J. Monaghan (Feb. 2007).
"An energy-conserving formalism for adaptive gravitational force softening in smoothed particle hydrodynamics and N-body codes".
In: *Monthly Notices of the Royal Astronomical Society* 374.4, pp. 1347–1358.
DOI: 10.1111/j.1365-2966.2006.11241.x.
arXiv: astro-ph/0610872 [astro-ph].

Price, Daniel J. (Feb. 2012).
"Smoothed particle hydrodynamics and magnetohydrodynamics".
In: *Journal of Computational Physics* 231.3, pp. 759–794.
DOI: 10.1016/j.jcp.2010.12.011.

Purcell, Chris W., James S. Bullock, and Stelios Kazantzidis (June 2010).
"Heated disc stars in the stellar halo".
In: *Monthly Notices of the Royal Astronomical Society* 404.4, pp. 1711–1718.
DOI: 10.1111/j.1365-2966.2010.16429.x. arXiv: 0910.5481 [astro-ph.GA].

Queiroz, A. B. A. et al. (July 2020). "The Milky Way's bar and bulge revealed by APOGEE DR16 and Gaia DR2". In: *arXiv e-prints*.
arXiv: 2007.12915 [astro-ph.GA].

Re Fiorentin, Paola, Mario G. Lattanzi, and Alessandro Spagna (Mar. 2019). "Evidence of a large-scale positive rotation-metallicity correlation in the Galactic thick disc".
In: *Monthly Notices of the Royal Astronomical Society* 484.1, pp. L69–L74. DOI: 10.1093/mnrasl/sly198. arXiv: 1810.07643 [astro-ph.GA].

Re Fiorentin, Paola et al. (Oct. 2015). "New Signatures of the Milky Way Formation in the Local Halo and Inner-halo Streamers in the Era of Gaia".
In: *The Astronomical Journal* 150.4, 128, p. 128. DOI: 10.1088/0004-6256/150/4/128. arXiv: 1508.03736 [astro-ph.GA].

Re Fiorentin, Paola et al. (Jan. 2021). "Icarus: A Flat and Fast Prograde Stellar Stream in the Milky Way Disk".
In: *The Astrophysical Journal Letters* 907.1, L16, p. L16. DOI: 10.3847/2041-8213/abd53d. arXiv: 2012.10957 [astro-ph.GA].

Read, J. I. (June 2014). "The local dark matter density".
In: *Journal of Physics G Nuclear Physics* 41.6, 063101, p. 063101. DOI: 10.1088/0954-3899/41/6/063101. arXiv: 1404.1938 [astro-ph.GA].

Recio-Blanco, A. et al. (July 2014). "The Gaia-ESO Survey: the Galactic thick to thin disc transition".
In: *Astronomy & Astrophysics* 567, A5, A5. DOI: 10.1051/0004-6361/201322944. arXiv: 1403.7568 [astro-ph.GA].

Reid, M. J. (July 2008). "Micro-arcsecond astrometry with the VLBA".
In: *A Giant Step: from Milli- to Micro-arcsecond Astrometry*. Ed. by W. J. Jin, I. Platais, and M. A. C. Perryman. Vol. 248. IAU Symposium, pp. 141–147. DOI: 10.1017/S1743921308018929.

Reid, M. J. and A. Brunthaler (Dec. 2004). "The Proper Motion of Sagittarius A*. II. The Mass of Sagittarius A*".
In: *The Astrophysical Journal* 616.2, pp. 872–884. DOI: 10.1086/424960. arXiv: astro-ph/0408107 [astro-ph].

Reid, M. J. et al. (Mar. 2014). "Trigonometric Parallaxes of High Mass Star Forming Regions: The Structure and Kinematics of the Milky Way".
In: *The Astrophysical Journal* 783.2, 130, p. 130. DOI: 10.1088/0004-637X/783/2/130. arXiv: 1401.5377 [astro-ph.GA].

Renzini, Alvio et al. (Aug. 2018). "The WFC3 Galactic Bulge Treasury Program: Relative Ages of Bulge Stars of High and Low Metallicity".
In: *The Astrophysical Journal* 863.1, 16, p. 16. DOI: 10.3847/1538-4357/aad09b. arXiv: 1806.11556 [astro-ph.GA].

Richter, Philipp (2017). "Gas Accretion onto the Milky Way". In: *Gas Accretion onto Galaxies*. Ed. by Andrew Fox and Romeel Davé. Vol. 430. Astrophysics and Space Science Library, p. 15. DOI: 10.1007/978-3-319-52512-9_2.

Riess, Adam G. et al. (Sept. 1998). "Observational Evidence from Supernovae for an Accelerating Universe and a Cosmological Constant". In: *The Astronomical Journal* 116.3, pp. 1009–1038. DOI: 10.1086/300499. arXiv: astro-ph/9805201 [astro-ph].

Riess, Adam G. et al. (July 2016). "A 2.4% Determination of the Local Value of the Hubble Constant". In: *The Astrophysical Journal* 826.1, 56, p. 56. DOI: 10.3847/0004-637X/826/1/56. arXiv: 1604.01424 [astro-ph.CO].

Robitaille, Thomas P. and Barbara A. Whitney (Feb. 2010). "The Present-Day Star Formation Rate of the Milky Way Determined from Spitzer-Detected Young Stellar Objects". In: *Astrophysical Journall* 710.1, pp. L11–L15. DOI: 10.1088/2041-8205/710/1/L11. arXiv: 1001.3672 [astro-ph.GA].

Rojas-Arriagada, A. et al. (May 2017). "The Gaia-ESO Survey: Exploring the complex nature and origins of the Galactic bulge populations". In: *Astronomy & Astrophysics* 601, A140, A140. DOI: 10.1051/0004-6361/201629160. arXiv: 1704.03325 [astro-ph.GA].

Rubin, V. C., Jr. Ford W. K., and N. Thonnard (Nov. 1978). "Extended rotation curves of high-luminosity spiral galaxies. IV. Systematic dynamical properties, Sa -> Sc." In: *The Astrophysical Journal Letters* 225, pp. L107–L111. DOI: 10.1086/182804.

— (June 1980). "Rotational properties of 21 SC galaxies with a large range of luminosities and radii, from NGC 4605 (R=4kpc) to UGC 2885 (R=122kpc)." In: *The Astrophysical Journal* 238, pp. 471–487. DOI: 10.1086/158003.

Salvatier, John, Thomas V. Wiecki, and Christopher Fonnesbeck (Apr. 2016). "Probabilistic programming in Python using PyMC3". In: *PeerJ Computer Science* 2, e55. ISSN: 2376-5992. DOI: 10.7717/peerj-cs.55.

Samland, M. and O. E. Gerhard (Mar. 2003). "The formation of a disk galaxy within a growing dark halo". In: *Astronomy & Astrophysics* 399, pp. 961–982. DOI: 10.1051/0004-6361:20021842. arXiv: astro-ph/0301499 [astro-ph].

Sanders, Jason L. and Payel Das (Dec. 2018).
"Isochrone ages for ∼3 million stars with the second Gaia data release".
In: *Monthly Notices of the Royal Astronomical Society* 481.3, pp. 4093–4110.
DOI: 10.1093/mnras/sty2490. arXiv: 1806.02324 [astro-ph.GA].

Sawala, Till et al. (Apr. 2016). "The APOSTLE simulations: solutions to the Local Group's cosmic puzzles".
In: *Monthly Notices of the Royal Astronomical Society* 457.2, pp. 1931–1943.
DOI: 10.1093/mnras/stw145. arXiv: 1511.01098 [astro-ph.GA].

Scannapieco, C. et al. (June 2012).
"The Aquila comparison project: the effects of feedback and numerical methods on simulations of galaxy formation".
In: *Monthly Notices of the Royal Astronomical Society* 423.2, pp. 1726–1749.
DOI: 10.1111/j.1365-2966.2012.20993.x. arXiv: 1112.0315 [astro-ph.GA].

Scannapieco, Cecilia et al. (Sept. 2010). "An observer's view of simulated galaxies: disc-to-total ratios, bars and (pseudo-)bulges".
In: *Monthly Notices of the Royal Astronomical Society* 407.1, pp. L41–L45.
DOI: 10.1111/j.1745-3933.2010.00900.x. arXiv: 1001.4890 [astro-ph.GA].

Schneider, S. E. and Y. Terzian (Nov. 1983).
"Planetary nebulae and the galactic rotation curve."
In: *The Astrophysical Journal Letters* 274, pp. L61–L64.
DOI: 10.1086/184151.

Schödel, R. et al. (June 2014).
"Surface brightness profile of the Milky Way's nuclear star cluster".
In: *Astronomy & Astrophysics* 566, A47, A47.
DOI: 10.1051/0004-6361/201423481. arXiv: 1403.6657 [astro-ph.GA].

Schönrich, Ralph, James Binney, and Walter Dehnen (Apr. 2010).
"Local kinematics and the local standard of rest".
In: *Monthly Notices of the Royal Astronomical Society* 403.4, pp. 1829–1833.
DOI: 10.1111/j.1365-2966.2010.16253.x. arXiv: 0912.3693 [astro-ph.GA].

Schultheis, M. et al. (Apr. 2017). "Baade's window and APOGEE. Metallicities, ages, and chemical abundances".
In: *Astronomy & Astrophysics* 600, A14, A14.
DOI: 10.1051/0004-6361/201630154. arXiv: 1702.01547 [astro-ph.GA].

Searle, L. and R. Zinn (Oct. 1978).
"Composition of halo clusters and the formation of the galactic halo."
In: *The Astrophysical Journal* 225, pp. 357–379. DOI: 10.1086/156499.

Skrutskie, M. F. et al. (Feb. 2006).
"The Two Micron All Sky Survey (2MASS)".
In: *The Astronomical Journal* 131.2, pp. 1163–1183. DOI: 10.1086/498708.

Slosar, Anže et al. (Apr. 2013). "Measurement of baryon acoustic oscillations in the Lyman-$\alpha$ forest fluctuations in BOSS data release 9".
In: *Journal of Cosmology and Astroparticle Physics* 2013.4, 026, p. 026.
DOI: 10.1088/1475-7516/2013/04/026. arXiv: 1301.3459 [astro-ph.CO].

Smith, Haywood and Heinrich Eichhorn (July 1996).
"On the estimation of distances from trigonometric parallaxes".
In: *Monthly Notices of the Royal Astronomical Society* 281.1, pp. 211–218.
ISSN: 0035-8711. DOI: 10.1093/mnras/281.1.211.
eprint: https://academic.oup.com/mnras/article-pdf/281/1/211/18540030/281-1-211.pdf.
URL: https://doi.org/10.1093/mnras/281.1.211.

Soffel, M. et al. (Dec. 2003).
"The IAU 2000 Resolutions for Astrometry, Celestial Mechanics, and Metrology in the Relativistic Framework: Explanatory Supplement".
In: *The Astronomical Journal* 126.6, pp. 2687–2706. DOI: 10.1086/378162.
arXiv: astro-ph/0303376 [astro-ph].

Sofue, Yoshiaki (Feb. 2017).
"Rotation and mass in the Milky Way and spiral galaxies".
In: *Publications of the Astronomical Society of Japan* 69.1, R1, R1.
DOI: 10.1093/pasj/psw103. arXiv: 1608.08350 [astro-ph.GA].

— (Apr. 2020).
"Rotation Curve of the Milky Way and the Dark Matter Density".
In: *Galaxies* 8.2, p. 37. DOI: 10.3390/galaxies8020037.
arXiv: 2004.11688 [astro-ph.GA].

Sofue, Yoshiaki and Vera Rubin (Jan. 2001).
"Rotation Curves of Spiral Galaxies".
In: *Annual Review of Astronomy and Astrophysics* 39, pp. 137–174.
DOI: 10.1146/annurev.astro.39.1.137.
arXiv: astro-ph/0010594 [astro-ph].

Sormani, Mattia C. et al. (Sept. 2020).
"Jeans modelling of the Milky Way's nuclear stellar disc".
In: *Monthly Notices of the Royal Astronomical Society*.
DOI: 10.1093/mnras/staa2785.

Soubiran, C., O. Bienaymé, and A. Siebert (Jan. 2003). "Vertical distribution of Galactic disk stars. I. Kinematics and metallicity".

In: *Astronomy & Astrophysics* 398, pp. 141–151.
DOI: 10.1051/0004-6361:20021615. arXiv: astro-ph/0210628 [astro-ph].

Spagna, A. et al. (Feb. 2010).
"Evidence of a thick disk rotation-metallicity correlation".
In: *Astronomy & Astrophysics* 510, L4, p. L4.
DOI: 10.1051/0004-6361/200913538. arXiv: 1002.0074 [astro-ph.GA].

Spagna, Alessandro et al. (May 2016).
"The Gaia mission: the dawn of Astrometric Cosmology? Status and prospects after 14 months of science operations".
In: *Journal of Physics Conference Series*. Vol. 718.
Journal of Physics Conference Series, p. 032005.
DOI: 10.1088/1742-6596/718/3/032005.

Spagna, Alessandro et al. (Apr. 2019). "The thick disk rotation-metallicity correlation, comparison with Galactic cosmological simulations".
In: *The Gaia Universe*, p. 38. DOI: 10.5281/zenodo.3059063.

Sparke, Linda S. and III Gallagher John S. (2006).
*Galaxies in the Universe - 2nd Edition*. DOI: 10.2277/0521855934.

Springel, V. (Dec. 2005). "The cosmological simulation code GADGET-2".
In: *Monthly Notices of the Royal Astronomical Society* 364, pp. 1105–1134.
DOI: 10.1111/j.1365-2966.2005.09655.x. eprint: astro-ph/0505010.

Springel, V. and L. Hernquist (Feb. 2003).
"Cosmological smoothed particle hydrodynamics simulations: a hybrid multiphase model for star formation".
In: *Monthly Notices of the Royal Astronomical Society* 339, pp. 289–311.
DOI: 10.1046/j.1365-8711.2003.06206.x. eprint: astro-ph/0206393.

Springel, V. et al. (Dec. 2008).
"The Aquarius Project: the subhaloes of galactic haloes".
In: *Monthly Notices of the Royal Astronomical Society* 391.4, pp. 1685–1711.
DOI: 10.1111/j.1365-2966.2008.14066.x. arXiv: 0809.0898 [astro-ph].

Springel, Volker (Sept. 2010).
"Smoothed Particle Hydrodynamics in Astrophysics".
In: *Annual Review of Astronomy and Astrophysics* 48, pp. 391–430.
DOI: 10.1146/annurev-astro-081309-130914.
arXiv: 1109.2219 [astro-ph.CO].

Starobinsky, A. A. (Mar. 1980).
"A new type of isotropic cosmological models without singularity".
In: *Physics Letters B* 91.1, pp. 99–102. DOI: 10.1016/0370-2693(80)90670-X.

Stephani, Hans et al. (2009). *Exact Solutions of Einstein's Field Equations*. DOI: 10.1017/CBO9780511535185.

Stinson, G. S. et al. (Nov. 2013). "MaGICC thick disc - I. Comparing a simulated disc formed with stellar feedback to the Milky Way". In: *Monthly Notices of the Royal Astronomical Society* 436.1, pp. 625–634. DOI: 10.1093/mnras/stt1600. arXiv: 1301.5318 [astro-ph.GA].

Tanabashi, M. et al. (Aug. 2018). "Review of Particle Physics*". In: *Physical Review D* 98.3, 030001, p. 030001. DOI: 10.1103/PhysRevD.98.030001.

The HIPPARCOS and TYCHO catalogues (Jan. 1997). *The HIPPARCOS and TYCHO catalogues. Astrometric and photometric star catalogues derived from the ESA HIPPARCOS Space Astrometry Mission*. Vol. 1200. ESA Special Publication.

Tornatore, L. et al. (Dec. 2007). "Chemical enrichment of galaxy clusters from hydrodynamical simulations". In: *Monthly Notices of the Royal Astronomical Society* 382, pp. 1050–1072. DOI: 10.1111/j.1365-2966.2007.12070.x. arXiv: 0705.1921.

Tsallis, Constantino (July 1988). "Possible generalization of Boltzmann-Gibbs statistics". In: *Journal of Statistical Physics* 52.1-2, pp. 479–487. DOI: 10.1007/BF01016429.

Tsallis, Constantino and Zochil Gonzalez Arenas (Apr. 2014). "Nonextensive statistical mechanics and high energy physics". In: *European Physical Journal Web of Conferences*. Vol. 71. European Physical Journal Web of Conferences, p. 00132. DOI: 10.1051/epjconf/20147100132.

Valenti, E. et al. (Mar. 2016). "Stellar density profile and mass of the Milky Way bulge from VVV data". In: *Astronomy & Astrophysics* 587, L6, p. L6. DOI: 10.1051/0004-6361/201527500. arXiv: 1510.07425 [astro-ph.GA].

Valentini, M. et al. (Apr. 2018). "Colour-magnitude diagram in simulations of galaxy formation". In: *ArXiv e-prints*. arXiv: 1805.00028.

Valentini, Milena et al. (Sept. 2017). "On the effect of galactic outflows in cosmological simulations of disc galaxies". In: *Monthly Notices of the Royal Astronomical Society* 470.3, pp. 3167–3193. DOI: 10.1093/mnras/stx1352. arXiv: 1705.10325 [astro-ph.GA].

Valentini, Milena et al. (May 2019). "Chemical evolution of disc galaxies from cosmological simulations".

In: *Monthly Notices of the Royal Astronomical Society* 485.1, pp. 1384–1404. DOI: 10.1093/mnras/stz492. arXiv: 1902.05955 [astro-ph.GA].

Valentini, Milena et al. (Jan. 2020). "Impact of AGN feedback on galaxies and their multiphase ISM across cosmic time". In: *Monthly Notices of the Royal Astronomical Society* 491.2, pp. 2779–2807. DOI: 10.1093/mnras/stz3131. arXiv: 1911.02572 [astro-ph.GA].

van Albada, T. S. and R. Sancisi (Dec. 1986). "Dark Matter in Spiral Galaxies". In: *Philosophical Transactions of the Royal Society of London Series A* 320.1556, pp. 447–464. DOI: 10.1098/rsta.1986.0128.

van der Marel, Roeland P., Nitya Kallivayalil, and Gurtina Besla (Mar. 2009). "Kinematical structure of the Magellanic System". In: *The Magellanic System: Stars, Gas, and Galaxies*. Ed. by Jacco Th. Van Loon and Joana M. Oliveira. Vol. 256, pp. 81–92. DOI: 10.1017/S1743921308028299. arXiv: 0809.4268 [astro-ph].

van Leeuwen, F. (Sept. 2008). "VizieR Online Data Catalog: Hipparcos, the New Reduction (van Leeuwen, 2007)". In: *VizieR Online Data Catalog*, I/311, pp. I/311.

van Leeuwen, F. et al. (July 2018). *Gaia DR2 documentation*. Gaia DR2 documentation.

Vera-Ciro, Carlos and Amina Helmi (Aug. 2013). "Constraints on the Shape of the Milky Way Dark Matter Halo from the Sagittarius Stream". In: *The Astrophysical Journal Letters* 773.1, L4, p. L4. DOI: 10.1088/2041-8205/773/1/L4. arXiv: 1304.4646 [astro-ph.GA].

Vincenzo, Fiorenzo et al. (July 2019). "The Fall of a Giant. Chemical evolution of Enceladus, alias the Gaia Sausage". In: *Monthly Notices of the Royal Astronomical Society* 487.1, pp. L47–L52. DOI: 10.1093/mnrasl/slz070. arXiv: 1903.03465 [astro-ph.GA].

Virtanen, Pauli et al. (2020). "SciPy 1.0: Fundamental Algorithms for Scientific Computing in Python". In: *Nature Methods* 17, pp. 261–272. DOI: 10.1038/s41592-019-0686-2.

Vogelsberger, Mark et al. (Jan. 2020). "Cosmological simulations of galaxy formation". In: *Nature Reviews Physics* 2.1, pp. 42–66. DOI: 10.1038/s42254-019-0127-2. arXiv: 1909.07976 [astro-ph.GA].

Wald, R. M. (1984). *General relativity*.

Watanabe, S. and M. Opper (2010). "Asymptotic equivalence of Bayes cross validation and widely

applicable information criterion in singular learning theory."
In: *Journal of machine learning research* 11.12.

Watkins, Laura L. et al. (Mar. 2019a). "Evidence for an Intermediate-mass Milky Way from Gaia DR2 Halo Globular Cluster Motions".
In: *The Astrophysical Journal* 873.2, 118, p. 118.
DOI: 10.3847/1538-4357/ab089f. arXiv: 1804.11348 [astro-ph.GA].

— (Mar. 2019b). "Evidence for an Intermediate-mass Milky Way from Gaia DR2 Halo Globular Cluster Motions".
In: *The Astrophysical Journal* 873.2, 118, p. 118.
DOI: 10.3847/1538-4357/ab089f. arXiv: 1804.11348 [astro-ph.GA].

Wegg, Christopher, Ortwin Gerhard, and Marie Bieth (May 2019). "The gravitational force field of the Galaxy measured from the kinematics of RR Lyrae in Gaia".
In: *Monthly Notices of the Royal Astronomical Society* 485.3, pp. 3296–3316.
DOI: 10.1093/mnras/stz572. arXiv: 1806.09635 [astro-ph.GA].

Wegg, Christopher, Ortwin Gerhard, and Matthieu Portail (July 2015). "The structure of the Milky Way's bar outside the bulge".
In: *Monthly Notices of the Royal Astronomical Society* 450.4, pp. 4050–4069.
DOI: 10.1093/mnras/stv745. arXiv: 1504.01401 [astro-ph.GA].

Wielen, R. (Sept. 1977). "The Diffusion of Stellar Orbits Derived from the Observed Age-Dependence of the Velocity Dispersion".
In: *Astronomy & Astrophysics* 60.2, pp. 263–275.

Wiersma, R. P. C., J. Schaye, and B. D. Smith (Feb. 2009). "The effect of photoionization on the cooling rates of enriched, astrophysical plasmas".
In: *Monthly Notices of the Royal Astronomical Society* 393, pp. 99–107.
DOI: 10.1111/j.1365-2966.2008.14191.x. arXiv: 0807.3748.

Wiltshire, D. L. (Aug. 2011). "What is dust? Physical foundations of the averaging problem in cosmology".
In: *Classical and Quantum Gravity* 28.16, p. 164006.
DOI: 10.1088/0264-9381/28/16/164006.
URL: https://doi.org/10.1088/0264-9381/28/16/164006.

Wolfram Research Inc. (2012). *Mathematica*. Website.
Version 9.x. Champaign, IL, 2012.
URL: https://www.wolfram.com/mathematica.

Wright, E. L. et al. (Sept. 1992). "Interpretation of the Cosmic Microwave Background Radiation Anisotropy Detected by the COBE Differential Microwave Radiometer".
In: *The Astrophysical Journal Letters* 396, p. L13. DOI: 10.1086/186506.

Xue, Xiang-Xiang, Hans-Walter Rix, and Gang Zhao (Nov. 2009). "The pairwise velocity difference of over 2000 BHB stars in the Milky Way halo". In: *Research in Astronomy and Astrophysics* 9.11, pp. 1230–1240. DOI: 10.1088/1674-4527/9/11/006.

Xue, Xiang-Xiang et al. (Aug. 2015). "The Radial Profile and Flattening of the Milky Way's Stellar Halo to 80 kpc from the SEGUE K-giant Survey". In: *The Astrophysical Journal* 809.2, 144, p. 144. DOI: 10.1088/0004-637X/809/2/144. arXiv: 1506.06144 [astro-ph.GA].

Yoshii, Y. (Jan. 1982). "Density distribution of faint stars in the direction of the north galactic pole." In: *Publications of the Astronomical Society of Japan* 34, pp. 365–379.

Yu, Jincheng and Chao Liu (Mar. 2018). "The age-velocity dispersion relation of the Galactic discs from LAMOST-Gaia data". In: *Monthly Notices of the Royal Astronomical Society* 475.1, pp. 1093–1103. DOI: 10.1093/mnras/stx3204. arXiv: 1712.03965 [astro-ph.GA].

Zheng, Y. et al. (Jan. 2019). "Revealing the Milky Way's Hidden Circumgalactic Medium with the Cosmic Origins Spectrograph Quasar Database for Galactic Absorption Lines". In: *The Astrophysical Journal* 871.1, 35, p. 35. DOI: 10.3847/1538-4357/aaf6eb. arXiv: 1710.10703 [astro-ph.GA].

Zoccali, M. (Aug. 2019). "The Stellar Population, 3D structure, and kinematics of the Galactic bulge". In: *Boletin de la Asociacion Argentina de Astronomia La Plata Argentina* 61, pp. 137–144.

Zoccali, M. et al. (Mar. 2017). "The GIRAFFE Inner Bulge Survey (GIBS). III. Metallicity distributions and kinematics of 26 Galactic bulge fields". In: *Astronomy & Astrophysics* 599, A12, A12. DOI: 10.1051/0004-6361/201629805. arXiv: 1610.09174 [astro-ph.GA].

Zwicky, F. (Jan. 1933). "Die Rotverschiebung von extragalaktischen Nebeln". In: *Helvetica Physica Acta* 6, pp. 110–127.

— (Oct. 1937). "On the Masses of Nebulae and of Clusters of Nebulae". In: *The Astrophysical Journal* 86, p. 217. DOI: 10.1086/143864.